Assessing the safety of engineered nanoparticles designed for therapeutic use

Inauguraldissertation

zur

Erlangung der Würde eines Doktors der Philosophie
vorgelegt der
Philosophisch-Naturwissenschaftlichen Fakultät
der Universität Basel

von

Stefan Kevin Siegrist

aus Basel (BS)

Basel, 2019

Genehmigt von der Philosophisch-Naturwissenschaftlichen Fakultät auf Antrag von

Prof. Dr. Jörg Huwyler
Prof. Dr. Martin Wilks

Basel, den 17.10.2017

Prof. Dr. Martin Spiess
Dekan

Notice the small things…

The rewards are inversely proportional.

Liz Vassey, Actress

Table of contents

Acknowledgements

Als Erstes möchte ich mich bei meinem Doktorvater, Jörg Huwyler, für seine immerwährende Unterstützung und Positivität während meiner Dissertation bedanken. Lieber Jörg, du hast es mir in dieser Zeit (meistens☺) sehr einfach gemacht, mich in der Forschung wohl zu fühlen. Dafür danke ich dir von Herzen.

Ein grosses Dankeschön geht an Martin Wilks für die sehr unkomplizierte Zusage zum Koreferat trotz vollem Terminplan.

A great big fat THANKS to Elizaveta Fasler-Kan. Deine grossartige Unterstützung und dein Enthusiasmus haben mir immer ein positives Gefühl gegeben. Es war mir eine grosse Freude mit dir arbeiten zu dürfen und eine Ehre dich in meinem Dissertations-Komitee zu haben.

Danken möchte ich auch der Gruppe der Pharmazeutischen Technologie, die mich auf diesem dreieinhalbjährigen Weg begleitet hat und die Zeit mit zahlreichen tollen Erinnerungen gefüllt hat. Ihr seid der Grund, warum ich immer gerne zur Arbeit gekommen bin. Im Speziellen bedanke ich mich bei Helene Kettiger, Philip Grossen, Dominik Witzigmann, Sandro Sieber, Leonie Wagner-Hattler und Urs Duthaler. Danke fürs Teilen des „Outlaw-Labors“, die unvergesslichen Ausflüge, Beer&Chill-Abende, die „Biidoo“-Anfälle und den einen oder anderen Streich bei der Arbeit. Ein weiteres grosses Dankeschön an Gaby Québatte, Maxim Puchkov, Pascal Detampel, Emre Cörek, Klara Kiene, Katharina Klados und Pascal Fluder. Danke euch für tolle Praktikumswochen, Tränen-Lacher, spannende Masterarbeiten und viele schöne Momente.

Danke auch an Susanne Schenk, Denise Ruoff, Christina Erb, Georg Schulz, Christos Bikis, Peter Thalmann, Bert Müller, Peter Wick, Pascal Zihlmann und die Mitarbeiter der European Synchrotron Radiation Facility. Ohne euch wäre diese Zeit auch nicht so reibungslos verlaufen.

Für die finanzielle Unterstützung danke ich dem Swiss Center for Applied Human Toxicology (SCAHT) herzlich.

An meine Familie und Freunde: Ich danke euch von Herzen für all die Unterstützung, die Aufmunterungen und die jederzeit geteilte Freude während dieser emotional nicht immer einfachen Reise.

Der grösste Dank geht an Bettina Rappo. Du warst jene Person, die alle Höhen und Tiefen ausnahmslos mit mir geteilt und durchgestanden hat. Du warst in jeder Situation mein Rückhalt. Ohne dich wäre vieles hiervon nicht möglich gewesen. Dafür werde ich dir immer dankbar sein.

Abbreviations

AB/TU	Wild type zebrafish strain AB/Tübingen
AFM	Atomic Force Microscopy
ASTM	American Society for Testing and Materials International
AuNP	Gold Nanoparticle(s)
AUC	Analytical Ultra-Centrifugation
BAG	Bundesamt für Gesundheit
BET	Nitrogen adsorption analysis
CLSM	Confocal laser scanning microscopy
cm	Centimeter(s)
CT	Computer Tomography
CTAB	hexadecyltrimethylammonium bromide
° C	degree(s) Celsius
DDS	Drug Delivery System
DLS	Dynamic Light Scattering
DoC	Duct of Cuvier
DPTG	di- and polymerized triacylglycerols
ECHA	Registration, Evaluation, Authorization, and Restriction of Chemicals
EGFP	Enhanced Green Fluorescent Protein
ELISA	Enzyme-Linked Immunosorbent Assay
ELS	Electrophoretic Light Scattering
EM	Electron microscopy
EMA	European Medicine Agency
ENM	Engineered Nanomaterial(s)
ENP	Engineered Nanoparticle(s)
EPA	United States Environmental Protection Agency
ESRF	European Synchrotron Radiation Facility
EU NCL	European Nanomedicine Characterization Laboratory
FDA	United States Food and Drug Administration
FITC	Fluorescein isothiocyanate
FT-IR	Fourier-Transform Infrared Spectroscopy
g	gram(s)
hpf	hours post fertilization
hpi	hours post injection
HTS	High-Throughput Screening
ICP-MS	Inductively Coupled Plasma Mass Spectrometry
ISO	International Organization of Standardization
JAK/STAT	Janus Kinase/Signal Transducer and Activator of Transcription
Kdrl:EGFP	fluorescent vasculature transgenic zebrafish line
LOAEL	Lowest Observed Adverse Effect Level
mg	milligram
MHC	Major Histocompatibility Complex
min	minute
ml	milliliter
mm	millimeter
mM	millimolar

mpeg1:Gal4;UAS:Kaede	fluorescent macrophage transgenic zebrafish line
MRI	Magnetic Resonance Imaging
MTT	3-(4,5-dimethylthiazol-2-yl)-2,5-diphenyltetrazolium bromide
mV	millivolt
µA	microampere
µCT	micro-computer tomography
µl	microliter
µm	micrometer
µg	microgram
ng	nanogram
nl	nanoliter
nm	nanometer
NMR	Nuclear Magnetic Resonance
NOAEL	No Observed Adverse Effect Level
NTA	Nanoparticle Tracking Analysis
OECD	Organization for Economic Co-operation and Development
PDI	Polydispersity index
PEG	Polyethylene glycol
PLGA	poly(lactide-*co*glycolide) copolymer
REACH	EU Regulation on Registration, Evaluation, Authorization of Chemicals
ROS	Reactive Oxygen Species
SAXS	Small Angle X-ray Spectroscopy
SCAHT	Swiss Center for Applied Human Toxicology
SEM	Scanning Electron Microscopy
SiNP	Silica Nanoparticle(s)
SPION	Superparamagnetic Iron Oxide Nanoparticle
SRµCT	Synchrotron Radiation Micro-Computer Tomography
TEM	Transmission Electron Microscopy
TEOS	Tetraethyl orthosilicate
Tg	transgenic
TRIS	2-Amino-2-hydroxmethyl-propane-1,3-diol
TRITC	Tetramethylrhodamine isothiocyanate
US NCL	United States Nanotechnology Characterization Laboratory
UV-vis	UV-visible Spectroscopy

Table of Figures

Zusammenfassung für Laien

Unter dem Begriff “Nano” versteht man im Volksmund die Bezeichnung von etwas verschwindend Kleinem, nicht wirklich Greifbarem, vielleicht sogar etwas Vernachlässigbarem. Der Begriff stammt vom altgriechischen Wort „*nanos*“ ab, was übersetzt Zwerg heisst. Die Mathematik definiert den Präfix „Nano“ als den milliardsten Teil einer Einheit. Folglich entspricht eine Milliarde Nanometer einem Meter. Tatsächlich kommen wir in unserem Alltag häufig unbewusst mit Materialien in Berührung, welche nur wenige Nanometer gross sind. Solche Nanomaterialien sind essentielle Bestandteile von Verpackungsmaterialien, Computern, Kosmetika, Textilien und pharmazeutischen Hilfsstoffen. 1957 hielt der spätere Nobelpreisträger Richard Feynman einen Vortrag über eine Vision. Er behauptete damals, dass die Medizin der Zukunft kleinste Maschinen und Roboter verwenden werde, um Krankheiten zu bekämpfen und Patienten zu heilen. Diese Maschinen würden kleiner sein als menschliche Zellen und könnten in definierter Zahl an den richtigen Ort gesteuert werden. Anfang der 1970er Jahre wurden Nanopartikel (sphärische Nanomaterialien) erstmals als potentiell erfolgsversprechende Anwendungen für die pharmazeutische und medizinale Forschung diskutiert. Sechzig Jahre nach Feynmans Vortrag ist seine Vision bis zu einem gewissen Grad Realität geworden. Heute gibt es mehr als 150 Anwendungen von Nanopartikeln in der Medizin. Sie sind oft sehr einfach herstellbar, dienen als Träger für empfindliche Wirkstoffe, werden als Kontrastmittel eingesetzt und sollen in der Krebstherapie als Wirkstoffe etabliert werden. Ihre Grösse bringt einen entscheidenden Vorteil gegenüber herkömmlichen Arzneiformen. Genau wie Feynman es beschrieben hatte, sind Nanopartikel klein genug**,** um zelluläre Barrieren zu überwinden. Zudem sind sie so potent, dass ihre Dosierung tiefer als jene von herkömmlichen Arzneistoffen gehalten werden kann. Ein weiterer Vorteil ist ihre enorme Partikeloberfläche, welche chemisch meist sehr einfach manipulierbar ist. Dadurch können Nanopartikel so verändert werden, dass sie zielgerichtet ihren Wirkort finden und gleichzeitig vor dem körpereigenen Immunsystem geschützt sind. All diese Aspekte machen die Nanomedizin zu einem der am schnellsten wachsenden Forschungszweigen des neuen Jahrtausends. Jedoch birgt der grösste Vorteil der Nanomedizin auch ein weitreichendes Risiko. Dank ihrer Grösse weisen Nanopartikel oft einzigartige Eigenschaften auf, welche denselben Materialien in grösserem Massstab fehlen. Zudem erhöht das Verhältnis von Grösse zu Oberfläche die

Reaktivität von Nanopartikeln um ein Vielfaches. Die Kombination dieser speziellen Eigenschaften verleiht Nanopartikeln das Gefahrenpotential, eine lange Bandbreite von ungewollten Nebenwirkungen auslösen zu können. Man weiss heute, dass nach dem Kontakt mit den meisten Zelltypen, Nanopartikel sehr einfach von diesen aufgenommen werden können. Diese Zellen bekunden danach jedoch oft Mühe den Abbau und das Ausstossen der Partikel zu regulieren. Das Unvermögen diese Fremdkörper wieder ausscheiden zu können, löst Stress in betroffenen Zellen aus. In vielen Fällen führt dies zu ungewollten Immunantworten wie etwa Hypersensibilität, Entzündungen oder Zelltod. Bewiesen wurde auch, dass einige Partikel nach Kontakt mit biologischen Flüssigkeiten anfangen Klumpen zu bilden. Setzen sich diese Klumpen im Körper dauerhaft fest, kann das ebenfalls erhebliche Konsequenzen für die Gesundheit nach sich ziehen. Gelangen solche Nanopartikel z.B. in die Blutbahn, sind Thrombosen und Embolien sehr realistische Spätfolgen. Um dies zu verhindern, setzen sich Regierungen, Behörden und Gesundheitsorganisationen in Zusammenarbeit mit Firmen und Universitäten seit Jahren verstärkt mit der Giftigkeit von Nanomaterialien auseinander (Nanotoxikologie). Durch ihre Einzigartigkeit wurde schnell klar, dass herkömmliche Sicherheitsmassnahmen und –vorschriften nicht ausreichen, um das toxische Potential von Nanomaterialien zu ergründen. Zahlreiche Ideen und Lösungsansätze für die Nanotoxikologie sind bis heute diskutiert worden und die Menge an erhobenen Daten wächst täglich. Jedoch sind sich Experten in mehreren Punkten noch immer uneinig. Angefangen bei geeigneten Dosierungen und Messmethoden bis hin zur Auslegung von experimentellen Daten ist noch kein Vorschlag von allen Beteiligten gleichermassen akzeptiert worden. Das Hauptproblem besteht darin, dass die Anwendungsvielfalt von Nanomaterialien zu gross ist, um eine einheitliche Regulierungs- und Sicherheitsstrategie aufstellen zu können. Der zurzeit vielversprechendste Ansatz ist, es Nanopartikel anhand ihrer Eigenschaften oder biologischen Interaktionen in Sicherheitsgruppen klassifizieren zu können. Die medizinale Anwendung von Nanopartikeln steckt noch immer in den Kinderschuhen, jedoch verhindert die Abwesenheit von klar strukturierten und anwendungsspezifischen Richtlinien den weiteren Aufschwung dieser Formulierungen.

Aus diesem Grund war es das Ziel dieser Dissertation, einen Lösungsansatz für die Sicherheitsevaluation von Nanomedizin-Formulierungen auszuarbeiten.

Als erstes wurden die Interaktionen und Reaktionen von Zellen auf unterschiedliche Nanopartikel analysiert und ausgewertet. Dabei lag der Fokus auf Nanopartikeln, deren Verwendung in der Pharmazie etabliert ist oder diskutiert wird. Anhand der erhobenen Daten konnten Verbindungen zwischen zellulären Reaktionen und bestimmten physikalisch-chemischen Eigenschaften von Partikeln bewiesen werden. Ebenso wurden unterschiedliche Reaktionen in verschiedenen Zelltypen beobachtet. Es konnte daraufhin festgestellt werden, dass das toxische Potential von Nanopartikeln abhängig ist von:

- der chemischen Zusammensetzung der Formulierung,
- den spezifischen physikalisch-chemischen Eigenschaften der Formulierung,
- und der biologischen Umgebung der Formulierung.

Um diese Beobachtungen im lebenden Tier zu überprüfen, wurden Nanopartikel mittels Injektion in die Blutbahnen von Zebrafischembryonen gespritzt. Embryonen des Zebrafisches sind durchsichtig und weisen ein ähnliches Immunsystem zum Menschen auf, was die Interpretation der Resultate vereinfachen kann. Zudem wird die Mehrheit aller heutigen Nano-Pharmazeutika via Injektion appliziert. Die embryonale Partikelverteilung und die Gesundheit des Tiers wurden anhand unterschiedlicher Methoden im Verlauf mehrerer Tage studiert und analysiert. Die Resultate erbrachten den Beweis, dass Nanopartikel bestimmte Voraussetzungen erfüllen müssen, um auch im Tier keine toxischen Ereignisse hervorrufen zu können. Unter der Berücksichtigung behördlicher Richtlinien, validierten Methoden und standardisierten Protokollen wurde schliesslich ein Entwurf zur ersten Strategie der Sicherheitsevaluation von medizinischen Nanopartikeln ausformuliert. Die Strategie besteht aus drei individuellen Testsystemen. Im ersten System werden die relevantesten physikalisch-chemischen Eigenschaften von Nanopartikeln für die medizinische Anwendung bestimmt und analysiert. Danach wird deren Verträglichkeit in einem neuartigen Gruppierungsverfahren getestet und evaluiert. Zum Schluss bietet die Strategie eine Sicherheitsprüfung individuell abgestimmt auf jede Gruppe. Diese anwendungsspezifische Strategie vereint bestehende Richtlinien mit neuartigen Testansätzen und ermöglicht so eine unkomplizierte, sachgerechte Entscheidungsfindung.

Summary

In 1959, physicist and Nobel laureate-to-be Richard Feynman held his famous speech “There’s Plenty of Room at the Bottom”. Herein he prophesized the upcoming of a new research field dedicated entirely to the nanometer scale. Six decades later we find ourselves amid the vision of Feynman where nanomaterials are omnipresent in daily life. Especially engineered nanoparticles (ENP) have gained enormous interest in medicine showing promising potentials as novel drug carrier systems, drug entities, and contrast agents. However, due to their size and physico-chemical properties, ENP inherit a unique toxicological profile that remains poorly understood. Moreover, the lack of generally accepted guidelines designed specifically for ENP prevents their proper safety regulation and risk assessment.

In collaboration with the Swiss Center for Applied Human Toxicology (SCAHT) and the Horizion2020 NanoReg2 consortium, we focused our research on establishing ENP-specific characterization strategies and assay toolboxes that should provide robust information on the safety of ENP-organism interactions.

Our results have shown that ENP toxicity is mediated by the chemical identity of a particle along with specific physico-chemical properties but also depends on the surrounding biological system. *In vitro*, *in vivo*, and *in situ* analyses ranging from simple viability studies to complex signaling pathway analysis have helped to link adverse effects and immune responses to different ENP types or specific properties thereof. Furthermore, we established the first protocol for the 3D-visualization of non-labeled ENP *in vivo* by synchrotron-radiation phase contrast x-ray micro-computer-tomography in therapeutically relevant dose-ranges. This novel method will aid to better understand the behavior of ENP after intravenous injection and may serve as a novel platform for the monitoring of ENP biodistribution and targeting.

Conclusively, the combined results obtained during this thesis have led to the proposal of a novel safety assessment strategy which specifically targets ENPs designed for therapeutic use. This proposal highlights the importance and the benefits of application-specific decision-making with a strong emphasis on physico-chemical characterization and *in vitro* hazard assessment. This strategy is meant to contribute to the ongoing establishment of much needed nano-specific safety guidelines and was developed to be in line with the interests of regulatory authorities and researchers alike.

Introduction

Engineered nanomaterials

The term “nano” is derived from the ancient Greek “*nānos” (νᾶνος)* that translates to the word dwarf. In the metric system, the prefix nano denotes the billionth part of a unit. Nanomaterials are entities displaying physical dimensions in the nanometer range (10^{-9} m – 10^{-8} m). The prevailing definition of a nanomaterial was set by the International Organization of Standardization (ISO)[1], the Organization for Economic Co-operation and Development (OECD)[2,3], and the American Society for Testing and Materials International (ASTM)[4]. According to this definition, the term nanomaterial encompasses all materials with at least one external (height, length, or width) or internal (e.g. pores) dimension in the range of approximately 1 – 100 nm. This size range is referred to as the nanoscale[1]. Since numerous materials naturally occur in the nanoscale and can also be referred to as nanomaterials, the term “engineered nanomaterial” (ENM) is used for man-made nanomaterials only. ENM are omnipresent in everyday life as regular components of consumable and durable goods. Developed on an industrial scale, they are used in e.g. printing cartridges[5], cosmetics[6], toiletries[7,8], food packaging[9], water purification[10], and most recently medical applications[11,12]. Their versatile use is based on physico-chemical benefits resulting from their size and shape. Being submicron entities, nanomaterials often display unique characteristics and properties that their larger sized counterparts completely lack[13–15].

Correct terminology of different nanomaterial subgroups

Nano-objects represent a form of nanomaterials and are commonly subdivided into nanoplatelets, nanorods or -tubes, and nanoparticles[1]. Often falsely referred to as being synonyms, these terms describe different nanomaterials according to the number of external dimensions in the nanoscale (**Figure I**). The term nano-object is the synonym all nanomaterials that bare at least one external dimension in the nanoscale. The subgroups of nanoplatelets, nanorods or -tubes, and nanoparticles are all nano-objects but feature specifically one, two, or three external dimensions in the nanoscale, respectively. Especially the ENM subcategory of engineered nanoparticles (ENP) have had vast impact on nanomedical research[16]. Today, the majority of approved medical nano-applications are ENP-based. The first intentional synthesis of nanoparticle was successfully conducted in 1875[17]. Michael Faraday chemically

reduced gold chloride, which led to the production of colloidal gold. However, the perception that it is a novelty to use ENP for medical purposes is not entirely correct.

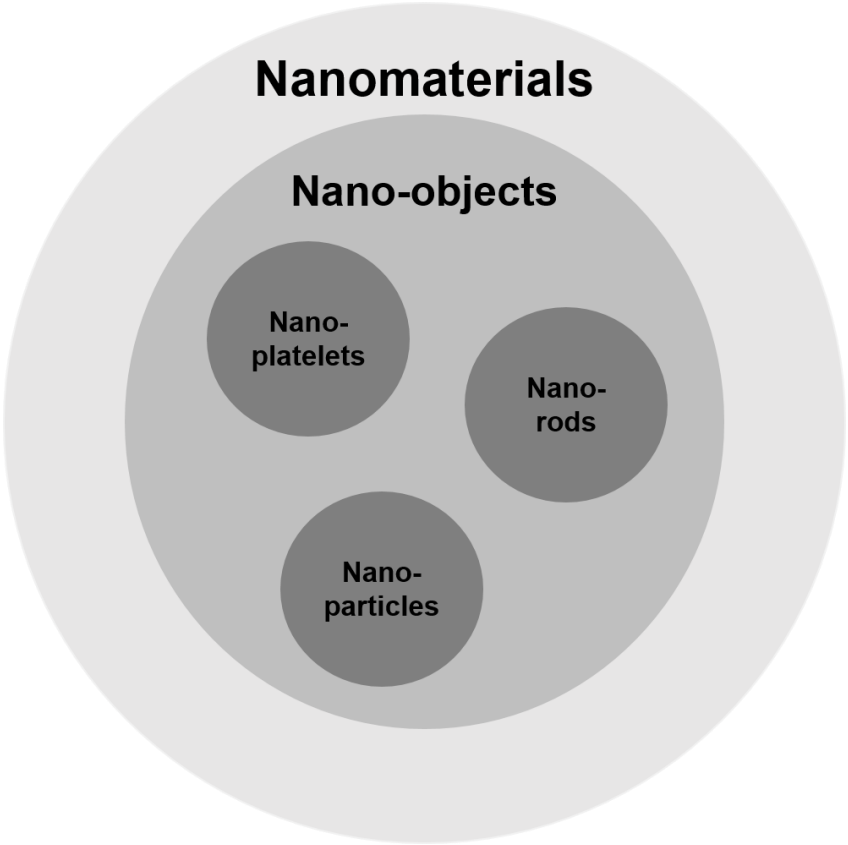

Figure I – Subgrouping of the different nanomaterials. *Nanomaterials are divided by the amount of displayed external and internal dimensions in the nanoscale. Nanomaterials encompass all materials that feature at least one internal or external dimension in the required size range of 1 – 100 nm. Nano-objects require at least one external dimension in the nanoscale. Distinct numbers of external dimensions at the nanoscale define the subgroups nanoplatelets (exactly one external dimension), nanorods or -tubes (exactly two external dimensions), and nanoparticles (all three external dimensions). Figure adapted from Kettiger[18].*

From the ancient to the present – History of nanoparticles in health care

Unknowingly, nanoparticles have been used in medicine and health care for several thousand years in form of colloidal gold or silver. **Figure II** highlights some of the historical milestones important for the nanomedicine of today. Historical transmissions dating back to the fifth century BC have indicated that the ancient Chinese and Indian cultures made medical use of colloidal gold[19]. In the same century, Hippocrates of Greece describes the benefit of silver dust in wound care and healing.[20] First indications of colloidal gold synthesis were found in transcriptions of the “Quinta essential auri” written by Paracelsus[19]. He described the formulation of “potable gold”[21] by adding gold chloride and vegetable extracts to oil or alcohols changing the solutions

color to a distinct red. Potable gold was used for the treatment of multiple conditions throughout the Middle Ages, including syphilis, diarrhea, or epilepsies.

Despite all the historical transmissions, it was not until 1900 that sub-visible particles were scientifically discussed to have medical relevance. According to the theory of the "magic bullet" by chemotherapy-pioneer Paul Ehrlich it should be possible to specifically neutralize specific pathogens without having to harm the pathogen host organism itself[22]. To do so, one would require the smallest of particles. At that time, colloidal silver was frequently used in wound healing and as an antimicrobial. With the discovery of the liposome in 1964[23] and the first in vivo studies conducted in 1971[24], research on medical ENP applications has gradually gained the attention of the global research community. In 1995 Liposomal doxorubicin (Doxil®/Caelyx™)[25–27] was the first medical nanoparticle to be approved by the United States Food and Drug Administration (FDA). Today, ENP are gaining evermore importance in life science and medical research sectors due to their potential use as drug carriers, imaging agents, and theranostics (a formulation that combines therapeutic and diagnostic properties). The nanomedicine research field currently has an estimated world market value of approximately 140 billion US dollars and regulatory approvals of medical nano-formulations are increasing on a yearly basis[28].

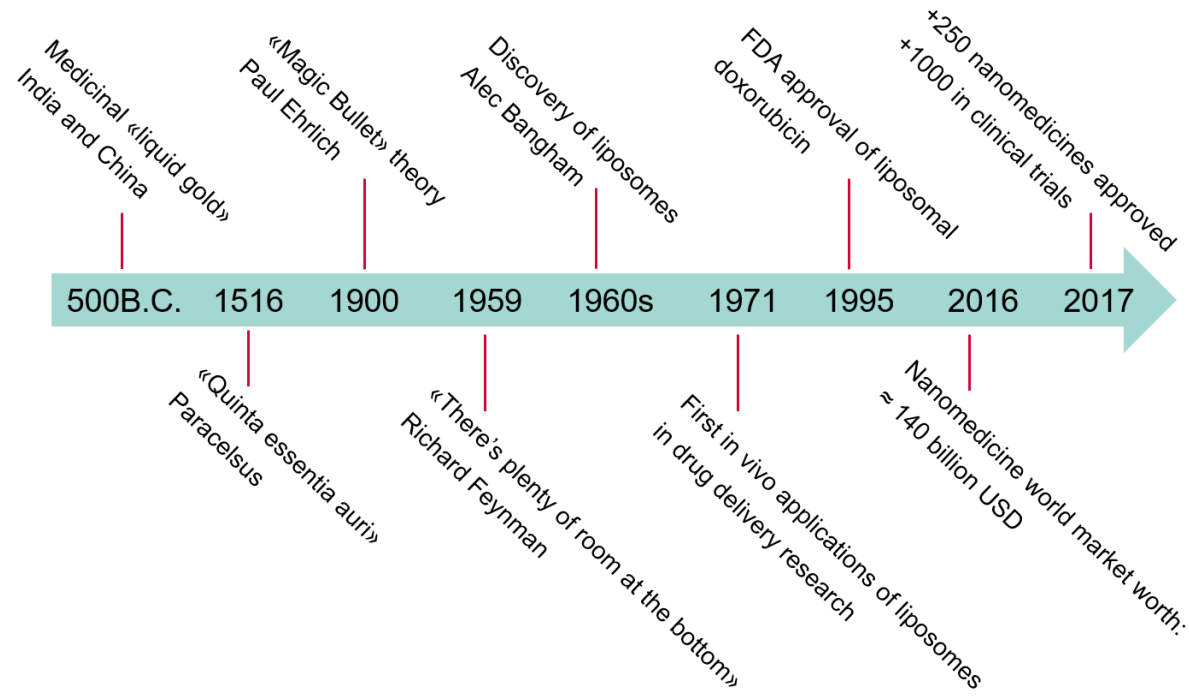

Figure II – Nanomedicine through the ages. *Engineered nanoparticles (ENP) have been used for millennia by various cultures for medical purposes. The term nanomedicine however did not emerge until recently.*

Benefits of engineered nanoparticles in medicine

As previously mentioned, ENP are the most used nanomaterials in nanomedicine. Organic nanoparticles (e.g. liposomes, polymersomes, dendrimers and drug-polymer conjugates) are mostly used to enhance formulation solubility[29] and are used as drug delivery systems (DDS)[30]. Inorganic nanoparticles such as gold and iron oxide nanoparticles find use as diagnostics or theranostic tools[31,32]. A plethora of other materials including silica[33,34], cerium[35], and silver[36] are also studied as promising alternatives for drug delivery, diagnostics, and theranostics.

Drug delivery systems (DDS)

Since the approval of Doxil®/Caelyx™ the most important and promising application of ENP is seen in their use as stability enhancers and novel DDS. With several products in clinical use nanoparticle-based DDS have proven to feature many advantageous characteristics[16,30]. Due to their unique physico-chemical properties, ENP can prolong the half-life of drugs in circulation by masking them from the immune system of the host. Additionally, this provides the advantage of causing minimal side effects thereby enhancing the safety of otherwise toxic formulations. Moreover, modifying the surface of an ENP chemically can lead to effective drug targeting or the promotion of controlled drug release. To date there are over 30 approved DDS based on ENP[16], most of them being organic (lipid[37] or polymer[38] based). However, inorganic ENP based on silica[39] or gold[40] for instance are attracting evermore attention in research[41].

Diagnostics

ENP have been reported to be utilized as tracers and contrast agents for several techniques (e.g. x-ray based[42], photoacoustics[43], fluorescence[44], MRI[45]). The most successful diagnostic applications however have been contrast agents consisting of heavy atom nanoparticles (e.g. gold and iron oxide ENP). Due to their high physical and electron density, these ENP provide high imaging contrast. Combined with the benefit of longer blood half-life than commonly used contrast agents (e.g. iodine[46]), lower dose administrations are enabled[43]. This in turn minimizes exposure and potential toxic effects triggered by ENP. Superparamagnetic iron oxide nanoparticles (SPIONs) coated with dextran or carboxydextran for example are used as liver tumor specific contrast agents for magnetic resonance imaging (MRI)[45]. More recently novel formulations of coated SPIONs are investigated for alternative targets and computer-

tomography techniques[47]. Gold (AuNP) are also frequently used or investigated as novel contrast agents for computer tomography (CT)[48,49] and MRI[50]. More exotic examples of nanoparticles discussed for diagnostics are gadolinium[51], platinum[52], tantalum[53], and ytterbium[54].

Theranostics

The goal of a theranostic treatment is combining therapeutic and diagnostic properties in a single formulation[55]. Theranostics should help to enable the use of the correct therapy for a distinct patient at the most beneficial time. Since it was discovered that ENP have the potential to be used as tracers but also display therapeutic effects, proposals of theranostic ENP have been constantly surfacing. The development of such multifunctional nanoparticles would allow immediate tracking of the therapeutic effect[56–58]. Certain approved SPION formulations show these theranostic characteristics[59,60]. These SPIONs can be traced throughout an organism by CT techniques and are triggered with magnetic impulses to induce hyperthermia in target tumor tissues.

Nanotoxicology

Nanotoxicology has been defined as *"[…] the study of the adverse effects of engineered nanomaterials (ENMs) on living organisms and the ecosystems, including the prevention and amelioration of such adverse effects. […]"*[61]. Their size, unique physico-chemical properties do not only account for a vast amount of beneficial properties. The same characteristics are also responsible for ENM to possess complex toxicological profiles. The fact that ENM may pose hazardous threats towards human health has been discussed continuously over the past decades. Monitoring the adverse effects of ENP *in vitro* and *in vivo* has brought forward an enormous amount of nanotoxicological data leading to a more profound understanding of ENP driven toxic effects. Today it is known that ENP-tissue interactions are dependent on incubation time and ENP dose. However, the toxicity of an ENP is driven by the chemical identity of the particle, the physico-chemical properties that ENP features, and the biological system a nanoparticle is exposed to[18].

As ENP enter an organism (e.g. via inhalation, ingestion, or injection) they will interact with their surroundings immediately. Nanoparticles are readily taken up by a large amount of different human cell types. The uptake mechanism predominantly endocytosis. The exact uptake route (pinocytosis or phagocytosis) is highly dependent

on the chemical identity of the particle, its physico-chemical properties, as well as the cell type[62,63]. Once inside a cell, nanoparticles can interact with organelles, enter the nucleus, change the pH of the cytosol, cause the generation of reactive oxygen species, activate signaling cascades, or disrupt the functionality of organelles and tubuli. These actions can cause a string of adverse outcomes on cellular level such as apoptosis, necrosis, and inflammation leading to either acute or chronic damage of the organism. However, due to a prevailing lack of specific ENM regulations and guidelines information on the underlying mechanisms triggering and maintaining ENM toxicity are scarce.

Shortcomings in nanosafety evaluations

Safety evaluation of ENM has been among the most intensely and controversially discussed topics linked to nanotechnology in the past two decades[64–70]. Classical toxicology and risk assessment approaches have been designed to regulate small molecules and bulk chemicals by authorities such as the European Chemicals Agency (ECHA), the United States Environmental Protection Agency (EPA), the European Medicine Agency (EMA), and the FDA. However, the inclusion of nanomaterials into these established approaches was never intended[71]. It is generally accepted that commonly used regulatory approaches do not meet the necessary requirements to assess the safety of ENM[72]. Due to these circumstances, no generally approved guidelines exist to specifically determine the safety of nanomedicines up to date[73]. Consequently, researchers from academia and industry have been collaborating with authorities to formulate strategies for nanosafety evaluations over recent years[61,74–76]. Despite these efforts several key topics remain controversial due to the interdisciplinary use of ENM. The countless discussions on general definitions, correct dosimetry, standardized measurement techniques, and ideal biological test systems have made it clear that regulating all ENM in the same manner is not possible. Instead it is the conception that regulatory guidelines on the evaluation of nanosafety should be tailored to fit the individual scopes of ENM.

Grouping

At present, a popular proposal to regulate nanosafety in an application specific manner is based on grouping strategies. By collecting the relevant experimental data, ENM can be grouped into defined classes or groups facilitating further regulatory decision-

making. Particularly in occupational safety and healthcare this strategy has found wide appreciation.

Grouping strategies are mainly based on criteria that are known to be related to the toxic profile of an ENM. Physico-chemical properties, exposure, or cellular effects are the most frequently used criteria for nanosafety evaluations. Designing grouping strategies that are tailored to fit specific ENM exposure scenarios can further improve risk assessment and the regulation of nanosafety. However, nanomedicine specific grouping strategies and risk assessment approaches have not been proposed so far. Consequently, grouping strategies with a focus on ENP administration via injection have also been widely neglected.

Nanoparticles used throughout this thesis

Various types of ENP were used throughout present thesis (**Figure III**). Choice of ENP was driven by the decision to work exclusively with nanoparticles that are currently used as approved nanomedical formulations or regularly discussed in nanomedical research. Due to the focus on nanotoxicology and nanosafety, a greater variety of inorganic ENP were studied than their organic counterparts which are proclaimed to be less toxic. Silica, gold and PLGA nanoparticles were all synthesized in-house. Iron oxide nanoparticles were synthesized and provided by collaborators.

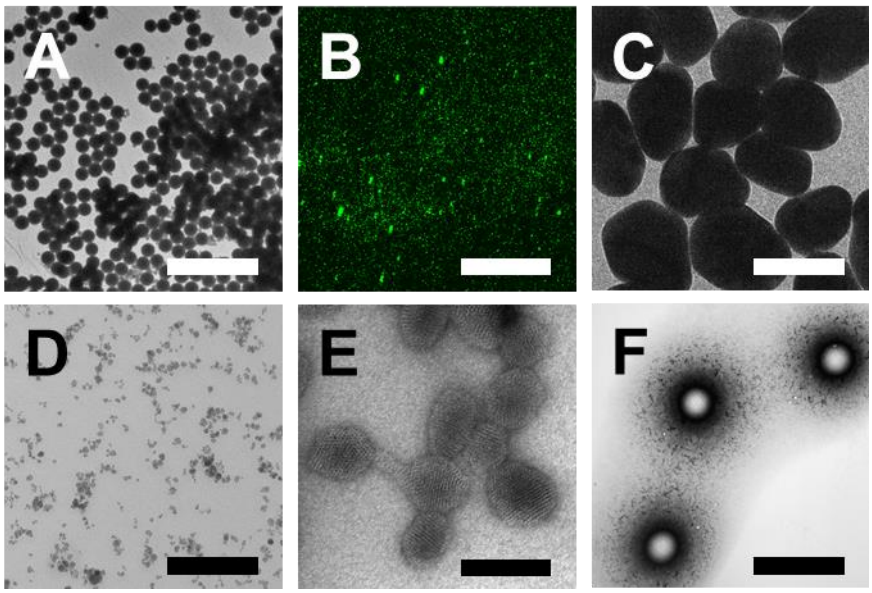

Figure III – Nanoparticles used throughout the thesis. *This figure shows transmission electron (TEM) micrographs (panels A, C D, E, F) and confocal laser scanning microscopy (CLSM) images (panel B) of all ENP discussed and studied in this thesis. The different panels show silica nanoparticles (panel A), fluorescent silica nanoparticles (B), gold nanoparticles (panel C), superparamagnetic iron oxide particles (panel D), mesoporous silica nanoparticles (panel E), and PLGA nanoparticles (panel F). Scale bars: panel A: 800nm, panel B: 2000nm, panel C: 25 nm, panel D: 300 nm, panel E: 200nm, panel F: 400 nm.*

Silica nanoparticles (SiNP, MSN)

Specific types of silica nanoparticles (Aerosil®) are extensively used as anti-caking agents enhancing the flowability in various pharmaceutical formulations (e.g. tablets and syrups). In recent years nonporous SiNP[34,39,77] and mesoporous SiNP (MSN)[78–80] have been continuously discussed as novel DDS and imaging probes. Nevertheless, their use should be carefully monitored as SiNP and MSN can cause a plethora of cytotoxic effects[62,81–85]. In contrast to other oxide nanoparticles however, the degradation (silicic acids) products of SiNP and MSN are regarded to be nontoxic[86].

SiNP were synthesized in a accordance to the Stöber method established in 1968[87]. This sol-gel reaction has become the standard procedure for the synthesis of nonporous, spherical, and uniformly sized SiNP, otherwise referred to as Stöber nanoparticles. By adding ammonia to a mixture of specific amounts of a alkoxysilane (typically tetraethyl orthosilicate (TEOS)), water, hydrolysis of the silane to silanol is triggered. The silanol monomers then condensate to form siloxane bonds from which eventually the SiNP start to grow based on the phenomenon named Ostwald ripening[88]. Different fluorescent labels (e.g. fluorescein isothiocyanate (FITC) and tetramethylrhodamine isothiocyanate (TRITC)) can also be introduced during the Stöber method by following the chemical procedure Branda et al.[89] have described.

MSN were synthesized according to the synthesis of Porta et al.[90]. Here, porosity was achieved by using the soft template surfactant hexadecyltrimethylammonium bromide (CTAB) as structural basis. The surfactant was removed after nanoparticle formation by acidic refluxing, which yielded the porous structure of the MSN.

Gold nanoparticles (AuNP)

Colloidal gold has been used for millennia in the treatment of physical and mental complaints. Today AuNP are mainly approved as diagnostic tools. They are used as contrast agents for x-ray and magnetism based radiology techniques such as CT and MRI[91,92]. Future applications also see AuNP introduced as theranostic tools[93] or drug carriers[40]. Gold nanoparticles are often regarded as inert, stable, and relatively safe ENP[94]. However caution must be taken as these particles are only slowly excreted and by these means can cause adverse outcomes due to biological persistence and agglomeration[94,95].

At present, two procedures are used more frequently than any other to synthesize AuNP. Both the Brust synthesis[96] and the Turkevich synthesis[97] rely on redox

chemistry to obtain colloidal gold. In both procedures Au^{3+} is reduced to elemental Au^0, but the reduction process is different. The AuNP used in this thesis were synthesized according to Turkevich due to the advantage of not having to use capping agents to prevent particle aggregation[98]. After dispersing tetrachloroaurate in water, Au^{3+} is reduced in the aqueous phase by adding trisodium citrate to the boiling dispersion. Additionally, the citrate in solution acts as the capping agent, largely preventing aggregation of the AuNP.

Superparamagnetic iron oxide nanoparticles (SPIONs)

The applications and benefits of SPIONs in nanomedicine have been highlighted earlier in present work. SPIONs are similarly used as gold nanoparticles and have become increasingly important for nanomedical applications due to their unique magnetic properties[59,60,99]. Toxicity-wise however SPIONs bare a higher risk than gold nanoparticles. Used for hyperthermia treatment of tumors[59], these ENP can cause a string of adverse effects leading to cytotoxicity[100–102]. Moreover, SPIONs are only stable in an aqueous surrounding if they are coated or their surface is altered[103,104]. Should this coating be stripped off or degrade before excretion the iron oxide core will disintegrate[105], releasing potentially harmful iron ions[106].

The SPIONs used throughout this thesis were synthesized under GMP conditions at the University of Erlangen by collaborators from the research group of Prof. Christoph Alexiou who are leading experts in the research on the applicability of SPIONs as nanomedicines[107].

Poly(lactide-coglycolide) (PLGA) nanoparticles

Poly(lactide-*co*glycolide) (PLGA) nanoparticles are organic ENP that have attracted considerable attention in the nanomedicine field. Due to the biocompatibility and biodegradability, FDA and EMA have approved the use of PLGA-based formulations for drug delivery[16,108]. Further benefits of PLGA nanoparticles are protection from degradation, enabling of sustained release, and straightforward surface modification[108,109]. In nanotoxicology and nanosafety studies they can be occasionally used as negative controls for the occurrence of toxic events and adverse effects.

Synthesis of poly(lactide-*co*glycolide) PLGA nanoparticles is generally achieved by mixing solutions of PLGA and di- and polymerized triacylglycerols (DPTG) to an emulsion with subsequent removal of the organic solvent[110].

The PLGA nanoparticles used throughout this thesis were additionally coated with alternating layers of polyelectrolytes covering a layer of immobilized enzymes (acid phosphatase or β-galactosidase)[111]. PLGA is an FDA approved biodegradable polymer of the aliphatic polyester family frequently used in drug delivery systems[109]. Originally used for the proof of concept of a new and improved crosslinked layer-by-layer (cLbL) concept, these ENP were also the subject of in vitro and in vivo nanosafety trials[111].

Physico-chemical characterization

In comparison to the characterization of small molecules – consisting mainly of chemical identity and purity determination – ENP require a far more demanding characterization process[112].

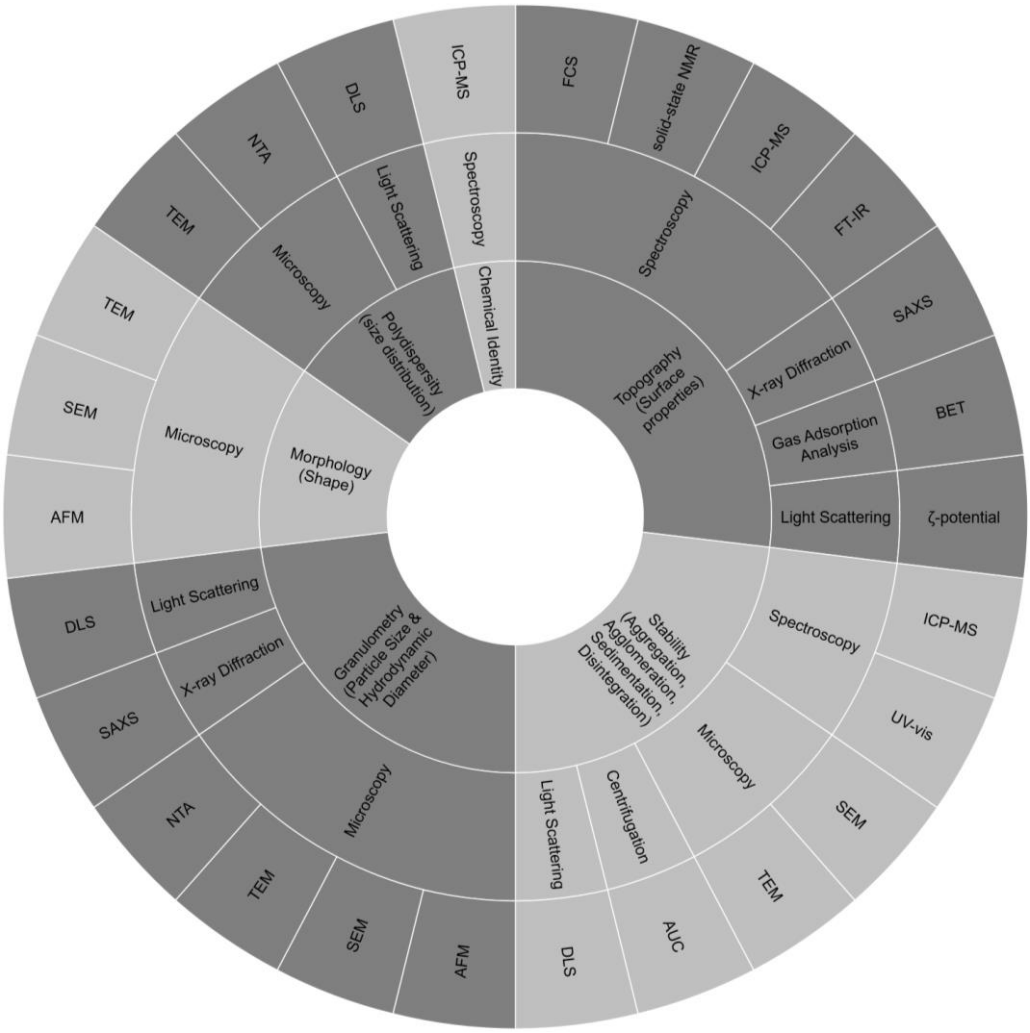

Figure IV – Possibilities of ENP physico-chemical characterization. *This diagram highlights the six most important physico-chemical parameters that can be measured for any ENP (chemical identity, granulometry, morphology, polydispersity, topography, and stability). Furthermore, the most frequently used measuring methodologies (microscopy, spectroscopy, light scattering, x-ray diffraction, centrifugation, gas adsorption analysis) and their respective techniques were listed to emphasize that there are multiple possibilities to characterize ENP.*

Arguably the most crucial part of nanosafety; profound physico-chemical characterization of ENP is therefore mandatory prior to the performance of toxicological studies[3,113]. Physico-chemical characterization should also be performed with purchased ENP to evade incorrect evaluation of characterization dependent data. Chemical identity (chemical composition), granulometry (particle size), morphology (shape), polydispersity (size distribution), topography (surface properties), and stability (aggregation, agglomeration, sedimentation, disintegration) are regarded as the six most important physico-chemical characteristics of any ENP as they all clearly define the toxic potential a nano-formulation (**Figure IV**). These parameters should be provided in any study discussing effects of ENP on biological systems. However, certain properties may add to this short list depending on the inspected ENP and the intended goal of the study (e.g. magnetism[114], purity[115]).

Chemical Identity

The chemical identity or chemical composition lays the basis to the palette of physico-chemical properties an ENP can inherit. Determining the chemical identity of an ENP is most frequently done with inductively coupled plasma mass spectroscopy (ICP-MS[116]). Despite being used frequently; this technique is not suitable for all types of ENP.

Granulometry (particle size and hydrodynamic diameter)

Size is the most important property of an ENP as the shear definition of a nanoparticle is dependent on the nanoscale. Moreover, size also defines the prominence of certain physico-chemical properties. A wide range of techniques are available to measure the granulometry of an ENP in the dry (particle size) or dispersive state (hydrodynamic diameter) all bearing their own benefits and limitations. Depending on the aim of further downstream experiments, one of the two parameters is more relevant than the other.

Microscopy techniques such as transmission electron microscopy (TEM[117]), scanning electron microscopy (SEM[118]), and atomic force microscopy (AFM[119]) are most frequently used to determine the particle size of an ENP. These techniques allow the visualization of single particles at high resolutions. However, due to the size of a micrograph and the need of relatively high particle numbers for statistical analysis, these techniques are usually time consuming. In recent years small angle x-ray scattering (SAXS[120]) has been promoted as an alternative method for particle size

measurements as well. It provides similar particle size results as TEM in less time, however SAXS does not render micrographs of the samples.

There is a significant difference between ENP size in dry versus dispersive state. In the dry state, the actual particle size can be measured. In the dispersive state, a layer of bulk liquid surrounding the ENP is considered during the measurement procedure as well. This is due to the light scattering based measurement technique and Brownian motion of the ENP in dispersion. This size is commonly referred to as the hydrodynamic diameter. To determine the hydrodynamic diameter of ENP the gold standard method is dynamic light scattering (DLS[121]). It provides statistically significant data fast, yet DLS is not as accurate as TEM. A rather novel technique is nanoparticle tracking analysis (NTA[122]) for dispersed ENP. NTA is basically a combination of DLS and microscopy.

Polydispersity (size distribution)

Polydispersity is practically always measured simultaneously to granulometry. The polydispersity index (PDI) is a dimensionless value between zero and one[123], that indicates how narrowly ENP size is distributed within one batch. High size distributions (> 0.2) indicate multiple ENP size populations in the sample, low values (< 0.2) of size distribution suggest the presence of only one size population. This is referred to as a monodisperse formulation and is often the aim in ENP syntheses. The standard measuring techniques are DLS[124], NTA[122], and TEM[125]. Drawbacks for TEM are the same as described for size measurements. The main shortcoming of DLS and NTA lies in the intensity-weighted analysis. Due to the dependence of scattered light, larger particles cause stronger signals which distort the size distribution results by a factor of 10^6 as compared to number distributions[121].

Morphology (Shape)

The morphology of ENP greatly influences their potential of exerting mechanical damage or being recognized by the immune system of an organism. Shapes with distinct edges are more likely to cause adverse effects than spherical formulations. Due to its definition, an ENP is shaped spherically or elliptic in most cases. The morphology of ENP can also be simultaneously measured to its size using microscopy techniques (TEM, SEM, AFM).

Topography (Surface)

Topography measurements bare information on the most exposed part of an ENP. The surface of an ENP is prone to encounter biological matter and therefore has a direct effect on the immediate surroundings. Parameters such as surface area, surface charge (zeta potential), and surface modifications (e.g. porosity) all influence tissue-ENP interactions.

The measurement techniques of choice for surface area and zeta potential are gas adsorption analysis (BET)[126] and electrophoretic light scattering (ELS[121]), respectively. BET analysis is based on measuring the amount of nitrogen desorption upon vaporization. Porosity and surface area can thus be calculated. ELS is based on the same technique electrophoresis and depends on the electrophoretic mobility of an ENP. The migration of ENP from one charged electrode to the oppositely charged one yields information on the surface charge of a nanoparticle. After ENP dispersion, ions from the solvent interact with the particle covering its surface entirely (Stern layer). During ENP movement the stern layer and a second ion layer (slipping plane) move with the ENP. The charge measured at the boarder of the slipping plane is the zeta potential. The zeta potential mainly serves as an indicator of ENP stability. A commonly used rule of thumb states that zeta potentials < -30 mV or > +30 mV indicate stability of an ENP in dispersion. It should be noted that the pH and the ion strength of a dissolution greatly influence the zeta potential. Without an indication of the pH value or the buffer used, zeta potential measurements are meaningless.

Furthermore, ENP surfaces can be altered with countless modifications (tracers, targeting molecules, coatings). There are numerous techniques to verify and inspect these modifications. The most common techniques are fluorescence correlation microscopy (FCS)[127,128], solid – state nuclear magnetic resonance (NMR)[18], ICP-MS[116], and Fourier-transform infrared spectroscopy (FT-IR)[129]. It should be noted that each of these techniques can only be used for specific ENP types or surface alterations. They cannot be chosen at will (in most of the cases).

Stability (Aggregation, Agglomeration, Sedimentation, Disintegration)

As medical ENP occur foremost in a dispersive state, colloidal stability is a key parameter to be determined. Stability of an ENP provides a decent shelf-live, minimizes undesired immune responses, facilitates circulation, and enhances bioavailability. Aggregation, agglomeration, or disintegration are often results of

coating abrasion due to the momentary environment of the ENP. This can lead to the triggering of adverse effects, sedimentation, mechanical tissue damage, immune reactions, and ENP elimination. Formulations such as SiNP, SPIONs, silver or copper nanoparticles all tend to aggregate or disintegrate over time in biological fluids. Monitoring these processes helps to determine the safety of a given ENP in solution. Furthermore, suitable optimizations can be chosen according to the behavior of the nanoparticle to minimize potential toxic effects.

Stability testing is often done by using DLS however there are several alternative methods such as ICP-MS, SEM, TEM, UV-vis spectroscopy, and analytical ultra-centrifugation (AUC)[130].

The controversy of the biocorona

Despite the importance that physico-chemical properties have on the toxic potentials of ENP, these properties can be dramatically altered as soon as ENP come in contact with biological fluids[131–133]. This alteration is commonly referred to as the biocorona[134,135]. It is supposed to be unique for every type of ENP and is often mentioned as a novel target to enhance the efficacy and safety of nanomedicines[24,136]. As biomolecules continuously adsorb to the surface of an ENP they eventually cover it entirely, masking its original synthetic surface. Consequently, ENP-tissue interactions are then driven by the amount and identity of adsorbed proteins and lipids forming the biocorona. However, the actual influence of the biocorona on toxicity is controversially discussed. The uncertainty of whether this biological coating is a dynamic or stable system has provoked more questions than brought forth answers concerning nanosafety. Amongst many more, Savolainen et al. have therefore proposed regular and careful characterization of the biocorona to further elucidate its impact on ENP behavior[76]. Even though multiple research groups have dedicated their work solely to the biocorona, at present there is no measuring technique that can determine the composition of the biocorona with significant accuracy. Thus, it is important to note, that the presence of the biocorona is widely accepted. Moreover, the determination of distinct parameters (particle size, zeta potential and stability) of ENP in biological fluids can indeed yield advantageous information on their behavior in *in vitro* and *in vivo* studies. However, if the biocorona cannot be accurately characterized, its impact remains hard to interpret during the evaluation of nanotoxicological results. Nevertheless, its presence can be appreciated by stating the following:

The unique physico-chemical characteristics of an ENP define the composition of its own biocorona. These characteristics therefore indirectly drive the influence of the biocorona on the behavior of the ENP. Thus, explicit correlations of the behavior and possible adverse effects of an ENP to its physico-chemical characteristics are correct, keeping in mind that these characteristics are directly responsible for the effects of the biocorona.

Nanotoxicological studies

The first documented nanotoxicological study was performed in 1971[24]. It consisted of an investigation of the behavior and effects that liposomal formulations have *in vivo*. Thereupon the authors could declare that the examined formulation did not show any signs of adverse effects and could therefore be regarded as safe.

Contemporary nanotoxicological studies mostly follow a three-tiered procedure. After physico-chemical characterization (Tier 1) cellular or animal model systems are exposed to ENP whereby crucial information on ENP-tissue interactions is retrieved (Tier 2). After completion of the data retrieval processes, the obtained results are analyzed and evaluated (Tier 3). Variations in ENP doses, exposure times and biological test system lead to a more sophisticated insight into the behavior of the ENP and its resulting impact on the surrounding tissues. Such insights may allow the correlation of observed adverse effects to specific physico-chemical properties of the tested ENP. By indicating that certain ENP properties trigger tissue interactions or adverse reactions, an initial estimate on the toxic potential of an ENP can be made. Elucidating the toxic potential of an ENP is the ultimate goal of any nanotoxicological study. The common starting point of investigating the toxicity of an ENP is determining its cytotoxicity in appropriate *in vitro* systems. The toxic potential of an ENP is not only unique because of its physico-chemical properties or chemical identity, its impact also depends greatly on the exposed biological system. In this sense, appropriate *in vitro* systems are cell-based systems that try to simulate the most probable surrounding of a nanoparticle in an *in vivo* situation.

Throughout this thesis the focus is set on ENP designed for therapeutic applications. The most popular administration route for nanomedicines is injection. After injection, nanomedical formulations are required to circulate throughout the vasculature and exit the bloodstream to reach its intended target within an organism without provoking immune reactions. Thus, the cell types which are primarily exposed to ENP encounters

and interactions during are blood cells (e.g. erythrocytes, leukocytes, platelets) and the cells lining the inner surface of the vasculature (endothelial cells). Nanotoxicological studies conducted in the scope of this thesis were mainly restricted to two different endothelial cell types: human blood-brain barrier cells (hCMEC/D3) and primary human umbilical vein endothelial cells (HUVEC). Macrophages are known to take up ENP via phagocytosis. These interactions have been extensively discussed in a comparative study with erythrocytes and non-phagocytotic cells by Kettiger et al.[81]

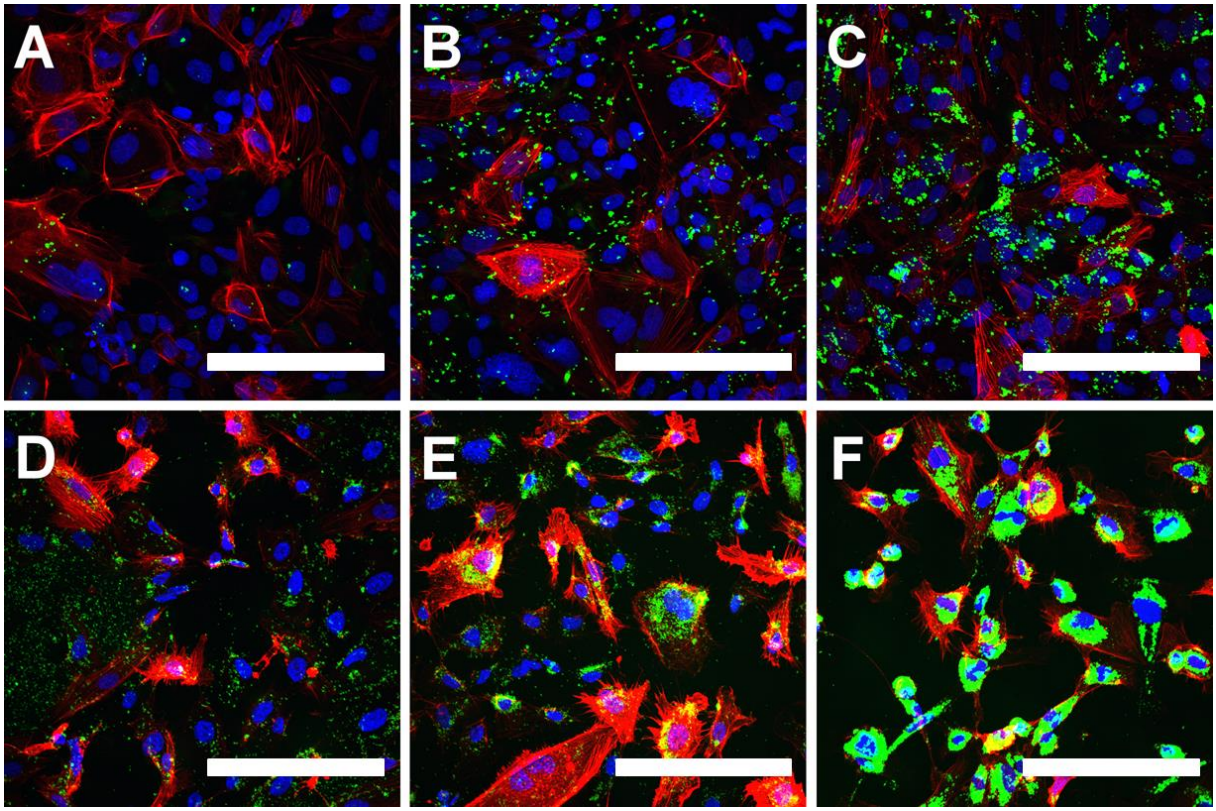

Figure V – Cellular uptake of nanoparticles over time. *Time dependent cellular uptake was visualized by confocal microscopy using fluorescent (FITC) labeled SiNP− (100 µg/ml). Incubation times for human blood-brain barrier cells (hCMEC/D3, panels A–C) and primary human umbilical vein endothelial cells (HUVEC, panel D–F) were 0 min, 35 min, and 4 h. Actin (red) was stained using Phalloidin-Rhodamine. Cell nuclei (blue) were stained using Hoechst 33342. Scale bars: 100 µm.*

Cytotoxicity

The impact of different ENP on cellular uptake, cellular viability, apoptosis & necrosis, generation of reactive oxygen species (ROS), and the triggering of different signaling pathways can be monitored by various techniques[62]. In every experiment ENP doses and exposure times should be varied in order to analyze the dose and time dependent dependence of ENP toxicity. Cellular uptake monitored over time ensures that later

detected toxic effects are a result of ENP uptake. These measurements can be conducted with confocal laser scanning microscopy (CLSM)[137], flow cytometry[138], and TEM[128]. Cell viability is one of the most meaningful determinants and can be monitored using the MTT assay[139,140]. This is a colorimetric technique based on NAD(P)H-dependent enzyme activity in viable cells which – despite its limitations[141,142] – features as one of the standard assays in nanotoxicology. Determining the present mechanism of cell death is highly relevant in nanotoxicology as the endpoints apoptosis and necrosis are understood to be triggered by different upstream-processes[143]. Apoptosis and necrosis events are commonly distinguished using fluorescent markers detected by CLSM or flow cytometry. Widely respected as one of the driving forces of nanoparticle toxicity, the generation of ROS is often discussed upon ENP uptake[144]. The DCFDA assay[145] represents the most frequently used technique to monitor the generation of ROS. Upon oxidative stress, a green dye is oxidized intracellularly to the fluorescent dichlorofluorescein (DCF). However, due to its relatively low sensitivity to different types of ROS an alternative approach using flow cytometry is advised[62]. Oxidative stress is often accused of being the main trigger of acute ENP toxicity. ROS are thought to promote apoptotic but also necrotic events *in vitro*. Moreover, the overproduction of ROS is supposed to cause inflammatory responses and other immune reactions. To clarify these proposals, enzyme-linked immunosorbent assay (ELISA)[146], flow cytometry, confocal microscopy, or western blot are adopted to investigate certain signaling pathways linked to the events of oxidative stress, apoptosis, necrosis and cellular defense[62]. The experimental methods used throughout this thesis are discussed in detail in the appropriate chapters (**Chapters I – IV**) of the section **Results** (pages 23 – 119).

Gaining the information on these parameters upon ENP interaction will help to distinctively link specific ENP properties to observed adverse effects. These insights can thus be indispensable for risk assessment and safety regulation. However, one must keep in mind that *in vitro* results cannot simply be extrapolated to the behavior of ENP *in vivo*[63,64]. *In vitro* studies are suitable to investigate mechanistic processes and serve as a first line safety assessment tool. *In vivo* studies on the other hand are crucial to verify the toxic phenomena encountered *in vitro*. Furthermore, *in vivo* studies have the advantage of monitoring the impact of an ENP on an entire organism over the

course of weeks (chronic toxicity), whereas *in vitro* studies offer confined systems observable for days (acute toxicity).

The choice of the appropriate animal model

Continuously emerging discoveries in the fields of nanotoxicology and nanomedicine have urged researchers to shift from mainly using nano-specific *in vitro* assays to incorporating combinations of *in vitro* and *in vivo* assays for their nanosafety research. This has led nanotoxicology from being an observational science to an upcoming predictive science[76,147]. In nanotoxicological research, the most commonly used models are the water flea (*Daphnia pulex*), fruit fly (*Drosophila melanogaster*), and the vertebrate models rat, mouse, and dog. Regarding the extrapolation of medically relevant data to the situation in humans, the animal models water flea and fruit fly are not feasible. However, the immense costs and limitations accompanying the use of otherwise common animal models for medical purposes has opened the discussion of implementing a “first-line” *in vivo* model specifically for nanosafety. Such a model should enable high-throughput screening (HTS) in a cost and time-effective manner bridging the gap between *in vitro* and higher *in vivo* model systems. One of these anticipated model organisms is the zebrafish embryo (*Danio rerio*), which is used recurrently in developmental biology.

The zebrafish is a fresh-water organism native to the Himalayan region[148]. It is a well-established model system in developmental biology and a promising *in vivo* model system for toxicology studies[149,150]. The zebrafish embryo is not a mammal, yet it is a vertebrate with a close homology to the genome of a human, especially pronounced in the development of the immune system, blood brain barrier, and endothelial cells[151–153]. This promising animal model inherits several other advantageous characteristics in comparison to routinely considered animal models in medical research. The most important benefits for nanotoxicological studies are its fast development[154] (**Figure VI**), low husbandry costs, and whole-body transparency in early life stages, allowing for real time microscopic *in vivo* examination[155,156]. Furthermore, the zebrafish embryo has a size of only a few millimeters and is therefore routinely used in HTS screenings of developmental and ecotoxicological studies. Furthermore, the zebrafish embryo animal model does not fall under any official ethics guidelines regarding animal testing before reaching an age of 144 hours post fertilization (hpf).

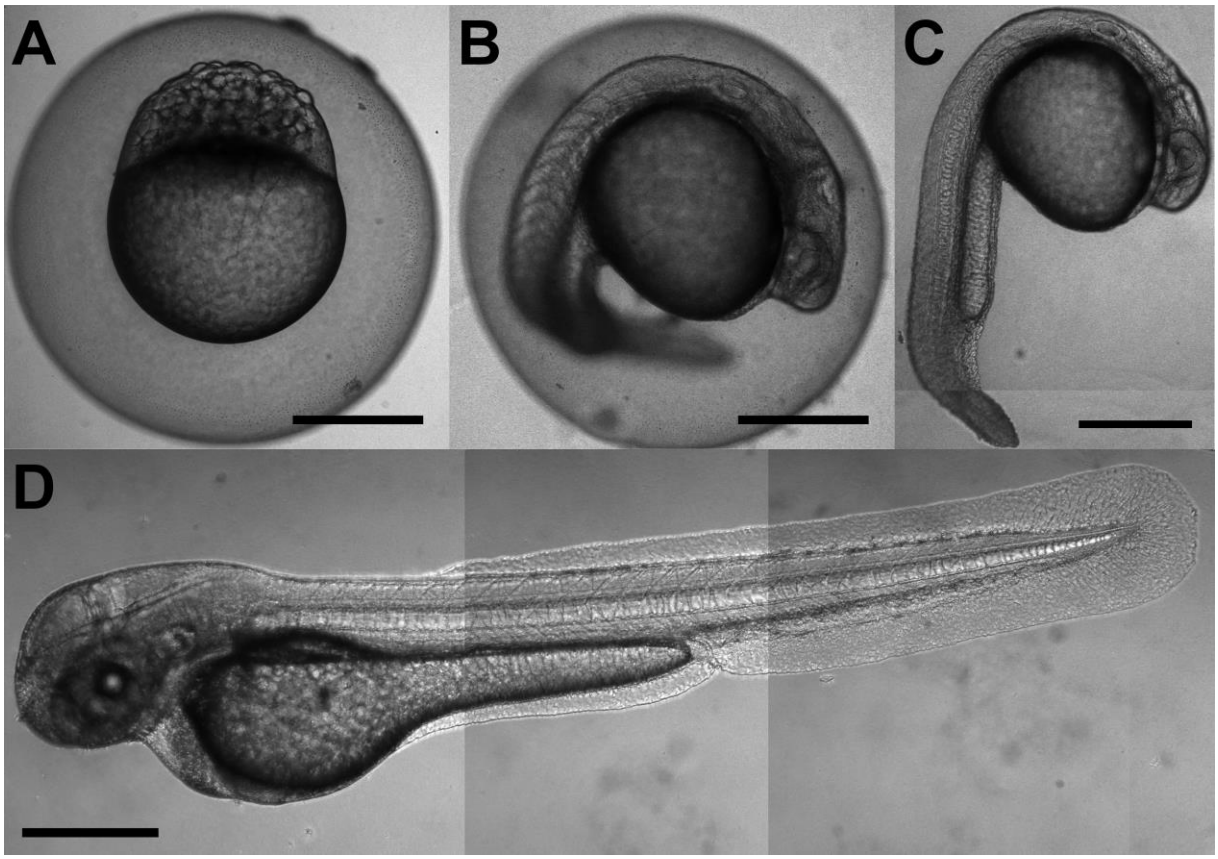

Figure VI – Developmental stages of the zebrafish embryo. *The development of a zebrafish embryo throughout the first two days post fertilization is documented in this figure. Zebrafish depicted at the 1000 cell state at 3 hours post fertilization (hpf, shown in panel A), at the 21-somite state 19 hpf (panel B),at the prim-6 state 25 hpf (panel C), and the long-pec state 48 hpf (panel D). Scale bars: 350 µm*

Zebrafish embryo in nanotoxicology

Assessing toxicity of ENP using the zebrafish requires ENP exposure via incubation or via injection. Toxicity is often assessed semi-quantitatively by monitoring embryo survival, motility, or the severity of phenotypic and morphological anomalies by staining the areas or structures of interest[157–159]. With regard to monitoring the safety of therapeutically relevant ENP, injection is preferred over incubation due to controlled dosimetry. Microinjection is predominantly performed into the the Duct of Cuvier (DoC), a temporal vascular structure running along the yolk sac on both sides of the embryo connecting the heart to the dorsal aorta. In **Figure VII** the recurrently used assays and visualization techniques of toxicity in zebrafish embryos are highlighted for the entire animal as well as the head separately. Bright field microscopy techniques allow the monitoring of anomalies or mutations such as edema of the heart, yolk sac deformation, or cartilage malformation (Fig. VII, A panels). Additionally, the abundance of transgenic lines (approximately 5000 individual Tg lines) offers a plethora of targets to choose from.

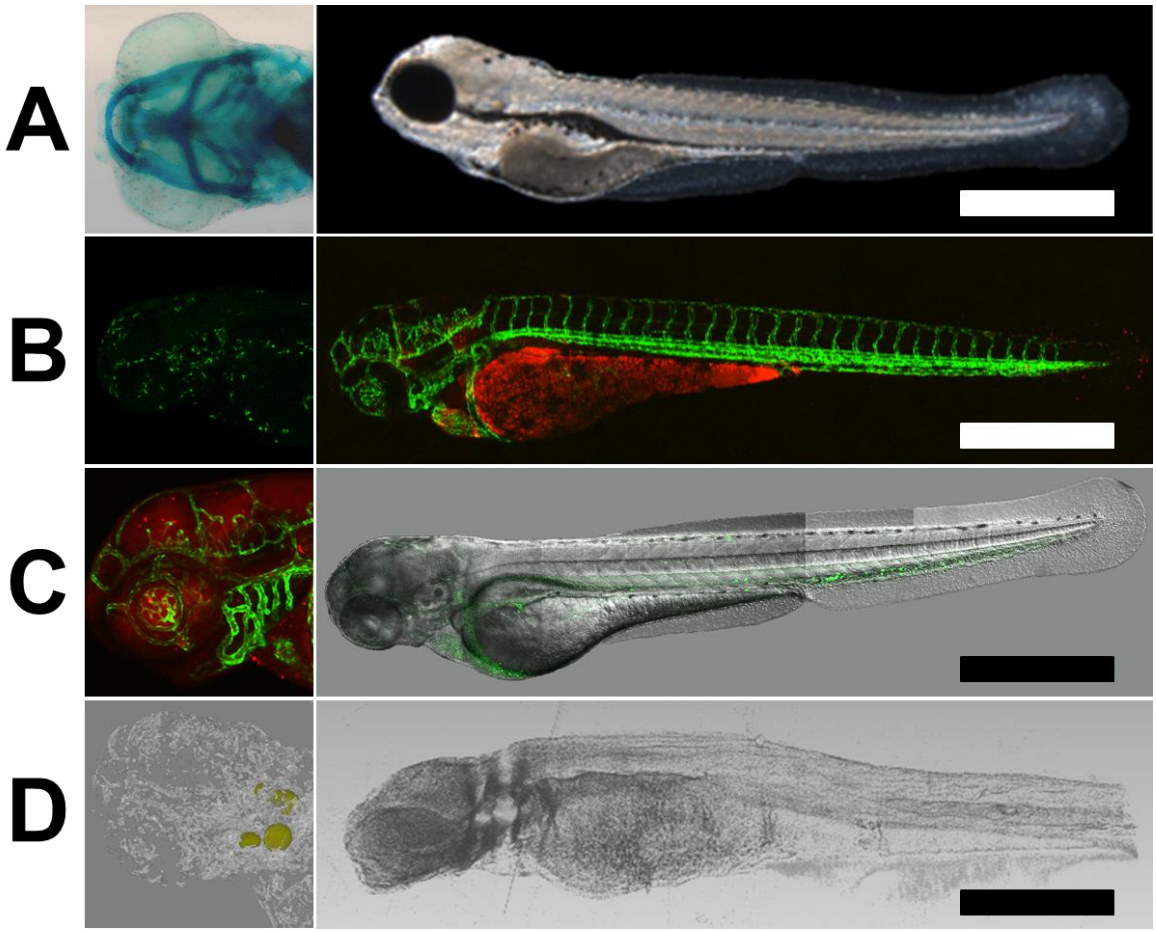

Figure VII – The zebrafish embryo animal model in nanotoxicology. *Bright field microscopy of wild type AB/TU embryos for monitoring malformations (large panel A) and cartilage anomalies (small panel A). Confocal microscopy of transgene (Tg) kdrl:EGFP embryos with fluorescently labeled vasculature (large panel B) and Tg mpeg1:Gal4;UAS:Kaede embryos with fluorescently labeled macrophages (small panel B) for biodistribution and toxicity assays (e.g. cell death and oxidative stress). Visualization of green (large panel C) and red (small panel C) fluorescent SiNP (FITC and TRITC modification) for biodistribution, targeting and stability monitoring. Absorption contrast µCT data reconstructions of wild type AB/TU embryos (large panel D) with highlighted otoliths (crystalline calcium carbonate structure of the inner ear) (small panel D) for novel non-invasive tracing techniques and targeting approaches.*

Fluorescent microscopy techniques such as CLSM and light sheet microscopy enable investigations of immune reactions (macrophage migration, apoptosis) or simply the accentuation of certain internal structures such as the vasculature (Fig. VII, B panels). Moreover, fluorescent microscopy techniques enable the tracing of fluorescently labeled ENP throughout the entire body of the fish (Fig. VII, C panels)[160]. Finally, X-ray based techniques such as CT, µCT, and synchrotron radiation µCT (SRµCT) are the subject of ongoing research for the visualization of non-labeled ENP and monitoring of ENP biodistribution *in vivo* (Fig. VII, D panels). Despite its portfolio of beneficial characteristics and the promising outlook of emerging as novel model organism for nanotoxicology, the zebrafish embryo still has to prove validity in a series of more advanced studies.

Aim of the thesis

The emergence of engineered nanoparticles (ENP) in medical applications has raised multiple concerns about their safety. However, there is a shortage of generally accepted guidelines regulating the safety of ENP designed for therapeutic use. Consequently, the aim of this thesis was to elucidate the interplay of key factors that drive nanoparticle-specific toxicity and develop a novel application-based safety assessment strategy for therapeutic ENP. Major project milestones were defined as follows:

Synthesis of inorganic nanoparticles used in therapeutic research

- How are silica and gold nanoparticles produced?
- How can these ENP be modified for nanotoxicological studies?

Physico-chemical characterization of ENP

- How relevant is physico-chemical characterization for toxicological studies?
- Which physico-chemical properties must be routinely determined?

In vitro screening of ENP toxicity

- How does one screen the toxicity of an ENP *in vitro*?
- What toxic outcomes triggered by ENP should be screened for hazard and safety assessment?

Alternative *in vivo* screening tool for nanotoxicology

- Is the zebrafish embryo a valid alternative *in vivo* model for nanotoxicology?
- Can biodistribution of non-labeled ENP be monitored in the zebrafish embryo?

Shortage of safety guidelines for nanoparticles designed for therapeutic use

- What are the most important aspects of determining the safety of ENP?
- Is there a possibility of establishing application-based guidelines for ENP?

Results

Chapter I

Selective stimulation of the JAK/STAT signaling pathway by silica nanoparticles in human endothelial cells.

***Siegrist S**, Kettiger H, Fasler-Kan E, Huwyler J*

Chapter II

Immobilization of enzymes on PLGA sub-micrometer particles by crosslinked layer-by-layer deposition.

*Sieber S, **Siegrist S**, Schwarz S, Porta F, Schenk SH, Huwyler J*

Chapter III

Monitoring the biodistribution of metal-based nanoparticles in a small animal model by synchrotron radiation micro-tomography

***Siegrist S**, Cörek E, Bikis C, Sieber S, Fluder P, Klados K, Detampel P, Puchkov M, Thalmann P, Schulz G, Alexiou Ch, Müller B, Huwyler J*

Chapter IV

Preclinical Hazard Evaluation Strategy for Nanomedicines

***Siegrist S**, Cörek E, Detampel P, Sandström J, Wick P, Huwyler J*

Chapter I

Toxicology in Vitro 42 (2017) 308–318

Contents lists available at ScienceDirect

Toxicology in Vitro

journal homepage: www.elsevier.com/locate/toxinvit

Selective stimulation of the JAK/STAT signaling pathway by silica nanoparticles in human endothelial cells

S. Siegrist[a], H. Kettiger[a,1], E. Fasler-Kan[b,c,2], J. Huwyler[a,*,2]

[a] Pharmaceutical Technology, University of Basel, Klingelbergstrasse. 50, 4056 Basel, Switzerland
[b] Department of Pediatric Surgery, University of Bern, Freiburgstrasse 15, 3010 Bern, Switzerland
[c] Department of Biomedicine, University of Basel, Hebelstrasse 20, 4031 Basel

ARTICLE INFO

Keywords:
Nanotoxicology
Silica nanoparticles
Reactive oxygen species
JAK/STAT
MHC class I

ABSTRACT

Silica nanoparticles (SiNP) are frequently used in pharmaceutical formulations. Intravenously administered, these particles are in close contact with the vascular endothelium. However, preliminary safety assessments of these novel excipients have indicated that SiNP are potentially cytotoxic and can trigger inflammation.

In order to elucidate mechanisms of SiNP mediated inflammation, cerebral microvascular endothelial cells and primary umbilical endothelial cells were incubated with SiNP at doses between 10 ng/ml and 250 μg/ml.

Two types of 110 nm SiNP with different surface charge were synthesized and characterized. Uptake, cell viability, apoptosis, necrosis, oxidative stress, as well as interferences with both JAK/STAT and NF-κB pathways were studied.

SiNP uptake leads to a cell viability decrease and promotes generation of reactive oxygen species (ROS) in a time- and dose-dependent manner. Furthermore, SiNP are able to trigger the activation of the STAT1 pathway. In contrast, no significant activation of STAT3, STAT6 or NF-κB could be detected. Additionally, modulation of the major histocompatibility complex (MHC) class I proteins was observed for cationic SiNP at low doses.

Our results show the potential of SiNP to trigger selective activation of inflammatory signaling pathways in endothelial cells and thereby contribute to a better understanding of the toxicological profile of SiNP.

1. Introduction

Silica nanoparticles (SiNP)[3] are increasingly used for technical or pharmaceutical applications. This includes their use as filler, desiccant, thickener for liquid dosage forms, or anticaking agent in powders. More recently, they were also proposed as nano-sized drug delivery systems or imaging probes (Ambrogio et al., 2011; Coti et al., 2009; Li et al., 2012; Tang and Cheng, 2013). Fluorescent SiNP can be used as tracers in vivo or as targeted carriers in cancer therapy (Arap et al., 2013; Wu et al., 2014) due to their beneficial characteristics in terms of size, the possibility to introduce surface modifications, and the high surface area to volume ratio. Among other administration routes, SiNP can be administered intravenously and hence reach their targets via the vascular system. However, these proposals have also raised concerns about their safety and biocompatibility (Fadeel, 2012; Guarnieri et al., 2014; Nel et al., 2006; Pietroiusti et al., 2013; Yildirimer et al., 2011). Being small enough to be readily taken up by cells, SiNP may accumulate within the organism leading to acute or chronic adverse effects. As an example, inflammatory responses to other types of nanoparticles were observed in toxicological studies on multiple occasions (Chia et al., 2015; Giovanni et al., 2015). Conclusively, questions about unspecific binding, cellular uptake routes, transcellular transport and potential toxic effects of SiNPs at the level of cellular barriers have led to much controversy over the safety of potential clinical applications (Cho et al., 2009; Guarnieri et al., 2014; Kettiger et al., 2013; Marzaioli et al., 2014). Serving as a selectively permeable barrier, endothelial cells separate the blood compartment from organs. The central nervous system is a prime example of an organ, where the endothelial cells have an important protective function by forming the so called blood-brain barrier (BBB) (Stevens et al., 2000). These cells are prone to interact with intravenously administered SiNP (Blechinger et al., 2013; Napierska et al., 2009), resulting in a potential impairment

* Corresponding author at: Pharmaceutical Technology, Pharmacenter, University of Basel, Klingelbergstrasse. 50, 4056 Basel, Switzerland.
E-mail address: Joerg.huwyler@unibas.ch (J. Huwyler).
[1] Present address: Faculty of Sciences and Engineering, Åbo Akademi University, Artillerigatan 6A, FI 20520 Turku, Finland.
[2] These authors contributed equally to this study.
[3] SiNP refers to silica nanoparticles in general. Throughout the publication the terms SiNP+ and SiNP− will be used consistently to distinguish between cationic and anionic silica

http://dx.doi.org/10.1016/j.tiv.2017.05.002
Received 30 November 2016; Received in revised form 22 March 2017; Accepted 2 May 2017
Available online 03 May 2017
0887-2333/

of brain tissue functionality, since uptake of nanoparticulate formulations by endothelial cells has been shown on previous occasions (Georgieva et al., 2011; Ye et al., 2013).

Previous studies have demonstrated that the immortalized human microvascular endothelial cell line hCMEC/D3 can be used as an in vitro model to study endothelial functionality (Fasler-Kan et al., 2010; Lopez-Ramirez et al., 2012; Poller et al., 2008; Weksler et al., 2013). These studies have shown that hCMEC/D3 cells share important characteristics with primary capillary endothelial cells. In particular, that hCMEC/D3 cells are responsive towards activation with pro-inflammatory cytokines including interferon-gamma (IFN-γ), interleukin 4 (IL-4), interleukin 6 (IL-6) and TNF-α leading to activation of JAK/STAT and NF-κB signaling pathways. Furthermore, expression of MHC class I and cell adhesion factors (cluster of differentiation molecules CD31 and CD34) confirm these endothelial cells are involved in antigen presentation, leukocyte recruitment and inflammation. The question arises therefore, if nanoparticle-induced disturbances of cell functionality and inflammation at the level of endothelial cells might be associated with activation of these signaling pathways.

It was the aim of the present study to investigate whether SiNP may trigger signaling pathways in endothelial cells, providing a mechanistic explanation for nanoparticle toxicity. Physico-chemical properties of SiNP (e.g. size, zeta potential, geometry, specific surface, chemical modifications) were controlled using established synthetic procedures (Kettiger et al., 2015). hCMEC/D3 cells were used to study cell uptake, cellular stress (ROS generation), viability (apoptosis and necrosis), and inflammatory responses. To identify cell-line specific effects, control experiments were performed using primary cultures of human endothelial cells (i.e. HUVEC; human umbilical vein endothelial cells). Interactions of SiNPs and endothelial cells were analyzed with respect to activation of pro-inflammatory signaling pathways, with a focus on JAK/STAT and NF-κB mediated signaling.

2. Materials and methods

All chemicals were of analytical grade and purchased from Sigma Aldrich (Saint Louis, MO) if not otherwise indicated. Phosphate buffered saline (Dulbecco's PBS consisting of 2.7 mM KCl, 1.5 mM KH_2PO_4, 137 mM NaCl, 8.9 mM Na_2HPO_4, pH 7.4) and rat tail collagen type 1 were also purchased from Sigma Aldrich. Monoclonal antibodies (mAbs) for flow cytometry and confocal laser scanning microscopy (CLSM) were purchased from Becton Dickinson (New Jersey, NJ). Cytokines were purchased from R&D Systems (Minneapolis, MN). The hCMEC/D3 cell line was obtained under license from INSERM, France. Cryopreserved HUVEC and cell culture media were purchased from BioConcept (Allschwil, Switzerland). Fetal calf serum (FCS) was obtained from Amimed (Allschwil, Switzerland).

2.1. Synthesis of silica nanoparticles (SiNP)

SiNPs were synthesized according to Stoeber (Stöber et al., 1968). In brief, water (20.3 ml), 30% ammonia solution (1 ml) and ethanol (150 ml) were mixed with tetraethylorthosilicate (TEOS, 8.9 ml) Reagents were added under continuous stirring (500 rpm) at room temperature. Either 224 µl or 931 µl of (3-Aminopropyl)triethoxysilane 98% (APTES, abcr, Karlsruhe, Germany) were then added to alter the net surface charge and obtain SiNP− and SiNP+, respectively. The reaction mixture was left to stir overnight. The resulting SiNP were collected by centrifugation (20 min, 20,000 × g, 22 °C), and washed with alcohol. Fluorescein isothiocyanate (FITC) labeled SiNP were synthesized with the co-condensation method as described by Branda et al. (2007). SiNP were dried under vacuum and stored in dry state at 4 °C in the dark. Prior to use, SiNP were redispersed in assay buffer (20 mM HEPES, 120 mM NaCl, pH 7.4) by sonication to obtain 1 mg/ml or 10 µg/ml stock solutions. These stock solutions were immediately diluted with FCS containing medium when used in cell based assays.

2.2. Physico-chemical characterization of nanoparticles

Hydrodynamic size, polydispersity index, and zeta potential were analyzed by differential (DLS) and electrophoretic light scattering (ELS) using a Delsa Nano C Particle Analyzer (Beckman Coulter Inc., Nyon, Switzerland). Scattered light was detected and analyzed as described elsewhere (Witzigmann et al., 2015). DLS measurements were performed in assay buffer to avoid interference with protein-agglomerates present in plasma or serum containing medium (Schmutz et al., 2011). To characterize SiNP shape and size transmission electron microscopy (TEM, CM-100, Philips, Amsterdam, Netherlands) was used, operating at 80 kV. At least 75 SiNP were measured for statistical soundness. Ultra-small-angle X-ray scattering (U-SAXS) was used as an additional method to determine SiNP size. Using a Smartlab X-ray Diffractometer (Rigaku, Tokyo, Japan), SiNP scattering profiles were collected at room temperature with Cu Kα radiation (λ = 1.541 Å) and 0–0.5 2θ scattering angle. Analysis was done with the Particle-/Pore-size Analysis Software NANO-Solver 3.7 provided with the instrument. Physico-chemical characterization experiments were performed with 1 mg/ml SiNP stock solutions in absence of FCS containing medium.

2.3. Dosimetry

Applied doses were the same for all in vitro assays (10 ng/ml, 100 ng/ml, 10 µg/ml, 50 µg/ml, 100 µg/ml, and 250 µg/ml). This dose range was chosen based on the following considerations: Cytokine mediated signaling can be triggered by very small doses of pro-inflammatory agents in the range of a few ng/ml. On the other hand, much higher doses of silica nanoparticles are frequently used in different experimental systems. For example, a SiNP dose range from 10 to 100 µg/ml covers concentrations frequently applied in ecotoxicological studies (Blaise et al., 2008). Toxicological effects of SiNP were studied in vivo using administered doses in the mouse of 50 mg/kg (Cho et al., 2009) resulting in an estimated plasma exposure of 50 µg/ml assuming a partitioning of SiNP to the extracellular fluid volume only (i.e. a volume of distribution of 0.2 l/kg). Acute toxicity of SiNP is observed at 5 times higher doses (i.e. LD_{50} doses of 262.45 ± 33.78 mg/kg for the mouse were reported by Yu et al., 2013). It was therefore decided to use for the present study an extended dose range covering > 4 orders of magnitude. This includes the highest expected plasma concentration, which can presumably be reached in animals (250 µg/ml). It should be noted, however, that local concentrations and thus exposure of the endothelium might be much higher in specific tissues or at the site of injection.

2.4. Cell cultures

hCMEC/D3 cells were cultured as described previously (Poller et al., 2008). Primary HUVEC cells were cultured according to protocols of the supplier (Provitro, Berlin, FRG) and were obtained from a local distributor (BioConcept). hCMEC/D3 and HUVEC were used at passages 25–35 (Poller et al., 2008) and passages 4–6 (Tavakol et al., 2016), respectively. All flasks, plates, and coverslips were coated with a 0.1 mg/ml rat tail collagen type 1 solution. Cell culture media contained penicillin/streptomycin (1% v/v). Cells were seeded into 75 cm^2 culture flasks and were cultured at 37 °C and 5% CO_2. For harvesting and passaging, cells were rinsed with phosphate buffered saline (PBS) and detached for 3 min (hCMEC/D3) or 5 min (HUVEC) with 2.5 ml trypsin/EDTA (0.05%) at 37 °C. For in vitro assays, cells were treated with accutase instead of trypsin for 4–5 min (hCMEC/D3) or 6–7 min (HUVEC) at 37 °C. Detachment was terminated by addition of 7.5 ml cell culture medium and cells were collected by centrifugation (190 × g for hCMEC/D3 or 250 × g for HUVEC, 5 min). All experiments were carried out in cell culture medium in presence of FCS, which leads to the formation of a biocorona. The identity of the biocorona formed on silica nanoparticles was extensively investigated previously by

Clemments et al. (2015).

2.5. Cellular uptake analysis by confocal laser scanning microscopy and flow cytometry

Cellular uptake was analyzed by CLSM and flow cytometry. For confocal microscopy analysis (FV-1000, Olympus, Tokyo, Japan), cells were grown on coated coverslips and incubated with FITC labeled SiNP for 35 min, 4 h, and 24 h under cell culture conditions. Cell nuclei were stained using Hoechst 33,342 (50 µg/ml) (ThermoFisher Scientific, Waltham, MA). Actin was visualized by incubation with 1 U/200 µl Phalloidin-Rhodamine (ThermoFisher Scientific). Images were taken using a 40 × PlanApo N oil immersion objective (NA 1.30). For flow cytometry, cells were grown in 12-well plates cells. They were detached as described above, transferred to flow cytometry sample tubes, and resuspended in PBS containing 0.2% fetal calf serum (FCS, BioConcept) before being analyzed using a FACS Canto II flow cytometer (Becton Dickinson, New Jersey, NJ) and FlowJo X software (FlowJo LLC, Ashland, OR).

2.6. Cell viability

The MTT assay was used to determine cell viability upon nanoparticle incubation. This colorimetric assay monitors NAD(P)H-dependent oxidoreductase enzyme activity of viable cells. The tetrazolium dye MTT 3-(4,5-dimethylthiazol-2-yl)-2,5-diphenyltetrazolium bromide (Roth, Karlsruhe, Germany) is thereby reduced to a water-insoluble and purple colored formazan. hCMEC/D3 and HUVEC cells were grown in 96–well plates (20,000 and 10,000 cells per well, respectively) and allowed to attach for 24 h prior to incubation for 4 h, 8 h, 16 h, or 24 h with SiNP, 20 µM terfenadine (positive control) or blank assay buffer (negative control). Formazan crystals were dissolved in dimethyl sulfoxide (DMSO, Roth, Karlsruhe, Germany) and absorption was measured using a Spectramax M2^e (Molecular Devices, Sunnyvale, CA).

2.7. Apoptosis and necrosis

The Alexa Fluor 488 Annexin V/Dead cell Apoptosis Kit (ThermoFisher Scientific) was used according to the instructions of the manufacturer to distinguish between apoptosis and necrosis. Cells were grown in 25 cm^2 culture flasks and were incubated with 1 µM staurosporin (positive control) or culture medium (negative control) for 24 h under cell culture conditions. Samples were analyzed by flow cytometry.

2.8. Oxidative stress

Generation of reactive oxygen species was monitored using the Total ROS/Superoxide Detection Kit (Enzo Life Sciences, Farmingdale, NY) according to instructions of the manufacturer. This kit detects a variety of reactive oxygen species, such as hydrogen peroxide (H_2O_2), peroxynitrite ($ONOO^-$), hydroxyl radicals (HO^-), nitric oxide (NO^-), and peroxy radicals (ROO^-). In brief, cells were grown in 12-well plates and incubated for 35 min with pyocyanin (positive control), blank assay buffer (negative control), and SiNP under cell culture conditions. Cells were detached as described above, transferred to FACS tubes and subsequently stained with dyes of the detection kit. Samples were analyzed by flow cytometry.

2.9. JAK/STAT activation

Activation of STAT1, STAT3 and, STAT6 was determined by flow cytometry. Cells were grown in 25 cm^2 culture flasks and incubated for 35 min with 5 ng/ml INF-γ (positive control), blank assay buffer (negative control), and SiNP under cell culture conditions. Subsequently, cells were detached as described above, fixed in 4% paraformaldehyde (10 min, 37 °C), and permeabilized with 90% methanol (30 min, 4 °C). Staining with the corresponding (i.e. STAT1/3/6) FITC-conjugated anti-phospho STAT mAbs was performed over night at 4 °C. Finally, cells were washed in PBS and their mean fluorescence intensity was analyzed by flow cytometry.

2.10. NF-κB activation

The activation of NF-κB was investigated by flow cytometry and CLSM. Cells were grown in 25 cm^2 culture flasks and incubated (37 °C and 5% CO_2) for 35 min with 5 ng/ml TNF-α (positive control), blank assay buffer (negative control), and SiNP. Cells were then fixed and permeabilized with a Fix/Perm solution (Becton Dickinson, New Jersey, USA) for 45 min. Staining with the fluorescein isothiocyanate conjugated Alexa Fluor 647 mouse anti-NF-κB mAb for phosphorylated p65 peptides was performed over night at 4 °C. Finally, cells were washed in PBS and their mean fluorescence intensity was analyzed by FACS. For CLSM samples were prepared and measured according to Fasler-Kan et al. (2013).

2.11. Major histocompatibility complex (MHC) class I and II modulation

Modulation of MHC class I and II was monitored by flow cytometry. Cells were grown in 25 cm^2 culture flasks and incubated (37 °C and 5% CO_2) for 48 h with 5 ng/ml INF-γ (positive control), blank assay buffer (negative control), and SiNP. After detachment as described above, cells were washed with PBS and stained overnight using the corresponding fluorescein isothiocyanate conjugated mouse anti-human mAbs for human leukocyte antigens HLA-ABC (MHC class I) or HLA-DR,DP,DQ (MHC class II). Mean fluorescence intensity of stained cells was analyzed by FACS.

2.12. PathScan

A PathScan Stress and Apoptosis Signaling Antibody Array (Cell Signaling Technologies, Danvers, MA) was used to monitor 19 different signaling molecules that play a role in regulating cellular stress response and apoptosis. The immunoassay was done according to the protocols provided by the supplier. Cells were incubated for 35 min under cell culture conditions with 250 µg/ml of either SiNP − or SiNP +.

2.13. Control experiments

Due to their unique physico-chemical characteristics, nanoparticles may cause artifacts in experimental systems. Plasma-protein binding to nanoparticles may alter their surface characteristics. Optical and/or adsorptive interference in spectroscopy or fluorescence-based methods (i.e. FACS and confocal fluorescence microscopy) may occur due to nanoparticle induced quenching of a fluorescent indicator dye, signal blockage, or direct interaction with a dye. The possibility of optical and adsorptive interference of SiNP was therefore addressed in all assays as described previously (Kettiger et al., 2015; Kroll et al., 2012). Control incubations up to the highest doses of SiNP revealed a potential for interference in one experimental setup only: In the ROS assay, a drop in signal at 250 µg/ml was attributed to quenching of the fluorescence indicator by optical and adsorptive interference. The corresponding data-point was therefore excluded from analysis (Fig. 3).

2.14. Statistical analysis

Assay results are expressed as means of independent sets of experiments ± standard deviation (SD), $n \geq 3$. Wherever indicated, significance was determined by one-way analysis of variance (ANOVA). Tukey's post-hoc test was performed to compare treated groups and the corresponding controls. Differences were considered to be significant at

Table 1
Characterization of silica nanoparticles (SiNP). Nanoparticles were analyzed by differential light scattering (DLS), transmission electron microscopy (TEM), and ultra-small-angle X-ray scattering (U-SAXS). Hydrodynamic diameter as a measure for size, polydispersity index (PDI), and the electrokinetic potential (zeta potential) were determined by DLS at pH 7.4 in assay buffer. Values marked with an asterisk (*) were measured in culture medium containing 10% fetal calf serum (FCS).

Silica nanoparticles	Size [nm] (TEM)	Size [nm] (TEM)*	Size [nm] (SAXS)	Size [nm] (DLS)	PDI (DLS)	Zeta potential [mV] (DLS)
SNP +	109.1 ± 11.4	121.4 ± 20.6*	102.7 ± 10.2	119.6	0.062	21.45
SNP −	113.3 ± 8.2	120.7 ± 19.5*	107.5 ± 8.4	121.5	0.018	− 22.85

$p < 0.05$. Used software was Origin 9.1 (OriginLab, Northampton, MA).

3. Results

3.1. Characterization of silica nanoparticles (SiNP)

Characterization of SiNP was done by Differential Light Scattering (DLS), Transmission Electron Microscopy (TEM) (as shown previously (Kettiger et al., 2015)), and Ultra-small-angle X-ray scattering (U-SAXS). We determined the most relevant properties, which are the hydrodynamic diameter, dry state particle size, zeta potential, polydispersity index, shape, and particle morphology (Table 1). DLS was as well used to monitor growth of SiNP during synthesis. The hydrodynamic diameter of SiNP + and SiNP − was almost identical and in the range of 120 nm, with a polydispersity below 0.2. To confirm the primary particle diameter, transmission electron microscopy and U-SAXS experiments were performed (Table 1). The actual particle sizes (110 nm) determined by both methods are consistent and slightly smaller than the values measured by DLS (120 nm). Measurements in culture medium containing 10% FCS also revealed no statistically significant change of the actual particle size. Unimodal size distribution of both particle preparations could be confirmed by statistical analysis of the sizes recorded with TEM. The zeta potential was determined for both particle types, was in the range of + 20 mV for SiNP + and − 20 mV for SiNP − (in HEPES, pH 7.4), and reflects different densities of surface bound amines due to varying amounts of APTES used during synthesis.

3.2. Cell viability and cellular uptake

The impact of increasing concentrations of SiNP on cell viability was studied in two human endothelial cell types (hCMEC/D3, HUVEC). Cellular viability was monitored by the MTT assay upon incubation for 24 h with SiNP + and SiNP − (Fig. 1). Both types of SiNP showed a concentration dependent toxicity towards endothelial cells. Toxic effects were more pronounced for cationic SiNP with a reduction in cell viability by approximately 50% and 60% in hCMEC/D3 (Fig. 1, panel A) and HUVEC (Fig. 1, panel F) cells, respectively, at particle concentrations of 100 µg/ml. Observed effects were less pronounced in hCMEC/D3 cells as compared to primary HUVEC cells. Results were confirmed using incubation times of 4 h, 8 h and 16 h (data not shown). Cytotoxicity was suspected to be a consequence of cellular uptake of SiNP. Therefore, time-dependent cellular uptake of SiNP was monitored by confocal microscopy using fluorescent (FITC) labeled SiNP. Both types of fluorescent SiNP are taken up by target cells as shown in Fig. 1, panels B–E (hCMEC/D3) and G–J (HUVEC) for particle concentrations of 100 µg/ml. As demonstrated for SiNP −, nanoparticles accumulate over time in the cytoplasm of the target cells (i.e. both hCMEC/D3 and HUVEC cells) as shown by a particulate intracellular staining pattern. At 35 min, most particles still reside outside of the cells; only a few were already taken up. Four hours after incubation, particles are preferentially located at the cell membrane. After 24 h, most of the inner cell volume is packed with internalized SiNP, forming a firm layer around the nucleus. Under these conditions, both cell types are deformed and start to lyse (Fig. 1, E and J). They are characterized by a disturbed arrangement of actin fibers. SiNP uptake was confirmed by flow cytometry (data not shown).

3.3. Apoptosis and necrosis induced by silica nanoparticle exposure

To further specify how cell death is caused in endothelial cells exposed to SiNP, apoptosis and necrosis was monitored in both hCMEC/D3 and HUVEC cells by flow cytometry. Dose- and time-dependent sets of experiments were conducted for both cells lines incubated with the two SiNP types. Cells were stained for Annexin V and were incubated with Propidium Iodide (PI). Resulting staining patterns were analyzed by flow cytometry (Fig. 2). Location of signals in the lower left quadrant of the pseudocolor flow cytometry plot (corresponding to Annexin V negative/PI negative cells) is representative for intact cells. Necrotic cells (Annexin V positive/PI positive cells) are located in the upper right quadrant. Apoptotic cells (Annexin V positive/PI negative cells) are located in the lower right quadrant. Annexin V negative/PI positive signals located in the upper left quadrant represent nuclear fragments (i.e. cell debris). As depicted, hCMEC/D3 cells treated for 24 h with 250 µg/ml of SiNP − (Fig. 2, panel C) or SiNP + (Fig. 2, panel D) shift to an apoptotic (66% of cells) or necrotic (80% of cells) stage, respectively. As a positive control, 1 µM staurosporin was used (Fig. 2, panel B and F). In HUVEC cells, both SiNP − (Fig. 2, panel G) and SiNP + (Fig. 2, panel H) show an increased toxicity under the same incubation conditions leading to a shift to a necrotic stage (> 70% of all cells under both conditions). The staining patterns are comparable to those obtained by the positive control staurosporin. Similar but less pronounced results were obtained at shorter incubation times (4 h, 8 h, and 16 h) and reduced SiNP concentrations (data not shown).

3.4. Nanoparticle induced generation of reactive oxygen species (ROS)

In a next set of experiments, we studied the generation of reactive oxygen species (ROS) since cytotoxic effects induced by SiNP are known to be consequence thereof. Uncontrolled overproduction of ROS leads to severe cytotoxic outcomes and often results in apoptotic and/or necrotic cell death. Consequently, generation of total ROS was measured by flow cytometry (Fig. 3). Dose-dependent generation of ROS was apparent within 35 min upon incubation with SiNP + and SiNP − and reached 47% and 66% of corresponding signals of the positive control (i.e. the bacterial toxin pyocyanin) for hCMEC/D3 and HUVEC cells, respectively. Again, cells incubated with SiNP + showed slightly higher generation of ROS than SiNP − in both endothelial cell types. HUVEC cells generated considerably more ROS than hCMEC/D3 cells regardless of the applied SiNP dose.

3.5. Activation of inflammatory signaling pathways and modulation of MHC class I expression by SiNP

Some cytokine mediated signaling pathways linked to cellular stress and cell death are known to have a close relationship to or are even dependent on ROS generation. We therefore studied pathways, which play an important role in inflammation and cell survival, such as the activation of JAK/STAT signaling pathways, activation of NF-κB, and induction of expression levels of the major histocompatibility complex (MHC class I and II) proteins by SiNP. Fig. 4 shows specific activation of

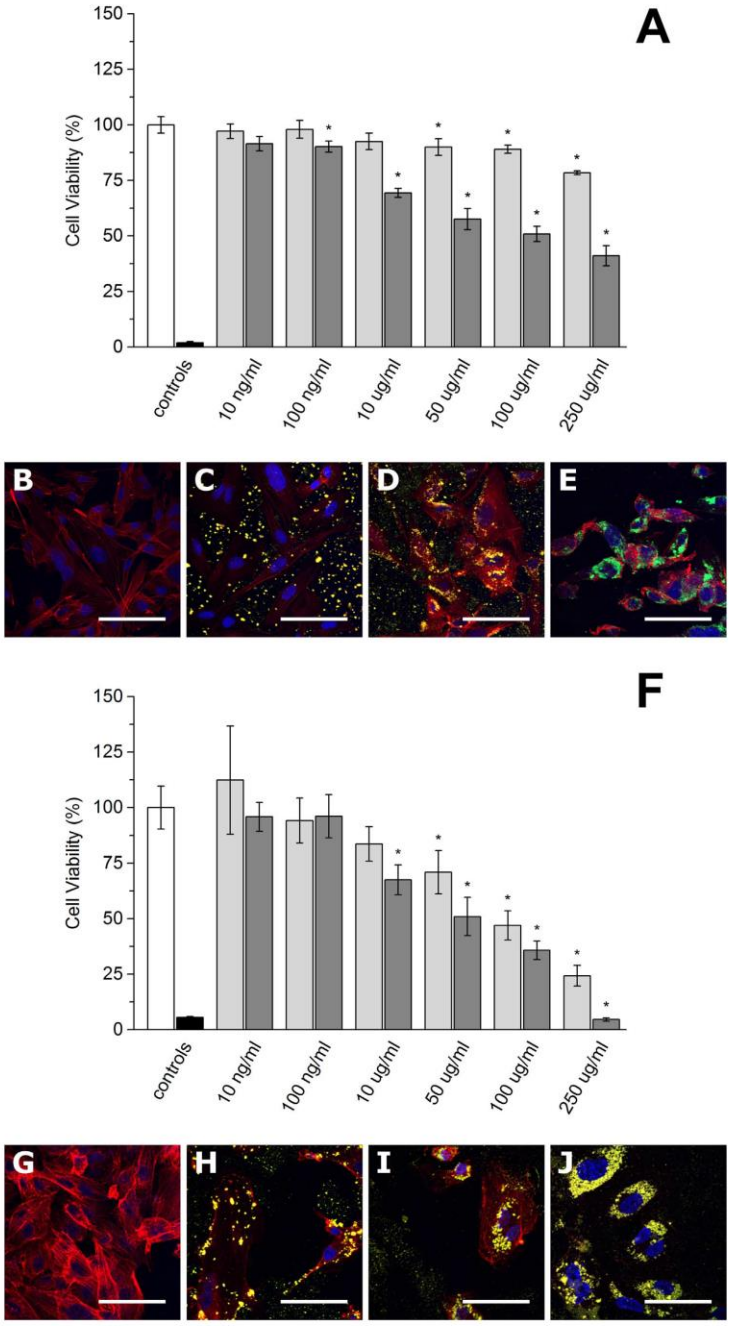

(caption on next page)

Fig. 1. Cell viability and SiNP uptake. hCMEC/D3 (A–E) and HUVEC cells (F–J) were incubated with SiNP. Cellular viability (A, F) was determined after 24 h by the MTT assay for both SiNP − (light grey bars) and SiNP + (dark grey bars). Indicated particle concentrations were used and compared to untreated cells (100% viability, white bars) and incubations with 20 μM Terfenadine (positive control, black bars). Values are means ± SD, n = 6. *: statistically significant differences between untreated and SiNP treated cells, $p < 0.05$. Time-dependent cellular uptake was visualized by confocal microscopy using fluorescent (FITC) labeled SiNP − (100 μg/ml). Incubation times for hCMEC/D3 (B–E) and HUVEC (G–J) were 0 min, 35 min, 4 h, and 24 h. Actin was stained using Phalloidin-Rhodamine. Cell nuclei were stained using Hoechst 33342. Scale bars: 80 μm.

STAT1 for SiNP + and SiNP − treated hCMEC/D3 cells at doses of 250 μg/ml (Fig. 4, A). Consistent with our previous results, SiNP + induced greater effects than SiNP −. HUVECs were more sensitive to SiNP treatments than hCMEC/D3 cells since lower concentrations of exposure (100 μg/ml) were needed to activate STAT1 (Fig. 4, B). In contrast, lower concentration levels did not reveal distinct activations of STAT1 for either cell type, suggesting a threshold based finding. NF-κB, STAT3, STAT6 and MHC class II were not stimulated or modulated in HUVEC and hCMEC/D3 upon SiNP exposure (data not shown). Furthermore, we observed an upregulation of MHC class I proteins when hCMEC/D3 cells were exposed to SiNP + in the ng/ml range (Fig. 5). We did not encounter this phenomenon at higher concentrations or in similarly treated HUVECs.

3.6. PathScan analysis of signaling molecules upon SiNP incubation

To further analyze our findings, we monitored 19 different signaling molecules that play a pivotal role in cellular stress response and apoptosis by using the PathScan stress and apoptosis signaling array and analyzing it on a high-resolution microarray scanner (Agilent Technologies, Santa Clara, CA). Our results show significantly elevated levels of Akt and p44/42 MAPK kinases as well as survivin and α-tubulin for all treatments. Furthermore, we found the levels of nuclear factor IκBα, Chk1, and Chk2 were significantly increased upon SiNP + exposure in both cell types. Additionally, we obtained significantly augmented signals of cytoplasmic signaling molecule Smad2, heat shock protein HSP27, and kinases p38 MAPK, SAPK/JNK, as well as of the pro-apoptotic Bcl-2 protein Bad and the apoptosis executioner enzyme caspase-7 specifically for HUVEC cells treated with SiNP + (Fig. 6 and Table S4). Surprisingly however, the apoptosis executioner enzyme caspase 3 was not detected. This can most likely be attributed to the short incubation time (35 min), which might not be sufficient to allow for a transition of signals from the apoptotic precursors p38, ChK1, and ChK2 – which were significantly augmented – to these effectors. Finally, we were also able to confirm that HUVEC were more sensitive to SiNP treatments than hCMEC/D3, as seen in earlier experiments.

4. Discussion

There is an increasing interest to use silica-based nanoparticles for the implementation of drug delivery strategies. This includes parenteral administration of SiNPs in oncology (Baek et al., 2015). However, many open questions still have to be addressed with respect to safety and biocompatibility of such particles. For example, interactions with cells of the immune system (e.g. mononuclear phagocytic cells) (Yu et al., 2013), proliferation of splenocytes (Lee et al., 2013) and haemolysis (Kettiger et al., 2015) were observed upon contact with SiNPs. Upon intravenous injection of SiNPs, endothelial cells are among the cell types that immediately come into close contact with these nanoparticles. It was therefore the aim of the present work to study interactions of SiNPs with endothelial cells with a special focus on cellular uptake and the resulting pro-inflammatory and toxic events. Therefore, two representative endothelial cell lines were used as model systems: Human immortalized hCMEC/D3 cells were used as well characterized cell culture model, which preserves typical endothelial characteristics (Poller et al., 2008). It was shown previously to be an appropriate model to study cytokine signaling pathways (Fasler-Kan et al., 2010). In addition, commercially available primary human umbilical vein cells (HUVEC) were chosen as an alternative endothelial model. These primary cells are considered to be a frequently used model system to study endothelial function, oxidative stress and inflammation related pathways (Onat et al., 2011). It is important to note that both cell models were chosen based on their typical endothelial characteristics rather than their origin from a specific tissue. It should further be pointed out, that nanoparticles which come in contact with biological fluids containing proteins and lipids, will be covered by a biocorona (Docter et al., 2015). In present work, all cell-based experiments were carried out in presence of FCS to mimic physiological conditions encountered by nanoparticles in vivo (Setyawati et al., 2015). At present, it remains to be elucidated to which degree the biocorona might affect nanoparticle toxicity. For this study, an extended dose range of 10 ng/ml to 250 μg/ml was defined based on considerations presented in the section "Materials and methods". At present, no generally accepted guidelines for dosing of nanoparticles have been approved, which makes correct dosing for nanotoxicological studies a challenge.

SiNP were used as a well characterized model (Kettiger et al., 2015). These solid formulations have a spherical geometry and a uniform size (~110 nm) with a narrow size distribution (PDI. 0.2). Presence of a hydration layer in DLS experiments can explain the slight increase in measured particle size of particles that are analyzed in solution. As described in Table 1 the only apparent difference between the SiNPs used in the present study is their positive (~+20 mV) or negative (~−20 mV) zeta potential. Particle agglomeration was not observed based on TEM or DLS analysis in HEPES buffer. Agglomeration over time was observed in presence of FCS in DLS, yet TEM analysis revealed no statistically significant differences in actual particles size to SiNP incubated in absence of FCS (Table 1). Upon prolonged incubation with endothelial cells, both types of SiNPs bind to target cells and are internalized within 4 h. This endocytic process may result from electrostatic interactions of cationic particles with the negative surface charge of phospholipid cell membranes (Pekker and Shneider, 2015). By using confocal microscopy, we were able to show that SiNPs accumulated and aggregated in the vicinity of the nucleus after 24 h incubation (Fig. 1). This indicates that SiNP are readily taken up by endothelial cells however do not migrate into the nucleus. Following SiNP uptake there was an obvious decrease of intact actin filaments accompanied by the accumulation of dead cells (Weber and Menko, 2006). Both findings imply that SiNP exert acute toxicity on endothelial cell viability.

Concentration-dependent cytotoxicity of SiNPs was paralleled by formation of reactive oxygen species such as H_2O_2, NO^-, HO^-, ROO^- and $ONOO^-$. Dose-dependent effects were seen in both hCMEC/D3 as well as primary HUVEC. Incubations with SiNP + led to higher generation of ROS than SiNP −, which can either be attributed to enhanced particle uptake or the effect of charge-dependent cytotoxicity (Fig. 3). It is known that cationic particles are more prone to be cytotoxic than their anionic counterparts (Fröhlich, 2012). Significant oxidative stress levels could already be detected at SiNP concentrations of 10 μg/ml, suggesting that SiNP possess the potential to provoke cellular responses at low doses.

As we demonstrate in the present work, excess generation of ROS due to SiNP uptake is always followed by the cytotoxic events of apoptosis and/or necrosis in both hCMEC/D3 cells and HUVEC (Fig. 2). The dose- and time-dependent morphological cellular stages of apoptosis and necrosis were confirmed in flow cytometry experiments, where forward scatter and side scatter of laser light was used to discriminate between cell morphologies associated with apoptosis and necrosis (Krysko et al., 2008) (data not shown). In general, cellular

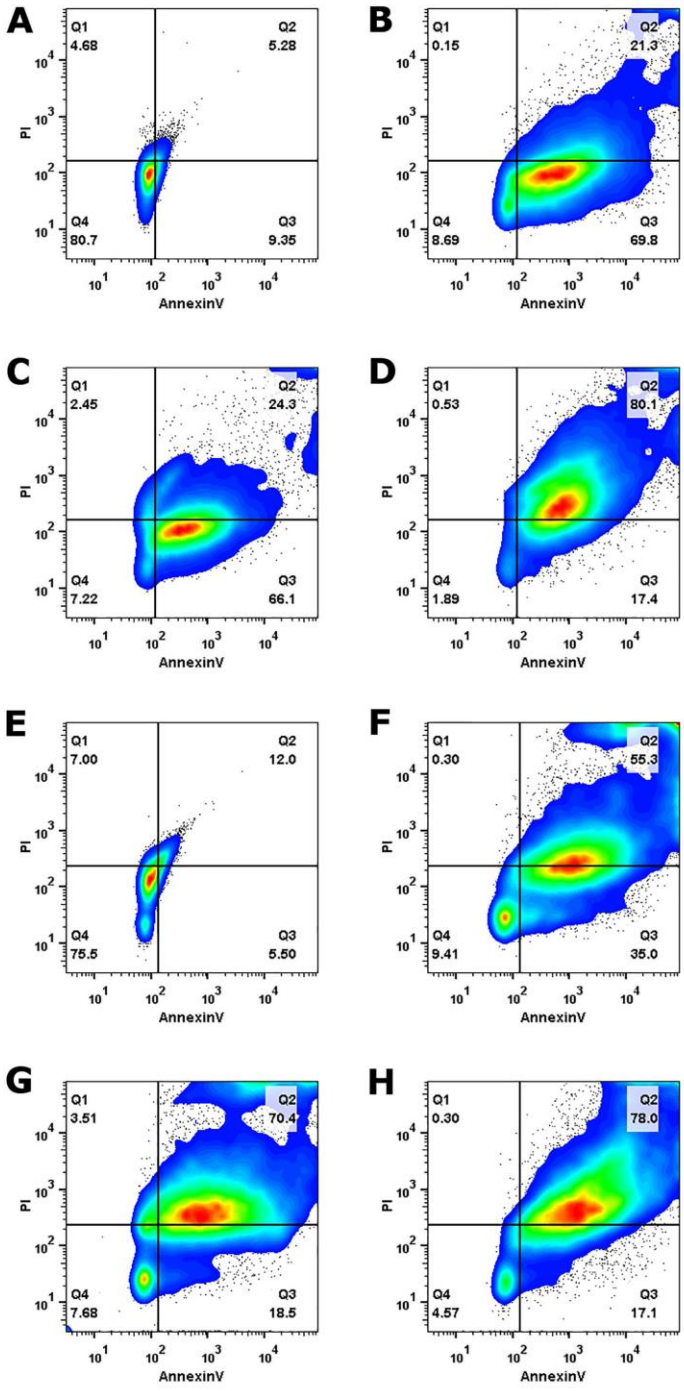

(caption on next page)

Fig. 2. Annexin V/PI staining and flow cytometry analysis of apoptotic and necrotic endothelial cells. Apoptosis and necrosis of hCMEC/D3 cells (A–D) and HUVEC (E–H) cells were induced by incubation for 24 h with SiNP. Cells were stained with Propidium Iodide (PI) and for Annexin V. Panel A and E: Negative control. Panel B and F: Positive control (1 µM staurosporin). Panel C and G: 250 µg/ml SiNP −. Panel D and H: 250 µg/ml SiNP +. Apoptotic cells (Annexin V positive/PI negative) populate the lower right quadrant of the pseudocolor FACS plot. Necrotic cells (Annexin V positive/PI positive) populate the upper right quadrant. Q-values shown for each quadrant designate the percentage of cells located in the respective quadrant. A statistical analysis is provided in Supplementary Table S1.

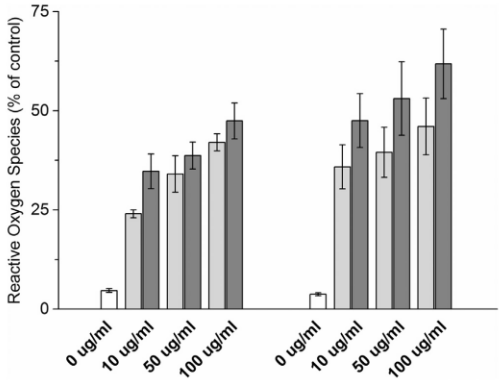

Fig. 3. Cellular generation of total reactive oxygen species (ROS). hCMEC/D3 cells were incubated with SiNP for 35 min. ROS generation was determined for SiNP − (light grey) and SiNP + (dark grey). Doses of 250 µg/ml could not be evaluated due to optical and adsorptive interference. White bar: untreated cells. Results are normalized to signals of the positive control (300 µM pyocyanin, 100% ± 15.3%). Values are means ± SD, n = 3.

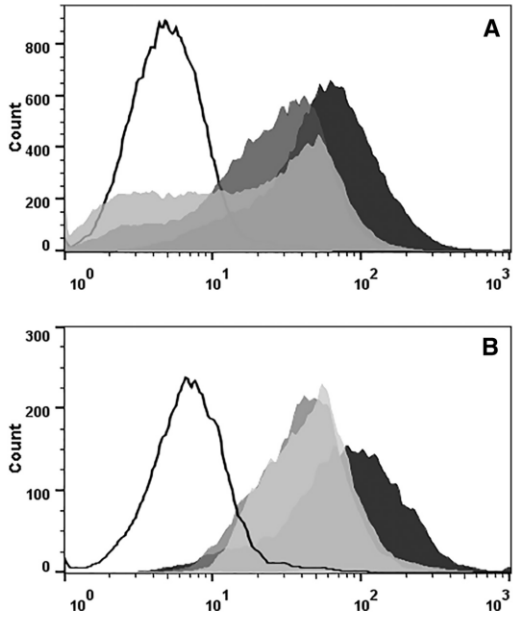

Fig. 4. SiNP mediated STAT1 activation. STAT1 activation was monitored by flow cytometry in hCMEC/D3 (A) and HUVEC (B). White histograms: Unstimulated cells (negative control). Black histograms: IFN–γ treated cells (positive control). Light grey histograms: stimulation by SiNP −. Dark grey histograms: stimulation by SiNP +. Concentrations of SiNP shown in this figure are 250 µg/ml and 100 µg/ml for hCMEC/D3 and HUVEC cells, respectively. Cells were incubated for 35 min prior to analysis. A statistical analysis is provided in Supplementary Table S2.

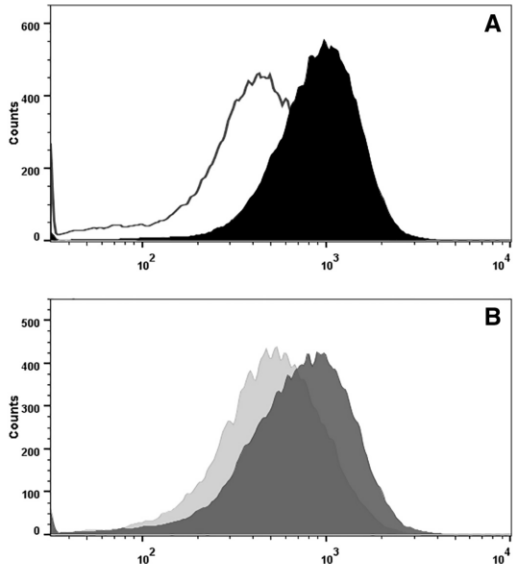

Fig. 5. Upregulation of MHC class I in response to SiNP treatment. MHC class I upregulation was monitored after 48 h incubation by flow cytometry in hCMEC/D3 cells. Results from the same experiment are shown with controls in panel A and incubations with SiNP in panel B. White histograms: Unstimulated cells (negative control). Black histogram: IFN–γ treated cells (positive control). Light grey histogram: stimulation by 10 ng/ml SiNP −. Dark grey histogram: stimulation by 10 ng/ml SiNP +. A statistical analysis is provided in Supplementary Table S3.

stress (Jiang et al., 2011; Naik and Dixit, 2011) and selective triggering of immune pathways are known to precede apoptosis and necrosis (Fleury et al., 2002; Kim and Lee, 2005). For example, Duan et al. (2013) could demonstrate interactions of SiNP with the Chk1-dependent G2/M checkpoint leading to DNA damage in HUVEC cells. More recently, Nakanishi et al. (2016) have stated that SiNP have the ability to trigger the production of pro-inflammatory cytokines in dendritic cells by activation of purinergic signaling. Other studies have demonstrated the interaction of ROS with the NF-κB pathway and the JAK/STAT pathway (Clempus and Griendling, 2006; Kim et al., 2013; Rada et al., 2011; Sharma et al., 2008) which are both essential pathways in inflammation and cell survival. Additionally ROS was found to trigger the activation of both NF-κB and the JAK/STAT pathway (Imran and Lim, 2013; Wu et al., 2011). We therefore analyzed the activation of these signaling pathways, along with the modulation of the major histocompatibility complex (MHC), following cellular exposures with SiNPs. NF-κB, STAT3, STAT6 and MHC class II did not seem to be significantly affected in HUVEC and hCMEC/D3 upon SiNP exposure (data not shown). However, we were able to observe significant activation of STAT1 (Fig. 4) and modulation of MHC class I (Fig. 5). Interestingly, MHC class I was upregulated in hCMEC/D3 cells at very low particle concentrations in the ng/ml range only, while HUVEC cells did not seem to be affected in terms of MHC modulation. This phenomenon may indicate that sub-acute doses of nanoparticles are able to cause interferences with cellular signaling. This may lead to weak and persisting adverse effects rather than immediate and acute

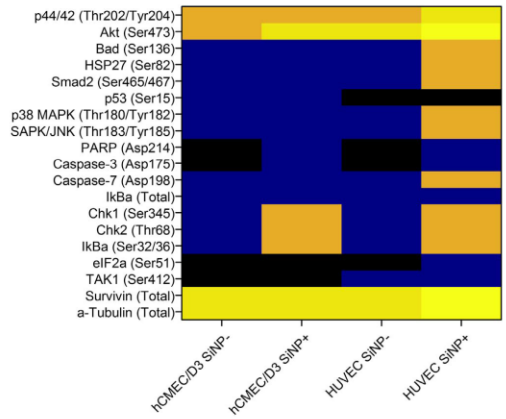

Fig. 6. PathScan analysis of cellular stress and apoptosis signaling molecules. The heatmap shows signals of 19 signaling molecules in rows and the corresponding treatment and cell lines in columns. Colors represent relative signal intensities as compared to untreated cells. Signals increase from black (< 5-fold increase) to blue (5-fold increase) to orange (15-fold increase) to yellow (50-fold increase) to bright yellow (≥ 100-fold increase). Level of significance of $p < 0.05$ as compared to untreated cells ($n = 8$ measurements) is met by all orange and yellow fields. A statistical analysis is provided in Supplementary Table S4. (For interpretation of the references to color in this figure legend, the reader is referred to the web version of this article.)

toxicity. Furthermore, concentration-dependent STAT1 activation by SiNPs was demonstrated in both hCMEC/D3 and HUVEC cells, whereas the latter showed stronger responses. Cellular uptake of SiNPs and generation of ROS was thus paralleled by STAT1 activation providing circumstantial evidence that these events are linked. Isolated pathways could not be further studied since ROS production under our assay conditions could not be completely blocked using inhibitors such as *N*-acetyl-L-cysteine (data not shown). To further confirm that the events of pathway activation, ROS generation, and cell death are nevertheless closely related, we monitored 19 individual signaling molecules involved in regulating ROS stress response and apoptosis (Fig. 6). We were able to show that kinases promoting cell survival (p44/42 MAPK ERK1/2) are activated upon SiNP treatment. Simultaneously, survival mediators such as apoptosis inhibitor-molecules (Akt, Survivin) are upregulated as a defensive response to SiNP treatment after 35 min incubations. In addition, significant signals related to inflammation and apoptosis (i.e. Smad2, p38 MAPK and SAPK/JNK) but also to STAT1 triggering could be detected as well (Kim and Lee, 2005; Solovyan and Keski-Oja, 2005; Wada and Penninger, 2004). These events precede upregulation of heat shock proteins (HSP27), apoptotic signaling markers (Chk1, Chk2, Bad, and Caspase-7), and NF-κB inhibition factors (IκBα) in HUVEC cells. In summary, this provides preliminary information on downstream signaling events linked to cellular stress (Batulan et al., 2016; Matt and Hofmann, 2016; Tang et al., 2013). Here again, HUVEC cells seem to be more sensitive towards SiNP uptake than hCMEC/D3 cells, suggesting that hCMEC/D3 signaling responses to SiNP treatments are slightly delayed due to slower uptake and onset of toxicity of SiNP in hCMEC/D3.

5. Conclusion

In summary, the presented work demonstrates that spherical SiNP induce intracellular ROS generation and induce cellular stress, apoptosis, and necrosis in a dose- and time-dependent manner in human cerebral microvascular endothelial cells (hCMEC/D3). Moreover, cationic SiNP show more severe cytotoxic effects than their anionic counterparts. These findings were confirmed in primary HUVEC cells, also showing their higher sensitivity to SiNP uptake than hCMEC/D3 cells throughout the study. Here, we demonstrate for the first time that SiNPs with both positive and negative zeta potentials can selectively activate the JAK/STAT signaling pathway. In addition, we also show that SiNP + have the potential to modulate MHC class I protein expression in hCMEC/D3 cells at very low doses. Hence, we conclude that SiNPs are capable of selectively triggering inflammatory signaling pathways in endothelial cells. Cellular damage leading to apoptosis and necrosis can be assumed to be the result of a complex interplay between ROS generation, cellular stress, modulation of MHC class I molecules and expression of the transcription factor STAT1. In view of the widespread use of SiNPs for biomedical applications, further mechanistic studies have to be conducted to clarify the exact mode of action leading to the toxic impact of these particles on a cellular level.

Declaration of interest

The authors have no conflicts in interest to declare.

Transparency document

The http://dx.doi.org/10.1016/j.tiv.2017.05.002 associated with this article can be found, in online version.

Acknowledgement

This work was supported by grants from the Swiss Center for Applied Human Toxicology (SCAHT) and the NanoReg2 Program (European Union Horizon 2020 research agreement 646221, 15.0200-3). Financial support from the Swiss National Science Foundation (grant 31003A_173057) provided to Dr. Helene Kettiger is gratefully acknowledged. We thank Dr. Susanne Schenk for technical assistance. Support of Dr. Daria Potashnikova (FACS analysis), Dr. Gabriela Québatte (U-SAXS analysis), Dr. Fabiola Porta (support with nanoparticle synthesis), and Dr. Christian Ruiz (microarray analysis) is acknowledged.

Appendix A. Supplementary data

Supplementary data to this article can be found online at http://dx.doi.org/10.1016/j.tiv.2017.05.002.

References

Ambrogio, M.W., Thomas, C.R., Zhao, Y.-L., Zink, J.I., Stoddart, J.F., 2011. Mechanized silica nanoparticles: a new frontier in theranostic nanomedicine. Acc. Chem. Res. 44, 903–913. http://dx.doi.org/10.1021/ar200018x.

Arap, W., Pasqualini, R., Montalti, M., Petrizza, L., Prodi, L., Rampazzo, E., Zaccheroni, N., Marchiò, S., 2013. Luminescent silica nanoparticles for cancer diagnosis. Curr. Med. Chem. 20, 2195–2211.

Baek, S., Singh, R.K., Khanal, D., Patel, K.D., Lee, E.-J., Leong, K.W., Chrzanowski, W., Kim, H.-W., 2015. Smart multifunctional drug delivery towards anticancer therapy harmonized in mesoporous nanoparticles. Nano 7, 14191–14216. http://dx.doi.org/10.1039/C5NR02730F.

Batulan, Z., Pulakazhi Venu, V.K., Li, Y., Koumbadinga, G., Alvarez-Olmedo, D.G., Shi, C., O'Brien, E.R., 2016. Extracellular release and signaling by heat shock protein 27: role in modifying vascular inflammation. Front. Immunol. 7, 285. http://dx.doi.org/10.3389/fimmu.2016.00285.

Blaise, C., Gagné, F., Férard, J.F., Eullaffroy, P., 2008. Ecotoxicity of selected nanomaterials to aquatic organisms. Environ. Toxicol. 23, 591–598. http://dx.doi.org/10.1002/tox.20402.

Blechinger, J., Bauer, A.T., Torrano, A.A., Gorzelanny, C., Bräuchle, C., Schneider, S.W., 2013. Uptake kinetics and nanotoxicity of silica nanoparticles are cell type dependent. Small 9, 3970–3980. http://dx.doi.org/10.1002/smll.201301004.

Branda, F., Silvestri, B., Luciani, G., Costantini, A., 2007. The effect of mixing alkoxides on the Stöber particles size. Colloids Surf. A Physicochem. Eng. Asp. 299, 252–255. http://dx.doi.org/10.1016/j.colsurfa.2006.11.048.

Chia, S.L., Tay, C.Y., Setyawati, M.I., Leong, D.T., 2015. Biomimicry 3D gastrointestinal spheroid platform for the assessment of toxicity and inflammatory effects of zinc oxide nanoparticles. Small 11, 702–712. http://dx.doi.org/10.1002/smll.201401915.

Cho, M., Cho, W.-S., Choi, M., Kim, S.J., Han, B.S., Kim, S.H., Kim, H.O., Sheen, Y.Y.,

Jeong, J., 2009. The impact of size on tissue distribution and elimination by single intravenous injection of silica nanoparticles. Toxicol. Lett. 189, 177–183. http://dx.doi.org/10.1016/j.toxlet.2009.04.017.
Clemments, A.M., Botella, P., Landry, C.C., 2015. Protein adsorption from biofluids on silica nanoparticles: corona analysis as a function of particle diameter and porosity. ACS Appl. Mater. Interfaces 7, 21682–21689. http://dx.doi.org/10.1021/acsami.5b07631.
Clempus, R.E., Griendling, K.K., 2006. Reactive oxygen species signaling in vascular smooth muscle cells. Cardiovasc. Res. 71, 216–225. http://dx.doi.org/10.1016/j.cardiores.2006.02.033.
Coti, K.K., Belowich, M.E., Liong, M., Ambrogio, M.W., Lau, Y.A., Khatib, H.A., Zink, J.I., Khashab, N.M., Stoddart, J.F., 2009. Mechanised nanoparticles for drug delivery. Nano 1, 16–39. http://dx.doi.org/10.1039/B9NR00162J.
Docter, D., Strieth, S., Westmeier, D., Hayden, O., Gao, M., Knauer, S.K., Stauber, R.H., 2015. No king without a crown—impact of the nanomaterial-protein corona on nanobiomedicine. Nanomedicine 10, 503–519. http://dx.doi.org/10.2217/nnm.14.184.
Duan, J., Yu, Y., Li, Y., Yu, Y., Li, Y., Zhou, X., Huang, P., Sun, Z., 2013. Toxic effect of silica nanoparticles on endothelial cells through DNA damage response via Chk1-dependent G2/M checkpoint. PLoS One 8, e62087. http://dx.doi.org/10.1371/journal.pone.0062087.
Fadeel, B., 2012. Clear and Present danger? Engineered nanoparticles and the immune system [WWW Document]. Swiss Med. Wkly. http://blog.smw.ch/ (accessed 5.11.16).
Fasler-Kan, E., Suenderhauf, C., Barteneva, N., Poller, B., Gygax, D., Huwyler, J., 2010. Cytokine signaling in the human brain capillary endothelial cell line hCMEC/D3. Brain Res. 1354, 15–22. http://dx.doi.org/10.1016/j.brainres.2010.07.077.
Fasler-Kan, E., Barteneva, N.S., Ketterer, S., Wunderlich, K., Reschner, A., Nurzhanova, A., Flammer, J., Huwyler, J., Meyer, P., 2013. Human cytokines activate JAK–STAT signaling pathway in porcine ocular tissue. Xenotransplantation 20, 469–480. http://dx.doi.org/10.1111/xen.12070.
Fleury, C., Mignotte, B., Vayssière, J.-L., 2002. Mitochondrial reactive oxygen species in cell death signaling. Biochimie 84, 131–141. http://dx.doi.org/10.1016/S0300-9084(02)01369-X.
Fröhlich, E., 2012. The role of surface charge in cellular uptake and cytotoxicity of medical nanoparticles. Int. J. Nanomedicine 7, 5577–5591. http://dx.doi.org/10.2147/IJN.S36111.
Georgieva, J.V., Kalicharan, D., Couraud, P.-O., Romero, I.A., Weksler, B., Hoekstra, D., Zuhorn, I.S., 2011. Surface characteristics of nanoparticles determine their intracellular fate in and processing by human blood–brain barrier endothelial cells in vitro. Mol. Ther. 19, 318–325. http://dx.doi.org/10.1038/mt.2010.236.
Giovanni, M., Yue, J., Zhang, L., Xie, J., Ong, C.N., Leong, D.T., 2015. Pro-inflammatory responses of RAW264.7 macrophages when treated with ultralow concentrations of silver, titanium dioxide, and zinc oxide nanoparticles. J. Hazard. Mater. 297, 146–152. http://dx.doi.org/10.1016/j.jhazmat.2015.04.081.
Guarnieri, D., Sabella, S., Muscetti, O., Belli, V., Malvindi, M.A., Fusco, S., De Luca, E., Pompa, P.P., Netti, P.A., 2014. Transport across the cell-membrane dictates nanoparticle fate and toxicity: a new paradigm in nanotoxicology. Nano 6, 10264–10273. http://dx.doi.org/10.1039/C4NR02008A.
Imran, M., Lim, I.K., 2013. Regulation of Btg2/TIS21/PC3 expression via reactive oxygen species–protein kinase C–NFκB pathway under stress conditions. Cell. Signal. 25, 2400–2412. http://dx.doi.org/10.1016/j.cellsig.2013.07.015.
Jiang, F., Zhang, Y., Dusting, G.J., 2011. NADPH oxidase-mediated redox signaling: roles in cellular stress response, stress tolerance, and tissue repair. Pharmacol. Rev. 63, 218–242. http://dx.doi.org/10.1124/pr.110.002980.
Kettiger, H., Schipanski, A., Wick, P., Huwyler, J., 2013. Engineered nanomaterial uptake and tissue distribution: from cell to organism. Int. J. Nanomedicine 8, 3255–3269. http://dx.doi.org/10.2147/IJN.S49770.
Kettiger, H., Sen Karaman, D., Schiesser, L., Rosenholm, J.M., Huwyler, J., 2015. Comparative safety evaluation of silica-based particles. Toxicol. in Vitro 30, 355–363. http://dx.doi.org/10.1016/j.tiv.2015.09.030.
Kim, H.S., Lee, M.-S., 2005. Essential role of STAT1 in caspase-independent cell death of activated macrophages through the p38 mitogen-activated protein kinase/STAT1/reactive oxygen species pathway. Mol. Cell. Biol. 25, 6821–6833. http://dx.doi.org/10.1128/MCB.25.15.6821-6833.2005.
Kim, H.J., Kim, C.-H., Ryu, J.-H., Kim, M.-J., Park, C.Y., Lee, J.M., Holtzman, M.J., Yoon, J.-H., 2013. Reactive oxygen species induce antiviral innate immune response through IFN-λ regulation in human nasal epithelial cells. Am. J. Respir. Cell Mol. Biol. 49, 855–865. http://dx.doi.org/10.1165/rcmb.2013-0003OC.
Kroll, A., Pillukat, M.H., Hahn, D., Schnekenburger, J., 2012. Interference of engineered nanoparticles with in vitro toxicity assays. Arch. Toxicol. 86, 1123–1136. http://dx.doi.org/10.1007/s00204-012-0837-z.
Krysko, D.V., Vanden Berghe, T., D'Herde, K., Vandenabeele, P., 2008. Apoptosis and necrosis: detection, discrimination and phagocytosis. Apoptosis 44, 205–221. http://dx.doi.org/10.1016/j.ymeth.2007.12.001.
Lee, S., Kim, M.-S., Lee, D., Kwon, T.K., Khang, D., Yun, H.-S., Kim, S.-H., 2013. The comparative immunotoxicity of mesoporous silica nanoparticles and colloidal silica nanoparticles in mice. Int. J. Nanomedicine 8, 147–158. http://dx.doi.org/10.2147/IJN.S39534.
Li, Z., Barnes, J.C., Bosoy, A., Stoddart, J.F., Zink, J.I., 2012. Mesoporous silica nanoparticles in biomedical applications. Chem. Soc. Rev. 41, 2590–2605. http://dx.doi.org/10.1039/C1CS15246G.
Lopez-Ramirez, M.A., Fischer, R., Torres-Badillo, C.C., Davies, H.A., Logan, K., Pfizenmaier, K., Male, D.K., Sharrack, B., Romero, I.A., 2012. Role of caspases in cytokine-induced barrier breakdown in human brain endothelial cells. J. Immunol. 189, 3130–3139. http://dx.doi.org/10.4049/jimmunol.1103460.
Marzaioli, V., Aguilar-Pimentel, J.A., Weichenmeier, I., Luxenhofer, G., Wiemann, M., Landsiedel, R., Wohlleben, W., Eiden, S., Mempel, M., Behrendt, H., Schmidt-Weber, C., Gutermuth, J., Alessandrini, F., 2014. Surface modifications of silica nanoparticles are crucial for their inert versus proinflammatory and immunomodulatory properties. Int. J. Nanomedicine 9, 2815–2832. http://dx.doi.org/10.2147/IJN.S57396.
Matt, S., Hofmann, T.G., 2016. The DNA damage-induced cell death response: a roadmap to kill cancer cells. Cell. Mol. Life Sci. 73, 2829–2850. http://dx.doi.org/10.1007/s00018-016-2130-4.
Naik, E., Dixit, V.M., 2011. Mitochondrial reactive oxygen species drive proinflammatory cytokine production. J. Exp. Med. 208, 417–420. http://dx.doi.org/10.1084/jem.20110367.
Nakanishi, K., Tsukimoto, M., Tanuma, S., Takeda, K., Kojima, S., 2016. Silica nanoparticles activate purinergic signaling via P2X7 receptor in dendritic cells, leading to production of pro-inflammatory cytokines. Toxicol. in Vitro 35, 202–211. http://dx.doi.org/10.1016/j.tiv.2016.06.003.
Napierska, D., Thomassen, L.C.J., Rabolli, V., Lison, D., Gonzalez, L., Kirsch-Volders, M., Martens, J.A., Hoet, P.H., 2009. Size-dependent cytotoxicity of monodisperse silica nanoparticles in human endothelial cells. Small 5, 846–853. http://dx.doi.org/10.1002/smll.200800461.
Nel, A., Xia, T., Mädler, L., Li, N., 2006. Toxic potential of materials at the nanolevel. Science 311, 622–627. http://dx.doi.org/10.1126/science.1114397.
Onat, D., Brillon, D., Colombo, P.C., Schmidt, A.M., 2011. Human vascular endothelial cells: a model system for studying vascular inflammation in diabetes and atherosclerosis. Curr. Diab. Rep. 11, 193–202. http://dx.doi.org/10.1007/s11892-011-0182-2.
Pekker, M., Shneider, M., 2015. Interaction between electrolyte ions and the surface of a cell lipid membrane. J. Phys. Chem. Biophys. 2015. http://dx.doi.org/10.4172/2161-0398.1000177.
Pietroiusti, A., Campagnolo, L., Fadeel, B., 2013. Interactions of engineered nanoparticles with organs protected by internal biological barriers. Small 9, 1557–1572. http://dx.doi.org/10.1002/smll.201201463.
Poller, B., Gutmann, H., Krähenbühl, S., Weksler, B., Romero, I., Couraud, P.-O., Tuffin, G., Drewe, J., Huwyler, J., 2008. The human brain endothelial cell line hCMEC/D3 as a human blood-brain barrier model for drug transport studies. J. Neurochem. 107, 1358–1368. http://dx.doi.org/10.1111/j.1471-4159.2008.05730.x.
Rada, B., Gardina, P., Myers, T.G., Leto, T.L., 2011. Reactive oxygen species mediate inflammatory cytokine release and EGFR-dependent mucin secretion in airway epithelial cells exposed to *Pseudomonas* pyocyanin. Mucosal Immunol. 4, 158–171.
Schmutz, H.-R., Detampel, P., Bühler, T., Büttler, A., Gygax, B., Huwyler, J., 2011. In vitro assessment of the formation of ceftriaxone–calcium precipitates in human plasma. J. Pharm. Sci. 100, 2300–2310. http://dx.doi.org/10.1002/jps.22466.
Setyawati, M.I., Tay, C.Y., Docter, D., Stauber, R.H., Leong, D.T., 2015. Understanding and exploiting nanoparticles' intimacy with the blood vessel and blood. Chem. Soc. Rev. 44, 8174–8199. http://dx.doi.org/10.1039/C5CS00499C.
Sharma, P., Chakraborty, R., Wang, L., Min, B., Tremblay, M.L., Kawahara, T., Lambeth, J.D., Haque, S.J., 2008. Redox regulation of interleukin-4 signaling. Immunity 29, 551–564. http://dx.doi.org/10.1016/j.immuni.2008.07.019.
Solovyan, V.T., Keski-Oja, J., 2005. Apoptosis of human endothelial cells is accompanied by proteolytic processing of latent TGF-[beta] binding proteins and activation of TGF-[beta]. Cell Death Differ. 12, 815–826.
Stevens, T., Garcia, J.G.N., Shasby, D.M., Bhattacharya, J., Malik, A.B., 2000. Mechanisms regulating endothelial cell barrier function. Am. J. Phys. Lung Cell. Mol. Phys. 279, L419–L422.
Stöber, W., Fink, A., Bohn, E., 1968. Controlled growth of monodisperse silica spheres in the micron size range. J. Colloid Interface Sci. 26, 62–69. http://dx.doi.org/10.1016/0021-9797(68)90272-5.
Tang, L., Cheng, J., 2013. Nonporous silica nanoparticles for nanomedicine application. Nano Today 8, 290–312. http://dx.doi.org/10.1016/j.nantod.2013.04.007.
Tang, J.-R., Michaelis, K.A., Nozik-Grayck, E., Seedorf, G.J., Hartman-Filson, M., Abman, S.H., Wright, C.J., 2013. The NF-κB inhibitory proteins IκBα and IκBβ mediate disparate responses to inflammation in fetal pulmonary endothelial cells. J. Immunol. Baltim. Md 1950 (190), 2913–2923. http://dx.doi.org/10.4049/jimmunol.1202670.
Tavakol, S., Hoveizi, E., Kharrazi, S., Tavakol, B., Karimi, S., Sorkhabadi, S.M.R., 2016. Organelles and chromatin fragmentation of human umbilical vein endothelial cell influence by the effects of zeta potential and size of silver nanoparticles in different manners. Artif. Cells Nanomed. Biotechnol.
Wada, T., Penninger, J.M., 2004. Mitogen-activated protein kinases in apoptosis regulation. Oncogene 23, 2838–2849. http://dx.doi.org/10.1038/sj.onc.1207556.
Weber, G.F., Menko, A.S., 2006. Actin filament organization regulates the induction of lens cell differentiation and survival. Dev. Biol. 295, 714–729. http://dx.doi.org/10.1016/j.ydbio.2006.03.056.
Weksler, B., Romero, I.A., Couraud, P.-O., 2013. The hCMEC/D3 cell line as a model of the human blood brain barrier. Fluids Barriers CNS 10, 16. http://dx.doi.org/10.1186/2045-8118-10-16.
Witzigmann, D., Sieber, S., Porta, F., Grossen, P., Bieri, A., Strelnikova, N., Pfohl, T., Prescianotto-Baschong, C., Huwyler, J., 2015. Formation of lipid and polymer based gold nanohybrids using a nanoreactor approach. RSC Adv. 5, 74320–74328. http://dx.doi.org/10.1039/C5RA13967H.
Wu, Y., Antony, S., Juhasz, A., Lu, J., Ge, Y., Jiang, G., Roy, K., Doroshow, J.H., 2011. Up-regulation and sustained activation of Stat1 are essential for interferon-γ (IFN-γ)-

induced dual oxidase 2 (Duox2) and dual oxidase A2 (DuoxA2) expression in human pancreatic cancer cell lines. J. Biol. Chem. 286, 12245–12256. http://dx.doi.org/10.1074/jbc.M110.191031.

Wu, X., Wu, M., Zhao, J.X., 2014. Recent development of silica nanoparticles as delivery vectors for cancer imaging and therapy. Nanomed. Nanotechnol. Biol. Med. 10, 297–312. http://dx.doi.org/10.1016/j.nano.2013.08.008.

Ye, D., Raghnaill, M.N., Bramini, M., Mahon, E., Aberg, C., Salvati, A., Dawson, K.A., 2013. Nanoparticle accumulation and transcytosis in brain endothelial cell layers. Nano 5, 11153–11165. http://dx.doi.org/10.1039/C3NR02905K.

Yildirimer, L., Thanh, N.T.K., Loizidou, M., Seifalian, A.M., 2011. Toxicology and clinical potential of nanoparticles. Nano Today 6, 585–607. http://dx.doi.org/10.1016/j.nantod.2011.10.001.

Yu, Y., Li, Y., Wang, W., Jin, M., Du, Z., Li, Y., Duan, J., Yu, Y., Sun, Z., 2013. Acute toxicity of amorphous silica nanoparticles in intravenously exposed ICR mice. PLoS One 8, e61346. http://dx.doi.org/10.1371/journal.pone.0061346.

Appendix

AnnexinV / PI analysis

Table S1 – statistical analysis of AnnexinV / PI flowcytometry assay (Figure 2). Analysis of variance (ANOVA) and Tukey's post-hoc test was performed to compare treated groups and the corresponding controls. Values denote the percentage of the cell population found in four different morphological states. Values marked with one asterisk (*): level of statistical significance $p < 0.05$ as compared to the respective negative controls (treatment with culture medium). Values marked with two asterisks (**): $p < 0.05$ as compared to the respective positive controls (treatment with staurosporin). Values are means ± standard deviation (n=3).

250 µg/ml Treatment	*Intact population*	*Apoptotic population*	*Necrotic population*	*Cell debris*
hCMEC/D3 + culture medium	80.43 ± 1.45	10.02 ± 1.98	5.42 ± 0.77	4.14 ± 0.49
hCMEC/D3 + SiNP-	8.69 ± 1.22 *	66.69 ± 5.27 *	21.38 ± 3.62 *	3.25 1.76
hCMEC/D3 + SiNP+	2.15 ± 0.61 *	17.76 ± 1.77 *	79.14 ± 2.81 **	0.91 0.49 *
hCMEC/D3 + staurosporin	8.67 ± 1.12 *	69.25 ± 4.94 *	21.10 ± 3.44 *	0.99 ± 0.69 *
HUVEC + culture medium	77.98 ± 1.97	7.57 ± 1.85	8.58 ± 2.60	5.91 ± 1.04
HUVEC + SiNP-	7.58 ± 1.44 *	21.22 ± 2.06 *	68.28 ± 1.63 **	2.96 ± 0.40 *
HUVEC + SiNP+	5.46 ± 0.67 *	15.70 ± 2.64 *	78.18 ± 2.60 **	0.63 ± 0.25 *
HUVEC + staurosporin	9.31 ± 1.42 *	38.16 ± 2.25 *	52.32 ± 2.75 *	0.20 ± 0.11 *

STAT1 analysis

Table S2 – statistical analysis of STAT1 activation assay (Figure 4). Analysis of variance (ANOVA) and Tukey's post-hoc test was performed to compare treated groups and the corresponding controls. Values are areas under the curve (AUC) as compared to negative control (cut off value: 95% percentile of negative control). Peak median values represent mean fluorescent intensity. Values marked with one asterisk (*): $p < 0.05$ as compared to the respective negative controls (treatment with culture medium). Values are means ± standard deviation (n=3).

Target	*STAT1 (250ug/ml)*	*Peak Median*
hCMEC/D3 + culture medium	5.25 ± 0.05	5.65 ± 0.95
hCMEC/D3 + SiNP-	57.30 ± 2.39 *	26.25 ± 9.87 *
hCMEC/D3 + SiNP+	74.63 ± 2.57 *	35.57 ± 12.58 *
hCMEC/D3 + staurosporin	91.90 ± 1.68 *	65.05 ± 12.02 *

Target	*STAT1 (100 ug/ml)*	*Peak Median*
HUVEC + culture medium	5.05 ± 0.25	8.67 ± 1.72
HUVEC + SiNP-	88.17 ± 2.16 *	43.20 ± 7.88 *
HUVEC + SiNP+	87.73 ± 1.81 *	45.07 ± 8.60 *
HUVEC + staurosporin	92.77 ± 1.51 *	72.10 ± 6.51 *

MHC class I analysis

Table S3 – statistical analysis of MHC class I modulation assay (Figure 5). Analysis of variance (ANOVA) and Tukey's post-hoc test was performed to compare treated groups and the corresponding controls. Values show the area under the curve (AUC) as compared to negative control (cut off value: 95% percentile of negative control). Peak median values represent mean fluorescent intensity. Values marked with an asterisk (*): $p < 0.05$ as compared to the respective negative controls (treatment with culture medium). Values are means ± standard deviation (n=3).

Target	*MHC class I (10ng/ml)*	*Peak Median*
hCMEC/D3 + culture medium	4.91 ± 0.25	409.00 ± 18.46
hCMEC/D3 + SiNP-	9.10 ± 1.55 *	469 ± 41.21
hCMEC/D3 + SiNP+	35.80 ± 3.23 *	738.67 ± 19.70 *
hCMEC/D3 + staurosporin	44.23 ± 2.90 *	892.33 ± 35.78 *

PathScan analysis

Table S4 – statistical analysis of PathScan assay (Figure 6). Analysis of variance (ANOVA) and Tukey's post-hoc test was performed to compare treated groups and the corresponding controls. Values denote x-fold increase of relative signal intensity (RSI) as compared to the respective negative controls. Values are means ± standard deviation (n=8). *: $p < 0.05$.

Target	hCMEC/D3 SiNP-	hCMEC/D3 SiNP+	HUVEC SiNP-	HUVEC SiNP+
p44/42 (Thr202/Tyr204)	26.6 ± 7.9 *	34.9 ± 4.3 *	29.4 ± 8.7 *	73.1 ± 9.8 *
Akt (Ser473)	38.8 ± 8.9 *	62.2 ± 4.4 *	50.3 ± 6.1 *	131.9 ± 9.7 *
Bad (Ser136)	6.7 ± 3.8	6.3 ± 1.2	7.8 ± 3.3	15.1 ± 2.8 *
HSP27 (Ser82)	6.6 ± 2.5	8.0 ± 2.2	8.7 ± 1.0	23.5 ± 6.6 *
Smad2 (Ser465/467)	7.3 ± 3.9	6.3 ± 0.9	8.4 ± 4.1	15.0 ± 4.5 *
p53 (Ser15)	5.3 ± 1.4	7.7 ± 3.1	1.1 ± 0.4	4.9 ± 2.0
p38 MAPK (Thr180/Tyr182)	8.5 ± 0.8	12.1 ± 2.5	8.7 ± 1.3	23.2 ± 5.8 *
SAPK/JNK (Thr183/Tyr185)	8.4 ± 0.6	12.0 ± 2.7	7.9 ± 1.3	22.5 ± 5.6 *
PARP (Asp214)	4.9 ± 1.2	6.9 ± 1.9	4.5 ± 1.3	12.0 ± 2.2
Caspase-3 (Asp175)	4.0 ± 1.0	7.6 ± 1.0	4.1 ± 0.9	12.4 ± 2.3
Caspase-7 (Asp198)	5.6 ± 0.4	8.2 ± 0.9	6.6 ± 1.2	17.9 ± 2.1 *
IκBα (Total)	9.6 ± 1.3	11.2 ± 2.8	5.0 ± 2.9	11.9 ± 5.7
Chk1 (Ser345)	11.0 ± 1.8	18.4 ± 1.1 *	7.1 ± 4.3	32.7 ± 1.9 *
Chk2 (Thr68)	10.5 ±1.1	18.8 ± 1.2 *	9.8 ± 1.7	36.4 ± 5.7 *
IκBα (Ser32/36)	9.2 ± 0.7	15.4 ± 1.5	10 ± 1.5	29.8 ± 4.3 *
eIF2α (Ser51)	1.5 ± 0.5	3.4 ± 0.7	1.6 ± 1.6	5.3 ± 1.9
TAK1 (Ser412)	3.5 ± 2.2	2.9 ± 2.5	6.0 ± 0.8	6.8 ± 5.9
Survivin (Total)	51.2 ± 4.8 *	67.1 ± 8.1 *	50.6 ± 5.9 *	103.7 ± 35.1 *
α-Tubulin (Total)	51.9 ± 3.4 *	66.2 ± 8.1 *	51.4 ± 6.1 *	107.0 ± 34.5 *

Full Paper

Macromolecular Journals

Macromolecular Bioscience

Immobilization of Enzymes on PLGA Sub-Micrometer Particles by Crosslinked Layer-by-Layer Deposition

Sandro Sieber, Stefan Siegrist, Stéphanie Schwarz, Fabiola Porta, Susanne H. Schenk, Jörg Huwyler*

Enzyme immobilization is of high interest for industrial applications. However, immobilization may compromise enzyme activity or stability due to the harsh conditions which have to be applied. The authors therefore present a new and improved crosslinked layer-by-layer (cLbL) approach. Two different model enzymes (acid phosphatase and β-galactosidase) are immobilized under mild conditions on biocompatible, monodisperse, sub-micrometer poly(lactide-*co*-glycolide) (PLGA) particles. The resulting PLGA enzyme systems are characterized regarding their size, surface charge, enzyme activity, storage stability, reusability, and stability under various conditions such as changing pH and temperature. The developed and characterized cLbL protocol can be easily adapted to different enzymes. Potential future uses of the technology for biomedical applications are discussed. PLGA-enzyme particles are therefore injected into the blood circulation of zebrafish embryos in order to demonstrate the in vivo stability and activity of the designed system.

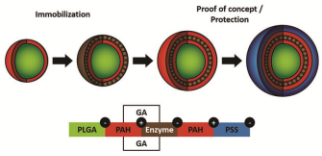

1. Introduction

Enzymes are increasingly used in industrial production due to their biocatalytic properties and potential. Examples include enantioselective production of active pharmaceutical ingredients[1] or the use of enzymes in food processing. The enzymatic treatment of milk, for example, results in lactose free milk products, which do not contain any residual lactose.[2,3] However, moderate chemical stability of many enzymes prevents their recovery from technical processes. This leads to high production costs and makes enzymes unsuitable for many applications.[4] In order to overcome these shortcomings, it was proposed to immobilize enzymes on surfaces or particles using different techniques. Through enzyme immobilization, different characteristics such as biological and chemical stability, kinetic properties, solubility and reusability can be improved. Today, a continuously growing number of immobilization techniques are available. They can mainly be divided into the immobilization on supports, entrapment, or crosslinking via the preparation of crosslinked enzyme aggregates (CLEAs) or crosslinked enzyme crystals (CLECs).[5]

Particles in the sub-micrometer range are ideal candidates for enzyme immobilization due to their high surface to volume ratio and therefore high enzyme loading capacity and the broad range of possible applications.[6] Despite the in most cases required preliminary activation of the underlying carrier and the specific reaction conditions, covalent attachment is still one of the most powerful methods for increasing enzyme stability upon immobilization.[4] However, most of these protocols require well defined and/or relatively harsh reaction conditions. As an alternative approach, physical adsorption

S. Sieber, S. Siegrist, S. Schwarz, Dr. F. Porta, Dr. S. H. Schenk, Prof. J. Huwyler
Division of Pharmaceutical Technology
Department of Pharmaceutical Sciences
University of Basel
Klingelbergstrasse 50, 4056 Basel, Switzerland
E-mail: joerg.huwyler@unibas.ch

DOI: 10.1002/mabi.201700015

based on electrostatic or hydrophobic/hydrophilic interactions can be used allowing enzymes to be adsorbed to the particle surface under mild conditions. The layer-by-layer (LbL) technique, which was already introduced in 1992 by Decher et al.,[7] offers a versatile and adaptable possibility to immobilize different enzymes on various carriers only based on their opposite electrostatic charge.[8] In this case, subsequent layers of polyelectrolytes and ionized enzymes are deposited on a solid support. The resulting "sandwich" configuration between electrolytes and enzymes allows for a high density of immobilized enzymes. A major drawback of this approach is the instability of the resulting carrier-enzyme systems resulting in enzyme desorption and the inability to wash and reuse enzyme-loaded particles.

In view of the shortcomings of both covalent and noncovalent coupling procedures, we present in this publication a novel crosslinked layer-by-layer (cLbL) immobilization technique. Combining covalent crosslinking and layer-by-layer deposition on sub-micrometer particles, the benefits of chemical and physical immobilization can both be exploited. This improved immobilization technique consists of a subsequent deposition of polyelectrolytes (PE) and enzymes on the surface of biodegradable (poly(lactide-*co*-glycolide)) (PLGA) particles using the layer-by-layer deposition technology. The coiled assembly of polyelectrolytes on the carrier facilitates multiple enzyme–PE interactions, which finally leads to an efficient and reproducible enzyme adsorption. Each PE–enzyme layer is subsequently stabilized by covalent crosslinking using glutaraldehyde (GA).[9] To this end, a PE with primary amino groups (i.e., poly(allylamine hydrochloride) (PAH)) was selected to allow for covalent crosslinking with amine groups present on enzymes. It was the goal of the present work to develop a cLBL enzyme immobilization technique and to demonstrate its applicability for industrial applications using two model enzymes (acid phosphatase and β-galactosidase). The established protocol can be adapted to different types of enzymes and allows for a fast and highly reproducible enzyme immobilization on sub-micrometer particles. Enzyme activity was monitored using colorimetric enzyme assays and Michaelis–Menten enzyme kinetics. Enzyme stability under stress conditions (i.e., storage, pH, and temperature), particle reusability, in vivo stability, and biocompatibility were investigated.

2. Experimental Section

2.1. Chemicals and Reagents

Acid phosphatase from potato (0.5–3.0 units mg^{-1}) (AP), β-galactosidase from *Aspergillus oryzae* (13.4 units mg^{-1}) (BGal), D-α-tocopherol polyethylene glycol 1000 succinate (DTPG), ethyl 3-aminobenzoate methane sulfonate (MS 222), halocarbon oil 27, 2-[4-(2-hydroxyethyl)piperazin-1-yl]ethanesulfonic acid (HEPES) buffer, paraformaldehyde, poly(allylamine hydrochloride) ($M_w \approx$15 000 or ≈17 500) (PAH), ester terminated poly(D,L-lactide-*co*-glycolide) (lactide:glycolide 65:35, M_w 40 000–75 000) (PLGA), poly(sodium 4-styrene sulfonate) ($M_w \approx$ 70 000) (PSS), *N*-phenylthiourea (PTU), NP-40, sodium deoxycholate, Tween 20 (polyoxyethylenesorbitan monolaurate), 2-mercaptoethanol, and 4-nitrophenol (4-NP) were purchased from Sigma-Aldrich (Sigma-Aldrich, Buchs, Switzerland). Dimethyl sulfoxide (DMSO), ethyl acetate, GA 50%, 5-Bromo-4-chlor-3-indoxyl-β-D-galactoside (X-β-Gal), potassium ferricyanide, potassium ferrocyanide, 2-nitrophenol-β-D-galactopyranoside (ONPG), 3-(4,5-dimethylthiazol-2-yl)-2,5-diphenyltetrazolium bromide (MTT), and 4-nitrophenylphosphate (4-NPP) were purchased from Carl Roth (Carl Roth GmbH, Karlsruhe, Germany). Agarose standard low was purchased from BioRad (BioRad, Hercules, CA). All other chemicals were of analytical grade and obtained from Merck, Darmstadt, Germany. Deionized water used for all experiments had a resistivity of 18.2 MΩ cm (Merck Millipore, Darmstadt, Germany). Activity of BGal was determined in citrate buffer (40×10^{-3} M citric acid, 60×10^{-3} M tri-sodium citrate, 1×10^{-3} M $MgCl_2$, 50×10^{-3} M 2-mercaptoethanol) at the indicated pH. If not differently noted, citrate buffers and H_2O used for particle enzyme preparation and enzyme activity assays contained 0.01% Tween 20 in order to prevent agglomeration and adsorption of processed PLGA particles on reaction container surfaces.

HEPG2 cells were cultured as described previously.[10] Primary human umbilical vein cells (HUVEC) and culture medium were from Provitro, Berlin, Germany. Primary HUVEC cells were cultured according to protocols of the supplier (Provitro, Berlin, Germany) and flasks or plates were coated with a 0.1 mg mL^{-1} rat tail collagen type 1 solution for enhanced monolayer formation. HEPG2 and HUVEC were used at passages 25–35 and passages 4–6 during MTT assays, respectively. 1% (v/v) penicillin/streptomycin was added to cell culture media.

Zebrafish embryo culture medium was prepared at final concentrations of 5×10^{-3} M sodium chloride, 0.25×10^{-3} M potassium chloride, 0.5×10^{-3} M magnesium sulfate, 0.15×10^{-3} M potassium dihydrogen phosphate, 0.05×10^{-3} M sodium phosphate dibasic, 0.5×10^{-3} M calcium chloride, 0.71×10^{-3} M sodium bicarbonate, 0.001% (w/v) methylene blue, pH 7.4.

Phosphate buffer used for all the X-β-Gal buffers was prepared at final concentrations of 23×10^{-3} M sodium phosphate monobasic, 77×10^{-3} M sodium phosphate dibasic, pH 7.3. X-β-Gal fixation buffer was prepared at a final concentration of 2% paraformaldehyde and 0.2% glutaraldehyde. X-β-Gal wash buffer was prepared at final concentrations of 2×10^{-3} M magnesium chloride, 0.02% sodium deoxycholate, and 0.02% NP-40. X-β-Gal staining buffer was prepared at final concentrations of 2×10^{-3} M magnesium chloride, 5×10^{-3} M potassium ferrocyanide, 5×10^{-3} M potassium ferricyanide, 0.02% sodium deoxycholate, 0.02% NP-40, and 1 mg mL^{-1} X-β-Gal.

2.2. PLGA Particle Preparation

PLGA particles were prepared as described previously.[11] Briefly, 100 mg of PLGA was solubilized in 1 mL of ethyl acetate overnight. The PLGA solution was added dropwise to 2 mL of a 0.3% (w/v) DTPG solution under vigorous agitation using a vortex

mixer. The emulsion was sonicated (three times for 10 s) in an ice water bath using a probe sonicator Sonifier 250 (Branson, Urdorf, Switzerland). The emulsion was diluted with 45 mL of a 0.3% (w/v) DTPG solution and stirred at 360 rpm for 3 h in order to fully evaporate the organic solvent. The resulting particles were washed three times by centrifugation using an Optima L-90K Ultracentrifuge (Beckman Coulter, Nyon, Switzerland) for 15 min at 17 000 × *g* and suspended in H_2O using a sonication bath. Particle concentration (mg mL^{-1}) in solution was determined by lyophilization of an aliquot (500 µL) of PLGA particles in H_2O. Particles were diluted to a final concentration of 2.85 mg mL^{-1} using H_2O.

2.3. Enzyme Immobilization

Following the new developed cLbL protocol, two different enzymes were separately immobilized on 0.5 mL of PLGA (2.85 mg mL^{-1}) particles. Subsequent layers of PAH, PSS, and GA crosslinked enzyme were deposited. In order to reach maximal enzyme adsorption, enzymes were always adsorbed onto an underlying layer of the opposite charged PE which was PAH in case of AP and PSS in case of BGal. For the particle layering with PEs, particles were incubated with 1 mL of 10 mg mL^{-1} PE (PAH in H_2O, PSS in citrate buffer pH 4.8) for 10 min on an orbital shaker using 1.5 mL plastic tubes. The excess of PEs was removed by centrifugation for 7 min at 10 000 × *g* followed by a washing step using 1 mL of H_2O or citrate buffer pH 4.8. Particles were resuspended by gentle sonication using a water bath sonicator (Sonorex; Bandelin, Berlin, Germany). For enzyme adsorption, PE layered PLGA particles were transferred into 4 mL glass vials and incubated with 1 mL of AP or BGal (5 or 20 mg mL^{-1}, respectively) in citrate buffer pH 4.8 for 15 min while stirred at 800 rpm. Thus, PLGA particles were loaded using an excess of enzyme under saturating conditions in order to minimize the time needed for enzyme adsorption. Covalent crosslinking of enzyme to PAH was performed by suspending a pellet of PE and enzyme layered PLGA particles in 1 mL GA (2.5%, v/v) in citrate buffer pH 4.8 followed by the same procedure as already described for the enzyme immobilization step. The excess of enzyme or GA was removed by centrifugation followed by three washing steps using 1 mL of citrate buffer pH 4.8. Particles were coated with two layers of GA crosslinked enzyme, in order to increase the amount of immobilized enzyme. As a proof of concept and to increased enzyme protection, PLGA particles coated with PEs and GA crosslinked enzyme were further coated with alternating layers of PEs. Five different types of cLbL particles were prepared. The composition of the particles is described using the following nomenclature: Using the model enzyme AP, PLGA PAH 2(AP GA) *x*(PAH PSS) particles were prepared and indicated as PLGA AP *x*PE, where *x* may adopt a value of 0, 1, or 2. Using BGal, corresponding particles were prepared, namely, PLGA PAH PSS 2(BGal GA) *x*(PAH PSS) and indicated as PLGA BGal *x*PE, where *x* may adopt a value of 0 or 1.

2.4. Characterization

Particle morphology and size were analyzed using a transmission electron microscopy (TEM) CM-100 Philips (FEI, Hillsboro, OR). Samples were stained on carbon coated copper grids using a 2% (w/v) uranyl acetate solution. Size and zeta potential of different PLGA enzyme particles were determined by dynamic light scattering (DLS) using a Delsa NanoC Particle Analyzer (Beckmann Coulter, Nyon, Switzerland). Size and zeta potential measurements of free enzymes at different pH values were carried out using a Zetasizer Nano ZSP and MPT-2 Multi-Purpose Titrator (Malvern, Herrenberg, Germany). All samples were measured in H_2O.

2.5. Michaelis–Menten Enzyme Kinetics

UV/vis spectroscopy was performed using a 96 well plate reader Spectramax M2^e (Molecular Devices, Sunnyvale, CA). All optical density measurements were carried out at a wavelength of 410 nm, using transparent 96 well plates and a sample volume of 200 µL.

Enzyme activity was determined according to Cooney.[12] One enzyme unit was defined as the amount of enzyme that hydrolyzes 1 µmol of its respective substrate per minute. All experiments were carried out at pH 4.8 since this represents the optimal working pH for both enzymes.

The Michaelis–Menten constant (K_m) and the maximum velocity (V_{max}) were determined as described in the following section. For AP, 50 µL of free or immobilized enzyme in citrate buffer pH 4.8 were incubated with 50 µL of 4-NPP in citrate buffer pH 4.8 with concentrations ranging from 0 to 8.5×10^{-3} M for 10 min at 37 °C and 700 rpm. The reaction was terminated by adding 100 µL of 1 M NaOH. In parallel, a blank of each sample was prepared by adding 50 µL of 4-NPP using the same concentration as mentioned above to a mixture of 50 µL free or immobilized enzyme in citrate buffer pH 4.8 and 100 µL 1 M NaOH. Samples and blanks were transferred to a 96 well plate and stored for 60 min at room temperature while slightly shaking in order to dissolve the PLGA particles. For BGal, 50 µL of free or immobilized enzyme in H_2O were incubated with 50 µL of ONPG in citrate assay 2× buffer pH 4.8 with concentrations ranging from 0 to 22×10^{-3} M for 10 min at 30 °C and 700 rpm. The reaction was terminated by adding 150 µL of 1 M sodium carbonate. In parallel, a blank of each sample was prepared by adding 50 µL of ONPG using the same concentration as mentioned above to a mixture of 50 µL free or immobilized enzyme in H_2O and 150 µL 1 M sodium carbonate. Samples and blanks were centrifuged for 7 min at 10 000 × *g*. In order to determine K_m and V_{max}, the model was fitted to the experimental data according to Equation (1). We observed an unspecific formation of background signal during the incubations due to chemical instability of the BGal substrate. This unspecific signal increased linearly over time and was subtracted from the experimental data. The Michaelis–Menten enzyme kinetics formula, adjusted for background signal, was defined as follows

$$V = \frac{V_{max} \times S}{S + K_M} - m \times S \quad (1)$$

where V_{max} = maximal velocity [µmol min^{-1} $unit^{-1}$], S = substrate concentration [µM], K_m = Michaelis–Menten constant [µM], and m = slope of unspecific background signal. Activity of enzymes was defined in terms of units, where one unit will hydrolyze 1.0 µmol of substrate per min under our assay conditions. Apparent enzyme efficiency E_{cat} was defined as V_{max}/K_M with units of [min^{-1} $unit^{-1}$].

2.6. Stress Test and Enzyme Stability

Enzyme activity was determined as described above under different stress conditions. Remaining activities were calculated as a percentage of the initial activity from untreated enzyme samples under the same activity assay conditions. pH sensitivity was measured by incubation of free and immobilized enzyme under the indicated conditions. Prior to OD measurements, particles were removed from solution by centrifugation for 7 min at 10 000 × *g*.

Temperature stress tests were performed by incubation of free and immobilized enzymes at temperatures ranging from 30 to 80 °C for 10 min. Samples were allowed to cool down to room temperature for another 10 min. The temperature treated enzyme solution was mixed with its substrate at an enzyme saturating concentration. To test storage stability, samples of free and immobilized enzymes were stored for 30 d at 4 °C in 1.5 mL plastic tubes. Remaining activities were calculated as a percentage of the initial activity of freshly prepared samples.

2.7. Repeated Use

Samples of immobilized enzymes were tested regarding their reusability. Enzyme loaded particles where separated from the incubation mix by centrifugation for 7 min at 10 000 × *g*. The collected pellet was washed with 1 mL of 0.01% Tween 20 in H_2O (w/v) followed by another activity assay. Remaining activities were indicated as percentage of the first activity assay.

2.8. Toxicity

The MTT assay was used to determine cell viability upon nanoparticle incubation. This colorimetric assay monitors NAD(P)H-dependent oxidoreductase enzyme activity of viable cells. The tetrazolium dye MTT 3-(4,5-dimethylthiazol-2-yl)-2,5-diphenyltetrazolium bromide is thereby reduced to a water-insoluble and purple colored formazan. 96 well plates were coated with a 0.1 mg mL^{-1} rat tail collagen type 1 solution prior to primary HUVEC seeding. HEPG2 and HUVEC cells were transferred to 96 well plates (20 000 and 10 000 cells per well, respectively) and allowed to attach for 24 h prior to incubation for 24 h with PLGA AP PE and PLGA BGal PE particles (10 ng mL^{-1}, 100 ng mL^{-1}, 10 µg mL^{-1}, 50 µg mL^{-1}, 100 µg mL^{-1}, and 250 µg mL^{-1}), 20×10^{-6} M terfenadine in 0.1% DMSO (positive control) or blank culture medium (negative control). Formazan crystals were dissolved in dimethyl sulfoxide and optical density was measured at 570 nm.

2.9. Zebrafish In Vivo Stability

A volume of 2 nL free BGal (5.2 units mL^{-1}) in H_2O 0.01% Tween 20 (w/v), PLGA BGal particles (0.5 units mL^{-1}) in H_2O 0.01% Tween 20 (w/v), and H_2O 0.01% Tween 20 (w/v) as a negative control were injected into blood circulation via the Duct of Cuvier of zebrafish embryos 2 d post fertilization in order to assess in vivo stability of the prepared formulation. Zebrafish embryos were kept in zebrafish culture media at 28 °C and bleached with PTU 1 d post fertilization. Prior to injection, zebrafish embryos were anesthetized using tricaine methanesulfonate (MS222) and immobilized in 0.3 % (w/v) agarose followed by injection using a micromanipulator (Wagner Instrumentenbau KG, Schöffengrund, Germany), a pneumatic Pico Pump PV830 (WPI, Sarasota, FL), and a Leica S8AP0 microscope (Leica, Wetzlar, Germany). 30 min post injection, zebrafish embryos were removed from the agarose. They were euthanized, washed with 2 mL X-β-Gal wash buffer, and incubated overnight at 4 °C in 2 mL of X-β-Gal fixation buffer. Fixed zebrafish embryos were washed three times for 5 min using 2 mL X-β-Gal wash buffer followed by staining in 2 mL of X-β-Gal staining buffer at 37 °C for 8 h. Active β-galactosidase cleaves the β-glycosidic bond of 5-Brom-4-chlor-3-indoxyl-β-D-galactoside (X-β-Gal), which results in blue precipitates of the insoluble dye. Samples were analyzed using a Leica DM6000B microscope using a 10× magnification. Single pictures were combined to a composite overview picture using ImageJ v1.51 picture processing software (open source software). All animal experiments were carried out in accordance with Swiss legislation on animal welfare.

2.10. Statistics

Values are means of $n \geq 3$ independent sets of experiments ± standard deviation (SD). Treatment groups were compared by one-way analysis of variance and Tukey's post hoc test. Statistically significant differences ($p \leq 0.05$) were marked by an asterisk. Used software was Origin 9.1 (OriginLab, Northampton, MA).

3. Results

Spherical PLGA microparticles were coated with layers of GA crosslinked enzyme and PEs. The resulting PLGA AP *x*PE particles were visualized by transmission electron microscopy. Uncoated PLGA particles (Figure 1A1,A2) had a regular and flat surface. The surface of these PLGA particles gradually changed after the addition of one enzyme layer and crosslinking using glutaraldehyde (Figure 1B1,B2) followed by two layers of opposite charged polyelectrolytes (Figure 1C1,C2). Particles had a uniform size and morphology. Enzymes and polyelectrolytes were deposited on the particle surface in form of clusters of plaques.

Size and size distribution of PLGA-enzyme particles were measured by DLS as summarized in Table 1. A hydrodynamic diameter of 494 ± 43 nm of a monodisperse particle population (polydispersity index (PDI) 0.16 ± 0.04) was determined for uncoated PLGA particles. Additionally, PLGA particles were analyzed by DLS after storage in water at 4 °C for 11 months. No change of particle size or PDI was observed (size 492.7 nm; PDI 0.155). An increase in size was observed after enzyme immobilization and subsequent addition of one or two layers of PEs. All PLGA AP PE particle preparations were monodisperse as shown by a PDI below 0.2. PLGA BGal PE particles showed a slightly increased PDI below 0.3. The change of zeta potential (i.e., the electrokinetic potential at the slipping/shear plane of a colloid particle) of PLGA particles after the application of subsequent opposite charged

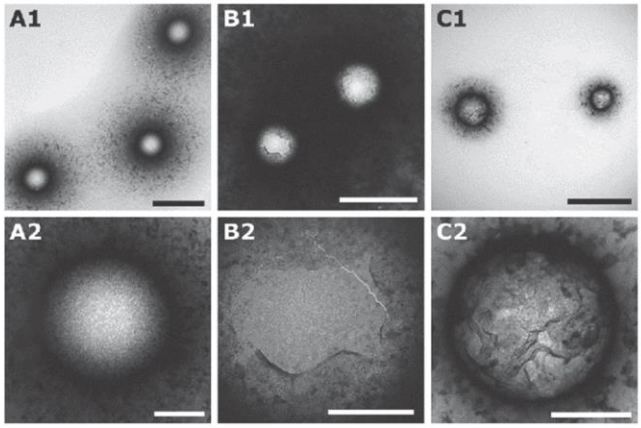

Figure 1. TEM analysis (negative staining) of uncoated PLGA particles (panels A1, A2), PLGA particles coated with acidic phosphatase (panels B1, B2), and PLGA particles coated with acid phosphatase and two layers of polyelectrolytes (panels C1, C2). Scale bars correspond to 1 µm (panels A1–C1) and 200 nm (panels A2–C2).

layers via the cLbL approach is presented in Figure 2. Bare PLGA particles showed a zeta potential around –40 mV. After addition of PAH, the zeta potential was raised to positive values. It should be noted that differences in the obtained zeta potential can be attributed to differences in molecular weight (chain length) of PAH used for the present studies (i.e., PAH of 15 000 g mol^{-1} for AP and PAH of 17 500 g mol^{-1} for BGal). Based on DLS measurements at different pH, the apparent isoelectric point of AP and BGal was estimated to be in the range of pH 4.2 and 6.4 under our assay conditions. AP and BGal are therefore negatively and positively charged at pH 4.8, respectively. Therefore, PLGA particles were layered with PAH (positively charged) or PSS (negatively charged), prior to enzyme immobilization. After enzyme immobilization, particles were coated with several layers of alternatingly charged polyelectrolytes to protect the bound enzymes. Successful layering was confirmed by the change of zeta potentials (Figure 2).

Table 1. Size and polydispersity index (PDI) of different PLGA-enzyme particles.

Enzyme	Particle	Size [nm]	PDI
–	PLGA	494.4 ± 43.2	0.156 ± 0.035
AP	PLGA AP	922.6 ± 5.4	0.175 ± 0.016
AP	PLGA AP PE	717.6 ± 18.5	0.172 ± 0.015
AP	PLGA AP 2 PE	764.9 ± 35.0	0.143 ± 0.069
BGal	PLGA BGal	635.8 ± 37.7	0.266 ± 0.017
BGal	PLGA BGal PE	648.7 ± 30.1	0.241 ± 0.012

PLGA particles carrying the two different immobilized enzymes acid phosphatase (AP) or β-galactosidase (BGal) and the indicated number of layers of polyelectrolytes (PE). Particles were analyzed using dynamic light scattering (DLS) ($n \geq 3$ experiments; values are means ± SD).

Free and immobilized enzymes were analyzed regarding their kinetic properties, which are summarized in Figure 3 and Table 2. In addition to the standard Michaelis–Menten constants, an apparent enzymatic efficiency (E_{cat}) was calculated. E_{cat} is defined as the ratio between V_{max} and K_M. In contrast to all formulations containing BGal (Table 2D–F), where no significant changes of kinetic properties were observed, formulations of AP (Table 2A–C) showed different values of K_m, V_{max}, and E_{cat}. An increased enzyme-substrate affinity was observed for both PLGA AP and PLGA AP PE as compared with free enzyme (Table 2). This was evident by a decreased K_m value. Taking into account concomitant changes of V_{max}, PLGA AP showed a 1.5 fold increased apparent enzymatic efficiency E_{cat}.

The different enzyme formulations were tested with respect to temperature and pH sensitivity, storage stability, and reusability. Immobilized AP did not show any changes regarding its temperature sensitivity when compared to free AP (Figure 4A). In contrast, immobilization of BGal on PLGA particles (Figure 4B) leads to an increased sensitivity toward elevated temperatures. Immobilized BGal did not show any improved stability against lower pH compared to free BGal (data not shown). However, the remaining activity of AP formulations increased with advanced states of immobilization after the pH of the reaction solution was reduced by one log unit. Compared with their activity at pH 4.8, the remaining activities of free AP, PLGA AP, and PLGA AP PE at pH 3.6 were 1.4% ± 0.1, 4.5% ± 0.2, and 13.0% ± 0.3, respectively. Comparing storage stability, free and immobilized formulations of AP possessed a remaining activity of around 60% after 30 d of storage irrespective of the used formulation (Figure 4C). BGal formulations retained almost 100% of their initial activity (Figure 4D). Enzymes were stored for 30 d at 4 °C. Reusability of enzymes was determined in terms of loss of activity during the course of five incubation and wash cycles (Figure 4E,F). These experiments were carried out with immobilized enzymes only since it is not possible to recover free enzyme from the incubation mix after the first activity determination. PLGA BGal particles kept around 80% of their initial activity after the fifth cycle of activity assays. A comparable result was

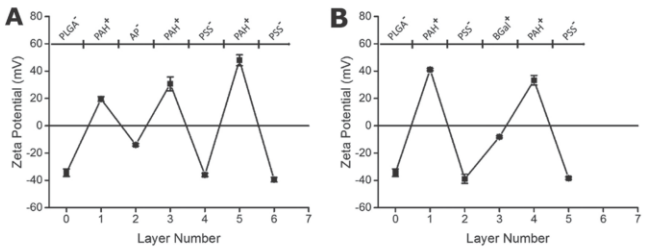

Figure 2. Alternating surface charge based on the cLbL immobilization approach of processed PLGA-enzyme particles. 0.15 mg mL^{-1} AP (panel A) or BGal (panel B) were immobilized on PLGA particles and further covered with the polyelectrolytes PAH and PSS according to the crosslinked layer-by-layer (cLbL) principle ($n \geq 3$ experiments; values are means ± SD).

obtained for PLGA AP particles, where around 65% of their initial activity was recovered.

To exclude a potential cellular toxicity of PLGA-enzyme particles, cell viability upon incubation was monitored in vitro using the HEPG2 and HUVEC cell lines. In Figure 5, the results of a 24 h 3-(4,5-dimethylthiazol-2-yl)-2,5-diphenyltertrazolium bromide (MTT) reduction assay are shown for both HEPG2 (Figure 5A) and HUVEC (Figure 5B). Up to a particle concentration of 100 μg mL^{-1} no statistically significant loss in cell viability could be seen. At the highest applied doses (250 μg mL^{-1}) of enzyme loaded particles only, a significant decrease in cell viability was observed.

The in vivo activity and stability of PLGA BGal particles was assessed in zebrafish embryos 2 d post fertilization (Figure 6). Two different staining patterns, obtained due to enzymatic formation of dark blue precipitates in vivo, were observed. Injection of free BGal resulted in a diffuse, faint and not localized color distribution whereas a dotted and localized staining pattern was obtained by injecting PLGA BGal particles. Particles seemed to accumulate within the posterior cardinal vein and the caudal vein. Zebrafish embryos were fixed and stained for BGal activity 30 min post intravenous injection of free or immobilized BGal into the Duct of Cuvier. There were no indications of acute toxicity (i.e., seizures, denaturation of tissue fluids or yolk, or heart failure) upon injection of enzyme or enzyme-loaded particles.

4. Discussion

The aim of this work was to develop and characterize an enzyme immobilization protocol (the cLbL protocol), which can be adapted to different particulate carriers and enzymes. Two our knowledge, this is the first time that different enzymes are immobilized on the surface of particles by a combination of both ionic interactions and covalent crosslinking using the same protocol. So far, combined coupling procedures were used only for industrial applications and coating of extended flat surfaces.[4] Our combined approach allowed us to immobilize enzymes by ionic interactions on PLGA particle surface and to subsequently stabilize the layered enzymes by covalent crosslinking under mild and nondestructive conditions. Loss of enzyme function (as often observed during crosslinking of enzymes using GA[13]) could be avoided, most probably

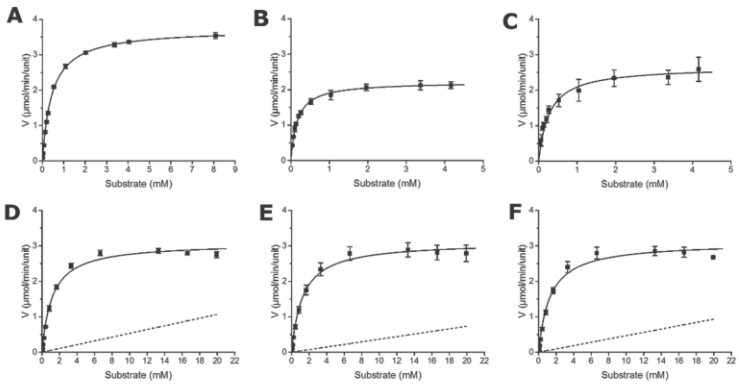

Figure 3. Enzyme kinetics of free and immobilized AP (panels A–C) and BGal (panels D–F). Michaelis–Menten enzyme kinetics of free AP (panel A), PLGA AP (panel B), PLGA AP PE (panel C), free BGal (panel D), PLGA BGal (panel E), and PLGA BGal PE (panel F). Solid lines: Fitted Michaelis–Menten kinetic model. Dotted lines: Subtracted background signal caused by unspecific conversion of educt. Values are means ± SD ($n \geq 3$).

Table 2. Michaelis–Menten kinetic parameters for free and immobilized AP and BGal.

Formulation	K_m [μM]	V_{max} [μmol min^{-1} unit^{-1}]	E_{cat} [min^{-1} unit^{-1}]
Free AP (A)	442.84 ± 28.96	3.73 ± 0.10	42.22 ± 1.62
PLGA AP (B)	165.80 ± 3.48	2.22 ± 0.12	66.84 ± 3.32
PLGA AP PE (C)	269.76 ± 17.66	2.66 ± 0.29	49.16 ± 3.15
Free BGal (D)	1151.36 ± 60.92	3.08 ± 0.07	10.73 ± 0.66
PLGA BGal (E)	1255.71 ± 16.03	3.11 ± 0.23	9.90 ± 0.75
PLGA BGal PE (F)	1361.03 ± 103.55	3.16 ± 0.20	9.33 ± 0.68

Kinetic parameters are calculated based on fitted experimental data ($n \geq 3$ experiments; values are means ± SD).

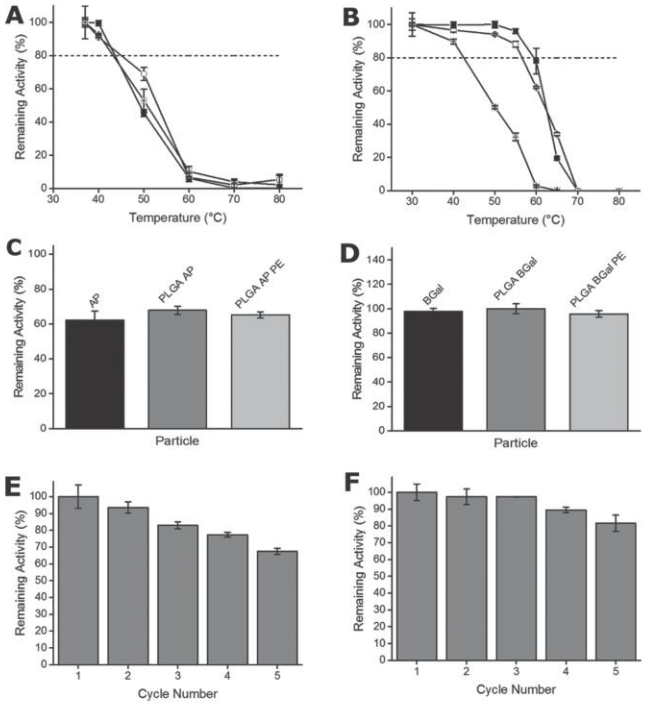

Figure 4. Stability tests of free and immobilized enzymes. Enzymatic activity of AP (panel A) and BGal (panel B) based formulations, which were kept for 10 min at the indicated temperature. Black squares: free enzyme, white circles: PLGA AP/BGal, asterisks: PLGA AP/BGal PE. Storage stability of free AP (panel C, black bar), PLGA AP (panel C, gray bar), PLGA AP PE (panel C, light gray bar), free BGal (panel D, black bar), PLGA BGal (panel D, gray bar), and PLGA BGal PE (panel D, light gray bar) after 30 d of storage at 4 °C. Reusability of PLGA AP (panel E) and PLGA BGal (panel F) as shown in terms of remaining activity after the indicated number of enzyme incubation and wash cycles. $n \geq 3$ experiments; values are means ± SD.

due to stabilization of enzymes in their active conformation prior to covalent linking. This approach can therefore be considered as a good alternative to enzyme immobilization via encapsulation, which often leads to unstable proteins.[14] Furthermore, enzyme leakage under changing pH conditions, which is one of the main drawbacks of physical enzyme adsorption,[15,16] did not occur.

The used enzymes acid phosphatase (AP) and β-galactosidase (BGal) carry opposite electrostatic charges under assay conditions demonstrating that anionic as well as cationic proteins can be immobilized by simple adjustment of the type and order of polyelectrolyte layers on the particle surface. Based on the isoelectric point and the enzymes natural working pH, the underlying particle can be layered either with an anionic or a cationic polyelectrolyte. Embedding the enzyme into polyelectrolytes provides a tridimensional network, which results in a much stronger enzyme adsorption compared to enzyme adsorption onto flat surfaces.[9] The extend of coating and thus the strength of electrostatic interactions was monitored by measuring the zeta potential of the particles. The usefulness and convenience of this analytical approach has already previously been recognized, but despite its importance there are very few protocols making use of it.[17] Adsorption of PSS always led to a surface charge of around –40 mV. PAH had a dual role: The addition of PAH to particles resulted in a strong positive surface charge[18] and the amino groups of PAH participated in crosslinking. The apparent isoelectric point of both enzymes of 4.2 and 6.4, respectively, was estimated by pH titration experiments combined with DLS size and zeta potential measurements (data not shown). Based on this result, the actual enzyme immobilization step was performed at pH 4.8 (activity assay condition for both enzymes) at which AP is negatively and BGal positively charged. The cLbL approach therefore allowed us to immobilize enzymes at their natural pH working conditions

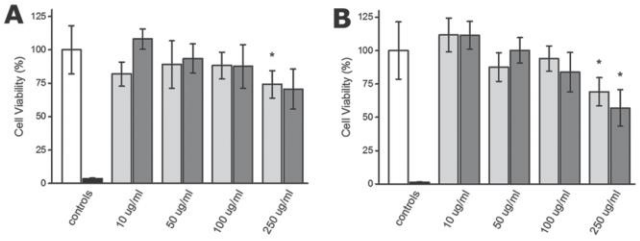

Figure 5. Cellular viability by the MTT assay. 24 h MTT viability testing for HEPG2 (panel A) and HUVEC cells (panel B) incubated with different concentrations of PLGA BGal PE (dark gray bars) and PLGA AP PE (light gray bars). Untreated cells were used as negative control (white bars, 100% viability). Positive control: 20×10^{-6} M terfenadine (black bars). Statistically significant differences as compared to 100% control are marked with an asterisk ($p > 0.05$).

where their active conformation is preserved.[19] In both cases, a change of the surface charge of carrier particles after enzyme addition was observed. Whereas the immobilization of AP completely changed the surface charge of the particle, the binding of BGal to the underlying particle was not sufficient to completely invert the zeta potential. Therefore, cationic PAH instead of anionic PSS was added on top of BGal in order to reach a positive zeta potential, which was required for addition of further PE layers.

PLGA, which is an extensively studied and Food and Drug Administration (FDA) approved polymer,[20,21] was used as the solid carrier for enzyme immobilization. PLGA particles were nonporous, monodisperse, and had a size in the sub-micrometer range. PLGA particle size was determined by DLS and TEM and a comparable diameter of around 500 nm was obtained. PLGA particle size can be tailored from a few to several thousand nanometers and therefore be adapted to the specific prerequisites of a given application.[22] From an industrial point of view, too small particles are difficult to recover from the reaction.[9] However, too big particles suffer from limited mass transport due to their decreased Brownian motion.[23] For the present study, relatively small particles were selected since they are characterized by a high surface to volume ratio resulting in a high enzyme loading capacity.[24] After the layering of AP and PEs on PLGA particles, DLS and TEM showed slightly different particle sizes. This can be explained by the dry state of the samples analyzed by TEM compared with the liquid state during DLS measurements. Whereas the solid PLGA particles are not influenced by these different states, the usually hydrated and fuzzy layers of strongly charged PEs[25] and enzymes dehydrate and therefore shrink under dry conditions.

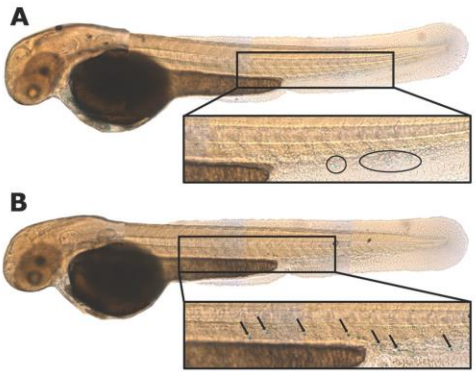

Figure 6. Enzymatic activity in vivo of PLGA BGal particles in the Zebrafish embryo. Free BGal (panel A) and PLGA BGal particles (panel B) were injected into the blood circulation of Zebrafish embryos via the Duct of Cuvier 2 d post fertilization. Arrows indicate areas of enzyme activity, which are characterized by formation of dark blue precipitates. Enzymatic activity was determined 30 min post injection.

The size of PLGA particles increased upon loading with enzymes. This is a consequence of particle aggregation due to a decrease in zeta potential from –40 mV to ≈0. Thus, the decrease in surface charge reduces electrostatic repulsion resulting in the reversible formation of particle aggregates.[26] After the addition of polyelectrolytes, however, the surface charge increased again leading (at least in the case of AP) to dismantling of aggregates.

Classic determination of kinetic parameters following the standard Michaelis–Menten kinetics was originally defined for homogenous systems ("well stirred compartments"), which is not necessarily applicable to nanoparticulate systems where phenomena such as mass diffusion limitations can occur. As a consequence, calculated K_m and V_{max} values of immobilized enzymes are approximations and cannot be compared to the corresponding parameters of free enzymes. Nevertheless, due to its simplicity and a lack of alternatives, the Michaelis–Menten model is, if properly used, still the accepted way for the comparison of kinetic parameters.[27] To validate the used enzyme assays, the activity of free AP and BGal was determined. The measured K_m values for both enzymes correspond to values published in literature.[28,29] Whereas kinetic parameters of free BGal did not change after immobilization, an improved catalytic efficiency of immobilized AP was observed. After immobilization of AP on PLGA particles, the affinity (i.e., K_M value) of AP toward its substrate 4-NPP was 2.5 fold increased and its V_{max} was slightly decreased. This resulted in an overall 1.5 fold increased apparent catalytic efficiency (E_{cat}). After covering the

immobilized AP with additional layers of PEs, the affinity and the V_{max} decreased but still remained on a higher level as compared to free AP. It is not uncommon to observe an increase in enzyme activity after immobilization. It has been suggested that stabilization of the active conformation or optimized orientation and exposure of the substrate binding site may be beneficial.[4,27] Substrate properties are another possible explanation for the observed changes of enzyme kinetics. 4-NPP, the substrate of AP, is zwitterionic and should therefore interact with the charged PE layer surrounding the enzyme. However, ONPG, the substrate of BGal, is not charged at assay conditions and therefore should only marginally be affected by the enzyme microenvironment.

Increased or unaltered enzyme activity does not have to go hand in hand with improved stability against elevated temperatures or changed pH conditions. BGal showed a decreased thermal stability after immobilization, which could be attributed to a decreased enzyme flexibility. This has previously been reported to be a key factor regarding thermal stability of enzymes.[30] In case of AP, an increased stability of the enzyme toward acidic reaction conditions was observed. It is tempting to speculate that PE act as a buffering system and thereby stabilize the pH of the enzyme microenvironment.[31] Both immobilized enzymes were, without any loss of activity, stored for 30 d at 4 °C and also their reuse with minor loss of activity was possible over at least five cycles of activity assays. This finding was surprising since previous reports by Ratzinger et al. indicated a 75% loss of enzyme activity when enzymes were stored under the same conditions as presented in this publication.[24] This advantage of high storage stability combined with good reusability of our novel cLBL approach is of high importance, especially regarding industrial applications.

The toxicity of PLGA enzyme PE preparations was assessed in two different cell lines. Human liver cancer cells (HEPG2) were used in order to represent the liver as the main organ of metabolism and nanoparticle accumulation. In order to assess nanoparticle safety upon injection, primary endothelial cells (HUVEC) were also incubated with increasing particle concentrations. No statistically significant effects were observed up to particle concentrations of 100 μg mL^{-1}, a dose which is accepted to represent physiologically relevant conditions.[10] Cell viability was significantly decreased only at the highest tested particle concentration of 250 μg mL^{-1}. Nevertheless, the results indicate a weak albeit potential toxicity of the tested formulations, which might be attributed to the two used polyelectrolytes PAH and PSS[8,32] or the crosslinking agent GA.

To get a first insight into stability and activity of PLGA based particles in vivo, zebrafish embryos were used as a relatively simple and easily accessible model system. Different nanoparticles such as liposomes, polystyrene beads, or PLGA have already been successfully tested in this vertebrate model.[33–35] There were no visible signs of acute toxicity upon injection. The subsequently applied staining for enzyme activity resulted in two distinct staining pattern. A diffusive blue color was obtained for free BGal whereas localized and defined blue dye precipitates resulted from PLGA BGal particles. We conclude that our particulate BGal enzyme formulation is active under in vivo conditions. The bright blue spots indicate that PLGA BGal particles remain stable and intact after injection for at least 30 min.

5. Conclusion and Outlook

During this study we developed and characterized a new and improved approach for enzyme immobilization. The described cLbL method is tunable and can be adopted to different enzymes based on their charge at a desired pH. Kinetic experiments revealed differences with respect to the apparent catalytic efficiency of the immobilized enzymes as compared to their unbound counterparts. While this parameter was unchanged or even increased for the tested enzymes, an extrapolation to other enzymes is difficult. However, the proposed test strategies offer the possibility to rapidly assess the performance of such systems. The present system shows a high stability and is therefore suited for industrial applications. In fact, stability of PLGA based particles can be adjusted from weeks to years depending on the ratio of lactic and glycolic acid.[20,36] However, future uses might as well include biomedical applications such as antigen immobilization on nanoparticulate carriers used for vaccination or immobilization of digestion enzymes like lactases or endopeptidases for the treatment of lactose intolerance or celiac disease.[37–39] Preliminary experiments in the zebrafish embryo model indeed demonstrate enzymatic activity in a biological environment (i.e., the blood circulation of a vertebrate). However, for such applications, the stability of the particulate carrier has to be reduced to ensure biotolerability. In addition, the used and potentially toxic crosslinking agent glutaraldehyde should be replaced by a biocompatible cross linking agent such as genipin.[40] Furthermore, the nonbiodegradable polymers PAH and PSS can be replaced by natural compounds such as alginates or chitosan.[41] Thus, the proposed cLbL protocol can be easily adopted for a broad range of applications.

Acknowledgements: The authors are thankful for the financial support of the "Stiftung zur Förderung des pharmazeutischen Nachwuchses in Basel" and the "Freiwillige Akademische Gesellschaft Basel," and declare no conflicts of interests. We thank the team of Prof. M. Affolter for providing zebrafish embryos.

Received: January 11, 2017; Revised: February 22, 2017; Published online: April 7, 2017; DOI: 10.1002/mabi.201700015

Keywords: crosslinking; enzyme immobilization; layer-by-layer; PLGA particles; zebrafish

[1] M. Kataoka, T. Miyakawa, S. Shimizu, M. Tanokura, *Appl. Microbiol. Biotechnol.* **2016**, *100*, 5747.
[2] Z. Grosová, M. Rosenberg, M. Rebros, M. Sipocz, B. Sedláčková, *Biotechnol. Lett.* **2008**, *30*, 763.
[3] Q. Husain, *Crit. Rev. Biotechnol.* **2010**, *30*, 41.
[4] C. Garcia-Galan, Á. Berenguer-Murcia, R. Fernandez-Lafuente, R. C. Rodrigues, *Adv. Synth. Catal.* **2011**, *353*, 2885.
[5] R. A. Sheldon, *Adv. Synth. Catal.* **2007**, *349*, 1289.
[6] S. Ding, A. A. Cargill, I. L. Medintz, J. C. Claussen, *Curr. Opin. Biotechnol.* **2015**, *34*, 242.
[7] G. Decher, J. D. Hong, J. Schmitt, *Thin Solid Films* **1992**, *210*, 831.
[8] O. S. Sakr, G. Borchard, *Biomacromolecules* **2013**, *14*, 2117.
[9] J. C. S. dos Santos, O. Barbosa, C. Ortiz, A. Berenguer-Murcia, R. C. Rodrigues, R. Fernandez-Lafuente, *ChemCatChem* **2015**, *7*, 2413.
[10] H. Kettiger, D. Sen Karaman, L. Schiesser, J. M. Rosenholm, J. Huwyler, *Toxicol. In Vitro Int. J. Publ. Assoc. BIBRA* **2015**, *30*, 355.
[11] R. L. McCall, R. W. Sirianni, *J. Vis. Exp. JoVE* **2013**, 51015, DOI:10.3791/51015.
[12] M. J. Cooney, *Methods Mol. Biol.* **2011**, *679*, 207.
[13] T. Haider, Q. Husain, *Int. J. Pharm.* **2008**, *359*, 1.
[14] W. Jiang, R. K. Gupta, M. C. Deshpande, S. P. Schwendeman, *Adv. Drug Delivery Rev.* **2005**, *57*, 391.
[15] O. Barbosa, C. Ortiz, Á. Berenguer-Murcia, R. Torres, R. C. Rodrigues, R. Fernandez-Lafuente, *RSC Adv.* **2013**, *4*, 1583.
[16] M. Hartmann, X. Kostrov, *Chem. Soc. Rev.* **2013**, *42*, 6277.
[17] J. M. Gómez, M. D. Romero, T. M. Fernández, E. Díez, *Bioprocess Biosyst. Eng.* **2012**, *35*, 1399.
[18] S. Chibowski, M. Knipa, *J. Dispersion Sci. Technol.* **2000**, *21*, 761.
[19] C. Mateo, J. M. Palomo, G. Fernandez-Lorente, J. M. Guisan, R. Fernandez-Lafuente, *Enzyme Microb. Technol.* **2007**, *40*, 1451.
[20] F. Danhier, E. Ansorena, J. M. Silva, R. Coco, A. Le Breton, V. Préat, *J. Controlled Release* **2012**, *161*, 505.
[21] H. K. Makadia, S. J. Siegel, *Polymers* **2011**, *3*, 1377.
[22] C. E. Astete, C. M. Sabliov, *J. Biomater. Sci. Polym. Ed.* **2006**, *17*, 247.
[23] H. Jia, G. Zhu, P. Wang, *Biotechnol. Bioeng.* **2003**, *84*, 406.
[24] G. Ratzinger, X. Wang, M. Wirth, F. Gabor, *J. Controlled Release* **2010**, *147*, 187.
[25] G. Decher, *Science* **1997**, *277*, 1232.
[26] J. Jiang, G. Oberdörster, P. Biswas, *J. Nanoparticle Res.* **2009**, *11*, 77.
[27] B. J. Johnson, W. Russ Algar, A. P. Malanoski, M. G. Ancona, I. L. Medintz, *Nano Today* **2014**, *9*, 102.
[28] S. Gargova, I. Pishtijski, I. Stoilova, *Biotechnol. Biotechnol. Equip.* **1995**, *9*, 47.
[29] C. Marzadori, C. Gessa, S. Ciurli, *Biol. Fertil. Soils* **1998**, *27*, 97.
[30] G. Feller, J. L. Arpigny, E. Narinx, C. Gerday, *Comp. Biochem. Physiol., Part A: Mol. Integr. Physiol.* **1997**, *118*, 495.
[31] E. Katchalski, I. Silman, R. Goldman, *Adv. Enzymol. Relat. Areas Mol. Biol.* **1971**, *34*, 445.
[32] E. Fröhlich, *Int. J. Nanomed.* **2012**, *7*, 5577.
[33] L. Evensen, P. L. Johansen, G. Koster, K. Zhu, L. Herfindal, M. Speth, F. Fenaroli, J. Hildahl, S. Bagherifam, C. Tulotta, *Nanoscale* **2016**, *8*, 862.
[34] F. Fenaroli, D. Westmoreland, J. Benjaminsen, T. Kolstad, F. M. Skjeldal, A. H. Meijer, M. van der Vaart, L. Ulanova, N. Roos, B. Nyström, *ACS Nano* **2014**, *8*, 7014.
[35] J. Yang, Y. Shimada, R. C. L. Olsthoorn, B. E. Snaar-Jagalska, H. P. Spaink, A. Kros, *ACS Nano* **2016**, *10*, 7428.
[36] T. G. Park, *Biomaterials* **1995**, *16*, 1123.
[37] S. A. Ansari, Q. Husain, *Biotechnol. Adv.* **2012**, *30*, 512.
[38] V. E. Bosio, G. A. Islan, Y. N. Martínez, N. Durán, G. R. Castro, *Crit. Rev. Biotechnol.* **2016**, *36*, 447.
[39] I. Caputo, M. Lepretti, S. Martucciello, C. Esposito, I. Caputo, M. Lepretti, S. Martucciello, C. Esposito, *Enzyme Res. Enzyme Res.* **2010**, *2010*, 2e174354.
[40] B. Manickam, R. Sreedharan, M. Elumalai, *Curr. Drug Delivery* **2014**, *11*, 139.
[41] J. Zhou, G. Romero, E. Rojas, L. Ma, S. Moya, C. Gao, *J. Colloid Interface Sci.* **2010**, *345*, 241.

Chapter III

Monitoring the biodistribution of metal-based nanoparticles in a small animal model by synchrotron radiation micro-tomography

Siegrist S.[1, †], Cörek E.[1, †], Bikis C.[2], Sieber S.[1], Fluder P.[1], Klados K.[1], Detampel P.[1], Puchkov M.[1], , Thalmann P.[2], Schulz G.[2], Alexiou Ch.[4], Müller B.[2], Huwyler J.[1,*]

[1]*Department of Pharmaceutical Technology, University of Basel, Klingelbergstrasse. 50, 4056 Basel, Switzerland;* [2]*Biomaterials Science Center, University of Basel, Gewerbestrasse 14, 4123 Allschwil, Switzerland;* [4]*Section for Experimental Oncology and Nanomedicine, Waldstraße 1,91054 Erlangen University of Erlangen, Germany*

[†]*These authors contributed equally to this study.*

**Correspondence: Prof. Jörg Huwyler, Pharmaceutical Technology, Pharmacenter, University of Basel, Klingelbergstrasse. 50, 4056 Basel, Switzerland. Tel: +41(0)612071513. E-mail: Joerg.huwyler@unibas.ch*

Keywords:
phase contrast x-ray micro-computer tomography, European Synchrotron Radiation Facility, superparamagnetic iron oxide nanoparticles, biodistribution, Zebrafish embryo,

Abstract

Engineered nanoparticles such as gold and superparamagnetic iron oxide nanoparticles are used contrast agents in cancer research. However, these engineered nanoparticles must be administered in high doses to gain significantly high contrast for the determination of their residence *in vivo*. Moreover, monitoring their biodistribution often implements the sectioning of the specimen making whole-body imaging impossible.

In order to achieve whole-body monitoring, a novel combination of *in* vivo model and analysis technique was implemented. Bare gold nanoparticles and human serum albumin coated superparamagnetic iron oxide nanoparticles were injected into 48 hours post fertilized zebrafish embryos and analyzed the biodistribution *in situ* by powerful phase contrast x-ray micro-computer tomography performed at the European Synchrotron Radiation Facility.

The gained results unveiled a procedure for detecting therapeutic doses of high-dense core engineered nanoparticles *in situ*. Visualization of nanoparticle biodistribution was achieved throughout the entire body in high resolution. To our knowledge this has not been shown in a comparable manner. Paramagnetic iron oxide nanoparticles were found to circulate through the embryo. Gold nanoparticles were not released into the bloodstream but remained in the vicinity of the injection site. The differences in visualized biodistributions of gold and iron oxide nanoparticles give insight into the importance of coating. Our findings demonstrate, that phase contrast imaging in combination with the zebrafish embryo model can be used to trace non-labeled nanoparticles in a non-invasive manner. Conclusively, the demonstrated results hold highly valuable benefits for nanotoxicological and medical research.

Introduction

Engineered nanoparticles (ENPs) are increasingly gaining attention as promising formulations for medical applications, especially in the field of imaging. Being able to monitor their biodistribution without any need of labelling provides crucial knowledge for risk assessment. While fluorescent and radioactive labelling is a common routine, the procedures are mostly based on the chemical alteration the ENP surface. This potentially changes the interaction patterns with biologic matter in comparison to those of the non-labelled medical nano-candidates significantly. Consequently, an appropriate risk assessment is not possible. In recent years commercial computer tomography (CT)[1] has been sought out as an alternative technique to trace ENP throughout a biological system by means of absorption[2,3]. In medical research, micro-computer-tomography (µCT) has been used to monitor the biodistribution of metal-based ENP *in vitro*, *ex vivo*, and *in vivo*[3–6] highlighting the feasibility of the method. Tietze et al.[7] used µCT to prove the concept of magnetic drug targeting of super-paramagnetic iron oxide nanoparticles (SPIONs). Furthermore, Chien et al.[8] used gold nanoparticles (AuNPs) as contrast agents for detection of cancer-related angiogenesis in mice and for kidney and tumor imaging[9]. In their work, Chien et al. furthermore successfully explored the implementation of powerful synchrotron radiation phase-contrast micro-computer-tomography (SRPµCT). This technique allows the discrimination of different materials based on their refractive index rather than their mass density. Therefore, SRPµCT provides higher contrast than commercial absorption contrast µCT and offers the determination of smaller structures or lesser amounts of material. Certain measures were taken in both studies to improve detection ENP. Tiezte et al administered 7 mg of SPIONs to an ex vivo system measuring 11 cm. Chien et al injected 200 µl of both AuNPs (15.5 mg/ml) and SPIONs (160mg/ml) into the femoral artery of mice that had been inoculated with tumor cells into the leg beforehand. Additionally, SRPµCT was performed on histological slices of the specimens rather than the entire animal. These actions were taken due to limitations in sample size and ENP doses. Applied ENP doses in both discussed studies were exceptionally high – with the exception of AuNPs used by Chien et al. – in order to increase their detection. Moreover, the main limiting factor for detecting ENP with SRPµCT is the distance between sample and scintillator[10], accounting for resolution and contrast. Hence the size of the sample should ideally be as small as possible. Due

to the size of common in vivo models however, the distance between sample and detector limits resolution and contrast to rather large ENP doses which could potentially be harmful to living organisms. Localizing medically relevant doses of nanoparticles in whole-body samples without using histological sectioning therefore still proves to be a major challenge. The combination of SRPμCT and the zebrafish model however, could finally solve this matter.

Zebrafish embryo as a new in vitro/in vivo model

The zebrafish embryo has been widely discussed as a veritable screening model for nanotoxicology. The vertebrate model features several benefits over commonly used in vivo models such as transparency, facilitated husbandry, small size (0.5-0.7 mm in diameter, 5-7 mm length[11]), and an immune system similar to humans[12].Moreover, incubation of the embryos with small molecules or nanoparticles is commonly done in occupational health research, proving the model to be suitable for toxicity studies[13–16]. Mircoinjections of these substances into a zebrafish embryo are routinely done into the Duct of Cuvier (DoC). The DoC is a temporary circulation channel (present until the first 72 hours post fertilization (hpf)) localized on both sides of the yolk sac that connects the heart to the dorsal aorta[17].

The goal of present work was to visualize the difference in biodistribution of gold nanoparticles (AuNPs) and superparamagnetic iron oxide nanoparticles (SPIONs) at low doses in whole zebrafish embryos using SRPμCT. AuNPs were synthesized according to the Turkevich method. SPIONs were provided from the University of Erlangen after being synthesized under GMP conditions[18]. Physico-chemical characterization of both AuNPs and SPIONs was done prior to in vivo experiments. To ensure that the injected ENP doses did not cause toxic effects, zebrafish embryo viability and malformation occurrence were monitored for 96 hours post injection (hpi) in preliminary experiments (supplementary table S5). Furthermore, bright field microscopy, commercial μCT, and histological sectioning were used in supplementary experiments to highlight the shortcomings of these visualization techniques for this study (supplementary information). Finally, *In situ* biodistribution analyses of both AuNPs and SPIONs were conducted with synchrotron radiation absorption contrast micro-computer-tomography (SRAμCT), and synchrotron radiation phase contrast micro-computer-tomography (SRPμCT). The results were analyzed to distinguish whether μCT techniques can provide relevant information on the biodistribution of low-

dosed non-labelled ENP upon injection. Furthermore, the results should prove that the zebrafish embryo is a powerful animal model for nanotoxicological risk assessment.

Materials and Methods

Synthesis of gold nanoparticles (AuNPs)

Gold nanoparticles were synthesized according to the Turkevich method[19]. In brief, trisodium citrate (170 mM, Fluka, Buchs, Switzerland) was added to boiling tetrachloroaurate (25 mM, Sigma-Aldrich, Buchs, Switzerland) in different ratios of 1:4 under constant stirring. After one minute, the typical color change from light-yellow over greyish-blue to ruby-red was observed. The dispersion was subsequently left to boil for an additional 15 minutes under constant stirring. Thereafter the dispersion was allowed to cool down to room temperature. The stable AuNP dispersion was transferred to brown glass vials and kept in the dark at 4.0° C for storage (detailed synthesis procedure and sample evaluation is described in the supplementary section of this work).

Synthesis of superparamagnetic iron oxide nanoparticles (SPIONs)

The superparamagnetic iron oxide nanoparticles (SPIONs) coated with lauric acid and human serum albumin ($SEON^{LA17HSA2}$) were synthesized by courtesy of Dr. Zaloga at the Friedrich-Alexander-University, Erlangen, Germany. Synthesis was done as described elsewhere [20]. For reasons of simplicity SEON particles are referred to as SPIONs throughout this study.

Physico-chemical characterization of nanoparticles

Analyses of particle size, hydrodynamic diameter, polydispersity index, and zeta potential of AuNPs and SPIONs were performed according to the procedure previously described elsewhere[21]. The methods used were differential and electrophoretic light scattering (DLS and ELS, Delsa Nano C Particle Analyzer, Beckman Coulter Inc., Nyon, Switzerland), and transmission electron microscopy (TEM, CM-100, Philips, Amsterdam, Netherlands). Physico-chemical characterization experiments were performed with in absence and presence of 5 % FCS containing medium.

Zebrafish barge culture

Experiments were conducted using the zebrafish wild type strain AB/Tübingen (AB/TU) and transgenic strain Tg(kdrl:EGFP). Adult zebrafish were kept in 20.0 L aerated tanks tempered to 28.0° C at a 10/14 hour light/dark cycle. Mating pairings were four females

and two males, and were carried out in breeding baskets. Eggs were collected the next morning, cleaned, sorted and transferred into petri dishes containing 25 ml 0.5X embryo-medium E2, which was prepared according to Sieber et al.[22] A maximum of 70 eggs were transferred into one petri dish and stored in an incubator (Aqualytic, Dortmund, Germany) at 28.0° C as long as they were not in use. E2 medium was renewed daily after egg sorting. Zebrafish embryos were dechorionated 24 hours post fertilization (hpf) by rupturing the chorion with two acupuncture needles (0.20x15 mm, Wandrey, Berlin, Germany) followed by careful extraction. Empty chorions were removed and E2 medium was renewed before placing the petri dishes back into the tempered zebrafish incubator (Aqualytic).

Nanoparticle microinjection

Nanoparticle microinjections were conducted according to the procedure described by Sieber et al.[22]. Injected nanoparticle volumes were 5 nl for AuNPs (3.3 mg/ml) and SPIONs (5.6 mg/ml). The exact fabrication of the injection needles as well as the procedure of keeping injection volumes consistent are described in detail in the supplementary section of this work.

Zebrafish euthanizing and fixation

For micro-tomography experiments embryos were first euthanized by being placed into 2.0 mL tricaine methanesulfonate stock 25 X (400.0 mg tricaine methanesulfonate, 97.9 mL water (Millipore 18-Ω), 2.1 mL trisaminomethane)) for 30 min. Subsequently, these embryos were fixed for one hour in 4.0 % paraformaldehyde (PFA) at one hour post injection (hpi). Thereafter, the fixed specimens were dehydrated by washing in ethanol with subsequently increasing concentrations (25.0 %, 50.0 %, 70.0 % and ≥ 99.8 %, Fluka) for 30 minutes each under constant shaking. The dehydrated zebrafish embryos could be stored in ethanol (≥ 99.8 %, Fluka) at 4.0° C for at least one week.

Sample preparation for x-ray scanning

Fixed zebrafish embryos were placed into the channel (diameter 0.8 mm) of a two-pieced, custom-made aluminum mold (3.0 cm x 2.0 cm x 2.0 cm). The embryo was air dried for one minute to ensure evaporation of any excess ethanol. Thereafter, the prepared mold was immersed vertically into liquid paraffin wax (80.0° C, Sigma-Aldrich, Buchs, Switzerland) allowing the channel containing the zebrafish embryo to fill with paraffin due to capillary forces. After a few minutes of cooling, the mold was opened and the paraffin rod containing the embedded embryo was removed with a blunt syringe. The paraffin rods were consequently stored at 4.0° C in the dark until further

use. Further information and results are found in the supplementary section of this work.

Synchrotron-based phase-contrast micro-computer-tomography (SRμCT)

Single-distance phase-contrast μCT was used for 3D visualization of nanoparticles injected into zebrafish embryos. The inline phase-contrast experiments were performed using a pco.edge 5.5 camera with a pixel size of 0.66 μm. In order to visualize the entire specimen, a maximum of two height steps per specimen were acquired. During the experiments, a pink beam with a mean photon energy of 19.5 keV was used. Due to its highly coherent beam, the required spatial resolution of the detector and the tomography instrumentation the experiments were carried out at the beamline ID19 at the European Synchrotron Radiation Facility in Grenoble, France.

Reconstruction of micro-tomograms

The synchrotron tomographic data from the ESRF was obtained in the European data format (EDF). Phase contrast information was introduced into projections with AnkaPhase (Version 2.1)[23] while performing flat-field and dark-field corrections. AnkaPhase is based on a single-distance non-iterative phase retrieval algorithm described by D. Paganin et al.[9]. Reconstruction of the single-slice images were generated by TomoPy, an open-source Python package for tomographic data processing and image reconstruction[9]. A delta-beta value of 1000 was used to obtain optimal contrast for the monitoring of the ENP. From the reconstructed single-slivce images, 3D reconstruction and processing was done by using the visualizing software VG STUDIO (Version 2.1, Volume Graphics GmbH, Heidelberg/Germany).

Statistical Analysis

Assay results are expressed as means of independent sets of experiments ± standard deviation (SD), $n \geq 3$. Wherever indicated, significance was determined by one-way analysis of variance (ANOVA). Tukey's post-hoc test was performed to compare the difference between the treated groups and the corresponding controls. Differences were considered to be significant at $p < 0.05$. Used software was Origin 9.1 (OriginLab, Northampton, MA).

Results

Characterization of engineered nanoparticles (SPIONs and AuNPs)

The physico-chemical properties particle size, hydrodynamic diameter, zeta potential, polydispersity index, and shape were measured for SPIONs and AuNPs. Analysis techniques used to perform characterization measurements were Differential Light Scattering (DLS), Electrophoretic Light Scattering (ELS), Transmission Electron Microscopy (TEM), and Ultra-small-angle X-Ray Scattering (U-SAXS). Furthermore, DLS measurements were carried out in presence and absence of 5 % FCS to monitor possible agglomeration behavior of the ENP. The obtained results are given in **Table 1**.

Table 1 – Characterization of engineered nanoparticles (ENPs). *Gold (AuNPs) and iron oxide (SPIONs) nanoparticles were characterized through differential light scattering (DLS), transmission electron microscopy (TEM), and ultra-small-angle x-ray scattering (U-SAXS). Hydrodynamic diameter, size, polydispersity index (PDI), and the electrokinetic potential (zeta potential) of the ENP were determined in purified water[1] and in 10 % FCS containing medium[2]. All experiments were done in three independent experiments(n=3). Details are given in the supplementary information section and supplementary tables S1 to S5.*

Engineered Nanoparticles	*Particle Size [nm] (TEM)*	*Hydrodynamic diameter [nm] (DLS)*	*PDI (DLS)*	*Zeta potential [mV] (DLS)*
AuNPs[1]	18.6 ± 4.6	29.6 ± 0.1	0.19 ± 0.2	-29.4 ± 0.8
SPIONs[1]	15.0± 3.7	61.0 ± 0.3	0.13 ± 0.01	-24.9 ± 1.0
AuNPs[2]	17.1 ± 3.9	94.9 ± 2.1	0.31 ± 0.5	-10.6 ± 0.9
SPIONs[2]	16.9 ± 3.3	60.7 ± 0.3	0.19 ± 0.02	-14.38 ± 0.9

Particle sizes of AuNPs and SPIONs dispersed in purified water were determined to be 18.6 ± 4.6 nm and 15.0 ± 3.7 nm, respectively. The corresponding hydrodynamic diameters were measured at higher values; 29.6 ± 0.1 for AuNPs and 61.0 ± 0.3 for SPIONs. Size distribution measurements yielded PDI values below 0.2 for both ENP formulations, when dispersed in purified water. Obtained zeta potentials of -29.4 ± 0.8 and -24.9 ± 1.0, were measured for AuNPs and SPIONs, respectively, in purified water at distinct pH 5.0. Hydrodynamic diameter and PDI values rose significantly in AuNP measurements containing FCS. The particle sizes of AuNPs and SPIONs dispersed in FCS containing medium (10 %) were determined to be 18.6 ± 4.6 nm and 15.0 ± 3.7 nm, respectively. Hydrodynamic diameters increased by more than four-fold (94.9 ± 2.1) and PDI values rose to 0.31 ± 0.5. FCS did not significantly affect hydrodynamic

diameter (60.7 ± 0.3) and PDI (0.19 ± 0.02) of SPIONs due to their human serum albumin (HSA) coating. However, the presence of FCS in solution affected zeta potentials of both AuNPs (-10.6 ± 0.9) and SPIONs (-14.38 ± 0.9). The shape of both AuNPs and SPIONs was determined to be spherical regardless of presence of FCS.

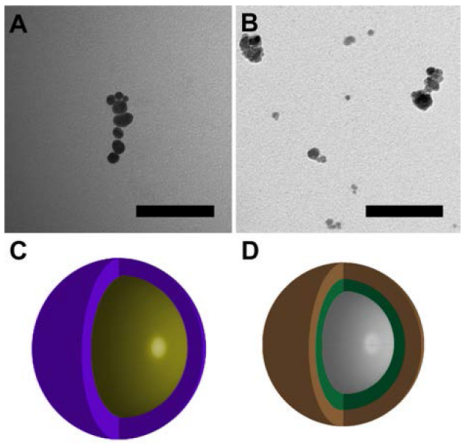

Figure 1 – Nanoparticle morphology. *Transmission electron microscopy (TEM) images of AuNPs (A) and SPIONs (B) as well as a schematic depiction of their chemical build up are depicted in this figure. In* panel *C AuNP are sown with a gold core (yellow) and a coating of citric acid (purple), In panel D, SPIONs are shown with their iron core (grey), a layer of lauric acid (green), and a final human serum albumin coating (brown). Scale bar= 100 nm.*

Synchrotron radiation Absorption contrast micro-computer-tomography (SRAμCT)

Preliminary experiments showed that both ENP were detectable by μCT (see supplementary figure S1). SRAμCT experiments of injected zebrafish embryos were performed at 1 hpi. High-resolution imaging was possible upto 0.66 μm/pixel. Retrieved single projections rendered clearly distinguishable signal differences of paraffin, air, and zebrafish soft tissue. 3D reconstruction of multiple projections combined enhanced the differentiation of those materials as well. However, neither ENP could be unquestionably detected in situ even though both AuNP and SPIONs display high particle densities (approximately 19 g/cm^3 and 5 g/cm^3, respectively). Moreover, the only internal zebrafish structures clearly distinguishable were the crystalline calcium carbonate structures (aragonite 2.83 g/cm^3) of the inner ear (otolithe) of the embryos. This structure was used throughout the study as points of reference for orientation.

Visual differences of absorption contrast and phase contrast µCT

Synchrotron radiation experiments utilize a monochromatic parallel beam instead of the polychromatic cone beam used in commercial µCT, enabling the visualization of ENP based on the refractive index of materials as visible in image rather than their mass density (B)[25]. The visual differences between SRAµCT and SRPµCT are achieved due to the fact that absorption contrast imaging gains absorption information of a sample whereas phase contrast imaging makes use of the refractive index of a material. In **Figure II** the differences between an unprocessed projection, an absorption contrast projection, and a phase contras projection are shown. Although panels A, B, and C are all the same projection, the visual information in all three differ greatly.

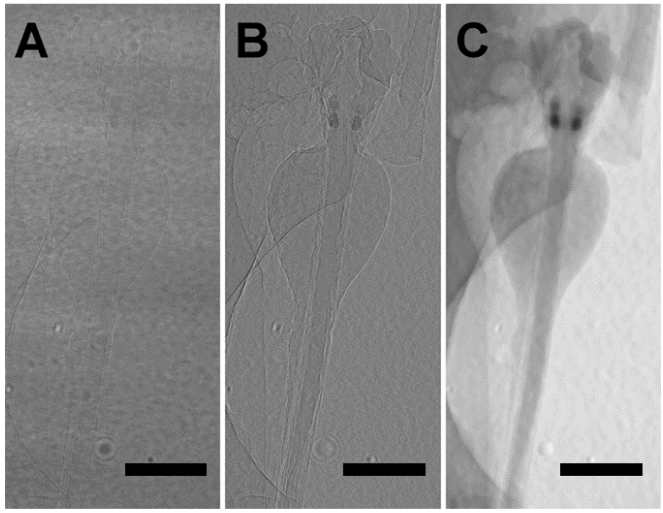

Figure 2 – Contrast differences in µCT. *Figure 2 depicts one uncorrected projection (A), one flat-field and dark-field corrected absorption contrast projection (B), and one flat-field and dark-field corrected phase contrast (C) images of a 96hpf zebrafish embedded in paraffin. Prjections were corrected with ANKAphase. Introducing flat-field and dark-field corrections lead to the subtraction of background noise in reconstructed projections. Introducing phase contrast information renders a projection with greyscales taking the refractive index of the scanned material into account. Increasing greyscale values show increasing densities whereby absorption contrast is dependent on mass density while phase contrast depends on the refractive index. Absorption contrast images show higher sharpness and lower contrast. Phase contrast images show lower sharpness and higher contrast, which is more suitable for soft tissue imaging. Scale bars: 500 µm*

In panel A, the unprocessed image does not include the phase information, instead the noise signal from the background and the scintillator blur out the image. After correcting for noise, the projection in panel B is generated. This projection features only the

absorption contrast information, rendering the paraffin and the zebrafish embryo visible. However, differences between structures are difficult to distinguish due to the similar density of paraffin and the soft tissue of the embryo. At this stage, the zebrafish does not contain any bony structures that would be seen due to the enhanced density. The only feature that can be seen with slightly more contrast due to its density is the crystalline calcium carbonate of the inner ear (otolithe). Each specimen displays two of these features on either side of the head. Finally, panel holds the projection with the most visual information. This information stems from the phase contrast technique that relies on gaining information depending on the refractive index of a material rather than is mass density. Here, a clear distinction between the different densities of the soft tissue embryo, the paraffin and the otolithes is possible. Due to the extreme differences in refractive indices of the tested ENP (AuNP: 0.27, SPIONs: 2.93) phase contrast imaging enables the visualization of these materials. However, visual information on the particles cannot be seen in projections, as the resolution of these images is too low to render signals from the 5 nl injections of both SPIONS and AuNP. To visualize ENP, a three-dimensional rendering of the reconstructed single slices with a resolution of 0.66 µm has to be performed.

Synchrotron radiation phase contrast micro-computer-tomography

SRPµCT was finally used to monitor the distribution of AuNP and SPIONs based on their refraction indices. 3D reconstructions revealed clearly distinguishable ENP. For the sake of orientation, the otoliths were colored blue. **Figure III** clearly shows AuNP (yellow) and SPIONs (red) residing inside the zebrafish embryo upon injection as in panels A and C hardly any signal is visible, indicating uptake rather than leakage at the injection site. Panels B and D are comparisons of the biodistributions of both ENP. In panel C, AuNP are seen to not circulate through the zebrafish. Instead they seem to adhere almost immediately to the tissue of the Duct of Cuvier (DoC). SPIONs were also found to reside at the injection site in comparably low amounts (panel D). Additionally, they were also found to frequent anterior and posterior cardinal vein as well as well as the dorsal aorta following the major blood vessels of the zebrafish embryo. No ENP were found to frequent any other areas of the zebrafish embryo and did not extravasate.

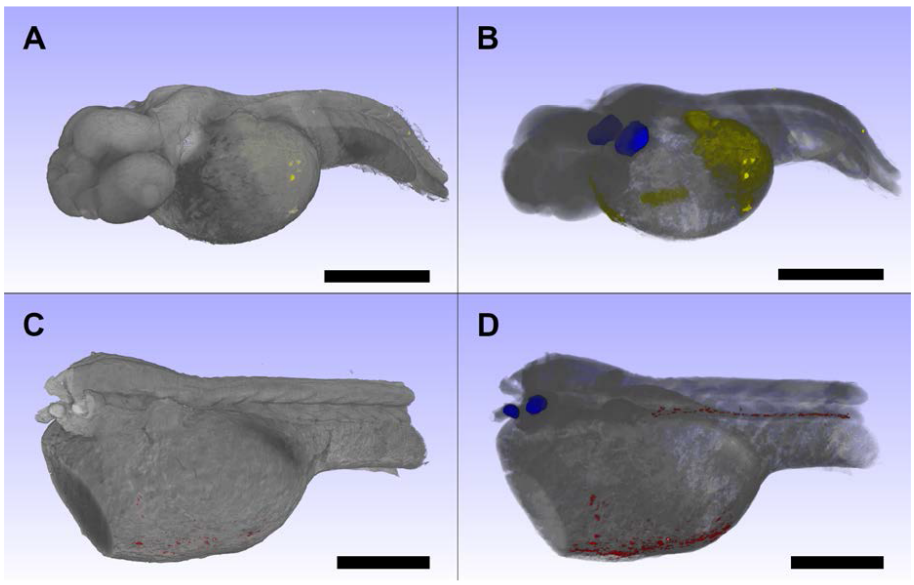

Figure 3 – 3D reconstructions of zebrafish embryos showing the biodistribution of AuNP and SPIONs. *3D reconstructions of synchrotron phase contrast projections of 1 hpi zebrafish embryos. Injections of 5 nl AuNPs (c= 3.3 mg/ml, RI: 0.2) and 5 nl SPIONs (c= 5.6 mg/ml: RI: 2.93) were performed into the Duct of Cuvier (DoC). The depictions show the zebrafish embryos (grey), AuNP (yellow), SPIONs (red), and Otoliths (blue). Opaque embryos with body surface (A, C) and transparent embryos with inner structures (B, D) highlight that both ENP reside inside the specimens. AuNP adhere to the surrounding tissue of the injection side (DoC). SPIONs are found to adhere less to the same tissue. However, they are clearly visible in the areas of the anterior cardinal vein (ACV), posterior cardinal vein (PCV), and the dorsal aorta (DA). Scale bars = 100 µm (A, B); 50 µm (C, D).*

Discussion

Determining the biodistribution of ENP in a non-invasive manner could help to elucidate the toxicological potential of the increasingly used pharmaceutical formulations like injectable radioagents or lipid drug nanocarriers. For its achievement, most ENP must be chemically enhanced to remain detectable after administration. Labeling ENP with fluorescent or radioactive tracers is routinely done[26]. Yet most labels are bound to the surface of the ENP, which may lead to a significant change in surface structure, charge, size, or solubility[27–30]. Moreover, the visualization of these formulations has frequently been conducted at dose levels exceeding medical doses by manifold due to the detection limit of either label or measuring technique. Alterations of the ENP-surface in combination with high dosing are therefore likely to bias the monitored biodistribution and cause adverse effects. The resulting false-positive or false-negative risk assessment readouts will consequently annihilate the chance of further elucidating the

toxic potential of such an ENP. MRI and CT techniques can provide some relief from the discussed issues as they are not invasive and can detect far lower doses of ENP. However, the distance between sample and scintillator has often proven to be a limiting factor for contrast and resolution in whole-body 3D imaging[10]. To tackle these prevailing issues, we combined SRPμCT with the zebrafish embryo model to enable high resolution imaging of AuNP and SPION biodistribution in low doses. AuNPs and SPIONs were characterized for their size, shape, hydrodynamic diameter and polydispersity (**Table 1** and **Figure 1**). Injection volumes were 5 nl for both AuNP (3.3 mg/ml) and SPIONs (5 mg/ml) reaching similar concentrations *in vivo* (0.24 mg/g) as Chien et al. for AuNP (0.138 mg/g). Concentrations of SPIONs (0.43 mg/g) however were well below those used by Chien et al. (1.42 mg/g). After injection, zebrafish embryos were euthanized and prepared for commercial absorption contrast μCT and SRPμCT. A novel sample preparation protocol described in the supplementary section of present work was established especially for the μCT analysis of zebrafish embryos. Absorption contrast μCT did not yield any visual information on the biodistribution of both ENP. Even though both materials express high physical densities (AuNPs: 19 g/cm^3, SPIONs: 5 g/cm^3), the concentration of ENPs was too low to be detected with the contrast levels achieved using the nanotom® or SRPμCT. The only internal signal that could be clearly separated from the soft tissue of the zebrafish embryo came from the crystalline calcium carbonate structures of the inner ears (otholits)[31]. SRPμCT finally provided high-resolution images of ENP biodistribution throughout the entire organism. 3D renderings of the zebrafish embryos or sections thereof revealed that AuNPs do not circulate through the vascular system after DoC injection and greatly adhere to the tissue of the DoC. SPIONs on the other hand were found to be distributed throughout the anterior and posterior cardinal vein (ACV, PCV) as well as the dorsal aorta (DA). SPIONS did not extravasate to other tissue layers outside of the vasculature and could otherwise only be found residing in the vicinity of the injection site. The different biodistributions are most probably dependent on the different coatings of AuNP and SPIONs. AuNP are stabilized by citric acid in solution. However, upon injection the citrate coating will degrade and lead to rapid agglomeration. This phenomenon was also observed while measuring the hydrodynamic size and zeta potential. SPIONs are coated with a chemically bound layer of human serum albumin. This coating will not wear of as fact as the citric acid layer of AuNP and will not trigger any immune reactions. To our knowledge, our results show the first successful

monitoring of low-dose ENP biodistribution in an entire zebrafish embryo at submicron resolution. We were therefore able to provide evidence that combing SRPμCT with the zebrafish embryo animal model is highly beneficial for monitoring the biodistribution of metal-based ENP at low doses. Both AuNP and SPIONs proved to have sufficiently high refractive indices (AuNP: 0.27, SPIONs: 2.93) to be clearly distinguished from the soft tissue of the zebrafish embryo. Rendering the obtained data into three-dimensional images also provided insights into the difference of non-labeled ENP biodistribution. Conclusively, this set up could be further improved to study the biodistribution of differently coated ENP for safety and applicatory reasons.

Conclusion

By using synchrotron radiation phase-contrast micro-tomography, we provide novel results on how the monitoring of nanoparticle biodistribution *in situ* can be performed. To our knowledge, we are the first to publish 3D rendered high-resolution images of the biodistribution of therapeutically relevant doses of ENP intravenously administered into zebrafish embryos. The low AuNP and SPION doses used in this study further underline the analytical power of this set up. Additionally, clear differences in the biodistribution of AuNPs and SPIONs could be shown. The obtained results have also led to an ongoing project focusing on enabling to monitor nanoparticles by SRPμCT that are not metal-based and solely designed as nano drug delivery systems, not contrast agents. This approach can provide much needed information on the behavior and the safety of ENP formulations designed for medical application.

Acknowledgement

This work was supported by grants from the Swiss Center for Applied Human Toxicology (SCAHT) and the NanoReg2 program (European Union Horizon 2020 research agreement 646221, 15.0200-3). We thank Dr. Susanne Schenk for assistance with the zebrafish barge culturing. Support of Roger Roth and Darryl Borland (aluminum mold design), as well as Ursula Sauder (Histology, BioEM Lab / C-CINA), and Dr. Wolf Heusermann (bright field microscopy) is greatly acknowledged. The authors would also like to thank Dr. Jan Zaloga from the University of Erlangen for providing the SPIONs used in the experiments. We thank Prof. Markus Affolter and Dr. Heinz Belting from the Biocenter of the University of Basel for providing the adult zebrafish specimens. The authors acknowledge the European Synchrotron Radiation Facility for provision of synchrotron radiation facilities and would like to thank Dr. Margie Olbinado for assistance while using beamline ID19.

Declaration of Interest

The authors have no conflicts in interest to declare.

References

1. Rubin, G. D. Computed Tomography: Revolutionizing the Practice of Medicine for 40 Years. *Radiology* **273,** S45–S74 (2014).
2. Shilo, M., Reuveni, Motiei, M. & Popovtzer, R. Nanoparticles as computed tomography contrast agents: current status and future perspectives. *Nanomed.* **7,** 257–269 (2012).
3. Ashton, J. R., West, J. L. & Badea, C. T. In vivo small animal micro-CT using nanoparticle contrast agents. *Front. Pharmacol.* **6,** (2015).
4. Clark, D. P. & Badea, C. T. Micro-CT of rodents: state-of-the-art and future perspectives. *Phys. Medica PM Int. J. Devoted Appl. Phys. Med. Biol. Off. J. Ital. Assoc. Biomed. Phys. AIFB* **30,** 619–634 (2014).
5. Cormode, D. P., Naha, P. C. & Fayad, Z. A. Nanoparticle Contrast Agents for Computed Tomography: A Focus on Micelles. *Contrast Media Mol. Imaging* **9,** 37–52 (2014).
6. Meir, R. & Popovtzer, R. Cell tracking using gold nanoparticles and computed tomography imaging. *Wiley Interdiscip. Rev. Nanomed. Nanobiotechnol.* n/a–n/a doi:10.1002/wnan.1480
7. Tietze, R. *et al.* Visualization of superparamagnetic nanoparticles in vascular tissue using XμCT and histology. *Histochem. Cell Biol.* **135,** 153–158 (2011).
8. Chien, C.-C. *et al.* Gold nanoparticles as high-resolution X-ray imaging contrast agents for the analysis of tumor-related micro-vasculature. *J. Nanobiotechnology* **10,** 10–10 (2012).
9. Hainfeld, J. F., Slatkin, D. N., Focella, T. M. & Smilowitz, H. M. Gold nanoparticles: a new X-ray contrast agent. *Br. J. Radiol.* **79,** 248–253 (2006).
10. Betz, O. *et al.* Imaging applications of synchrotron X-ray phase-contrast microtomography in biological morphology and biomaterials science. I. General aspects of the technique and its advantages in the analysis of millimetre-sized arthropod structure. *J. Microsc.* **227,** 51–71 (2007).
11. Parichy, D. M., Elizondo, M. R., Mills, M. G., Gordon, T. N. & Engeszer, R. E. Normal Table of Post-Embryonic Zebrafish Development: Staging by Externally Visible Anatomy of the Living Fish. *Dev. Dyn. Off. Publ. Am. Assoc. Anat.* **238,** 2975–3015 (2009).
12. Sieber, S. *et al.* Zebrafish as an early stage screening tool to study the systemic circulation of nanoparticulate drug delivery systems in vivo. *J. Control. Release Off. J. Control. Release Soc.* **264,** 180–191 (2017).
13. Kovrižnych, J. A. *et al.* Acute toxicity of 31 different nanoparticles to zebrafish (Danio rerio) tested in adulthood and in early life stages – comparative study. *Interdiscip. Toxicol.* **6,** 67–73 (2013).
14. Bambino, K. & Chu, J. Zebrafish in Toxicology and Environmental Health. *Curr. Top. Dev. Biol.* **124,** 331–367 (2017).
15. Clemente, Z. *et al.* Fish exposure to nano-TiO2 under different experimental conditions: Methodological aspects for nanoecotoxicology investigations. *Sci. Total Environ.* **463,** 647–656 (2013).
16. Nagel, R. DarT: The embryo test with the Zebrafish Danio rerio--a general model in ecotoxicology and toxicology. *ALTEX* **19 Suppl 1,** 38–48 (2002).
17. Benard, E. L. *et al.* Infection of Zebrafish Embryos with Intracellular Bacterial Pathogens. *J. Vis. Exp. JoVE* 3781 (2012). doi:10.3791/3781

18. Zaloga, J. *et al.* Pharmaceutical formulation of HSA hybrid coated iron oxide nanoparticles for magnetic drug targeting. *Eur. J. Pharm. Biopharm.* **101,** 152–162 (2016).
19. Turkevich, J., Cooper Stevenson, P. & Hillier, J. A study of the nucleation and growth processes in the synthesis of colloidal gold. *Discuss. Faraday Soc.* **11,** 55–75 (1951).
20. Zaloga, J. *et al.* Pharmaceutical formulation of HSA hybrid coated iron oxide nanoparticles for magnetic drug targeting. *Eur. J. Pharm. Biopharm.* **101,** 152–162 (2016).
21. Siegrist, S., Kettiger, H., Fasler-Kan, E. & Huwyler, J. Selective stimulation of the JAK/STAT signaling pathway by silica nanoparticles in human endothelial cells. *Toxicol. Vitro Int. J. Publ. Assoc. BIBRA* **42,** 308–318 (2017).
22. Sieber, S. *et al.* Immobilization of Enzymes on PLGA Sub-Micrometer Particles by Crosslinked Layer-by-Layer Deposition. *Macromol. Biosci.* **17,** n/a-n/a (2017).
23. Weitkamp, T., Haas, D., Wegrzynek, D. & Rack, A. *ANKAphase* : software for single-distance phase retrieval from inline X-ray phase-contrast radiographs. Erratum. *J. Synchrotron Radiat.* **20,** 205–205 (2013).
24. Paganin, D., Mayo, S. C., Gureyev, T. E., Miller, P. R. & Wilkins, S. W. Simultaneous phase and amplitude extraction from a single defocused image of a homogeneous object. *J. Microsc.* **206,** 33–40 (2002).
25. Davis, T. J., Gao, D., Gureyev, T. E., Stevenson, A. W. & Wilkins, S. W. Phase-contrast imaging of weakly absorbing materials using hard X-rays. *Nature* **373,** 595–598 (1995).
26. van Schooneveld, M. M. *et al.* A fluorescent, paramagnetic and PEGylated gold/silica nanoparticle for MRI, CT and fluorescence imaging. *Contrast Media Mol. Imaging* **5,** 231–236 (2010).
27. Yildirimer, L., Thanh, N. T. K., Loizidou, M. & Seifalian, A. M. Toxicology and clinical potential of nanoparticles. *Nano Today* **6,** 585–607 (2011).
28. Samberg, M. E., Oldenburg, S. J. & Monteiro-Riviere, N. A. Evaluation of silver nanoparticle toxicity in skin in vivo and keratinocytes in vitro. *Environ. Health Perspect.* **118,** 407–413 (2010).
29. Chen, Y. S., Hung, Y. C., Liau, I. & Huang, G. S. Assessment of the in vivo toxicity of gold nanoparticles. *Nanoscale Res Lett* **4,** (2009).
30. Hanot, C. C., Choi, Y. S., Anani, T. B., Soundarrajan, D. & David, A. E. Effects of Iron-Oxide Nanoparticle Surface Chemistry on Uptake Kinetics and Cytotoxicity in CHO-K1 Cells. *Int. J. Mol. Sci.* **17,** 54 (2016).
31. Haddon, C. & Lewis, J. Early ear development in the embryo of the Zebrafish, Danio rerio. *J. Comp. Neurol.* **365,** 113–128 (1996).

Monitoring the biodistribution of metal-based nanoparticles in a small animal model by synchrotron radiation micro-tomography

Supplementary information

Siegrist S.[1, †], Cörek E.[1, †], Bikis C.[2], Sieber S.[1], Fluder P.[1], Klados K.[1], Detampel P.[1], Puchkov M.[1], , Thalmann P.[2], Schulz G.[2], Alexiou Ch.[4], Müller B.[2], Huwyler J.[1,*]

[1]*Department of Pharmaceutical Technology, University of Basel, Klingelbergstrasse. 50, 4056 Basel, Switzerland;* [2]*Biomaterials Science Center, University of Basel, Gewerbestrasse 14, 4123 Allschwil, Switzerland;* [4]*Section for Experimental Oncology and Nanomedicine, Waldstraße 1,91054 Erlangen University of Erlangen, Germany*

[†]*These authors contributed equally to this study.*

**Correspondence: Prof. Jörg Huwyler, Pharmaceutical Technology, Pharmacenter, University of Basel, Klingelbergstrasse. 50, 4056 Basel, Switzerland. Tel: +41(0)612071513. E-mail: Joerg.huwyler@unibas.ch*

Engineered nanoparticles (ENP)

Synthesis of gold nanoparticles (AuNP)

One of the most common ways to synthesize AuNP is the Turkevich method[1]. Here 0.2 mL trisodium citrate (38.8 mM, Fluka, Buchs, Switzerland) are added to 20.0 mL boiling tetrachloroaurate (0.3 mM, Sigma-Aldrich, Buchs, Switzerland) under constant stirring. A change in color from light yellow to greyish-blue and further to ruby-red indicates the formation of the gold colloids and is usually visible after approximately one minute. The dispersion can then be left boiling for an additional 30 minutes under constant stirring. Thereafter, the dispersion is allowed to cool to room temperature.

The Turkevich method results in dispersions with nanoparticle concentrations of around 0.25 mg/ml. This concentration had proven to be too low to detect when the injecting a maximum of 8 nl into a 48 hpf zebrafish embryo in preliminary experiments (data not shown) As a consequence, various syntheses of AuNP were performed by mixing varying amounts of tetrachloroaurate ($HAuCl_4$; 1.0 mM, 2.0 mM, 4.0 mM, 10.0 mM and 15.0 mM, Sigma-Aldrich) and trisodium citrate ($Na_3C_6H_5O_7$; 4.0 mM, 8.0 mM, 16.0 mM, 40.0 mM and 60.0 mM, Fluka) at constant molar ratios of 1:4 as done in the Turkevich method. Tetrachloroaurate (Sigma-Aldrich) and trisodium citrate (Fluka) were heated separately to 75.0° C in a thermomixer (Thermomixer comfort, Eppendorf, Hamburg, Germany) for 15 minutes. Trisodium citrate (Fluka) and tetrachloroaurate (Sigma-Aldrich) were mixed and left to react for a further 20 minutes at 75.0° C. The resulting colloids were allowed to cool down to room temperature. AuNP were kept in brown glass vials in the dark at 4.0° C for storage.

In **Table S1** the concentrations of gold colloids (mg/ml) present in the different mixtures of tetrachloroaurate and trisodium citrate are given.

Table S1 – Concentrations of $HAuCl_4$, $Na_3C_6H_5O_7$ and AuNP for synthesis. *$HAuCl_4$ and $Na_3C_6H_5O_7$ were mixed at constant molar ratios of 1:4 during synthesis.*

Batch	Concentration $HAuCl_4$ [mM]	Concentration $Na_3C_6H_5O_7$ [mM]	Concentration AuNP [mg/ml]
AuNP1	1.0	4.0	0.8
AuNP2	2.0	8.0	1.7
AuNP3	4.0	16.0	3.3
AuNP4	10.0	40.0	8.3
AuNP5	15.0	60.0	12.5

Additionally, all formulated batches of AuNP (AuNP1 to AuNP5) were characterized by differential light scattering and transmission electron microscopy after reaching room temperature. During this process the different batches were evaluated and compared in order to determine the most suitable formulation for the injection studies. The authors focused on size, hydrodynamic diameter, polydispersity, zeta potential and stability over time. These results are presented in **Table S2**.

Table S2 – Physico-chemical characterization of AuNP series. *Size was measured by transmission electron microscopy (TEM). Hydrodynamic diameter and polydispersity index were measured by dynamic light scattering (DLS). Zeta potential was measured by electrophoretic light scattering (ELS). The Polydispersity index (PDI) is indicated to the second decimal figure due to significance. Values are means ± standard deviations of independent experiments (n=3).*

Batch	Particle Size [nm]	Hydrodynamic diameter [nm]	PDI	Zeta Potential [mV]
AuNP1	33.4 ± 5.8	35.1 ± 1.4	0.37	-10.7
AuNP2	25.4 ± 5.3	28.2 ± 2.2	0.38	-18.1
AuNP3	18.6 ± 4.6	29.6 ± 0.1	0.19	-29.4
AuNP4	14.7 ± 3.0	887.5 ± 40.3	0.31	-39.2
AuNP5	21.1 ± 5.7	845.8 ± 97.9	0.31	-38.2

Batches AuNP1 to AuNP3 were stable in storage at 4°C for at least 48 hours. Batches AuNP4 and AuNP5 revealed to be non-stable dispersions, as aggregation and sedimentation of these AuNP were observed. The performed measurements of hydrodynamic diameter and particle size also supported these findings. While batches AuNP1 to AuNP3 showed similar values of the hydrodynamic diameter to the respective particle size measurements, hydrodynamic diameter of the batches AuNP4 and AuNP5 were measured at 60-fold and 40-fold values to their particle size counterparts, respectively. These results indicate aggregation and agglomeration overtime. Sedimentation of these two specimens were observed by macroscopic evaluation after 1 hour. Furthermore, obtained values for polydispersity show that most formulations are polydisperse with PDI values ranging from 0.31 to 0.38. The only monodisperse formulation was batch AuNP3 showing a value (0.19) below 0.2.

Commercial absorption-contrast micro-computer-tomography (µCT)

For µCT measurements paraffin rods containing one zebrafish embryo were pinned onto the needle of the sample holder which was then fixed on the precision rotation stage of the system. The absorption contrast measurements were performed using a nanotom® m (phoenix|x-ray, GE Sensing & Inspection Technologies GmbH, Wunstorf,

Germany) equipped with a 180.0 kV / 15.0 W nanofocus X-ray source. The experiments were performed using an acceleration voltage of 60.0 kV and a beam current of 240.0 µA. Taking advantage of the cone beam geometry a resulting pixel length of 1.0 µm was adjusted. 1440 equiangular projections over 360° were reconstructed by phoenix datos|x 2.0.1 - RTM (GE Sensing & Inspection Technologies GmbH, Wunstorf, Germany). After reconstruction, the 3D data sets were visualized using the software VG Studio Max 2.1 (Volume Graphics GmbH, Heidelberg, Germany). Measurements were performed at the Biomaterials Science Center, University of Basel.

Control experiments nanotom®

To guarantee the detection of the injected ENP during µCT experiments, preliminary experiments with a nanotom® were conducted to visualize the both. Herefore, were filter papers were soaked with of AuNP and SPIONs, dried and placed in a 1.5 ml Eppendorf tube containing molten paraffin wax. The tubes were fixed vertically onto a custom-made holder and measured by the nanotom®. Furthermore, the authors were interested in the visible contrast between the different ENPs, paraffin, filter paper, air, and the Eppendorf tubes. **Figure S I** represents the absorptions contrast images obtained with the commercial µCT. The black background (air) could be significantly differentiated from all other signals other than water which was present in enclosed in paraffin (**1**). Paraffin and the Eppendorf tubes also seemed to have the similar absorption values (**1 and 8**). The main focus was the visualization of both AuNP3 (**2**) and SPIONs (**3**) (3.3 mg/ml and 5.6 mg/ml, respectively). Both ENP could clearly be distinguished as fine white lines suggesting their incorporation into the filter paper mesh grid. Also it should be pointed out, that SPIONs gave higher absorption signals than gold despite their lower mass density (AuNP: 19 g/cm^3, SPIONs: 5 g/cm^3). The reason for this was the almost two-fold higher concentration of SPIONs. For comparison, silica nanoparticles (density of approximately 2 mg/ml) at concentrations of 20 mg/ml (**4**) and 10 mg/ml (**5**) were monitored as well. However, only the higher concentrated sample of silica count be detected faintly. Additionally, lyophilized AuNP were monitored (**6**) in absence of paraffin. Plane filter paper in paraffin (**7**) and just paraffin (**8**) did not show different contrasts to the Eppendorf tube.

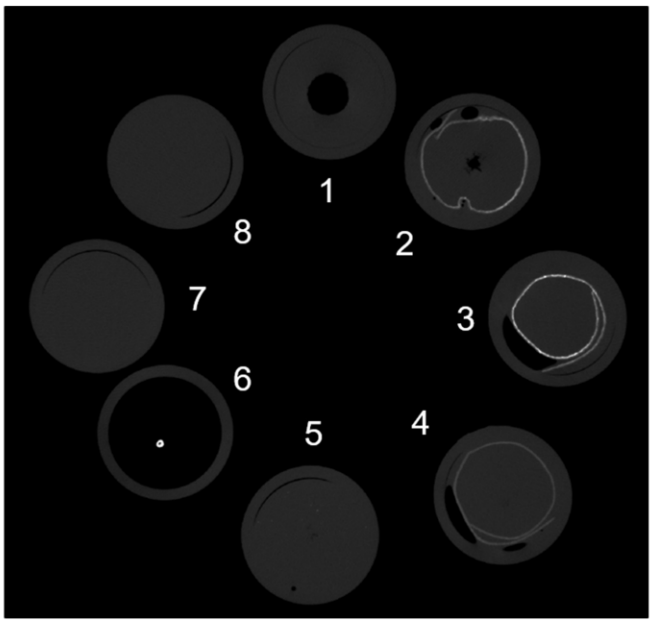

Figure S I – Control experiments. *To ensure detection of AuNP3 and SPIONs is possible in nanotom®. The background is visible in black, the Eppendorf tubes in grey. White areas showing dense materials like the AuNPs and SPIONs, whereby higher intensities are equal to higher densities. Eppendorf tubes containing: control with paraffin and water (1), gold nanoparticles c= 3.3 mg/ml (2), SPIONs c= 5.6 mg/ml (3), silica nanoparticles c= 20 mg/ml (4), silica nanoparticles c= 10 mg/ml (5), lyophilized gold nanoparticles (6), paraffin and filter paper (7), and paraffin (8).*

Consequently, the results of the preliminary experiments led to the consideration of SPIONs and AuNP3 for the biodistribution studies in the zebrafish.

For the reasons of simplicity AuNP3 are referred to as AuNPs in the original manuscript.

Furthermore, it was important to the authors that both formulations could be injected consistently without clotting the injection needle and that the maximum administered dose was non-toxic towards the embryo up to 144 hpf and 96 hpi.

Injection calibration

Injection needle manufacturing and injection volume consistency

Needles for microinjection were made of normal glass capillaries (O.D. 1.2 mm, I.D. 0.69 mm, Sutter Instrument, Novato, CA) by using a Flaming/Brown™ micropipette puller (P-97, Sutter Instrument, Novato, CA) and manipulated with distinct parameters to guarantee reproducible functionality (Heat: 500, Pull: 100, Velocity: 200, Time: 40). Needles were coated in order to prevent adhesion of ENP by filling them with polysorbate 80 (0.1 %) the evening before injection. Shortly before use, needles were rinsed with Millipore 18-Ω water. Microinjection needles were filled with nanoparticle dispersion by back loading (SPIONs were injected in Millipore 18-Ω water, AuNP were injected in the citrate buffer they were synthesized in) using Microloader™ tips (20.0 µL, Eppendorf, Hamburg, Germany) and mounted onto a PiccoNozzle Kit (5430-ALL, WPI, Sarasota, FL) thereafter. The needles were loaded with 100 µl of nanoparticle dispersion and opened by clipping the tip with blunt forceps (#5, Dumont, Montignez, Switzerland). To ensure no clotting of the needles and consistent injection volumes test injections into immersion oil (Leica Microsystems, Wetzlar, Germany) were performed to measure the consistency of the droplet sizes.

Table S3 – conversion of droplet size measured with eyepiece graticule to droplet size volume.

Objective Magnification	Graticule Magnification	Droplet diameter [mm]	Droplet volume [nl]
1X	10X	1.24	1
1.3X	10X	1.61	1
1.6X	10X	1.99	1
2X	10X	2.48	1
2.5X	10X	3.10	1
4X	10X	4.96	1
5X	10X	6.20	1
6.3X	10X	7.82	1
8X	10X	9.93	1

The droplet diameters were measured with an eyepiece graticule and were manipulated by adjustments of the injection time (ms) and the exhaust pressure (mbar) to consistently receive a droplet volume of 1 nl to 8 nl (see **Table S3 and Table S4** for details). These test injection series were done after every new back loading or changing of the needle and always before injecting into the live specimen. This repeated procedure made the injection volumes highly reproducible throughout the experiments.

Table S4 – Droplet volumes used for injection with corresponding droplet diameter at 80X magnification.

Injection volume [nl]	Droplet diameter [mm]	Magnification
1	9.93	80X
3	14.32	80X
5	16.97	80X
8	19.85	80X

Zebrafish viability

Viability after injection

Gold and iron ENP are both anticipated to be used frequently as future contrast agents in x-ray examinations in humans and animals alike. However, the authors were concerned about the dosing of these formulations, since ex vivo and in vitro proof of concept experiments are commonly performed without choosing appropriate doses. To ensure that the doses used do not affect the zebrafish embryo until reaching its larval stage (144 hpf) the authors monitored the viability and malformation occurrence in 48 hpf zebrafish embryos injected with various doses of AuNP and SPIONs (1 nl, 3 nl, 5 nl, and 8 nl) over the course of 96 hours (**Table S5**). If a statistically significant difference to the untreated control population was observed, the dose was deemed unfit for further biodistribution assays.

Table S5 – Statistical analysis of zebrafish embryo viability 96 hours post injection (hpi). *Analysis of variance (ANOVA) and Tukey's post-hoc test was performed to compare viability of specimens treated with gold and iron oxide ENP and untreated zebrafish embryos. Values represent the number of live specimens (144 hpf) after 96 hpi of 1 nl, 3 nl, 5 nl, and 8 nl injections. Values significantly different to the negative control (zebrafish embryos treated with E2 medium) are marked with an asterisk (*): $p < 0.05$). Values are means ± standard deviation of n=3 experiments, where each condition was monitored with n=30 zebrafish embryos. The embryos were always injected at an age of 48 hpf.*

Condition	Live embryos	Deceased embryos	Visible malformation
1 nl injection			
AuNP3	29.67 ± 0.47	1	0
SPIONs	27.3 ± 2.08	8	0
3 nl injection			
AuNP3	29.33 ± 0.94	2	0
SPIONs	28.7 ± 0.58	4	0
5 nl injection			
AuNP3	29.33 ± 0.47	2	0
SPIONs	28.3 ± 1.16	5	0
8 nl injection			
AuNP3	26.33 ± 1.25*	9	3
SPIONs	25.3 ± 1.53*	14	4
controls			
AuNP3	29.67 ± 0.47	1	0
SPIONs	29.3 ± 0.16	4	0

Sample preparation and control experiments

Bleaching

In order to improve detectability of ENP after microinjection by bright field microscopy, the pigment cell formation in zebrafish embryos were suppressed. The therefore obligate conversion of tyrosine to melanin was inhibited by adding 0.5 mL of 1-pehnol-2-thiourea (PTU) stock 50 X (36.5 mg 1-phenol-2-thiourea, 24.0 mL purified water) to petri dishes with dechorionated zebrafish embryos 24 hpf after E2 medium renewal.

Bright field Microscopy

The zebrafish embryos were fixed in 4 % PFA for 30 minutes and dehydrated with increasing ethanol dilutions from 25, 50, 75 and 96 Vol.-% for 15 minutes each and stored in analytical ethanol (> 96 Vol.%). Each embryo was embedded using the embedding medium Euparal (Carl Roth) on microscope slides and dried for 2-3 days. For analyzing and imaging, the bright field microscope Leica DM6000 was used with objectives of 10, 20 and 40x magnification.

Due to the prerequisite of non-labeling, bright field microscopy was performed to analyze the biodistribution of AuNP and SPIONs. Upon injection, bright field microscopy did enable the localization of relevant internal zebrafish structures. However, visualization of injected SPIONs and AuNP were mostly impaired. Inconsistent bleaching of the embryos made a clear distinction between ENP and pigment cells nearly impossible. Furthermore, limited resolution of the microscope prevented more detailed visualization that might have been able to compensate for the inconsistent bleaching. Nevertheless, agglomerates of SPIONs could be detected in the lateral aorta (LA), the anterior cardinal vein (ACV), the posterior cardinal vein (PCV), and the Duct of Cuvier (DoC) close to the injection site (IS). AuNP agglomerates on the other hand could only be localized at the injection site (IS).

Histological examination by transmission electron microscopy

Euthanised zebrafish embryos were decapitated using a surgical scalpel (blade no. 20). Heads and bodies were fixed separately in Karnovsky fixative (paraformaldehyde 3.0 %, glutaraldehyde 0.5 % in phosphate buffered saline (PBS) 10.0 mM, pH 7.4) for one hour. After washing with PBS the samples were fixed in osmium tetroxide (1.0 %) for one hour. After a second washing step with water, the samples were dehydrated by washing in ethanol with subsequently increasing concentrations (50.0 % and 70.0 %) for ten minutes each. Thereafter, samples were stained with a mixture of ethanol

and uranyl acetate (70.0 %ethanol and 2.0 % uranyl acetate) for one hour. Then the samples were further dehydrated by two washing steps with ethanol (90.0 % and 100.0 %) for 10 minutes each. The samples were infiltrated with epoxy resin (EPON) prior to embedding by placing them subsequently in acetone for ten minutes, a mixture of EPON and acetone (1:1) for two hours and pure EPON for 4 hours. The infiltrated samples where then embedded in EPON for 24 hours at 60.0° C. Histological sections of 60.0 nm thickness were obtained by cutting the embedded samples with a diamond blade. Sections were stained with uranyl acetate (6.0 %) for one hour and lead acetate for 2 minutes and examined by transmission electron microscopy (Morgagni 268D, FEI, Hillsboro, OR) at an operating voltage of 80.0 kV. Sample preparation, histological sectioning and transmission electron microscopy were conducted at BioEM Lab / C-CINA.

To confirm bright field microscopy observations, histological slices of zebrafish embryos were analyzed by transmission electron microscopy (TEM). AuNP and SPIONs were detectable on electron micrographs. Moreover, the identical distribution differences between AuNP and SPIONs were observed as hypothesized in bright field microscopy experiments. SPIONs were found in sections of the anterior and posterior trunk-region (LA, ACV and PCV), in the Duct of Cuvier (DoC) at the injection site (IS)[2]. Large AuNP agglomerates were localized in the Duct of Cuvier (DoC) exclusively. The histological examination also proved, that both ENP could not penetrate the yolk after intravenous microinjection or extravasate to any other tissue. However, entire specimen imaging was not possible with this technique. Due to a slice thickness of 60 nm only limited sections of the zebrafish embryo were able to be visualized. Additionally, the slicing process could mechanically force ENP into other tissues and internal structures biasing the observed results.

Novel sample preparation method for µCT analysis of zebrafish embryos

Micro-computer-tomography (µCT) provides high-resolution imaging, where sample detection relies greatly on material density. Furthermore, the technique is non-invasive, allows the analysis of very small samples, and enables distinguishing low-density differences. However, standardized protocols regarding the preparation of zebrafish embryos for the µCT analysis do not exist. In the following we therefore describe a novel sample preparation protocol for zebrafish embryos.

After ENP injection, euthanizing and fixation, zebrafish embryos were embedded into paraffin rods (0.8 mm diameter, 2 cm length). The custom made, two-pieced aluminum

mold enabled quick and reproducible embedding (**Figure S IV**). The embedding channel diameter facilitated zebrafish embryo alignment as it was measured to be only 0.2 mm wider (on average) than a 72 hpf embryo. This also allowed total encasing of the embryo with paraffin protecting it from any mechanical damage during transportation and analysis. Air-drying of the embryo ensured that no excess of ethanol or water could compromise the paraffin embedding, leading to potential movement of the specimen during tomographic measurements. Furthermore, the paraffin rod was tailored to a thickness that withstood radiation measurements at the nanotom® (several hours) and the ESRF (45 min) without deformation. Additionally, minimization of the paraffin rod diameter allowed the sample to be moved as closely as possible to either the radiation source of the nanotom® or to the detector of the synchrotron beam for maximum resolution.

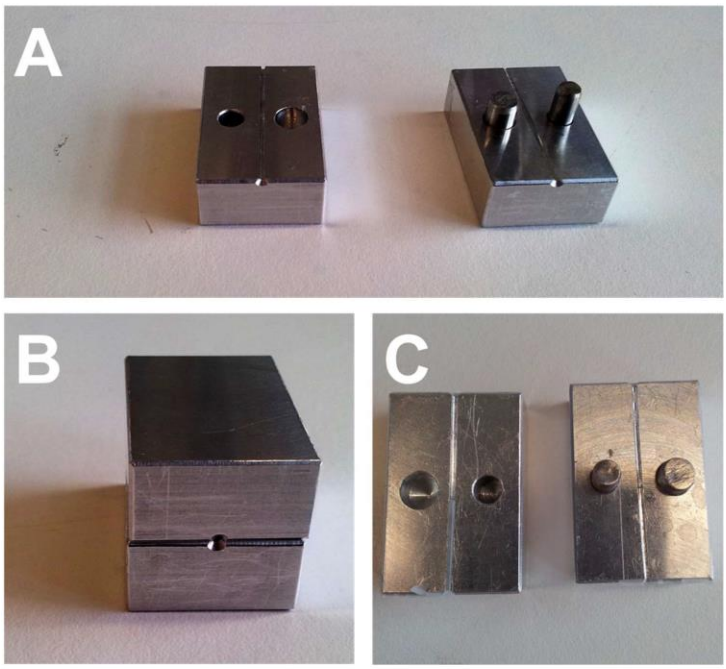

Figure S II – Preparation mold for injected zebrafish embryos. *The samples were prepared to be interchangeably used in nanotom® and synchrotron measurements. Embryos were fixed, dehydrated, and embedded into paraffin. The paraffin rods were poured in a custom made, aluminum mold with an embedding channel diameter of 0.8 mm (**A**). The small diameter of the rods ensured maximum resolution in x-ray experiments paired with good transport and experiment stability (**B**). Before measuring, the rods (**C**) were lifted out of the mold with a blunt needle and fixed onto the sample holders to avoid movement of the specimen during x-ray imaging.*

The aragonite crystals of the inner ear (otoliths)

In preliminary nanotom® experiments ENP in zebrafish embryos could not be visualized. However, the crystalline calcium carbonate structures (aragonite) of the inner ear structures (otoliths) showed high absorption contrast due to their large mass (**Figure S V**). Since a zebrafish embryo does not delevope hard tissue (bone) until after 144 hpf, these aragonite structures further served as aids for orientation.

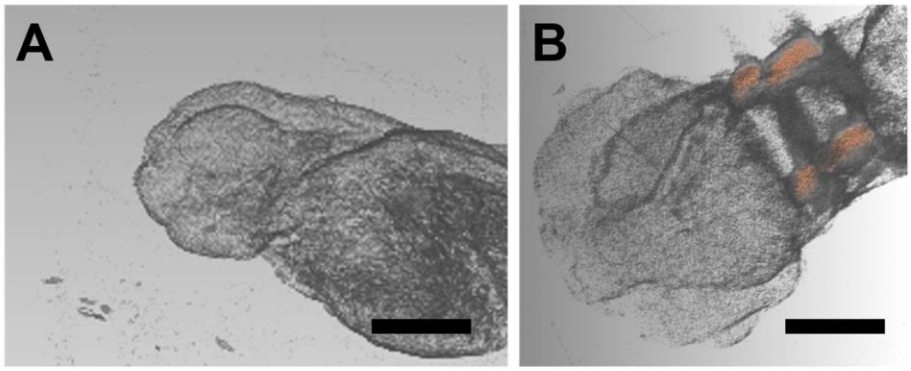

Figure S III – Commercial µCT analysis of a zebrafish embryo (48 hpf). *No ENP could be detected in any zebrafish embryo during trials performed with the nanotom®. At least detection close to the injection site (DoC) were expected(**A**). However, the signal coming from the otoliths aids the orientation, since zebrafish embryos did not develop any bony structures in this life stage (**B**). The otoliths are marked in red. Scale bars:100 µm (**A**) and 50 µm (**B**)*

Chapter IV

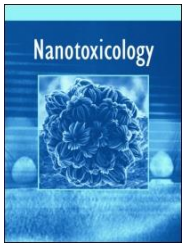

Nanotoxicology

ISSN: 1743-5390 (Print) 1743-5404 (Online) Journal homepage: http://www.tandfonline.com/loi/inan20

Preclinical hazard evaluation strategy for nanomedicines

Stefan Siegrist, Emre Cörek, Pascal Detampel, Jenny Sandström, Peter Wick & Jörg Huwyler

To cite this article: Stefan Siegrist, Emre Cörek, Pascal Detampel, Jenny Sandström, Peter Wick & Jörg Huwyler (2018): Preclinical hazard evaluation strategy for nanomedicines, Nanotoxicology, DOI: 10.1080/17435390.2018.1505000

To link to this article: https://doi.org/10.1080/17435390.2018.1505000

Published online: 05 Sep 2018.

NANOTOXICOLOGY
https://doi.org/10.1080/17435390.2018.1505000

Taylor & Francis
Taylor & Francis Group

REVIEW ARTICLE

OPEN ACCESS Check for updates

Preclinical hazard evaluation strategy for nanomedicines

Stefan Siegrist[a]*, Emre Cörek[a]*, Pascal Detampel[a], Jenny Sandström[b], Peter Wick[c] and Jörg Huwyler[a]

[a]Division of Pharmaceutical Technology, Pharmacenter, University of Basel, Basel, Switzerland; [b]Swiss Centre for Applied Human Toxicology, Basel, Switzerland; [c]Laboratory for Patricles-Biology Interactions, Empa Swiss Federal Laboratories for Materials Science and Technology, St. Gallen, Switzerland

ABSTRACT

The increasing nanomedicine usage has raised concerns about their possible impact on human health. Present evaluation strategies for nanomaterials rely on a case-by-case hazard assessment. They take into account material properties, biological interactions, and toxicological responses. Authorities have also emphasized that exposure route and intended use should be considered in the safety assessment of nanotherapeutics. In contrast to an individual assessment of nanomaterial hazards, we propose in the present work a novel and unique evaluation strategy designed to uncover potential adverse effects of such materials. We specifically focus on spherical engineered nanoparticles used as parenterally administered nanomedicines. Standardized assay protocols from the US Nanotechnology Characterization Laboratory as well as the EU Nanomedicine Characterisation Laboratory can be used for experimental data generation. We focus on both cellular uptake and intracellular persistence as main indicators for nanoparticle hazard potentials. Based on existing regulatory specifications defined by authorities such as the European Medicines Agency and the United States Food and Drug Administration, we provide a robust framework for application-oriented classification paired with intuitive decision making. The Hazard Evaluation Strategy (HES) for injectable nanoparticles is a three-tiered concept covering physicochemical characterization, nanoparticle (bio)interactions, and hazard assessment. It is cost-effective and can assist in the design and optimization of nanoparticles intended for therapeutic use. Furthermore, this concept is designed to be adaptable for alternative exposure and application scenarios. To the knowledge of the authors, the HES is unique in its methodology based on exclusion criteria. It is the first hazard evaluation strategy designed for nanotherapeutics.

ARTICLE HISTORY
Received 3 May 2018
Revised 25 June 2018
Accepted 20 July 2018

KEYWORDS
Nanoparticles; nanomedicine; hazard assessment; safe-by-design

1. Introduction

Engineered nanoparticles (ENP) were first introduced to the market as pharmaceutical indications in 1957 and 1959, when iron dextran and sucrose products of Sanofi Aventis and Vifor were approved for the intravenous treatment of iron deficiency in patients with chronic kidney disease. Since the approval of the anti-cancer drug Doxil®/Caelyx® by the United States Food and Drug Administration (FDA) in 1995, the number of yearly approved ENP formulations designed for medical purposes are steadily increasing (Etheridge et al. 2013; Pelaz et al. 2017; Weissig, Pettinger, and Murdock 2014; Witzigmann et al. 2015). Today, it is well accepted that ENP have an undisputable potential as drug carriers (Bozzuto and Molinari 2015; Coti et al. 2009; Puri et al. 2009), imaging agents (Arap et al. 2013; Toy et al. 2014; Unterweger et al. 2017), vaccines (Gregoriadis 1985; Gregory, Titball, and Williamson 2013; Zhao et al. 2014), and theranostic tools (Ambrogio et al. 2011; Elgqvist 2017; Xie, Lee, and Chen 2010). Nevertheless, ENP are not risk-free substances and safety concerns towards these novel formulations have to be addressed (Fadeel 2012; Wolfram et al. 2015). ENP may induce adverse side effects, which is not the case for the bulk chemicals they are composed of (Nel et al. 2006; Shvedova, Kagan, and Fadeel 2010; Singh 2015; Yildirimer et al. 2011). For example,

CONTACT Jörg Huwyler joerg.huwyler@unibas.ch Division of Pharmaceutical Technology, Pharmacenter, University of Basel, Klingelbergstrasse 50, 4056 Basel, Switzerland.
*Both authors contributed equally to the present work.

physicochemical characteristics such as particle size, shape, and surface properties (e.g. charge) have proven to influence the toxicological profile of ENP heavily regardless of their chemical composition (Berger 2009; Buzea, Pacheco, and Robbie 2007; Park et al. 2011). It is therefore generally believed that ENP cannot be regulated in the same way as bulk chemicals (Feliu and Fadeel 2010). In particular, a more detailed understanding of how and why nanoparticles interact with biological systems has to be developed (Dusinska et al. 2009; Guadagnini et al. 2015; Seaton et al. 2010). However, due to the shortage of nano-specific safety guidelines, nanomedicines are not regulated differently from 'ordinary' pharmaceuticals up to date. The awareness of nanoparticle toxicity has sensitized researchers and authorities alike to address these concerns and in turn has led to an increasing interest in phenomena related to 'nanotoxicology' (Gallud and Fadeel 2015; Gebel et al. 2014; Krug 2014).

Over the past decades, a plethora of research has been conducted on various ENP to better understand how and why nanoparticles are potentially toxic. It was found that nanoparticles entering an organism start to interact with their surroundings immediately (Kettiger et al. 2013; Unfried et al. 2007; Wu and Lu 2016). The nature of these interactions is dependent on the physicochemical identity of the nanoparticles, their surface properties, as well as the environment they encounter (Figure 1)(Fubini, Ghiazza, and Fenoglio 2010; Joris et al. 2016; Kim et al. 2015; Yang et al. 2017).

Today, it is known that many ENP are readily taken up by numerous cell types and have the ability to cross intra-cellular barriers as well as inter-cellular spaces (Guarnieri et al. 2014; Saraiva et al. 2016; Shimizu, Nakamura, and Watano 2016). Depending on type, dose, and incubation time, ENP can cause, e.g. the generation of reactive oxygen species, activate the complement system, or disrupt the functionality of membranes and cellular barriers (Guo et al. 2015; Moghimi and Simberg 2017; Sayes, Banerjee, and Romoser 2009; Siegrist et al. 2017). These actions lead to acute or chronic damage in the organism culminating in serious outcomes such as inflammation, gene aberrations, and severe organ damage (Nemmar et al. 2016; Vermeij et al. 2015; Wen et al. 2017). Yet – albeit all the efforts of elucidating nanotoxicological patterns – no standardized procedures exist to uniformly determine the safety of ENP. Ongoing debates about general definitions, ideal test systems, or how to group and classify ENP prevent the harmonization of existing safety and testing guidelines (Bleeker et al. 2013; Mühlebach, Borchard, and Yildiz 2015; Scott-Fordsmand et al. 2014; Whitesides 2003). Complicating this matter further, a number of clinical applications (e.g. in oncology) rely explicitly on cytotoxic effects induced by nanomedicines. Here, toxic effects are thus part of their mode of action (MoA) (Bao et al. 2015; Hung et al. 2016). Today, finding a consensus on how to evaluate the safety of ENP is one of the most controversially discussed topics among researchers (Nel et al. 2006), regulatory bodies (Stone et al. 2014), and authorities (van Teunenbroek 2017) alike.

The term nanotoxicology is generally defined as *'[…] the study of the adverse effects of engineered nanomaterials (ENM) on living organisms and the ecosystems, including the prevention and amelioration of such adverse effects. […]'* (Oberdörster 2010). This definition comprises environmental safety as well as adverse drug effects and consumer health thereby targeting every possible nanomaterial (including ENP). In contrast to this highly condensed and straightforward definition, the process of studying, preventing, or minimizing adverse effects caused by nanomaterials is very complex. So far it has not been possible to reach a consensus on how the safety on nanomaterials should be assessed using efficient methods and protocols, which are accepted by regulatory bodies. The reasons are manyfold: lack of defined reference material to benchmark the outcome of the tested material, lack of consensus on predictive endpoints for human toxicity, technical limitations of the tests for ENP (e.g. interference), and batch-to-batch differences due to insufficient control over the manufacturing process. For the past two decades, many government and non-government associations have tried to work out how to tackle this problem. Resulting from their work, the proposal to group or categorize nanomaterials for downstream risk and safety assessments has found large appreciation (Dekkers et al. 2016; Fadeel, Pietroiusti, and Shvedova 2017; Oomen et al. 2015). How to group nanomaterials will mostly be determined by their

toxicological profile or the underlying mechanisms thereof. However, it is at present still common to evaluate the safety of nanomaterials on a case-by-case basis due to the lack of standardized experimental data needed for establishing a grouping strategy. This is a time-consuming and costly procedure, which is especially undesirable in medicinal research. The most common grouping strategies (please refer to the following reflection papers of the European Medicines Agency (EMA) as provided in the References section: Data requirements for intravenous iron-based nano-colloidal products developed with reference to an innovator medicinal product; Joint MHLW/EMA reflection paper on the development of block copolymer micelle medicinal products;Reflection paper on surface coatings: general issues for consideration regarding parenteral administration of coated nanomedicine products; Reflection paper on the data requirements for intravenous liposomal products developed with reference to an innovator liposomal product; Reflection paper on nanotechnology-based medicinal products for human use.) are based on categorizing nanomaterials according to physicochemical properties, nanoparticle-cell interactions, exposure threats, or endpoint toxicity (Arts et al. 2015; Sayes, Smith, and Ivanov 2013; Simkó, Tischler, and Mattsson 2015). These strategies all target different aspects of nanomaterial toxicity and can provide vital information on the nature of nanomaterial-based toxicity. These approaches are often tailored to fit specific exposure risk scenarios of involuntary inhalation or voluntary oral ingestion (Bolt 2014; Gebel et al. 2014; Hadrup et al. 2015). Intentional therapeutic exposure upon injection on the other hand is only rarely referred to or even specifically ruled out of present grouping concepts (Arts et al. 2015). Yet, there are several reasons why the definition of such a strategy would be highly beneficial. First, for medical applications, where ENP formulations offer increasing therapeutic options, injection is the preferred route of administration. This route of administration leads to a defined and measurable exposure in contrast to inhalation or ingestion scenarios. Second, with the correct choice of biological models, it is possible to distinguish between intentional pharmacological effects (i.e. cytotoxicity as a MoA in cancer) and off-target effects. Third, with more than 75 FDA approved ENP, over 100 in clinical trials and hundreds more in research (Bobo et al. 2016; Witzigmann et al. 2015), the need for nano-specific regulation and safety assessment strategies for medical candidates is obvious.

2. Aim

It is the aim of the present work to provide a proposal for a novel hazard evaluation strategy to determine the safety of ENP designed for the use as injectable nano-pharmaceutics (Figure 2). It is important to note that inhalable and ingestible dosage forms were explicitly excluded from this study. Inhalables are based on particle size distributions that exceed the nano-range (Brown et al. 2013). Oral nanomedicines mostly consist of nanocrystals, which enhance solubility of poorly soluble drugs (Etheridge et al. 2013; Junghanns and Müller 2008). As they dissolve rapidly upon contact with gastric or intestinal fluids, these materials do not penetrate the body in the form of nanoparticles. Here, we propose a stepwise approach to assess the safety of nanomedicines (Figure 2). First, ENP are required to meet specific physicochemical properties to allow for their use as injectable nanoparticles (iNP). Second, a novel classification system divides selected candidates into hazard classes based on cellular uptake and intracellular persistence. Third, ENP are evaluated based on their safety classification using a distinct set of standardized toxicological assays as conducted by the US Nanotechnology Characterization Laboratory and European Nanomedicine Characterization Laboratory (USNCL and EUNCL, respectively). The US- and EUNCL assist the respective regulatory agencies (EMA and FDA) during the approval process of medical applications containing nanomaterials. Finally, the retrieved information serves a multitude of downstream processes such as safe-by-design, safety predictions, risk assessment, data mining, and grouping.

The three-tiered strategy allows us to identify suitable ENP for injection in an application-oriented and effective manner. Its structure could aid in minimizing the risk of adverse responses when moving from *in vitro* to *in vivo* testing as well as costly failures during later stages of their development. Our strategy is thus based on the International Organization of Standardization (ISO) definition of the term 'nanoparticle' and takes up a similar

classification approach as used, for example, in the Biopharmaceutics Classification System (BCS) to estimate the oral bioavailability of drugs (Amidon et al. 1995; ISO 2015). The concept uses standardized testing protocols from the USNCL and EUNCL to specifically assess the hazardous potential of ENP. Ultimately, the HES approach should promote an application-oriented decision-making process. It will contribute to informed and effective ENP hazard assessment and can be combined with future grouping strategies for read-across purposes.

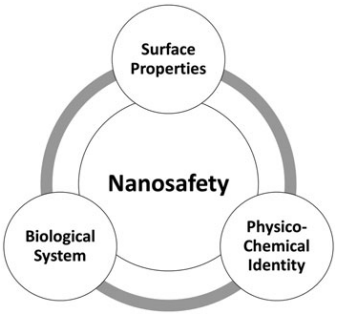

Figure 1. Nanosafety. Together with the biological system, the surface properties and physicochemical identity define the toxic potential of any engineered nanoparticle.

3. The hazard evaluation system for injectable nanoparticles (HES)

Approved nanomedicines designed for parenteral administration are very diverse with respect to their chemical identity, size, geometry, surface modifications, ζ-potential, and intended clinical uses. Very often, these formulations share certain physicochemical properties. They are mostly spherical or display an aspect ratio (AR) $\leq$ 3:1, have particle diameters below one micron (Buzea et al. 2007), and are stable as dispersions. However, this knowledge does not directly provide any information on the behavior or safety of an ENP after injection. ENP may provoke toxicity in a dose- and time-dependent manner upon interaction with biological systems. This includes, for example, recognition, phagocytosis or endocytosis, and processing of the immune system (macrophages) on a cellular level (Bartneck et al. 2010b; Sabella et al. 2014; Tiwari, Takashi, and Behari 2010; Weissleder, Nahrendorf, and Pittet 2014). On a whole-organism level, such interactions may lead to

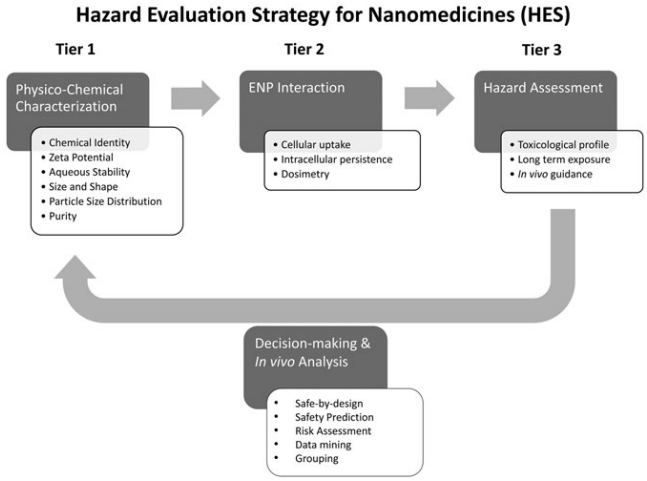

Figure 2. Hazard Evaluation System for Injectable Nanoparticles (HES). The HES hazard evaluation strategy is based on a three-tiered approach, which combines physicochemical characterization of engineered nanoparticles (ENP), ENP interaction, and hazard assessment. This test strategy can be used to (i) determine if a given ENP qualifies as a parentally administered medical application and (ii) identify potential safety issues of injected nanomedicines at early stages of their development. Furthermore, linking the findings from tiers 2 and 3 to the physicochemical properties determined in tier 1 can serve as the basis for *in vivo* testing strategies, risk assessment strategy set up and future grouping criteria. This will help to design and optimize ENP through safe-by-design principles and support personalized medicine initiatives.

augmented circulation time, accumulation, retarded clearance, off-target interactions, organ damage, and chronic adverse effects. We strongly believe that the two key factors, directly providing preliminary information on these biological interactions and the ensuing *in vivo* consequences, are cellular uptake (Oh and Park 2014; Yameen et al. 2014) and intracellular persistence (Laux et al. 2017; Lee et al. 2013). High uptake and high persistency may trigger inflammatory events (Fadeel et al. 2017; Kennedy, Wilson, and Barakat 2009). Low quantities of ENP uptake by cells other than macrophages and low intracellular persistency over time is indicative of limited biological interactions. In the latter case, phagocytosis by macrophages (Bartneck et al. 2010a) or extracellular events such as platelet aggregation or complement activation should be closely monitored. Due to the possibility of linking physicochemical properties with nanoparticle-cell interactions *in vitro*, the risk of provoking adverse effects *in vitro* and *in vivo* (e.g. toxicity or elimination) can be minimized significantly.

The Hazard Evaluation System for Injectable Nanoparticles (HES) was designed as a concept to specifically test the suitability of ENP as injectable pharmaceutics. The three tiers – as shown graphically in Figure 2 – are physicochemical characterization (1), ENP interaction (2), and hazard assessment (3).

The ENP are physicochemically characterized before progressing to *in vitro* toxicity studies. Following the characterization, cellular uptake and intracellular persistence of the formulations are determined to categorize them into hazard groups for more detailed hazard assessment. Dedicated hazard assessment processes designed for every group ensure the recognition of hazardous potential associated to a pharmaceutical candidate. Every tier includes specific assays, measuring techniques, controls and definitions that are discussed in detail in the following sections. Formulations failing to meet the requirements of tier 1 to tier 3 are not further considered in the HES approach and are required to proceed in case-by-case evaluations. Such formulations are not necessarily considered unfit as injectable pharmaceutics; however, due to their innovation or unconventional characteristics represent classes of formulations where vital information is still lacking. Thus, the safety of these candidates must be evaluated case-by-case until enough data are acquired in order to expand the HES framework or separately establish a novel testing strategy. An important component of the proposed concept is the retrospective analysis of results (decision-making and *in vivo* analysis, Figure 2). Data mining and data analysis will offer the possibility to perform informed safety predictions and to implement grouping and modeling strategies. Such a rational approach will be the basis for future safe-by-design strategies.

3.1. Tier 1: Physicochemical characterization

In the first tier of the HES, the candidate materials enter a defined physicochemical characterization cascade (see flowchart Figure 3). The cascade serves as a systematic preselection sequence, in which ENP are tested according to six criteria: chemical identity, ζ-potential (zeta potential), aqueous stability, shape, size and size distribution, and contamination. Depending on the outcome of this initial screen, an ENP either qualifies to be further investigated in the HES or must yet undergo a 'case-by-case' safety assessment, as mentioned earlier. The chemical identity, ζ-potential, and aqueous stability of an ENP are not directly a safety issue in most cases. Nevertheless, knowing these three parameters is a prerequisite for their further experimental assessment. Having this knowledge beforehand can give insight into how an ENP sample behaves in dispersion, or in what manner it may interact with buffers or biological fluids. A formulation that fulfills all physicochemical requirements (as summarized in Figure 3**)** also fits the physicochemical definition of an injectable nanoparticle and can therefore enter tier 2 of the HES.

Each one of the basic physicochemical properties of ENP should be measured using a standardized protocol. For the HES, we propose to use the written and recommended protocols of either the USNCL or the EUNCL. Both US- and EUNCL work together with the FDA or the European Medicines Agency (EMA), respectively. Furthermore, both NCL institutions do not only act as advisors to regulatory agencies but also provide assistance for small and medium-sized enterprises, spin-offs and newcomers towards nanomaterial characterization and product submission approvals. This assures that the assay

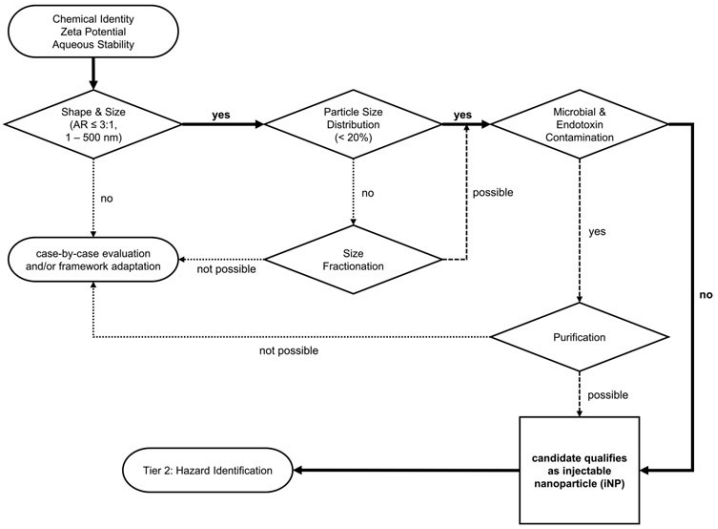

Figure 3. Physico-chemical characterization of nanoparticle properties. The physicochemical characterization of ENP represents tier 1 of the Hazard Evaluation System for Injectable Nanoparticles (HES). After the chemical identity, ζ-potential, and aqueous stability are determined, size, particle size distribution, and purity are examined. In this step-by-step approach, an ENP either moves on through the HES cascade or its safety has to be evaluated separately case-by-case depending on the results obtained during characterization. A candidate passing the entire cascade (Tier 1) qualifies as an injectable nanoparticle according to the HES guideline and moves on to ENP interaction (Tier 2, Figure 4). AR: Aspect Ratio.

protocols are well in-line with current testing standards and are re-evaluated on a regular basis.

In addition, proposals for alternative measurement techniques are provided as well. These techniques are not used by the US- or EUNCL but find much appreciation throughout their respective research fields. Furthermore, not all techniques suggested by the NCLs are available as a standard in every laboratory. References to selected protocols are listed in the appropriate sections of this publication.

3.1.1. Chemical identity

The chemical identity of an ENP should be assessed first as it may have an impact on the setup of further experiments regardless if the ENP is the active agent or its carrier system. Should any chemical contaminations (e.g. synthesis residues) be detected during the assay, it is strongly advised to purify the formulation before advancing further in tier 1 (Garbovskiy 2017). Batch-to-batch variability should be held as low as possible and must be recorded for at least three independently manufactured formulations.

Different analysis techniques can be used to gain information on the chemical identity of an ENP. The most commonly used technique is Inductively Coupled Plasma Mass Spectrometry (ICP-MS) (Fabricius et al. 2014). With ICP-MS entire samples or single nanoparticles (detection limit in nanogram per liter range) can be analyzed in very short time and high precision. Furthermore, ICP-MS can be coupled to several analytical separation methods whereby speciation and quantification measurements can also be performed. The USNCL provides four different protocols on how to characterize the chemical identity of nanomaterials all including ICP-MS techniques (USNCL-PCC-8, USNCL-PCC-9, USNCL-PCC-11, and USNCL-PCC-14). As an alternative, different techniques including High Performance Liquid Chromatography (HPLC) are also being used to analyze nanomaterials that are mainly carbon, or nonmetal based (Álvarez-Fuentes et al. 2012; Itoh et al. 2016).

Alternatively, Nanoscale Fourier-Transformation Infrared Spectroscopy (nano-FTIR) can also be used to determine the chemical identity of nanoparticles

(Huth et al. 2012). Fourier-Transformation Infrared Spectroscopy (FTIR) is commonly used in chemistry to identify chemical structure of materials or to verify the chemical purity of a synthesis product. Nano-FTIR is a combination of FTIR and scattering-type Scanning Near-field Optical Microscopy (s-SNOM) based on Atomic Force Microscopy (AFM) in non-contact mode. The technique allows measurements on ultra-small probe quantities with a spatial resolution of 10 nm–20 nm. Nano-FTIR has already been successfully used to identify polymers and nanocomposites or in investigations regarding the elucidation of secondary protein structures as well as bacterial membranes (Amenabar et al. 2013).

Another important technique is the Microscale Thermogravimetric Analysis (μ-TGA). It is used to characterize the surface coating and purity of nanoparticles, especially when they are introduced to a biological environment (Mansfield et al. 2014). This method is very sensitive and can be used to determine the amount of coating on the nanoparticle surface. These experiments are done in an inert atmosphere at temperatures over 1000 °C (Dongargaonkar and Clogston 2018).

Alternatively, quantitative NMR can be used to characterize nanoparticles to reveal structural and dimensional information. Especially the coatings can be analyzed to explore characteristics like the ligand density on the surface (Guo and Yarger 2018).

3.1.2. Aqueous stability and ζ-potential

The lack of aqueous stability provokes agglomeration and sedimentation, which may trigger immune responses such as phagocytosis, generation of reactive oxygen species (ROS), or inflammatory reactions. Moreover, agglomeration-flocculates can sediment and in extreme cases could clot capillaries causing mechanical distress and serious pain. Since there is no generally accepted protocol on the measurement of ENP stability, the authors propose the following: *'The aqueous stability of ENP should exceed the duration of the longest tests proposed in the tiers of the hazard evaluation strategy (HES). We therefore propose that ENP dispersions should not display any significant changes in particle size, shape, and particle size distribution over the course of at least one week, at a defined pH and at 37 °C using a physiological buffer system.'*

However, depending on specific project requirements and application needs, this basic protocol can be adjusted to a specific time frame (e.g. short-term application) or for factors that can affect the stability profile, such as the mechanism of the payload delivery or surface modifications. Furthermore, additional test might be needed to demonstrate prolonged stability during storage at room temperature or at 4 °C in a specific container (e.g. plastic infusion bag or glass vials). It should also be noted that the stability of an ENP may change after dispersion in biological fluids (Aguilar-Castillo et al. 2015; Moore et al. 2015). Thus, performing stability measurements in biological fluids may yield valuable information as well and should be carried out. Aqueous stability measurements follow the same protocols used for particle size, shape, and particle size distribution. Method descriptions and protocols are covered in detail by the appropriate standardized protocols (see Section '3.1 Tier 1: Physicochemical characterization').

The aqueous stability of any nanomaterial dispersion is often related to the surface charge (ζ-potential) of the nanoparticle. For this reason, ζ-potentials of ENP should be measured prior to analyzing their aqueous stability (Bhattacharjee 2016). Formulations that display positive or negative ζ-potentials are generally considered to be stable in water whereas nanoparticles with a ζ-potential near neutral tend to agglomerate (Clogston and Patri 2011). It should, however, be noted that highly positive charged particles have the potential to be acute cytotoxic (Dobrovolskaia et al. 2012). On the other hand, ζ-potential values directly depend on the pH of nanoparticle dispersions as pH influences protonation and deprotonation of the nanoparticles (Berg et al. 2009). Thus, ζ-potentials should always be determined at pH values that resemble the ones of the ENP storage solutions and ideally represent physiological conditions (i.e. ideally above 30 mV or below −30 mV). The protocols ensuring correct measurements of ζ-potentials and pH are referenced as USNCL-PCC-2 and USNCL-PCC-13, respectively. The preferred ζ-potential measuring technique is electrophoretic light scattering (ELS) whereas pH is predominantly measured with semi-micro combination pH electrodes.

3.1.3. Shape

The International Standards Organization (ISO) provides definitions for the terms nanomaterial, nanoobject, nanofiber, nanoplatelet, and nanoparticle based on their external and internal dimensions. In this sense, external dimensions describe length, width, and height of a material whereas surface structures (e.g. pores) and internal structures are acknowledged as internal dimensions (ISO 2015). As an exclusion criterion, the HES approach considers external dimensions of ENP only, yet taking into account that internal dimensions may well influence stability or the MoA.

As mentioned before, most commercially available nano-pharmaceutics are spherical in shape or have an aspect ratio of $\leq$3:1. Therefore, only nanoparticles that display an aspect ratio (AR) $\leq$3:1 are considered for further investigations in the HES. So called high aspect ratio nanomaterials (HARN) (Oberdörster, Stone, and Donaldson 2007) are excluded from the process. This includes the fiber-like single or multiwalled carbon nanotubes (SWCNT or MWCNT, respectively). Although these nanomaterials are at present heavily studied, they show typical signs of complications associated to HARN. HARN may inflict mechanical cell or tissue damage often due to rigidity and size (e.g. leading to frustrated phagocytosis). Moreover, their geometry bears a higher risk of recognition by the immune system. Considering these facts, HARN are not ideal nanomaterials for parenteral applications and have not been used as such up to date. Consequently, HARN are also excluded from the HES and must be evaluated on a case-by-case basis.

Transmission Electron Microscopy (TEM) (Pyrz and Buttrey 2008), Scanning Electron Microscopy (SEM) (Goldstein et al. 2014), and cryoEM (Crawford et al. 2011) are commonly used to study the shape of nanoparticles. The chemical identity of a nanoparticle dictates which of these techniques should be applied. The procedures using TEM and SEM can be carried out according to the protocols USNCL-PCC-7 and USNCL-PCC-15, respectively. Additionally, the EUNCL provides a protocol for cryoEM analysis (EUNCL-PCC-20).

3.1.4. Particle size

Particle size is arguably the most important characteristic in the first HES tier since various definitions of the term 'nanoparticle' are based entirely on primary particle size. We propose the implementation of a novel size range specifically suiting ENP designed for injection. Such candidates normally cover a size range of 1–500 nm rather than the regulatory definition of 1–1000 nm. Candidates averaging sizes below 1 nm or above 500 nm are subjected to case-by-case evaluations and are excluded from the HES.

We feel that, in this particular case, the novel ENP size range of 1 nm to 500 nm is a valid alternative to existing definitions of the International Standards Organization (ISO), the Organization for Economic Co-operation and Development (OECD), the European Commission, the US Environmental Protection Agency, or regulatory authorities in charge of pharmaceuticals. In many cases, nanoobjects are defined by a size of approximately 1– 100 nm (often referred to as the nanoscale) (ISO 2015; Krug and Wick 2011; Potočnik 2011; Serpone and Horikoshi 2013). The lower limit of 1 nm was set to specifically exclude single atoms and small atom groups. The upper limit of 100 nm was set to emphasize on the existence of so called 'quantum size effects' (Boilard et al. 2013; Krug and Wick 2011; Zhang et al. 2009) often originating from band-gap differences directly influenced by particle size (Chukwuocha, Onyeaju, and Harry 2012). Due to their submicron size, ENP may thus display unique characteristics that their bulk counterparts lack completely. The National Nanotechnology Initiative (NNI) states that quantum effects are size driven and in turn govern the behavior and properties of nanomaterials (NSCT/CoT/NSET 2014). A number of properties such as fluorescence, electrical conductivity, magnetic permeability, and chemical reactivity are affected when particles stay below the critical size of 100 nm (Navya and Daima 2016; Uskoković 2013). However, this 100 nm cutoff value remains controversial, for different reasons. Numerous regulatory organizations feel that the present justification of the upper size limit (100 nm) is not scientifically appropriate and should be extended with more qualifiers (such as particle size distribution and spatial dimensions) (Jong 2010; Lovestam 2010; Potočnik 2011). Additionally, it has been acknowledged that health and safety aspects with nanomaterials do not abruptly end at 100 nm (ISO 2015). In view of these debates and the

growing interest in pharmaceutical and medical nano-applications, the FDA has considered an augmentation of the upper scale limit to 1000 nm (FDA 2005). Most other regulatory authorities have also adopted this scale enlargement over the past years. However, the FDA also states that setting the cutoff at one micron is not at all trouble-free as this size incorporates an even greater palette of diverse materials (e.g. pigments, quartz, sand). The FDA, therefore, states that it might be beneficial not to cover all nanomaterials within one definition but rather set definitions according to the applicatory field of the material in question (FDA 2005).

Taking these facts into account, the HES size definition for injectable nanoparticles was considered to be appropriate for medical regulation purposes. The lower limit of the HES size definition (i.e. 1 nm) is based on widely accepted nanoparticle definitions from authorities and regulatory bodies whereby atoms and small molecules are excluded. Its upper limit (i.e. 500 nm) newly considers the activity of immune cells and their ubiquitous presence in the vasculature system. It is generally accepted that uptake of intact nanoparticles through cell membranes is mediated by active transport (e.g. receptor mediated endocytosis) (Zhang et al. 2009). These uptake routes depend on particle size. Objects smaller than 500 nm are readily internalized via different types of endocytosis (e.g. clathrin versus caveolin-mediated transport) (Champion, Katare, and Mitragotri 2007; Kettiger et al. 2013). However, objects larger than 500 nm mostly lack this ability and are prone to be predominantly exposed to phagocytosis, which is an immune cell-specific process (Aderem 2003). Therefore, limiting ENP size to 500 nm rules out size-dependent involvement of immune cells in cellular uptake of ENP or immune mediated reactions. Finally, since injectables are not designed to trigger phagocytosis, the upper size limit of 500 nm in the HES definition of an iNP was chosen.

Alternatively, some nanoparticles are designed to be fusiogenic (e.g. cationic liposomes). For example, liposomes with integrated lipopeptides in the bilayer were able to fuse with plasma membranes and to empty their cargo into the cytoplasm of their target cells (reviewed by Li et al. (2017)). Under such conditions, active transport will not be involved and the mentioned size definitions have to be adjusted.

Size measurements must be interpreted with caution since the term 'particle size' is often used interchangeably to describe the primary particle size as well as the hydrodynamic diameter of an ENP. Primary particle size denominates the true particle diameter, whereas the hydrodynamic diameter takes the first layer of solvent into account as well (Hackley and Clogston 2011). Hence, the hydrodynamic diameter should always be larger than the primary particle diameter and is therefore the decisive parameter when it comes to the discussed size limitations. Nevertheless, both parameters should be measured as either one can have an impact at later stages of the HES. The standard methods to measure hydrodynamic diameters of ENP are based on the technique of Dynamic Light Scattering (Kaszuba et al. 2008) (DLS, protocol USNCL-PCC-1). Here, Nanoparticle Tracking Analysis (NTA) (Hole et al. 2013; Maguire et al. 2017; Mehn et al. 2017) is frequently used as an alternative method. Atomic Force Microscopy (Rao et al. 2007) (AFM, protocol USNCL-PCC-6) and TEM (Pyrz and Buttrey 2008) (protocol USNCL-PCC-7) are typically used to determine primary particle sizes. Other techniques that are used to describe primary particle sizes include: Small-Angle X-Ray Scattering (SAXS) (Li, Senesi, and Lee 2016; Vippola et al. 2016) and electrospray differential mobility analysis (ES-DMA) (Guha et al. 2012).

3.1.5. Particle size distribution

The Scientific Committee on Emerging and Newly Identified Health Risks (SCENHIR) sub-categorizes nanoparticles into three categories depending on the range of particle size distributions. In contrast, we propose a more stringent approach. It demands particle size distributions to be as narrow as possible (Jong 2010). In physiological buffer, a particle size distribution limit of 20% or a polydispersity index value (PDI) of <0.2 based on an intensity-based Z-average diameter value is proposed. This limit is chosen because a PDI of <0.2 is considered to reflect monodispersity (Panchal et al. 2014; Roberson and Weltje 2014). However, the viscosity and refractive index of the solvent, ionic strength of the media, temperature, concentration of ENP,

handling of ENP (e.g. filtration, sonication) should be considered for comparing different PDI values across studies. It should be noted that a PDI <0.2 for parenteral applications might be smaller than the corresponding value defined for other therapeutic applications. For example, for dermal delivery of liposomes, a PDI <0.3 has been deemed acceptable to reflect monodisperse ENP-drug preparations. In addition, the PDI will change in presence of proteins due to protein adsorption or the presence of protein agglomerates. If the condition of monodispersity is not fulfilled, size fractionation (Akthakul et al. 2005; Robertson et al. 2016) or filtering (Droppo 2006) may be used to narrow down the particle size distribution of particle populations. The method of choice to determine hydrodynamic particle size distributions and polydispersity is DLS according to protocol USNCL-PCC-1. In addition, true particle size distributions of ENP should be confirmed by SEM and TEM (FDA 2005; Jong 2010; Lovestam 2010).

3.1.6. Microbial contamination and endotoxins

A well-known issue with ENP submitted for pharmaceutical or medical approval is purity (Li and Boraschi 2016). The presence of impurities is the most common reason regulatory bodies neglect pharmaceutical formulations or applications during the approval sequence. Purity refers to the absence of chemical or biological contamination. As chemical impurities must be checked for and identified previously during the analysis of the chemical identity; this step of the HES focuses on biological contamination (i.e. bacteria, mycoplasma, or endotoxin). The USNCL defines a number of assays to assess contamination levels of nanomaterials. At least endotoxin (USNCL-STE-1.1 until 1.4), bacterial (USNCL-STE-2.1 and 2.2), and mycoplasma contaminations (USNCL-STE-3) should be monitored. Purity is an intrinsic property of any iNP. In case of the presence of contaminants, ENP should be sterilized and depyrogenized by using standard techniques such as autoclaving, filtration, or gamma-irradiation (Li et al. 2013; Vetten et al. 2014; Zheng et al. 2011). If, however, impurities are still detected thereafter, which cannot be removed by a modified production process, the candidate falls out of the HES and must be further assessed in a case-by-case evaluation. Because standard sterilization techniques can influence the stability and physicochemical properties of ENP, it must be ensured that the properties of postprocessed ENP are not significantly changed.

3.1.7. Physicochemical definition of an injectable nanoparticle (iNP)

The physicochemical definition of an iNP takes all the previously discussed issues into account and summarizes tier 1 of the Hazard Evaluation Strategy for Injectable Nanoparticles (HES) as follows: *'An injectable nanoparticle (iNP) is defined as a nanoparticle measuring between 1 nm to 500 nm in all three external dimensions (height, length, width), whereas the length of the longest to the shortest axis of the nanoparticle do not differ by more than three-fold (aspect ratio 3:1). Additionally, iNP particle size distributions should be below 20% (polydispersity indices of <0.2) as determined in a physiological buffer system. Also, the aqueous stability should not be affected over the course of 7 days when measured at a distinct pH and 37 °C. Finally, an iNP must be endotoxin-free and should not show chemical, bacterial, or mycoplasma contamination.'*

3.2. Tier 2: ENP interaction

In the second tier of the HES, a novel classification system divides iNP into four different risk categories depending on two biological readouts, which are linked to particle persistence in biological systems and cellular exposure. In this novel ENP interaction concept (Figure 4), iNP are grouped according to the criteria of cellular uptake and intracellular persistence. We propose that these two parameters are key for iNP safety in circulation. In the HES plot, the intensity of cellular uptake and intercellular persistence increases from the top left to bottom right quadrant of the plot. This does not generally imply that high uptake and persistence of iNP bear the highest risk for a patient. Depending on the intended use of the iNP, high uptake and persistence are part of the MoA. Yet, the multitude of possible adverse effects is augmented when uptake and persistence are high. Consequently, iNP grouped into category IV necessitate a more detailed safety assessment as compared to iNP

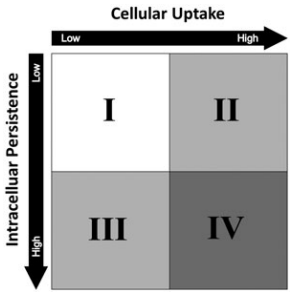

Figure 4. The HES ENP interaction. The HES ENP interaction divides nanoparticles into four different groups. The grouping strategy is based on cellular uptake and intracellular persistence of an iNP. By monitoring these two parameters, distinct hazard assessment strategies can be designed for individual ENP interaction groups. As a general rule, the higher the category the higher the number of possible hazards and thus the number of required safety assessments. It should be noted that the generation of ROS or an involvement and activation of the immune system has a major impact on the interpretation of the HES classification. For example, humoral responses mediated by the complement system may lead to hemolysis and platelet aggregation. Cellular immune responses may lead to particle depletion.

falling into lower risk categories (Category IV < III < II < I).

Neither USNCL nor EUNCL provides standardized protocols for measuring cellular uptake or intercellular persistence as this does not lie in the scope of their work. Therefore, experimental methods are proposed in the following sections to address these issues.

3.2.1. Cellular uptake

The techniques to measure cellular uptake can vary depending on the type of iNP and the availability of analytical technologies. Ideally, confocal-, dark-field-, and EM-microscopy (qualitative assessment) can be combined with flow cytometry, HPLC, single particle or single cell ICP-MS, or a combination of the latter techniques (quantitative assessment). The prerequisite for quantitative assessments is, however, knowing the initial administered dose. After a desired incubation time, the quantity of iNP and their residues is measurable in the supernatant as well as in the cell sample. This enables determining the quantity of iNP taken up. Measurements should be performed at time points 30 min, 4 h, 8 h, and 24 h. The indicator for low cellular uptake would then be defined as any quantity of iNP taken up in the first 8 h of incubation being below a certain cut-off value (percentage of total iNP dose). Alternatively, high cellular uptake levels would be represented by any quantity of iNP taken up in the first 8 h of incubation exceeding that same cutoff value. With this respect, erythrocytes may serve as negative control (minimal uptake) and macrophages as positive control (maximal uptake).

Cellular uptake of iNP should be monitored in the cell type, which is most likely to interact first with iNP after injection. After intravenous injection of iNP, for example, these are vascular endothelial cells as they line the blood vessels and the lymphoid system (Félétou 2011). Endothelial cells are known to readily take up nanoparticles (in contrast to, e.g. erythrocytes) (Siegrist et al. 2017). This can lead to severe cytotoxic effects that in turn damage the vascular system and potentially the tissue residing behind it, causing complications and pain in the patient. Furthermore, the endothelium acts as a semi-selective barrier and co-controls the migration of white blood cells into and out of the blood stream (Yuan and Rigor 2010). Endothelial dysfunction plays, therefore, a pivotal role in vascular diseases (Deanfield et al. 2005) and is often regarded as the early trigger of events such as arteriosclerosis (Davignon and Ganz 2004). We, therefore, believe that monitoring endothelial uptake of iNP *in vitro* provides essential information on endocytosis and cellular clearance of iNP. Intended target cells of the iNP should be excluded from these measurements, since the focus of these experiments is an ENP interaction in non-target cells. While the exact structure of the biocorona is controversially discussed (e.g. existence and relevance of a 'soft' protein corona), the detailed composition is very variable and highly fluctuating over time even *in vitro* (Casals et al. 2010; Docter et al. 2015). Furthermore, recent studies show that proteins adsorbed to nanoparticles *in vitro* are rapidly exchanged *in vivo* (Chen et al. 2017). Although, in the future, *in vitro* tests might permit to predict the role and influence of the biocorona *in vivo*, currently our understanding and ability of extrapolating the impact from *in vitro* to *in vivo* is insufficient. Therefore, future tests assessing the biocorona of nanoparticle might complement our test strategy.

For protein interactions of biomedical applied nanoparticles, see Shannahan (2017). This topic is further reviewed by Treuel et al. (2015), Ke et al. (2017), and Neagu et al. (2017).

3.2.2. Intracellular persistence

Intracellular persistence is monitored in the same cell type, preferably even in the same sample, as cellular uptake. The first measurements should be performed 8 h and 24 h after incubation, thereafter once every 24 h for a week. In the sense of a precautionary approach, low intracellular persistency is defined if the amount of iNP taken up after 24 h decreases by 80% until the fifth day of the measurement. High intracellular persistence is given, if less than 80% of the iNP taken up in the first 24 h has been degraded.

Measuring intracellular persistence can either be performed by confocal and EM microscopy or ICP-MS (Lee et al. 2013). While microscopy techniques will only yield qualitative results, ICP-MS allows for quantitative analyses. However, cellular samples are destroyed under ICP-MS in contrast to microscopy techniques. It should be emphasized, that intracellular persistence is not equivalent to chemical or colloidal stability as it is being tested for in tier 1 of the HES. Even though the two parameters can certainly be linked, the ability of an organism to degrade or eliminate an iNP underlies different and often more complex mechanisms than particle agglomeration or disintegration in aqueous solution.

Experimental results on cellular uptake are expected to be dose- and time-dependent. They are not only closely related to the number of nanoparticles taken up, but can vary depending on the capacity of cells to degrade or eliminate them after uptake. Thus, intracellular persistence correlates to intracellular accumulation and exposure. It is therefore expected that adverse effects gain in severity with increasing levels of uptake and persistence, in particular if iNP are administered repeatedly.

3.2.3. Dosimetry and dose

It is important to note that correct dosimetry is paramount for any type of nanosafety evaluation and ENP risk assessment (Teeguarden et al. 2007). Cellular uptake, intracellular persistence, and toxicity are in most cases dose-dependent. For *in vitro* studies on nanoparticles, appropriate doses range from ng/ml to μg/ml (Siegrist et al. 2017). To translate the dose-range from *in vitro* and *in vivo* experiments to humans (human equivalent dose, HED), no-observed-adverse-effect-level (NOAEL) values from corresponding animal experiments are used. The animal-derived NOAEL is multiplied with a conversion factor (k_m), which is different for each species. It is based on the body surface area and is set by the FDA. After calculating the HED, a maximum recommended starting dose (MRSD) is evaluated. Dividing HED values by a safety or uncertainty factor (often a factor of 10) is the common procedure to calculate an MRSD and reduce the risk of possible adverse effects in humans. The MRSD is given in milligrams per kilogram body weight (mg/kg), which can be reproducibly calculated for each individual (FDA 2005; Nair and Jacob 2016). Table 1 highlights the maximum recommended dose and route of administration of selected nanomedicine formulations approved by the FDA. The given doses correspond to the highest recommended dose for a person weighing 60 kg with a body surface area of 1.69 m^2. For reasons of completeness, nanocrystals – which are administered at very high doses – are also listed in Table 1. However, these oral dosage forms cannot be designated as iNP based on criteria of the HES as discussed in previous sections. Nevertheless, therapeutic doses of injectable nanomedicines typically cover three orders of magnitude depending on the indication, as the selection of approved nanomedicines in Table 1 shows.

In accordance with regulatory guidelines on pharmaceutical applications, we therefore recommend that a no-observed-adverse-effect-level (NOAEL) as well as a maximum recommended starting dose (MRSD) specifically for iNP should be established routinely. Nano-specific HED and k_m values should be calculated on a case-by-case basis considering the unique toxicological profile of nanoparticles and their intended clinical application. This should be done for the final formulation, which will be administered to the patient. If the preclinical formulations substantially differ from the final product formulations, the previously measured values should be updated. We recommend that for injectable nanomedicines, the dose units should uniformly be given in mg/kg (rather than U/kg or mg/

Table 1. Applied doses of FDA approved nanomedicines. Dose, dosing interval, administration route(s), and supplement size of selected FDA approved nanomedicines.

Name (Company), Year of approval	Dose	Interval	Administration	Supplement size
Selected examples of inorganic based injected nanoparticles				
Feridex®/Endorem® (AMAG pharmaceuticals), 1996 (2008)	0.65 mg/kg	Once	i.v.	56 mg/5 ml
Ferrlecit® (Sanofi Avertis), 1999	2.1 mg/kg	Once	i.v.	62.5 mg/5 ml
Feraheme®/ferumoxytol (AMAG pharmaceuticals), 2009	8.5 mg/kg	Twice a week	i.v.	510 mg/17 ml
Venofer® (Luitpold Pharmaceuticals), 2000	16.7 mg/kg	Once	i.v.	100 mg/5 ml, 200 mg/10 ml
INFeD® (Sanofi Avertis), 1957	45.9 mg/kg	Once	i.v.	100 mg/2 ml
Selected examples of injected nanocrystals				
Abraxane®)/ABI-007 (Celgene), 2005, 2012, 2013	7.7 mg/kg	Every 3 weeks	i.v.	100 mg/20 ml
Ryanodex® (Eagle Pharmaceuticals), 2014	11.7 mg/kg	Once	i.v.	250 mg/5 ml
Selected examples of lipid based injected nanoparticles				
Marqibo®\ (Onco TCS), 2012	67.7 μg/kg	Weekly	i.v.	5 mg/31 ml
Visudyne® (Bausch and Lomb), 2000	0.18 mg/kg	Once	i.v.	15 mg/7 ml
AmBisome®\ (Gilead Sciences), 1997	0.82 mg/kg	Daily	i.v.	50 mg/10 ml
DaunoXome® (Galen), 1996	1.2 mg/kg	Every 2 weeks	i.v.	50 mg/25 ml
Onivyde® (Merrimack), 2015	2.1 mg/kg	Every 2 weeks	i.v.	43 mg/10 ml
Doxil®/Caelyx® (Janssen), 1995, 2005, 2008	1.5 mg/kg	Monthly	i.v.	20 mg/10 ml, 50 mg/30 ml
DepoDur® (Pacira Pharmaceuticals), 2004	0.25 mg/kg	Once	lumbar-epidural	10 mg/ml
DepoCyt® (Sigma Tau), 1996	0.83 mg/kg	Every 2 weeks	intrathecal	50 mg/5 ml
Curosurf®/Poractant alpha (Chiesei farmaceutici), 1999	2.9 mg/kg	Once	intratracheal	120 mg/1.5 ml, 240 mg/3 ml
Selected examples for injected polymeric drugs				
Mircera®/Methoxy polyethylene glycol-epoetin beta (Hoffman-La Roche), 2007	0.7 μg/kg	Every 2 weeks	s.c. or i.v	50–1000 μg/ml
PegIntron® (Merck), 2001	1.8 μg/kg	Weekly	s.c.	50–150 μg/0.5 ml
Cimzia®/certolizumab pegol (UCB), 2008, 2009, 2013, 2013	6.7 mg/kg	Monthly	s.c.	200 mg/ml
Oncaspar®/pegaspargase (Enzon Pharmaceuticals), 1994	0.88 mg/kg	Every 2 weeks	i.m. or i.v.	3750 U/5 ml (> 85 IU/kg)
Macugen®/ Pegaptanib (Bausch & Lomb), 2004	5.0 μg/kg	Every 6 weeks	intravitreal	0.3 mg/ml
Selected examples for oral or dermal applied nanoparticles or polymeric drugs				
Zanaflex® (Acorda), 2002	66.5 μg/kg	3x daily	oral	2 mg, 4 mg, 6 mg capsules 4 mg tablets
Megace ES® (Par Pharmaceuticals), 2001	10.4 mg/kg	Daily	oral	625 mg/ 5 ml
Estrasorb® (Novavax), 2003	58 mg/kg	Daily	topical	4.35 mg/1.74 g foil

Highest recommended doses are shown and are normalized to 60 kg body weight and 1.69 m^2 body surface area (FDA, 2005).
The supplement size shows the amount of drug per sample unit.
Therapeutically used doses vary by three orders of magnitude.
i.m.: intramuscular; s.c.: subcutaneous; i.v.: intravenous.

m^2) as proposed in 2005 by the FDA for initial clinical trials (FDA 2005).

3.3. Tier 3: Hazard assessment

As described in Figure 4, the ENP interaction system of iNP is subdivided into four categories that depend on uptake and persistence.

- Category I – low cellular uptake and low intracellular persistence
- Category II – high cellular uptake and low intracellular persistence
- Category III – low cellular uptake and high intracellular persistence
- Category IV – high cellular uptake and high intracellular persistence

The assignment of an iNP to one of the four HES risk categories (Figure 4) dictates which set of assays must be performed to assess the safety of the formulation in question. As the four categories are related to possible adverse outcomes, the assay cascades become more elaborate with increasing uptake and persistence of the iNP. However, this does not necessarily suggest increasing levels of nanoparticle toxicity: For example, an iNP in category II may show greater toxic potential than a counterpart entering category IV. We propose eight different parameters in total, which should be monitored throughout hazard assessment. These parameters cover complement activation, platelet aggregation, hemolysis, oxidative stress, cell viability, phagocytosis, inflammation, and DNA damage. An overview of assays recommended by the USNCL or the EUNCL is given in Table 2. This includes measurement technique, assay type, specific category affiliation, and a protocol reference. It should be noted that the incorporation of different toxicogenomics techniques such as genomics, proteomics, and metabolomics may complement or eventually replace a number of biochemical or cell based assays mentioned in Table 2 since there is a growing interest in these approaches in the nanosafety community (Fröhlich 2017). In general, the HES approach is highly dependent on the selection of specific assays and endpoints that best represent the critical hazard criteria that are relevant to the *in vivo* situation. Therefore, the approach should provide some flexibility in revisiting and updating the specific subsets of assays as the science evolves.

The most common routes of administration summarized under the term injection are intravenous, subcutaneous, and intramuscular. Complement activation, platelet aggregation, and hemolysis are risks associated with intravenously injected iNP. Such adverse effects are less likely if iNP are not in direct contact with the lymphoid system and bloodstream (Turner et al. 2011). Nevertheless, we believe it is important to test for these events routinely for any

Table 2. Hazard assessment portfolio. This table shows the nine possible parameters that can be determined in the HES Tier 3.

Target	Assay	Technique	Risk category	Protocol
Present techniques				
Complement activation	Antibody presentation	ELISA	Category I – IV	USNCL-ITA-5.1 EUNCL-ITA-005.2
Platelet aggregation	Whole blood assay	Bioassay	Category I – IV	EUNCL-ITA-02.1 EUNCL-ITA-02.2
Hemolysis	Colorimetric assay	Spectroscopy	Category I – IV	EUNCL-ITA-01
Cell viability	MTT	Spectroscopy	Category I – IV	EUNCL-GTA-01
	WST8	Spectroscopy		USNCL-GTA-2
Phagocytosis	THP-1 uptake	Spectroscopy Microscopy	Category I, III, IV	USNCL-ITA-9
Oxidative stress	DCF-HA	Flow Cytometry	Category II, III, IV	USNCL-ITA-7 USNCL-GTA-3
Cytotoxicity	LDH	Spectroscopy		USNCL-GTA-4 USNCL-GTA-7
DNA damage	Micronucleus assay, Ames assay, COMET assay	Microscopy, Spectroscopy	Category III, IV	OECD
Inflammation	ELISA	Microarray	Category IV	EUNCL-ITA-10
	NFk-B, STAT, CD34	Western Blot		EUNCL-ITA-30
	MHC I / MHC II	Flow Cytometry		EUNCL-ITA-31
Future techniques				
Unbiased approaches	Genomics, Proteomics, Metabolomics	Screening and sequencing	Category II-IV	*Under evaluation for regulatory purposes*

According to the risk category and injection type, a subset of assays is selected for hazard assessment of a given iNP.
All assay protocols (except for DNA damage) listed in this table are validated and approved by the US NCL or the EU NCL.
Novel unbiased approaches are at present under evaluation for regulatory purposes.

type of iNP-injection based on the observations that platelet aggregation and complement activation can be observed after s.c. (Ermidou-Pollet et al. 2005) and i.m (Atkinson, Taylor, and Chetty 1985) injections of nanomaterials (Meng et al. 2011). Moreover, hemolysis has been reported to occur after i.m. diclofenac-therapy as well (Ahrens et al. 2004). Figure 5 provides a summary of the required safety assessments for each category of iNP.

3.3.1. Application of the hazard assessment concept

In the following sections, the case of super-paramagnetic iron oxide nanoparticles (SPIONs) is discussed to demonstrate the applicability and validity of the HES recommendations provided in Figure 5. These iNPs are used as imaging agents and therapeutics to treat glioblastoma, iron deficiency anemia, and iron deficiency in chronic kidney disease (Kievit and Zhang 2011; McCormack 2012; Ros et al. 1995; Weinstein et al. 2010). We were able to match one specific type of SPION to every ENP interaction group and to discuss the proposed HES test strategy in the light of observed *in vitro* and *in vivo* toxic effects. SPIONs were categorized based on FDA compliant preclinical test procedures. Temporal changes in the surface coating of the ENP are not considered. This approach can be justified since storage stability under physiological conditions was assessed based on criteria discussed above.

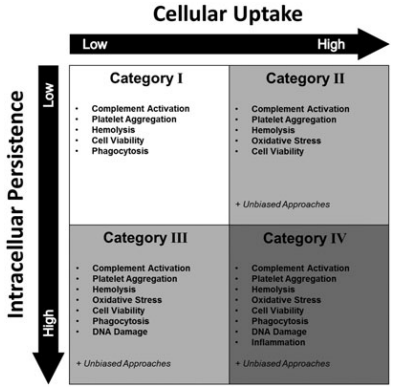

Figure 5. Recommended HES hazard assessments for iNP. Depending on the outcomes in tier 2, an iNP is proposed to pass a hazard assessment cascade individually tailored for one of the four risk categories. Increasing levels of uptake and persistence require more elaborate assay cascades. The eight assays include complement activation, platelet aggregation, hemolysis, oxidative stress, cell viability, phagocytosis, inflammation, and DNA damage.

Category I: Pegylated SPIONs proposed as theranostics do not seem to be acutely toxic to rats after injection. In animal experiments, viability did not decrease over the course of three weeks (Jarockyte et al. 2016). Moreover, neither significant endocytic uptake nor accumulation of the particles was detectable leading to an extended systemic circulation and a prolonged contact with blood cells. These particles are considered to be well tolerated. However, PEGylation may potentially cause complement activation (leading to the hypersensitivity syndrome 'C activation-related pseudo allergy – CARPA') and represents a possible risk (Verhoef and Anchordoquy 2013). Based on these considerations, a test strategy with a focus on complement activation, platelet aggregation, and hemolysis is recommended. Moreover, even though no notable viability decrease was observed, there is a regulatory need of assuring that ENP do not affect cell viability. It is, therefore, required to test cell viability as well.

Category II: Unlike their PEGylated counterparts, endocytic cellular uptake is commonly observed with uncoated SPIONs (Singh et al. 2010). These nanoparticles are rapidly degraded within the lysosomal compartment placing them in the risk category II. *In vitro*, their degradation has been shown to trigger cytotoxic events such as mitochondrial oxidative stress and a significant cell viability decrease. *In vivo*, phagocytosis and hypersensitivity have been reported to be the consequence of treatment of rats with this type of SPIONs (Mahmoudi et al. 2012; Park 2003; Szebeni et al. 2015).

Category III: Approved drug formulations, such as Rienso (Friedrich et al. 2015) or Feraheme (Lu et al. 2010) are SPIONs coated with a layer of polyglucose sorbitol carboxymethylether (PSC). They are used to treat iron deficiency in patients suffering from chronic kidney disease. The PSC layer contributes to low cellular uptake and high persistence, simultaneously minimizing cytotoxic effects (low platelet aggregation and phagocytosis). In patients with a

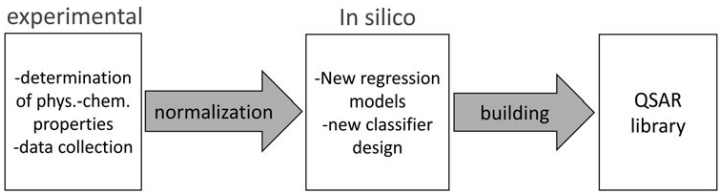

Figure 6. Workflow of a QSAR based grouping and modeling approach. Quantitative structure-activity relationships (QSAR) are used to correlate physicochemical properties of nanoparticles and cytotoxic effects. QSAR model libraries support grouping of ENP.

history of allergies, hypersensitivity was shown to be a likely side-effect (Lu et al. 2010). This is an example of a nanoparticle that would have successfully passed the proposed HES hazard assessment in category III.

Category IV: *In situ*-coated lauric acid ferrofluid ($SEON^{LA}$) (Friedrich et al. 2015; Zaloga et al. 2014) was used to validate the effect of different lauric acid coatings on SPIONs towards the application as a drug delivery system *in vitro* as well as *in vivo*. The formulation displayed high levels of cellular uptake (Zaloga et al. 2014) paired with a high biopersistence (Cicha 2016) *in vitro*. However, this formulation proved to be cytotoxic. Cell viability decreased and generation of reactive oxygen species combined with DNA damage were observed (Friedrich et al. 2015; Zaloga et al. 2014). Moreover, the tendency of $SEON^{LA}$ to agglomerate while in circulation is indicative of a liability for phagocytosis, complement activation, platelet aggregation and hemolysis. The proposed HES test strategy for category IV ENP would have been appropriate to uncover these risks.

4. HES compared to existing hazard evaluation strategies

The HES provides an application-oriented and effective hazard evaluation cascade based on a novel classification approach and well-accepted protocols. To our knowledge, the HES is the first hazard evaluation strategy that targets solely the pharmaceutical applicability of injectable ENP and does this in a unique manner.

To underline this statement, we compared our strategy to three alternative grouping and hazard evaluation strategies that were proposed either by regulatory authorities or by academia. The chosen strategies use different approaches and levels of complexity to determine nanomaterial safety.

4.1. QSAR-based grouping and modeling

The two-tiered strategy groups metal oxide nanoparticles based on their physicochemical characteristics and subsequently uses a quantitative structure-activity relationships (QSARs) analysis to identify statistical correlations with cytotoxic effects (Sayes et al. 2013). Such a QSAR approach was used previously as well to group non-nano substances based on structural similarities (ECHA 2013). Defined physicochemical properties of nanoparticles are measured using a screening approach, normalized, and statistically analyzed. This approach relies on *in silico* pattern recognition techniques and predictive modeling. The workflow is schematically depicted in Figure 6.

This test strategy was validated based on the analysis of silver, copper, nickel, iron, and zinc nanoparticles. Nanoparticles were suspended in aqueous media according to a defined protocol. The measured properties included engineered particle size, agglomerate size in water, ζ-potential, pH, and age of suspension. The measured biological response was the production of ROS. In order to compare results, the raw data was normalized *'[…] by dividing each raw data value by the standard deviation in its respective data type […]'* (Sayes et al. 2013). Statistical methods (i.e. principal component analysis – PCA and correlation analysis – CA) were used to group the metal oxide nanoparticles (Tämm et al. 2016). In contrast to the HES, this QSAR approach was specifically designed to support the analysis of metal nanoparticles. Considering that a solid validation of the HES will provide a large

Table 3. Nanoparticle risk assessment based on dose exposure. Starting from a deposited dose, the dose rate or dose equivalents of nanoparticles deposited in specific target tissues or organs are estimated.

Deposited dose (*D*)	Dose rate (*DR*)	Committed tissue dose (*TD*)	Equivalent dose (*ED*)	Effective dose (*DEff*)
Deposited surface area (*SA*) per mass of living matter (*M*)	Mean absorbed dose (D_{mean}) in target tissue (*tiss*) at time point (*t*)	Quantity of *D* taken up over a defined time period (τ)	*TD* weighted by nanoparticle - specific weighting factors (w_N)	Tissue - weighted (W_T) sum of *ED* in all tissues/organs
$D = SA/M$	$DR = D_{mean,tiss}\ (t)$	$TD = \int_0^{\tau} DR\ dt$	$ED = w_N \cdot TD$	$DEff = \Sigma w_T \cdot ED$

The toxic impact of nanoparticles on specific organs can thus be approximated. The nanoparticle dose units are square meters per kilogram (m^2/kg). The term deposited surface area (SA) corresponds to the total surface area of nanoparticles the sample (M) is potentially exposed to.
Table adapted from Simkó et al. (2014).

amount of processable data, data mining and QSAR analysis could aid to establish a future grouping strategy for iNP. For metal oxide nanoparticles this has already been shown by Zhang et al. (2012) where the ENP band gap was used to develop predictive paradigm for oxidative stress and inflammation (Zhang et al. 2012).

4.2. Dosimetry-based risk assessment

In this approach, nanoparticles can be grouped as safe or unsafe in relation to the applied nanoparticle dose, which in this case is uniformly defined in square meters per kilogram (m^2/kg) (Simkó, Nosske, and Kreyling 2014). Weighting factors are introduced to account for differences in physicochemical properties of ENP. The concept provides an elegant solution on how to calculate the dose rate (DR), committed tissue dose (TD), equivalent dose (ED), and effective dose (DEff) of a nanoparticle formulation based on the knowledge of the original deposited nanoparticle dose (D) (Table 3).

The reactivity and thus toxic potential of different nanoparticles at a given dose can be determined by calculating the ED considering several nanoparticle-specific properties (i.e. nanoparticle weighting factors, W_N). The W_N chosen by the authors were specific surface area, surface texture, ζ-potential, particle morphology, band gap energy levels for metal as well as metal oxide nanoparticles, and particle dissolution/dissociation rates. This concept supports our notion that a careful dose assessment is indispensable to compare and interpret experiments and studies. Although the HES does provide its own proposal on dosimetry as well, the two concepts differ significantly. In principle, the dosimetry concept is designed to enable risk assessments for any nanomaterial in any tissue or organ and groups nanomaterials thereafter. However, at present, the concept has limitations due to the lack of tissue- and organ-specific data and was applied to the analysis of metal particles only.The HES assumes that toxicity does not occur at a defined exposure but is based on dose-response relationships. The HES does not define exposure limits for toxicity but rather uncovers potential hazards.

4.3. The 'DF4Nano' concept

In 2015, the European Centre for Ecotoxicology and Toxicology of Chemicals 'Nano Task Force' (ECETOC) has published a new decision-making framework on nanomaterial grouping (Arts et al. 2015). The DF4NanoGrouping approach is a multi-tiered grouping strategy that *'[…] uses the 'functionality' of nanomaterials for grouping rather than relying on intrinsic material properties alone […].'* With the strict exception of medical or therapeutic ENP, nanomaterials can be grouped with the DF4Nano approach according to the adverse outcome pathway (AOP) concept (Ankley et al. 2010). An AOP is designed to establish a link between a sequence of measurable key events and an adverse outcome. The DF4Nano is the first AOP concept specific to nanomaterials. The strategy is divided into four main parts as shown in Figure 7. Starting with defining and measuring intrinsic material properties, the concept takes system-dependent nanomaterial properties into account before determining their impact on cells and entire systems (organs, organisms). The experimental section is divided into three tiers of *in vitro* assay cascades. In tier 1, basic physicochemical properties for ENM are determined. This includes the determination of particle size, surface area, shape, aspect ratio, chemical composition, aqueous solubility, and impurities. Thereafter, system-dependent properties such as exposure, uptake, biodistribution, biopersistence, and cellular effects are monitored in tier 2. *In vivo* studies are

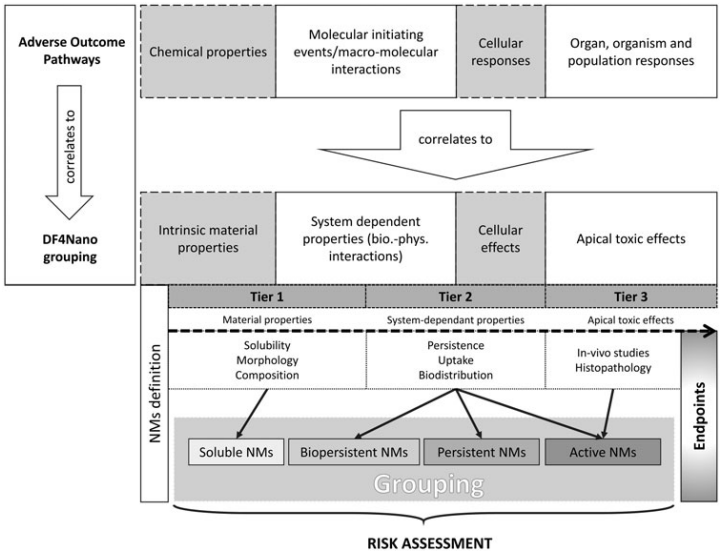

Figure 7. Overview of the DF4NanoGrouping approach of ECETOC. The DF4NanoGrouping strategy designed for nanomaterials adopts the Adverse Outcome Pathway (AOP) approach designed for chemicals. Generally, the grouping is divided into four steps where intrinsic material properties, system dependent properties, cellular effects, and apical toxic effects are determined. The experimental part of the concept is a three-tiered assay cascade. Nanomaterials are grouped into soluble, biopersistent, passive or active nanomaterials. The DF4NanoGrouping strategy is not applicable for nanomedicines or nano-therapeutics. It is explicitly designed for the risk assessment of environmental and accidental nanomaterial exposure. Adapted from Arts et al. (2015).

carried out in tier 3. Based on this concept, four main nanomaterial groups are defined (i.e. soluble, biopersistent, passive and active nanomaterials). Biopersistence refers to insoluble high-aspect-ratio (HARN) nanomaterials. Passive nanomaterials include non-fibrous, biopersistent materials that have the tendency to agglomerate in biological fluids. In contrast to active materials, they lack chemical reactivity. The thresholds and limitations defining the decision-making process of grouping in the DF4Nano concept are based on regulatory standards and authority proposals.

The DF4NanoGrouping concept is a rather complex grouping approach that is – to a certain extent – similar to the HES approach. However, the two concepts group nanomaterials based on different parameters. The DF4Nano concept is based on solubility and reactivity, whereas the HES categorizes nanoparticles according to cellular uptake and intracellular persistence. The DF4Nano concept cannot be used for the grouping and risk assessment of medical and therapeutic nanomaterials. The HES, on the other hand, does feature a possibility of establishing both for injectable nanomedicines. In contrast to the DF4Nano concept, however, the HES is not based on a systematic screening approach but combines a subset of individual experiments and specific exclusion criteria to generate standardized data needed for risk assessment.

5. Discussion

The proposed Hazard Evaluation System for Injectable Nanoparticles (HES) is a three-tiered hazard evaluation concept that was specifically designed for injectable nanoparticles (iNP) used as nanomedicines. To demonstrate that the approach poses a valid alternative or extension to existing grouping and risk assessment strategies, we compared the HES to three alternative screening and risk assessment strategies.

In Table 4, an overview of all 28 measured experimental parameters of the four discussed concepts is provided. ζ-potential, shape, size, and aspect ratio were the key properties for most

Table 4. Overview of relevant hazard evaluation determinants.

Parameters	QSAR-based concept	Dosimetry concept	DF4Nano concept	HES
Physicochemical properties (tier I)				
Chemical identity				X
Shape		X	X	X
Size	X	X	X	X
Aspect ratio		X	X	X
PDI		X	X	X
ζ-potential	X	X	X	X
Agglomeration size	X			
Surface area		X	X	
Surface texture		X		
pH	X			X
Solubility/Stability		X	X	X
Suspension age	X			
Contamination/Impurity			X	X
System-dependent properties (tier II)				
Exposure		X		
Biopersistence			X	
Intracellular persistence				X
Systemic uptake		X	X	
Cell specific uptake				X
Cellular effects			X	X
Concentration/Dosimetry	X	X		X
Bioactivity		X		
Biodistribution			X	
Toxic endpoints (tier III)				
Complement activation				X
Platelet aggregation				X
Hemolysis				X
Oxidative stress	X	X	X	X
Cytotoxicity	X	X	X	X
Cell viability			X	X
Phagocytosis		X	X	X
DNA damage				X
Inflammation			X	X

Comparison between the HES and three alternative hazard evaluation approaches.
The four discussed strategies use different combinations of experimental parameters, which cover physicochemical properties (tier I), system-dependent properties (tier II), and toxic endpoints (tier III).

concepts. Any experimental result should be critically evaluated considering the aspects of contamination, impurity, and dosimetry. This comparison shows that the HES uses the highest number of measured parameters. However, the HES (in contrast to the other strategies) is not a screening approach but uses an informed decision-making process to minimize the number of needed experiments. The HES follows thereby an intuitive and straightforward decision-making path.

In terms of future applications of the concept, several scenarios can be envisaged. First, preclinical safety evaluations will be facilitated since the HES is based on physicochemical exclusion criteria. Non-qualifying materials can be identified and the number of *in vitro* experiments can be minimized. Second, the number of *in vitro* experiments can be further reduced based on selective application of toxicological assays. This approach is cost-effective. Third, a careful *in vitro* evaluation of test materials at early stages of the development process helps to avoid costly *in vivo* experiments at later stages. This is in line with the 3R principles of animal welfare. Fourth, the HES concept will help to mitigate the risk of off-target effects *in vivo*. Fifth, it is tempting to speculate that a systematic evaluation of nanomaterials will form the basis for future grouping strategies. It will, thus, be possible to correlate physicochemical properties with hazard categories of injectable nanopharmaceuticals. This knowledge can guide the design of novel and/or optimized nanomaterials according to safe-by-design principles (as presented by the NanoReg and Prosafe European initiatives) to assist both regulatories and industry. It addresses issues regarding nanomaterial safety, both in products and processes (Gottardo 2017). The HES works towards this principle by focusing on injectable nanoparticles. By proposing a stepwise strategy based on key parameters, the HES encourages developers to consider safety during the different steps of product design.

6. Conclusions

The motivation of this project was to develop an application-oriented, cost-effective, robust, and user-friendly hazard assessment concept for nanopharmaceuticals. To the knowledge of the authors, HES is the first hazard evaluation concept focusing entirely on the application of nanoparticles as injectable formulations. Validation of the HES approach using well characterized reference materials will be an important next step towards its acceptance and implementation by research scientists as well as regulatory authorities.

Acknowledgments

We express our gratitude to Prof. Dr. Martin Wilks (Swiss Centre for Applied Human Toxicology – SCAHT), Dr. Andrea Haase ("Bundesinstitut für Risikobewertung – BfR" and the NanoReg2 consortium), Dr. Christoph Studer ("Bundesamt für Gesundheit – BAG"), and Dr. Blanca Suarez (TEMAS AG) for their valuable inputs on the novel hazard evaluation strategy.

Disclosure statement

Dr. P. Wick is executive board member of the EUNCL.

Funding

This work was financially supported by the Swiss Centre for Applied Human Toxicology (SCAHT), the NanoReg2 program (European Union Horizon 2020 research agreement 646221, 15.0200-3), and the NanoScreen Materials Challenge co-founded by the Competence Centre for Materials Science and Technology (CCMX).

References

Aderem, A. 2003. "Phagocytosis and the Inflammatory Response." *The Journal of Infectious Diseases* 187 (s2): S340–S345. doi:10.1086/374747

Aguilar-Castillo, B. A., J. L. Santos, H. Luo, Y. E. Aguirre-Chagala, T. Palacios-Hernandez, and M. Herrera-Alonso. 2015. "Nanoparticle Stability in Biologically Relevant Media: influence of Polymer Architecture." *Soft Matter* 11 (37): 7296–7307. doi:10.1039/C5SM01455G

Ahrens, N., L. Schewior, E. Garbe, H. Kiesewetter, and A. Salama. 2004. "Massive Haemolysis after Intramuscular Diclofenac in a Patient Who Apparently Tolerated Oral Medication." *Vox Sanguinis* 86 (1): 71–74. doi:10.1111/j.0042-9007.2004.00389.x

Akthakul, A., A. I. Hochbaum, F. Stellacci, and A. M. Mayes. 2005. "Size Fractionation of Metal Nanoparticles by Membrane Filtration." *Advanced Materials* 17 (5): 532–535. doi:10.1002/adma.200400636

Álvarez-Fuentes, J., L. Martín-Banderas, I. Muñoz-Rubio, M. A. Holgado, and M. Fernández-Arévalo. 2012. "Development and Validation of an RP-HPLC Method for CB13 Evaluation in Several PLGA Nanoparticle Systems [WWW Document]." *The Scientific World Journal* 2012: 737526. doi:10.1100/2012/737526

Ambrogio, M. W., C. R. Thomas, Y.-L. Zhao, J. I. Zink, and J. F. Stoddart. 2011. "Mechanized Silica Nanoparticles: A New Frontier in Theranostic Nanomedicine." *Accounts of Chemical Research* 44 (10): 903–913. doi:10.1021/ar200018x

Amenabar, I., S. Poly, W. Nuansing, E. H. Hubrich, A. A. Govyadinov, F. Huth, R. Krutokhvostov, L. Zhang, M. Knez, J. Heberle. J., et al. 2013. "Structural Analysis and Mapping of Individual Protein Complexes by Infrared Nanospectroscopy." *Nature Communications* 4 (1): 3890. Ncomms doi:10.1038/ncomms3890

Amidon, G. L., H. Lennernäs, V. P. Shah, and J. R. Crison. 1995. "A Theoretical Basis for a Biopharmaceutic Drug Classification: The Correlation of in Vitro Drug Product Dissolution and in Vivo Bioavailability." *Pharmaceutical Research* 12: 413–420. doi:10.1023/A:1016212804288

Ankley, G. T., R. S. Bennett, R. J. Erickson, D. J. Hoff, M. W. Hornung, R. D. Johnson, D. R. Mount, J. W. Nichols, C. L. Russom, P. K. Schmieder, et al. 2010. "Adverse Outcome Pathways: A Conceptual Framework to Support Ecotoxicology Research and Risk Assessment." *Environmental Toxicology and Chemistry* 29 (3): 730–741. doi:10.1002/etc.34

Arap, W., R. Pasqualini, M. Montalti, L. Petrizza, L. Prodi, E. Rampazzo, N. Zaccheroni, and S. Marchiò. 2013. "Luminescent Silica Nanoparticles for Cancer Diagnosis." *Current Medicinal Chemistry* 20 (17): 2195–2211. doi:10.2174/0929867311320170005

Arts, J. H. E., M. Hadi, M.-A. Irfan, A. M. Keene, R. Kreiling, D. Lyon, M. Maier, K. Michel, T. Petry, U. G. Sauer, et al. 2015a. "A Decision-Making Framework for the Grouping and Testing of Nanomaterials (DF4nanoGrouping)." *Regulatory Toxicology and Pharmacology* 71 (2): S1–S27. doi:10.1016/j.yrtph.2015.03.007

Atkinson, P. M., D. I. Taylor, and N. Chetty. 1985. "Inhibition of Platelet Aggregation by Ketamine Hydrochloride." *Thrombosis Research* 40 (2): 227–234. doi:10.1016/0049-3848(85)90333-0

Bao, H., X. Yu, C. Xu, X. Li, Z. Li, D. Wei, and Y. Liu. 2015. "New Toxicity Mechanism of Silver Nanoparticles: Promoting Apoptosis and Inhibiting Proliferation." *PLoS One* 10 (3): e0122535. doi:10.1371/journal.pone.0122535

Bartneck, M., H. A. Keul, S. Singh, K. Czaja, J. Bornemann, M. Bockstaller, M. Moeller, G. Zwadlo-Klarwasser, and J. Groll. 2010a. "Rapid Uptake of Gold Nanorods by Primary Human Blood Phagocytes and Immunomodulatory Effects of Surface Chemistry." *ACS Nano* 4 (6): 3073–3086. doi:10.1021/nn100262h

Bartneck, M., H. A. Keul, G. Zwadlo-Klarwasser, and J. Groll. 2010b. "Phagocytosis Independent Extracellular Nanoparticle Clearance by Human Immune Cells." *Nano Letters* 10 (1): 59–63. doi:10.1021/nl902830x

Berg, J. M., A. Romoser, N. Banerjee, R. Zebda, and C. M. Sayes. 2009. "The Relationship between pH and Zeta Potential of ~30 Nm Metal Oxide Nanoparticle Suspensions Relevant to in Vitro Toxicological Evaluations." *Nanotoxicology* 3 (4): 276–283. doi:10.3109/17435390903276941

Berger, M. 2009. "Size matters. Comparing the toxicity of micro- to nanoparticles" [WWW Document]. Accessed August 21 2017. http://www.nanowerk.com/spotlight/spotid=10128.php

Bhattacharjee, S. 2016. "DLS and Zeta Potential – What They Are and What They Are Not?." *Journal of Controlled Release* 235: 337–351. doi:10.1016/j.jconrel.2016.06.017

Bleeker, E. A. J., W. H. de Jong, R. E. Geertsma, M. Groenewold, E. H. W. Heugens, M. Koers-Jacquemijns, D. van de Meent, J. R. Popma, A. G. Rietveld, S. W. P. Wijnhoven, et al. 2013. "Considerations on the EU Definition of a Nanomaterial: Science to Support Policy Making." *Regulatory Toxicology and Pharmacology* 65 (1): 119–125. doi:10.1016/j.yrtph.2012.11.007

Bobo, D., K. J. Robinson, J. Islam, K. J. Thurecht, and S. R. Corrie. 2016. "Nanoparticle-Based Medicines: A Review of FDA-Approved Materials and Clinical Trials to Date." *Pharmaceutical Research* 33 (10): 2373–2387. doi:10.1007/s11095-016-1958-5

Boilard, S. P., P. R. Amyotte, F. I. Khan, A. G. Dastidar, and R. K. Eckhoff. 2013. "Explosibility of Micron- and Nano-Size Titanium Powders." *Journal of Loss Prevention in the Process Industries* 26 (6): 1646–1654. doi:10.1016/j.jlp.2013.06.003

Bolt, H. M. 2014. "Grouping of Nanomaterials for Risk Assessment." *Archives of Toxicology* 88 (12): 2077–2078. doi:10.1007/s00204-014-1416-2

Bozzuto, G., and A. Molinari. 2015. "Liposomes as Nanomedical Devices." *International Journal of Nanomedicine* 10: 975–999. doi10.2147/IJN.S68861

Brown, J. S., T. Gordon, O. Price, and B. Asgharian. 2013. "Thoracic and Respirable Particle Definitions for Human Health Risk Assessment." *Particle and Fibre Toxicology* 10 (1): 12. doi:10.1186/1743-8977-10-12

Buzea, C., I. I. Pacheco, and K. Robbie. 2007. "Nanomaterials and Nanoparticles: sources and Toxicity." *Biointerphases* 2 (4): MR17–MR71. doi:10.1116/1.2815690

Casals, E., T. Pfaller, A. Duschl, G. J. Oostingh, and V. Puntes. 2010. "Time Evolution of the Nanoparticle Protein Corona." *ACS Nano* 4 (7): 3623–3632. doi:10.1021/nn901372t

Champion, J. A., Y. K. Katare, and S. Mitragotri. 2007. "Particle Shape: A New Design Parameter for Micro- and Nanoscale Drug Delivery Carriers." *Official journal of the Controlled Release Society* 121 (1–2): 3–9. doi:10.1016/j.jconrel.2007.03.022

Chen, F., G. Wang, J. I. Griffin, B. Brenneman, N. K. Banda, V. M. Holers, D. S. Backos, L. Wu, S. M. Moghimi, and D. Simberg. 2017. "Complement Proteins Bind to Nanoparticle Protein Corona and Undergo Dynamic Exchange In Vivo." *Nature Nanotechnology* 12 (4): 387–393. doi:10.1038/nnano.2016.269

Chukwuocha, E. O., M. C. Onyeaju, and T. S. T. Harry. 2012. "Theoretical Studies on the Effect of Confinement on Quantum Dots Using the Brus Equation World Journal of Condensed Matter Physics 2 (2): 96–100. doi:10.4236/wjcmp.2012.22017

Cicha, I. 2016. "Strategies to Enhance Nanoparticle-Endothelial Interactions under Flow." *Journal of Cellular Biotechnology* 1 (2): 191–208. doi:10.3233/JCB-15020

Clogston, J. D., and A. K. Patri. 2011. "Zeta Potential Measurement." *Methods in Molecular Biology (Clifton, N.J.)* 697: 63–70. doi:10.1007/978-1-60327-198-1

Coti, K. K., M. E. Belowich, M. Liong, M. W. Ambrogio, Y. A. Lau, H. A. Khatib, J. I. Zink, N. M. Khashab, and J. F. Stoddart. 2009. "Mechanised Nanoparticles for Drug Delivery." *Nanoscale* 1 (1): 16–39. doi:10.1039/b9nr00162j

Crawford, R., B. Dogdas, E. Keough, R. M. Haas, W. Wepukhulu, S. Krotzer, P. A. Burke, L. Sepp-Lorenzino, A. Bagchi, and B. J. Howell. 2011. "Analysis of Lipid Nanoparticles by Cryo-EM for Characterizing siRNA Delivery Vehicles." *International Journal of Pharmaceutics* 403 (1–2): 237–44. doi:10.1016/j.ijpharm.2010.10.025

Davignon, J., and P. Ganz. 2004. "Role of Endothelial Dysfunction in Atherosclerosis." *Circulation* 109 (23_suppl_1): III-27–III-32. doi:10.1161/01.CIR.0000131515.03336.f8

Deanfield, J., A. Donald, C. Ferri, C. Giannattasio, J. Halcox, S. Halligan, A. Lerman, G. Mancia, J. J. Oliver, A. C. Pessina, et al., Working Group on Endothelin and Endothelial Factors of the European Society of Hypertension. 2005. "Endothelial Function and Dysfunction. Part I: Methodological Issues for Assessment in the Different Vascular Beds: A Statement by the Working Group on Endothelin and Endothelial Factors of the European Society of Hypertension." *Journal of Hypertension* 23 (1): 7–17. doi:10.1097/00004872-200501000-00004

Dekkers, S., A. G. Oomen, E. A. J. Bleeker, R. J. Vandebriel, C. Micheletti, J. Cabellos, G. Janer, N. Fuentes, S. Vázquez-Campos, T. Borges, et al. 2016. "Towards a Nanospecific Approach for Risk Assessment." *Regulatory Toxicology and Pharmacology* 80: 46–59. doi:10.1016/j.yrtph.2016.05.037

Dobrovolskaia, M. A., A. K. Patri, J. Simak, J. B. Hall, J. Semberova, S. H. De Paoli Lacerda, and S. E. McNeil. 2012. "Nanoparticle Size and Surface Charge Determine Effects of PAMAM Dendrimers on Human Platelets in Vitro." *Molecular Pharmaceutics* 9 (3): 382–393. doi:10.1021/mp200463e

Docter, D., D. Westmeier, M. Markiewicz, S. Stolte, S. K. Knauer, and R. H. Stauber. 2015. "The Nanoparticle Biomolecule Corona: lessons Learned – Challenge Accepted?" *Chemical Society Reviews* 44: 6094–6121. doi:10.1039/C5CS00217F

Dongargaonkar, A. A., and J. D. Clogston. 2018. "Quantitation of Surface Coating on Nanoparticles Using Thermogravimetric Analysis." In *Characterization of Nanoparticles Intended for Drug Delivery*, *Methods in Molecular Biology*, edited by McNeil S, 57–63. New York, NY: Humana Press. doi:10.1007/978-1-4939-7352-1_6

Droppo, I. G. 2006. "*Filtration in Particle Size Analysis.*" *In Encyclopedia of Analytical Chemistry*, edited by R. A. Meyers and R. B. Flippen. Hoboken, New Jersey: John Wiley & Sons, Ltd. doi:10.1002/9780470027318.a1506

Dusinska, M., M. Dusinska, L. Fjellsbø, Z. Magdolenova, A. Rinna, E. Runden Pran, A. Bartonova, E. Heimstad, M. Harju, L. Tran. et al. 2009. "Testing Strategies for the Safety of Nanoparticles Used in Medical Applications." *Nanomed* 4 (6): 605–607. doi:10.2217/nnm.09.47

ECHA. 2013. "Grouping of Substances and Read-Across – ECHA" [WWW Document]. Accessed August 28 2017. https://echa.europa.eu/support/registration/how-to-avoid-unnecessary-testing-on-animals/grouping-of-substances-and-read-across

Elgqvist, J. 2017. "Nanoparticles as Theranostic Vehicles in Experimental and Clinical Applications—Focus on Prostate and Breast Cancer." *International Journal of Molecular Sciences* 18 (5): 1102. doi:10.3390/ijms18051102

Ermidou-Pollet, S., H. Nounopoulos, N. Sdougas, M. Szilágyi, and S. Pollet. 2005. "Influence of Subcutaneous Injection of Essential Fatty Acids on the Stress-Induced Modifications of Rat Platelet Aggregation and Membrane Lipid Composition." *Acta Biologica Hungarica* 56 (3–4): 247–259. doi:10.1556/ABiol.56.2005.3-4.8

Etheridge, M. L., S. A. Campbell, A. G. Erdman, C. L. Haynes, S. M. Wolf, and J. McCullough. 2013. "The Big Picture on Small Medicine: The State of Nanomedicine Products Approved for Use or in Clinical Trials." *Nanomedicine: Nanotechnology, Biology, and Medicine* 9 (1): 1–14. doi:10.1016/j.nano.2012.05.013

European Medicines Agency - Multidisciplinary - Data requirements for intravenous iron-based nano-colloidal products developed with reference to an innovator medicinal product [WWW Document], n.d. Accessed January 19 2018. http://www.ema.europa.eu/docs/en_GB/document_library/Scientific_guideline/2015/03/WC500184922.pdf

European Medicines Agency - Multidisciplinary - Joint MHLW/EMA reflection paper on the development of block copolymer micelle medicinal products [WWW Document], n.d. Accessed January 19 2018. http://www.ema.europa.eu/docs/en_GB/document_library/Scientific_guideline/2013/02/WC500138390.pdf

European Medicines Agency - Multidisciplinary - Reflection paper on surface coatings: general issues for consideration regarding parenteral administration of coated nanomedicine products [WWW Document], n.d. Accessed January 19 2018. http://www.ema.europa.eu/docs/en_GB/document_library/Scientific_guideline/2013/08/WC500147874.pdf

European Medicines Agency - Multidisciplinary - Reflection paper on the data requirements for intravenous liposomal products developed with reference to an innovator liposomal product [WWW Document], n.d. Accessed January 19 2018. http://www.ema.europa.eu/docs/en_GB/document_library/Scientific_guideline/2013/03/WC500140351.pdf

European Medicines Agency - Multidisciplinary - Reflection paper on nanotechnology-based medicinal products for human use [WWW Document], n.d. Accessed 19 Jan 2018. http://www.ema.europa.eu/docs/en_GB/document_library/Regulatory_and_procedural_guideline/2010/01/WC500069728.pdf

Fabricius, A.-L., L. Duester, B. Meermann, and T. A. Ternes. 2014. "ICP-MS-Based Characterization of Inorganic Nanoparticles—Sample Preparation and off-Line Fractionation Strategies." *Analytical and Bioanalytical Chemistry* 406 (2): 467–479. doi:10.1007/s00216-013-7480-2

Fadeel, B. 2012. *Clear and Present Danger? Engineered Nanoparticles and the Immune System [WWW document]*. Swiss Med. Wkly. Accessed May 11 2016. http://blog.smw.ch/

Fadeel, B., A. Pietroiusti, and A. A. Shvedova. 2017. *Adverse Effects of Engineered Nanomaterials: Exposure, Toxicology, and Impact on Human Health*. Cambridge, Massachusetts: Academic Press.

FDA. 2005. "Guidance for Industry on Estimating the Maximum Safe Starting Dose in Initial Clinical Trials for Therapeutics in Adult Healthy Volunteers." Availability [WWW Document]. Fed. Regist. Accessed August 24 2017. https://www.federalregister.gov/documents/2005/07/22/05-14456/guidance-for-industry-on-estimating-the-maximum-safe-starting-dose-in-initial-clinical-trials-for

Félétou, M. 2011. "The Endothelium: Part 1: Multiple Functions of the Endothelial Cells—Focus on Endothelium-Derived Vasoactive Mediators." In *Integrated Systems Physiology: From Molecule to Function to Disease*, edited by D. Neil Granger and Joey P. Granger, 1–306. San Rafael (CA): Morgan & Claypool Life Sciences.

Feliu, N., and B. Fadeel. 2010. "Nanotoxicology: No Small Matter." *Nanoscale* 2 (12): 2514–2520. doi:10.1039/c0nr00535e

Friedrich, R. P., C. Janko, M. Poettler, P. Tripal, J. Zaloga, I. Cicha, S. Dürr, J. Nowak, S. Odenbach, I. Slabu. et al. 2015. "Flow Cytometry for Intracellular SPION Quantification: Specificity and Sensitivity in Comparison with Spectroscopic Methods." *International Journal of Nanomedicine* 10: 4185–4201. doi:10.2147/IJN.S82714

Fröhlich, E. 2017. "Role of Omics Techniques in the Toxicity Testing of Nanoparticles." *Journal of Nanobiotechnology* 15 (1): 84. doi:10.1186/s12951-017-0320-3

Fubini, B., M. Ghiazza, and I. Fenoglio. 2010. "Physico-Chemical Features of Engineered Nanoparticles Relevant to Their Toxicity." *Nanotoxicology* 4 (4): 347–363. doi:10.3109/17435390.2010.509519

Gallud, A., and B. Fadeel. 2015. "Keeping It Small: Towards a Molecular Definition of Nanotoxicology." *European Journal of Nanomedicine* 7: 143–151. doi:10.1515/ejnm-2015-0020

Garbovskiy, Y. 2017. "Biological Contamination of Nanoparticles and Its Manifestation in Optical Absorbance Measurements." *Analytical Chemistry* 89 (14): 7282–7285. doi:10.1021/acs.analchem.7b01766

Gebel, T., H. Foth, G. Damm, A. Freyberger, P.-J. Kramer, W. Lilienblum, C. Röhl, T. Schupp, C. Weiss, K.-M. Wollin, et al. 2014. "Manufactured Nanomaterials: Categorization and Approaches to Hazard Assessment." *Archives of Toxicology* 88 (12): 2191–2211. doi:10.1007/s00204-014-1383-7

Goldstein, A., Y. Soroka, M. Frušić-Zlotkin, I. Popov, and R. Kohen. 2014. "High Resolution SEM Imaging of Gold Nanoparticles in Cells and Tissues." *Journal of Microscopy* 256 (3): 237–247. doi:10.1111/jmi.12179

Gottardo, S. 2017. "NANoREG Framework for the Safety Assessment of Nanomaterials - EU Science Hub - European Commission [WWW Document]." *EU Science Hub*. Accessed March 7 2018. https://ec.europa.eu/jrc/en/publication/eur-scientific-and-technical-research-reports/nanoreg-framework-safety-assessment-nanomaterials

Gregoriadis, G., 1985. Liposomes for drugs and vaccines. *Trends Biotechnol*. 3: 235–241. doi:10.1016/0167-7799(85)90014-9

Gregory, A. E., R. Titball, and D. Williamson. 2013. "Vaccine Delivery Using Nanoparticles." *Frontiers in Cellular and Infection Microbiology* 3: 13. doi:10.3389/fcimb.2013.00013

Guadagnini, R., B. Halamoda Kenzaoui, L. Walker, G. Pojana, Z. Magdolenova, D. Bilanicova, M. Saunders, L. Juillerat-Jeanneret, A. Marcomini, A. Huk, et al. 2015. "Toxicity Screenings of Nanomaterials: Challenges Due to Interference with Assay Processes and Components of Classic in Vitro Tests." *Nanotoxicology* 9 (Supp1): 13–24. doi:10.3109/17435390.2013.829590

Guarnieri, D., S. Sabella, O. Muscetti, V. Belli, M. A. Malvindi, S. Fusco, E. De Luca, P. P. Pompa, and P. A. Netti. 2014. "Transport across the Cell-Membrane Dictates Nanoparticle Fate and Toxicity: A New Paradigm in Nanotoxicology." *Nanoscale* 6 (17): 10264–10273. doi:10.1039/C4NR02008A

Guha, S., M. Li, M. J. Tarlov, and M. R. Zachariah. 2012. "Electrospray–Differential Mobility Analysis of Bionanoparticles." *Trends Biotechnol* 30 (5): 291–300. doi:10.1016/j.tibtech.2012.02.003

Guo, C., Y. Xia, P. Niu, L. Jiang, J. Duan, Y. Yu, X. Zhou, Y. Li, and Z. Sun. 2015. "Silica Nanoparticles Induce Oxidative Stress, Inflammation, and Endothelial Dysfunction in Vitro via Activation of the MAPK/Nrf2 Pathway and Nuclear Factor-κB Signaling." *International Journal of Nanomedicine* 10: 1463–1477. doi:10.2147/IJN.S76114

Guo, C., and J. L. Yarger. 2018. "Characterizing Gold Nanoparticles by NMR Spectroscopy." *Magnetic Resonance in Chemistry*. doi:10.1002/mrc.4753. [Epub ahead of print]

Hackley, V. A., and J. D. Clogston. 2011. "Measuring the Hydrodynamic Size of Nanoparticles in Aqueous Media Using Batch-Mode Dynamic Light Scattering." In *Characterization of Nanoparticles Intended for Drug Delivery*, edited by S. E. McNeil, 35–52. Totowa, NJ: Humana Press. doi:10.1007/978-1-60327-198-1_4

Hadrup, N., A. K. Sharma, M. Poulsen, and E. Nielsen. 2015. "Toxicological Risk Assessment of Elemental Gold following Oral Exposure to Sheets and Nanoparticles - A Review." *Regulatory Toxicology and Pharmacology* 72 (2): 216–221. doi:10.1016/j.yrtph.2015.04.017

Hole, P., K. Sillence, C. Hannell, C. M. Maguire, M. Roesslein, G. Suarez, S. Capracotta, Z. Magdolenova, L. Horev-Azaria, A. Dybowska, et al. 2013. "Interlaboratory Comparison of Size Measurements on Nanoparticles Using Nanoparticle Tracking Analysis (NTA)." *Journal of Nanoparticle Research* 15 (12): 2101. doi:10.1007/s11051-013-2101-8

Hung, H.-I., O. J. Klein, S. W. Peterson, S. R. Rokosh, S. Osseiran, N. H. Nowell, and C. L. Evans. 2016. "PLGA Nanoparticle Encapsulation Reduces Toxicity While Retaining the Therapeutic Efficacy of EtNBS-PDT In Vitro." *Scientific Reports* 6 (1): 33234. doi:10.1038/srep33234

Huth, F., A. Govyadinov, S. Amarie, W. Nuansing, F. Keilmann, and R. Hillenbrand. 2012. "Nano-FTIR Absorption Spectroscopy of Molecular Fingerprints at 20 Nm Spatial Resolution." *Nano Letters* 12 (8): 3973–3978. doi:10.1021/nl301159v

ISO. 2015. "ISO/TS 80004-2:2015(en), Nanotechnologies — Vocabulary — Part 2: Nano-objects." [WWW Document]. Accessed August 28 2017. https://www.iso.org/obp/ui/#iso:std:iso:ts:80004:-2:ed-1:v1:en

Itoh, N., E. Yamamoto, T. Santa, T. Funatsu, and M. Kato. 2016. "Effect of Nanoparticle Surface on the HPLC Elution Profile of Liposomal Nanoparticles." *Pharmaceutical Research* 33 (6): 1440–1446. doi:10.1007/s11095-016-1886-4

Jarockyte, G., E. Daugelaite, M. Stasys, U. Statkute, V. Poderys, T.-C. Tseng, S.-H. Hsu, V. Karabanovas, and R. Rotomskis. 2016. "Accumulation and Toxicity of Superparamagnetic Iron Oxide Nanoparticles in Cells and Experimental Animals." *International Journal of Molecular Sciences* 17 (8): 1193. doi:10.3390/ijms17081193

Jong, W. 2010. "Scientific Basis for the Definition of the Term 'nanomaterial'." [WWW Document] Accessed 28 August 2017. http://ec.europa.eu/health/scientific_committees/emerging/docs/scenihr_o_032.pdf

Joris, F., D. Valdepérez, B. Pelaz, S. J. Soenen, B. B. Manshian, W. J. Parak, S. C. De Smedt, and K. Raemdonck. 2016. "The Impact of Species and Cell Type on the Nanosafety Profile of Iron Oxide Nanoparticles in Neural Cells." *Journal of Nanobiotechnology* 14 (1): 69. doi:10.1186/s12951-016-0220-y

Junghanns, J.-U. A. H., and R. H. Müller. 2008. "Nanocrystal Technology, Drug Delivery and Clinical Applications." *International Journal of Nanomedicine* 3 (3): 295–310.

Kaszuba, M., D. McKnight, M. T. Connah, F. K. McNeil-Watson, and U. Nobbmann. 2008. "Measuring Sub Nanometre Sizes Using Dynamic Light Scattering." *Journal of Nanoparticle Research* 10 (5): 823–829. doi:10.1007/s11051-007-9317-4

Ke, P. C., S. Lin, W. J. Parak, T. P. Davis, and F. Caruso. 2017. "A Decade of the Protein Corona." *ACS Nano* 11 (12): 11773–11776. doi:10.1021/acsnano.7b08008

Kennedy, I. M., D. Wilson, and A. I. Barakat; HEI Health Review Committee. 2009. "Uptake and Inflammatory Effects of Nanoparticles in a Human Vascular Endothelial Cell Line." *Research reports - Health Effects Institute* 136: 3–32.

Kettiger, H., A. Schipanski, P. Wick, and J. Huwyler. 2013. "Engineered Nanomaterial Uptake and Tissue Distribution: From Cell to Organism." *International Journal of Nanomedicine* 8: 3255–3269. doi:10.2147/IJN.S49770

Kievit, F. M., and M. Zhang. 2011. "Surface Engineering of Iron Oxide Nanoparticles for Targeted Cancer Therapy." *Accounts of Chemical Research* 44 (10): 853–862. doi:10.1021/ar2000277

Made Materials Interfacing with the Nano-Cosmos of Biological Systems." *Annual Review of Pharmacology and Toxicology* 50 (1): 63–88. doi:10.1146/annurev.pharmtox.010909.105819

Siegrist, S., H. Kettiger, E. Fasler-Kan, and J. Huwyler. 2017. "Selective Stimulation of the JAK/STAT Signaling Pathway by Silica Nanoparticles in Human Endothelial Cells." *Toxicology In Vitro* 42: 308–318. doi:10.1016/j.tiv.2017.05.002

Simkó, M., D. Nosske, and W. G. Kreyling. 2014. "Metrics, Dose, and Dose Concept: The Need for a Proper Dose Concept in the Risk Assessment of Nanoparticles." *International Journal of Environmental Research and Public Health* 11 (4): 4026–4048. doi:10.3390/ijerph110404026

Simkó, M., S. Tischler, and M.-O. Mattsson. 2015. "Pooling and Analysis of Published in Vitro Data: A Proof of Concept Study for the Grouping of Nanoparticles." *International Journal of Molecular Sciences* 16 (11): 26211–26236. doi:10.3390/ijms161125954

Singh, A. K. 2015. *Engineered Nanoparticles: Structure, Properties and Mechanisms of Toxicity*. Cambridge, Massachusetts: Academic Press.

Singh, N., G. J. Jenkins, R. Asadi, and S. H. Doak. 2010. "Potential Toxicity of Superparamagnetic Iron Oxide Nanoparticles (SPION)." *Nano Rev* 1 (1): 5358. doi:10.3402/nano.v1i0.5358

Stone, V., S. Pozzi-Mucelli, L. Tran, K. Aschberger, S. Sabella, U. Vogel, C. Poland, D. Balharry, T. Fernandes, S. Gottardo, et al. 2014. "ITS-NANO - Prioritising Nanosafety Research to Develop a Stakeholder Driven Intelligent Testing Strategy." *Particle and Fibre Toxicology* 11 (1): 9. doi:10.1186/1743-8977-11-9

Szebeni, J., S. Fishbane, M. Hedenus, S. Howaldt, F. Locatelli, S. Patni, D. Rampton, G. Weiss, and J. Folkersen. 2015. "Hypersensitivity to Intravenous Iron: classification, Terminology, Mechanisms and Management." *British Journal of Pharmacology* 172 (21): 5025–5036. doi:10.1111/bph.13268

Tämm, K., L. Sikk, J. Burk, R. Rallo, S. Pokhrel, L. Mädler, J. J. Scott-Fordsmand, P. Burk, and T. Tamm. 2016. "Parametrization of Nanoparticles: development of Full-Particle Nanodescriptors." *Nanoscale* 8 (36): 16243–16250. doi:10.1039/C6NR04376C

Teeguarden, J. G., P. M. Hinderliter, G. Orr, B. D. Thrall, and J. G. Pounds. 2007. "Particokinetics in Vitro: dosimetry Considerations for in Vitro Nanoparticle Toxicity Assessments." *Toxicological Sciences* 95 (2): 300–312. doi:10.1093/toxsci/kfl165

Tiwari, D., J. Takashi, and J. Behari. 2010. "Dose-Dependent In-Vivo Toxicity Assessment of Nanoparticle in Wistar Rats." *Toxicology Mechanisms and Methods* 21 (1): 13–24. doi:10.3109/15376516.2010.529184

Toy, R., L. Bauer, C. Hoimes, K. B. Ghaghada, and E. Karathanasis. 2014. "Targeted Nanotechnology for Cancer Imaging." *Advanced Drug Delivery Reviews* 76: 79–97. doi:10.1016/j.addr.2014.08.002

Treuel, L., D. Docter, M. Maskos, and R. H. Stauber. 2015. "Protein Corona – from Molecular Adsorption to Physiological Complexity." *Beilstein Journal of Nanotechnology* 6: 857–873. doi:10.3762/bjnano.6.88

Turner, P. V., T. Brabb, C. Pekow, and M. A. Vasbinder. 2011. "Administration of Substances to Laboratory Animals: Routes of Administration and Factors to Consider." *Journal of the American Association for Laboratory Animal Science* 50 (5): 600–613.

Unfried, K., C. Albrecht, L.-O. Klotz, A. Von Mikecz, S Grether-Beck, R.P.F. Schins. 2007. "Cellular responses to nanoparticles: Target structures and mechanisms." *Nanotoxicology* 1: 52–71. doi:10.1080/00222930701314932

Unterweger, H., C. Janko, M. Schwarz, L. Dézsi, R. Urbanics, J. Matuszak, E. Őrfi, T. Fülöp, T. Bäuerle, J. Szebeni. et al. 2017. "Non-Immunogenic Dextran-Coated Superparamagnetic Iron Oxide Nanoparticles: A Biocompatible, Size-Tunable Contrast Agent for Magnetic Resonance Imaging." *International Journal of Nanomedicine* 12: 5223–5238. doi:10.2147/IJN.S138108

Uskoković, V. 2013. "Entering the Era of Nanoscience: Time to Be so Small." *Journal of Biomedical Nanotechnology* 9 (9): 1441–1470. doi:10.1166/jbn.2013.1642

van Teunenbroek, T. 2017. "NANoREG, A Common European Approach to the Regulatory Testing of Nanomaterials." [WWW Document]. www.nanoreg.eu. Accessed December 21 2017. http://www.rivm.nl/en/About_RIVM/Mission_and_strategy/International_Affairs/International_Projects/Completed/NANoREG/NANoREG_Results_Repository_sub_page_Final_Report

Verhoef, J. J., and T. J. Anchordoquy. 2013. "Questioning the Use of PEGylation for Drug Delivery. Drug Deliv." *Drug Delivery and Translational Research* 3 (6): 499–503. doi:10.1007/s13346-013-0176-5

Vermeij, E. A., M. I. Koenders, M. B. Bennink, L. A. Crowe, L. Maurizi, J.-P. Vallée, H. Hofmann, W. B. Berg, L. van den, P. L. E. M. van, Loo, and F. A. J. van de. 2015. "The in-Vivo Use of Superparamagnetic Iron Oxide Nanoparticles to Detect Inflammation Elicits a Cytokine Response but Does Not Aggravate Experimental Arthritis." *PLoS One* 10 (5): e0126687. doi:10.1371/journal.pone.0126687

Vetten, M. A., C. S. Yah, T. Singh, and M. Gulumian. 2014. "Challenges Facing Sterilization and Depyrogenation of Nanoparticles: effects on Structural Stability and Biomedical Applications." *Nanomedicine: Nanotechnology, Biology, and Medicine* 10 (7): 1391–1399. doi:10.1016/j.nano.2014.03.017

Vippola, M., M. Valkonen, E. Sarlin, M. Honkanen, and H. Huttunen. 2016. "Insight to Nanoparticle Size Analysis—Novel and Convenient Image Analysis Method versus Conventional Techniques." *Nanoscale Research Letters* 11 (1): 169. doi:10.1186/s11671-016-1391-z

Weinstein, J. S., C. G. Varallyay, E. Dosa, S. Gahramanov, B. Hamilton, W. D. Rooney, L. L. Muldoon, and E. A. Neuwelt. 2010. "Superparamagnetic Iron Oxide Nanoparticles: diagnostic Magnetic Resonance Imaging and Potential Therapeutic Applications in Neurooncology and Central Nervous System Inflammatory Pathologies, A Review."

Journal of Cerebral Blood Flow & Metabolism 30 (1): 15–35. doi:10.1038/jcbfm.2009.192

Weissig, V., T. K. Pettinger, and N. Murdock. 2014. "Nanopharmaceuticals (Part 1): Products on the Market." *International Journal of Nanomedicine* 9: 4357–4373. doi:10.2147/IJN.S46900

Weissleder, R., M. Nahrendorf, and M. J. Pittet. 2014. "Imaging Macrophages with Nanoparticles." *Nature Materials* 13 (2): 125–138. doi:10.1038/nmat3780

Wen, H., M. Dan, Y. Yang, J. Lyu, A. Shao, X. Cheng, L. Chen, and L. Xu. 2017. "Acute Toxicity and Genotoxicity of Silver Nanoparticle in Rats." *PLoS One* 12 (9): e0185554. doi:10.1371/journal.pone.0185554

Whitesides, G. M. 2003. "The "Right" Size in Nanobiotechnology." *Nature Biotechnology* 21 (10): 1161–1165. doi:10.1038/nbt872

Witzigmann, D., M. Camblin, J. Huwyler, and V. Balasubramanian. 2015. "Nanomaterials: Therapeutic Applications."In *The Encyclopedia of Biomedical Polymers & Polymeric Biomaterials*, edited by M. Mishra, 5364–5378. New York: Taylor & Francis.

Wolfram, J., M. Zhu, Y. Yang, J. Shen, E. Gentile, D. Paolino, M. Fresta, G. Nie, C. Chen, H. Shen. et al. 2015. "Safety of Nanoparticles in Medicine." *Current Drug Targets* 16 (14): 1671–1681. doi:10.2174/1389450115666140804124808

Wu, X., Z.-R. Lu. 2016. "Nanoparticle–Tissue Interaction.." In *Nanomaterials in Pharmacology. Methods in Pharmacology and Toxicology*, edited by Z.-R. Lu, S. Sakuma, 201–218. New York, NY: Humana Press. doi:10.1007/978-1-4939-3121-7

Xie, J., S. Lee, and X. Chen. 2010. "Nanoparticle-Based Theranostic Agents." *Advanced Drug Delivery Reviews* 62 (11): 1064–1079. doi:10.1016/j.addr.2010.07.009

Yameen, B., W. I. Choi, C. Vilos, A. Swami, J. Shi, and O. C. Farokhzad. 2014. "Insight into Nanoparticle Cellular Uptake and Intracellular Targeting." *30th Anniversary Special Issue* 190: 485–499. doi:10.1016/j.jconrel.2014.06.038

Yang, Y., Z. Qin, W. Zeng, T. Yang, Y. Cao, C. Mei, and Y. Kuang. 2017. "Toxicity Assessment of Nanoparticles in Various Systems and Organs." *Nanotechnology Reviews* 6: 279. doi:10.1515/ntrev-2016-0047

Yildirimer, L., N. T. K. Thanh, M. Loizidou, and A. M. Seifalian. 2011. "Toxicology and Clinical Potential of Nanoparticles." *Nano Today* 6 (6): 585–607. doi:10.1016/j.nantod.2011.10.001

Yuan, S. Y., and R. R. Rigor. 2010. *The Endothelial Barrier*. San Rafael, California: Morgan & Claypool Life Sciences.

Zaloga, J., C. Janko, J. Nowak, J. Matuszak, S. Knaup, D. Eberbeck, R. Tietze, H. Unterweger, R. P. Friedrich, S Duerr, et al. 2014. "Development of a Lauric Acid/Albumin Hybrid Iron Oxide Nanoparticle System with Improved Biocompatibility." *International Journal of Nanomedicine* 9: 4847–4866. doi:10.2147/IJN.S68539

Zhang, H., Z. Ji, T. Xia, H. Meng, C. Low-Kam, R. Liu, S. Pokhrel, S. Lin, X. Wang, Y.-P. Liao, et al. 2012. "Use of Metal Oxide Nanoparticle Band Gap to Develop a Predictive Paradigm for Oxidative Stress and Acute Pulmonary Inflammation." *ACS Nano* 6 (5): 4349–4368. doi:10.1021/nn3010087

Zhang, S., J. Li, G. Lykotrafitis, G. Bao, and S. Suresh. 2009. "Size-Dependent Endocytosis of Nanoparticles." *Advanced Materials* 21 (4): 419–424. doi:10.1002/adma.200801393

Zhao, L., A. Seth, N. Wibowo, C.-X. Zhao, N. Mitter, C. Yu, and A. P. J. Middelberg. 2014. "Nanoparticle Vaccines." *Vaccine* 32 (3): 327–337. doi:10.1016/j.vaccine.2013.11.069

Zheng, J., J. D. Clogston, A. K. Patri, M. A. Dobrovolskaia, and S. E. McNeil. 2011. "Sterilization of Silver Nanoparticles Using Standard Gamma Irradiation Procedure Affects Particle Integrity and Biocompatibility." *Journal of Nanomedicine & Nanotechnology* S5 (01): 001. doi:10.4172/2157-7439.S5-001

Discussion

The versatility of ENP has made these materials promising candidates for use as novel drug delivery systems, imaging tools, or active agents. However, these versatile materials are also capable of provoking multiple adverse effects. The assessment of ENP safety is therefore an ongoing concern among researchers and authorities alike. ENP are equipped with an exceptional array of physico-chemical properties that lead to the inheritance of their toxicological potential. As size can influence the display of these properties, the hazardous health risk of every ENP is potentially unique. To understand how an ENP is received by tissues (**Chapter I**; pages 23 – 35) or organisms (**Chapters II & III**; pages 36 – 45 & 46 – 74) upon administration and interaction, three general parameters need to be determined. These parameters are the chemical identity of the particle, its physico-chemical properties, and the biologic system they encounter. In terms of research this requires the characterization of an ENP, the monitoring of its cytotoxicity, and the investigation of the behavior of an ENP in an entire organism (**Figure VII**). Furthermore, these investigations should be carried out in the most reproducible manner possible to avoid contradicting results and controversial perceptions of nanosafety. How to conduct such investigations effectively is one of the most discussed topic in nanosafety. The content of this thesis was therefore committed to further improve the knowledge of nanotoxicology (**Chapters I & II**; pages 23 – 35 & 36 – 45) and expedite the assessment of nanosafety regulation (**Chapters III & IV**; pages 46 – 74 & 75 – 119), especially for the field of ENP designed for therapeutic use.

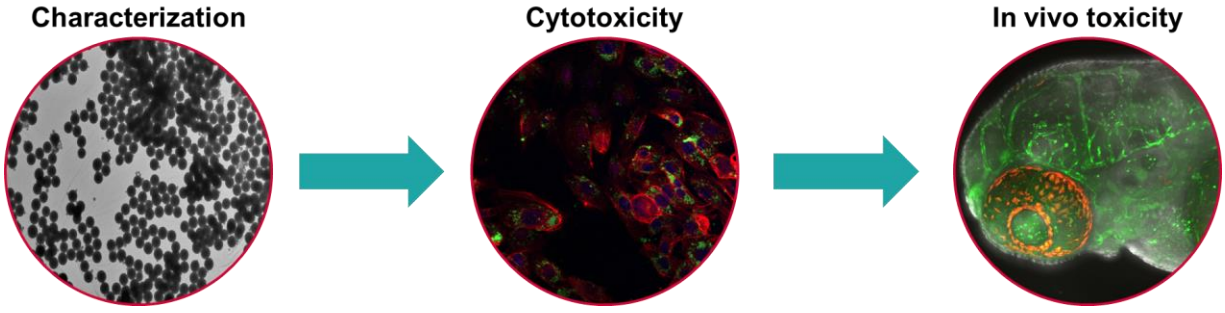

Figure VIII – Workflow in nanotoxicological research. *Characterization, cytotoxicity, and in vivo toxicity monitoring are a prerequisite of determining the mechanism and impact of specific nanoparticle toxicity. Due to the lack of guidelines, the diversity of investigational set ups and interpretations of these three parameters have led to controversial points of view on how to correctly determine nanosafety.*

Synthesis of inorganic nanoparticles used in therapeutic research

Described as a major benefit, the synthesis of many ENP is often referred to as straightforward and highly reproducible. Indeed, an ENP can be chemically tailored to fit a vast amount of needs. Specific organ or tissue targeting methods such as the approach of hepatocyte targeting by using asialofetuin-conjugated liposomes[161] are greatly dependent on ENP surface modifications[162]. The implementation of fluorescent markers is a further, routinely used modification of ENP surfaces for *in vitro* and *in vivo* observations of e.g. cellular uptake, or stability as shown in **Chapter I** (pages 23 – 35). However, most often ENP surfaces are altered to enhance the biocompatibility of these materials. Despite well-documented chemical procedures on how to produce ENP, the aspect of safety by design is often neglected. This is because many of the commonly used ENP syntheses were initially not intended to result in products for medical research[87,97]. Only since nanomedicine has become increasingly interesting did the issue of safety by design become more important. Hence modifications are routinely done to ensure better tolerability of ENP by a target organism. Polyethylene glycol (PEG) is an FDA approved polymer that is most frequently used for this purpose due to its high solubility and biocompatibility[163]. Other are options of coating being applied are dextran[164] and human serum albumin (HSA)[60] as used in **Chapter III** (pages 46 – 74).

Although straightforward synthesis approaches are common, high reproducibility between batches of any nanoparticle is not guaranteed. Reproducibility of ENP is often dependent on parameters such as temperature, pressure, purity of the reactants, sterility, reaction time, and the researcher performing the synthesis. In research laboratories, these limitations can seldom all be covered. If in these cases the physico-chemical properties of ENP are not determined after every synthesis, false interpretations of further downstream results are inevitable.

Physico-chemical characterization of ENP

The physico-chemical characterization of an ENP marks the starting point of both nanotoxicological research and nanosafety assessments alike. Because the toxic potentials of ENP are highly dependent on their unique physico-chemical properties, thorough characterization is key to understand the outcome of *in vitro* or *in vivo* studies. In **Chapter IV** (pages 75 – 119) seven physico-chemical properties were defined as the most important parameters to be determined for therapeutic ENP candidates:

chemical identity, zeta potential, aqueous stability, particle size, shape, size distribution, and purity.

The chemical identity, zeta potential and aqueous stability of an ENP should be among the first determined characteristics. Knowing the chemical identity of a formulation can already give important insights into the behavior and reactivity of an ENP formulation. Additionally, zeta potential and aqueous stability are indicators for agglomeration, aggregation, and sedimentation. Furthermore, negative zeta potentials have proven the inheritance of a lesser toxic potential than their positive counterparts.

The key physico-chemical characteristic of an ENP however, is undoubtedly its size. Not only is the definition of a nanoparticle entirely size-dependent; but small size mostly correlates to facilitated cellular uptake, low persistence, and cytotoxicity, as well as lesser elimination due to phagocytosis. Moreover, an adjustment of the nanoscale specifically for therapeutic ENP would be beneficial as nanoparticles are taken up by endocytosis at larger sizes than 100 nm. The new proposal discussed in **Chapter IV** (pages 75 – 119) sees this upper limit being raised to 500 nm marking the size boundary where no endocytosis apart from phagocytosis takes place.

As nanoparticles are also three-dimensional objects, size distribution and shape are two additional characteristics that influence the toxicity of an ENP or its readout. ENP are mostly regarded as being spherical. By definition however, a nanoparticle is not obliged to any shape but must have an aspect ratio of ≤ 3:1. Nevertheless, the aim of synthesizing spherical ENP should be pursued since this is the shape that minimizes immune responses and maximizes the circulation half-life. Size distributions should be kept as narrow as possible. First, to ensure that the size of a formulation remains within the nanoscale, secondly, narrow size distributions allow for better allocation of adverse effects to specific ENP properties ensuring higher safety. Therefore, the size distribution within an ENP batch should ideally not exceed 20 % (PDI 0.2). Finally, most of the therapeutic candidates launched for approval by authorities are not successful due to contaminations most prominently introduced during synthesis. Due to sterility issues bacteria and mycoplasma adhering to the surface are most often the prime reason for rejection of the formulation by regulators.

Determining these seven physico-chemical parameters for every ENP formulation provides the needed information to draw the correct conclusions from *in vitro* or *in vivo* toxicity study results when trying to link an adverse outcome to a specific ENP feature.

In vitro screening of ENP toxicity

Screening the effects that ENP can have on *in vitro* systems is the most common approach of gaining knowledge in nanotoxicological research. Depending on the goal of the screening, the main challenges are the choice of the optimal cell-based system, ENP type, ENP dose, and incubation parameters (e.g. time, temperature).

Most nanotoxicological screenings bare the motivation of detecting a reaction from the biological test system after interacting with an ENP. Therefore, high ENP doses, optimized treatment conditions, and appropriate cell types are chosen to achieve this goal.

A different approach should be used when determining the toxic potential of an ENP designed for therapeutic use. Here, the cellular model(s) should reflect the tissue most likely to be exposed to the therapeutic ENP in question. Furthermore, testing a dose range spanning across multiple orders of magnitude is necessary to determine the specific ENP associated adverse effects, the dose levels at which no adverse effect (NOAEL) and the lowest adverse effect (LOAEL) are encountered. Finally, ENP toxicity is time-dependent requiring a series of experiments in which the occurrence of possible adverse effects is screened for in defined intervals.

Since there are no defined guidelines on how to examine the toxicity of ENP for medical purposes, the array of toxic effects that should be monitored is not demarcated.

The extensive study described in **Chapter I** (pages 23 – 35)[62] is an example of how the principal adverse effects caused by ENP can be screened and interpreted. The study shows that generation of ROS and significant cell death in form of apoptosis and necrosis is the results of SiNP uptake in human endothelial cells. Furthermore, signaling experiments revealed that ROS triggers the activation of the inflammation and apoptosis linked JAK/STAT pathway before apoptotic activity is detected. At the same time, cellular defense mechanisms such as the activation of NFκ-B could not be observed. Even though the production of the apoptosis-inhibiting protein Survivin meant that the immune defense of endothelial cells was partly functioning, incubated cells were not able to manage the prevailing ENP exposure. An exception was found at lowest ENP doses where the modulation of MHC class I, low ROS generation and no significant cell viability decrease suggested a functioning cellular defense after more than 48h of incubation. These observations point out the capability of selectively

triggering signaling pathways with differently modified ENP. Notably, these observations are restricted to acute adverse effects triggered by ENP.

In the specific case of evaluating the toxic potential of a formulation designed for therapeutic use, monitoring further parameters (e.g. intracellular persistence, hemolysis) with additional cell-based systems is a prerequisite (**Chapter IV;** pages 75 – 119).

To monitor the ability of ENP to cause chronic toxicity on the other hand, *in vivo* screenings are a necessity.

Alternative in vivo screening tool for nanotoxicology

Due to several key characteristics the zebrafish embryo model has emerged as a potential *in vivo* model for nanotoxicology. Transparency, fast development, and small size make this animal a promising prospect for toxicological studies with the possibility of implementing HTS as well. Moreover, their extensive use in developmental biology has led to the availability of an enormous amount of transgenic lines to monitor angio-, organo-, or immunogenesis as well as the routine use of microinjection. Finally, the zebrafish is a vertebrate with close genome homology to the human (especially to the immune system).

In **Chapters II & III** (pages 36 – 45 & 46 – 74) the zebrafish embryo is used as an alternative *in vivo* model system, firstly to monitor the safety and biodistribution of ENP and secondly to exploit its use as nanotoxicological tool.

The stability and activity of PLGA nanoparticles were monitored using the zebrafish embryo model to verify their biomedical use in **Chapter II** (pages 36 – 45)[111]. The study revealed that the zebrafish embryo is an ideal small animal model for the monitoring of fluorescently labeled ENP. Furthermore, the stability of ENP formulations can be observed over days, proving the versatility of the model. Due to the possibility of observing the biodistribution of fluorescent ENP the behavior of an ENP presents information on the safety of the formulations, further supporting the use of the zebrafish in nanotoxicological studies and nanosafety assessments[160].

Biodistribution is one crucial parameter that needs to be investigated for ENP designed for therapeutic use. As described previously, this is possible for fluorescently labeled ENP after injection into the zebrafish. However, tracing non-labeled ENP is not as straightforward. However, this would be highly beneficial, especially for therapeutic ENP candidates.

Thus, monitoring the biodistribution of AuNP and SPIONs after injection into zebrafish embryos was investigated in **Chapter III** (pages 46 – 74). Different techniques (bright field microscopy, computer tomography, histology) were used to gain an overview of possibilities to monitor ENP biodistribution in vivo. The outcome of the study suggested that commercial microscopy techniques did not represent a valid alternative as the ENP could not be distinguished with certainty. Histological investigations had proven not to be suitable either. Despite its diminutive size the zebrafish had to be sectioned into a number of samples exceeding the possibility of whole-body evaluations. However, SRμCT was found to pose a valid alternative, as the biodistribution of non-labeled ENP was able to be monitored throughout an entire organism for the first time. The insights provided by this novel combination of analysis technique and animal model further underline the value of the zebrafish animal model for nanotoxicology. However, the intention should not be to replace existing animal models with the zebrafish. This model should find its application as an early *in vivo* screening tool to bridge the gap from cell-based investigations to higher organisms such as the mouse or rat. Due to its physical features and possibility of HTS the zebrafish embryo could serve as a time- and cost-effective alternative for routine toxicity screening processes.

Shortage of safety guidelines for nanoparticles designed for therapeutic use

Although being aware of the shortage of nano-specific regulatory guidelines, authorities have not decided on how nanosafety should be regulated. From a regulatory point of view, there are four major issues responsible for this shortage:

- *Analytics:* No robust and effective toolbox is available to characterize nanomaterials and quantify ENP exposure in test systems.
- *Screening methods in vivo:* Specific methods to be integrated into a test and risk assessment strategy are inexistent and must be identified.
- *Reference System:* Lack of reference ENP to validate test and risk assessment strategies ensuring robust results.
- *Grouping:* Strategies to differentiate nanomaterials and to group similar materials are controversial.

Combining the results and insights obtained in **Chapters I – III** (pages 23 - 74) a proposal for a preclinical safety guideline for injectable nanomedicines was generated. This approach discussed in **Chapter IV** (pages 75 – 119) highlights the importance of application-specific safety assessment of ENP. Furthermore, the importance of distinct physico-chemical characterization is discussed as well as the choice of *in vitro* test systems, analysis techniques, and assay protocols. The strategy is based on the intent of fast and application-oriented decision making, including a novel definition for ENP designed for injection (iNP) as well as a novel hazard assessment approach. ENP interactions in this case are based on the two fundamental events prone to trigger nanotoxicological outcomes: cellular uptake and intracellular persistence. Depending on the levels of cellular uptake and intracellular persistence the examined ENP are categorized into one of four different classes. Hazard assessment for each class consists of a specific assay cascade to ensure maximum safety of the ENP before clinical trials. This preclinical safety guideline is the first of its kind, as there are no nanomedicine specific approaches existent and none of the existing safety strategies cover the evaluation of ENP exposure specifically after injection.

Outlook

ENP have successfully broken onto the scene as promising alternatives for multiple medical applications. There use as DDS, diagnostic tools, and theranostic applications has stimulated an ever-growing community of researchers to tackle more common medical issues such as cancer, Alzheimer, or iron deficiency. To help pave the way for the successful achievement of these goals several efforts in nanotoxicology and nanosafety are being made.

Introduction of standardized *in vitro* and *in vivo* characterization techniques and test systems (e.g. µCT and zebrafish embryo) would help greatly to generate less contradictory knowledge on the interactions of ENP with biological targets. Furthermore, this would lead to a more uniform view on how to regulate these promising materials and in turn accelerate the implementation of standard testing protocols.

Institutions such as the US Nanotechnology Characterization Laboratory (US NCL) and the European Nanomedicine Characterization Laboratory (EU NCL) have begun to set up assay cascades for the testing of ENM that are intended for medical applications available for the public. Furthermore, they are consulted by regulatory authorities and manufacturers alike for the assistance with characterization and safety testing of ENM. In the future such institutions will have gained extensive knowledge of the intentions of both parties alongside developing an expertise in specific ENM safety evaluation, which in turn can be accessed by the public. Consequent use of their expertise would lead to a more uniform approach of testing across the field of nanotoxicology providing more comparable data and focused trouble-shooting.

In their most recent communication on nano-related definitions, the FDA has stated that it could be favorable to regulate ENM in an application-orientated manner, which may help to clear up prevailing confusion and controversial views on the topic of nanosafety. This statement shows that a change of thinking is underway where the solution of successfully regulating ENM is no longer a one strategy approach, but where it is advisable that certain applicatory fields promote their own distinct regulation of ENM. For the field of nanomedicine this would be highly favorable.

Conclusion

Throughout this work the main parameters important for the safety of ENP designed for therapeutic use were assessed, analyzed, and discussed. This provided several novelties in cell signaling, in vivo imaging, and in hazard assessment. It could be shown that differently charged nanoparticles can selectively trigger signaling pathways in a dose and time-dependent manner. Different silica-based ENP were shown to activate the JAK/STAT pathway and modulate of MHC class I. The correlation between these findings and further adverse effects such as generation of ROS, apoptosis, and necrosis has underlined the hypothesis that after nanoparticle uptake specific toxicological cascades are triggered. Furthermore, the implementation of the zebrafish embryo model into safety and biodistribution studies proved that this novel vertebrate model would be an ideal complementary *in vivo* system for nanotoxicological studies. By combining the zebrafish with powerful synchrotron-based computer tomography the biodistribution of non-labeled ENP administered in therapeutic doses could be visualized for the first time in an entire animal model. The combination of all obtained results and insights led to the proposal of a safety guideline specifically for injectable nanoparticles incorporating the most important factors of physico-chemical characterization, ENP interaction, and hazard assessment. This application-oriented approach is based on exclusion criteria, facilitates regulatory decision-making, and incorporates standardized assay protocols to form a robust and highly feasible strategy. The proposal represents the very first safety guideline issued specifically for the preclinical development of nanomedicines.

Bibliography

1. ISO. ISO/TS 80004-2:2015(en), Nanotechnologies — Vocabulary — Part 2: Nano-objects. (2015). Available at: https://www.iso.org/obp/ui/#iso:std:iso:ts:80004:-2:ed-1:v1:en. (Accessed: 28th August 2017)
2. Serpone, N. & Horikoshi, S. Microwaves in Nanoparticle Synthesis: Fundamentals and Applications. (2013). Available at: http://www.wiley.com/WileyCDA/WileyTitle/productCd-3527331972.html. (Accessed: 28th August 2017)
3. Krug, H. F. & Wick, P. Nanotoxicology: an interdisciplinary challenge. *Angew. Chem. Int. Ed Engl.* **50,** 1260–1278 (2011).
4. ASTM. ASTM E2456 - 06(2012) Standard Terminology Relating to Nanotechnology. (2012). Available at: https://www.astm.org/Standards/E2456.htm. (Accessed: 8th September 2017)
5. Kim, Y. *et al.* Emissions of Nanoparticles and Gaseous Material from 3D Printer Operation. *Environ. Sci. Technol.* **49,** 12044–12053 (2015).
6. Lohani, A., Verma, A., Joshi, H., Yadav, N. & Karki, N. Nanotechnology-Based Cosmeceuticals. *ISRN Dermatol.* **2014,** 843687 (2014).
7. Raj, S., Jose, S., Sumod, U. S. & Sabitha, M. Nanotechnology in cosmetics: Opportunities and challenges. *J. Pharm. Bioallied Sci.* **4,** 186–193 (2012).
8. McCormick, P. G. Nanoparticles in Sunscreens: Fact and Fiction. *Cosmetics & Toiletries* (2013). Available at: http://www.cosmeticsandtoiletries.com/regulatory/nanotech/Nanoparticles-in-Sunscreens-Fact-and-Fiction-232514661.html. (Accessed: 8th September 2017)
9. Bumbudsanpharoke, N., Choi, J. & Ko, S. Applications of Nanomaterials in Food Packaging. *J. Nanosci. Nanotechnol.* **15,** 6357–6372 (2015).
10. Pradeep, T. & Anshup. Noble metal nanoparticles for water purification: A critical review. *Thin Solid Films* **517,** 6441–6478 (2009).
11. Murthy, S. K. Nanoparticles in modern medicine: State of the art and future challenges. *Int. J. Nanomedicine* **2,** 129–141 (2007).
12. Salata, O. Applications of nanoparticles in biology and medicine. *J. Nanobiotechnology* **2,** 3–3 (2004).
13. Boilard, S. P., Amyotte, P. R., Khan, F. I., Dastidar, A. G. & Eckhoff, R. K. Explosibility of micron- and nano-size titanium powders. *J. Loss Prev. Process Ind.* **26,** 1646–1654 (2013).
14. Zhang, Z., Xu, L., Li, H. & Kong, J. Wavelength-tunable luminescent gold nanoparticles generated by cooperation ligand exchange and their potential application in cellular imaging. *RSC Adv.* **3,** 59–63 (2012).
15. Auffan, M. *et al.* Towards a definition of inorganic nanoparticles from an environmental, health and safety perspective. *Nat. Nanotechnol.* **4,** 634–641 (2009).
16. Bobo, D., Robinson, K. J., Islam, J., Thurecht, K. J. & Corrie, S. R. Nanoparticle-Based Medicines: A Review of FDA-Approved Materials and Clinical Trials to Date. *Pharm. Res.* **33,** 2373–2387 (2016).
17. Faraday, M. The Bakerian Lecture: Experimental Relations of Gold (and Other Metals) to Light. *Philos. Trans. R. Soc. Lond.* **147,** 145–181 (1857).
18. Kettiger, H. E. Silica nanoparticles and their interaction with cells : a multidisciplinary approach. (University_of_Basel, 2014).
19. Dykman, L. & Khlebtsov, N. Gold Nanoparticles in Biology and Medicine: Recent Advances and Prospects. *Acta Naturae* **3,** 34–55 (2011).
20. Yapijakis, C. Hippocrates of Kos, the father of clinical medicine, and Asclepiades of Bithynia, the father of molecular medicine. Review. *Vivo Athens Greece* **23,** 507–514 (2009).
21. Naggar, M. E., Shehadi, I., Abdou, H. E. & Mohamed, A. A. Gilded Hope for Medicine. *Inorganics* **3,** 139–154 (2015).
22. Strebhardt, K. & Ullrich, A. Paul Ehrlich's magic bullet concept: 100 years of progress. *Nat Rev Cancer* **8,** 473–480 (2008).

23. Bangham, A. D. & Horne, R. W. Negative staining of phospholipids and their structural modification by surface-active agents as observed in the electron microscope. *J. Mol. Biol.* **8,** 660-IN10 (1964).
24. Gregoriadis, G., Leathwood, P. D. & Ryman, B. E. Enzyme entrapment in liposomes. *FEBS Lett.* **14,** 95–99 (1971).
25. Emanuel, N., Kedar, E., Bolotin, E. M., Smorodinsky, N. I. & Barenholz, Y. Preparation and characterization of doxorubicin-loaded sterically stabilized immunoliposomes. *Pharm Res* **13,** 352–359 (1996).
26. Emanuel, N., Kedar, E., Bolotin, E. M., Smorodinsky, N. I. & Barenholz, Y. Targeted delivery of doxorubicin via sterically stabilized immunoliposomes: pharmacokinetics and biodistribution in tumor-bearing mice. *Pharm Res* **13,** 861–868 (1996).
27. Barenholz, Y. (Chezy). Doxil® — The first FDA-approved nano-drug: Lessons learned. *J. Controlled Release* **160,** 117–134 (2012).
28. Grand View Research. Nanomedicine Market Size, Growth | Global Industry Report, 2013-2025. (2017). Available at: http://www.grandviewresearch.com/industry-analysis/nanomedicine-market. (Accessed: 9th September 2017)
29. Emerich, D. F. & Thanos, C. G. Targeted nanoparticle-based drug delivery and diagnosis. *J. Drug Target.* **15,** 163–183 (2007).
30. Zhang, L. *et al.* Nanoparticles in Medicine: Therapeutic Applications and Developments. *Clin. Pharmacol. Ther.* **83,** 761–769 (2008).
31. Cole, L. E., Ross, R. D., Tilley, J. M., Vargo-Gogola, T. & Roeder, R. K. Gold nanoparticles as contrast agents in x-ray imaging and computed tomography. *Nanomed.* **10,** 321–341 (2015).
32. Neuwelt, A. *et al.* Iron-Based Superparamagnetic Nanoparticle Contrast Agents for MRI of Infection and Inflammation. *AJR Am. J. Roentgenol.* **204,** W302–W313 (2015).
33. Ambrogio, M. W., Thomas, C. R., Zhao, Y.-L., Zink, J. I. & Stoddart, J. F. Mechanized Silica Nanoparticles: A New Frontier in Theranostic Nanomedicine. *Acc. Chem. Res.* **44,** 903–913 (2011).
34. Tang, L. & Cheng, J. Nonporous silica nanoparticles for nanomedicine application. *Nano Today* **8,** 290–312 (2013).
35. Das, S. *et al.* Cerium oxide nanoparticles: applications and prospects in nanomedicine. *Nanomed.* **8,** 1483–1508 (2013).
36. Kim, J. S. *et al.* Antimicrobial effects of silver nanoparticles. *Nanomedicine Nanotechnol. Biol. Med.* **3,** 95–101 (2007).
37. Fenske, D. B. & Cullis, P. R. Liposomal nanomedicines. *Expert Opin. Drug Deliv.* **5,** 25–44 (2008).
38. Liechty, W. B., Kryscio, D. R., Slaughter, B. V. & Peppas, N. A. Polymers for Drug Delivery Systems. *Annu. Rev. Chem. Biomol. Eng.* **1,** 149–173 (2010).
39. Wu, X., Wu, M. & Zhao, J. X. Recent development of silica nanoparticles as delivery vectors for cancer imaging and therapy. *Nanomedicine Nanotechnol. Biol. Med.* **10,** 297–312 (2014).
40. Kumar, A., Zhang, X. & Liang, X.-J. Gold nanoparticles: Emerging paradigm for targeted drug delivery system. *Pearl 30th Anniv. Ed. Nanotechnol. Regen. Med.* **31,** 593–606 (2013).
41. Ojea-Jiménez, I. *et al.* Engineered inorganic nanoparticles for drug delivery applications. *Curr. Drug Metab.* **14,** 518–530 (2013).
42. Hahn, M. A., Singh, A. K., Sharma, P., Brown, S. C. & Moudgil, B. M. Nanoparticles as contrast agents for in-vivo bioimaging: current status and future perspectives. *Anal. Bioanal. Chem.* **399,** 3–27 (2011).
43. Cormode, D. P., Naha, P. C. & Fayad, Z. A. Nanoparticle Contrast Agents for Computed Tomography: A Focus on Micelles. *Contrast Media Mol. Imaging* **9,** 37–52 (2014).
44. Lisy, M.-R. *et al.* Fluorescent bacterial magnetic nanoparticles as bimodal contrast agents. *Invest. Radiol.* **42,** 235–241 (2007).
45. Wang, Y.-X. J. Superparamagnetic iron oxide based MRI contrast agents: Current status of clinical application. *Quant. Imaging Med. Surg.* **1,** 35–40 (2011).

46. Singh, J. & Daftary, A. Iodinated Contrast Media and Their Adverse Reactions. *J. Nucl. Med. Technol.* **36,** 69–74 (2008).
47. Tietze, R. *et al.* Visualization of superparamagnetic nanoparticles in vascular tissue using XμCT and histology. *Histochem. Cell Biol.* **135,** 153–158 (2011).
48. Hainfeld, J. F. *et al.* Micro-CT enables microlocalisation and quantification of Her2-targeted gold nanoparticles within tumour regions. *Br. J. Radiol.* **84,** 526–533 (2011).
49. Lee, N., Choi, S. H. & Hyeon, T. Nano-sized CT contrast agents. *Adv. Mater. Deerfield Beach Fla* **25,** 2641–2660 (2013).
50. van Schooneveld, M. M. *et al.* A fluorescent, paramagnetic and PEGylated gold/silica nanoparticle for MRI, CT and fluorescence imaging. *Contrast Media Mol. Imaging* **5,** 231–236 (2010).
51. Regino, C. A. S. *et al.* A dual CT-MR dendrimer contrast agent as a surrogate marker for convection-enhanced delivery of intracerebral macromolecular therapeutic agents. *Contrast Media Mol. Imaging* **3,** 2–8 (2008).
52. Chou, S.-W. *et al.* In vitro and in vivo studies of FePt nanoparticles for dual modal CT/MRI molecular imaging. *J. Am. Chem. Soc.* **132,** 13270–13278 (2010).
53. Oh, M. H. *et al.* Large-scale synthesis of bioinert tantalum oxide nanoparticles for X-ray computed tomography imaging and bimodal image-guided sentinel lymph node mapping. *J. Am. Chem. Soc.* **133,** 5508–5515 (2011).
54. Pan, D. *et al.* An early investigation of ytterbium nanocolloids for selective and quantitative 'multicolor' spectral CT imaging. *ACS Nano* **6,** 3364–3370 (2012).
55. Jeelani, S. *et al.* Theranostics: A treasured tailor for tomorrow. *J. Pharm. Bioallied Sci.* **6,** S6–S8 (2014).
56. Kono, K. *et al.* Multi-functional liposomes having temperature-triggered release and magnetic resonance imaging for tumor-specific chemotherapy. *Biomaterials* **32,** 1387–1395 (2011).
57. de Smet, M., Heijman, E., Langereis, S., Hijnen, N. M. & Grüll, H. Magnetic resonance imaging of high intensity focused ultrasound mediated drug delivery from temperature-sensitive liposomes: An in vivo proof-of-concept study. *J. Controlled Release* **150,** 102–110 (2011).
58. Phillips, W. T., Goins, B. A. & Bao, A. Radioactive liposomes. *Wiley Interdiscip. Rev. Nanomed. Nanobiotechnol.* **1,** 69–83 (2009).
59. Kalber, T. L. *et al.* Hyperthermia treatment of tumors by mesenchymal stem cell-delivered superparamagnetic iron oxide nanoparticles. *Int. J. Nanomedicine* **11,** 1973–1983 (2016).
60. Zaloga, J. *et al.* Pharmaceutical formulation of HSA hybrid coated iron oxide nanoparticles for magnetic drug targeting. *Eur. J. Pharm. Biopharm.* **101,** 152–162 (2016).
61. Oberdörster, G. Safety assessment for nanotechnology and nanomedicine: concepts of nanotoxicology. *J. Intern. Med.* **267,** 89–105 (2010).
62. Siegrist, S., Kettiger, H., Fasler-Kan, E. & Huwyler, J. Selective stimulation of the JAK/STAT signaling pathway by silica nanoparticles in human endothelial cells. *Toxicol. In Vitro* **42,** 308–318 (2017).
63. Kettiger, H., Schipanski, A., Wick, P. & Huwyler, J. Engineered nanomaterial uptake and tissue distribution: from cell to organism. *Int. J. Nanomedicine* **8,** 3255–3269 (2013).
64. Oberdörster, G., Oberdörster, E. & Oberdörster, J. Nanotoxicology: An Emerging Discipline Evolving from Studies of Ultrafine Particles. *Environ. Health Perspect.* **113,** 823–839 (2005).
65. Service, R. F. Nanotoxicology. Nanotechnology grows up. *Science* **304,** 1732–1734 (2004).
66. Seaton, A., Tran, L., Aitken, R. & Donaldson, K. Nanoparticles, human health hazard and regulation. *J. R. Soc. Interface* **7,** S119–S129 (2010).
67. Whitesides, G. M. The 'right' size in nanobiotechnology. *Nat Biotech* **21,** 1161–1165 (2003).
68. Scott-Fordsmand, J. J. *et al.* A unified framework for nanosafety is needed. *Nano Today* **9,** 546–549 (2014).
69. Krug, H. F. Nanosafety Research—Are We on the Right Track? *Angew. Chem. Int. Ed.* **53,** 12304–12319 (2014).

70. Haase, A., Tentschert, J. & Luch, A. Nanomaterials: a challenge for toxicological risk assessment? *EXS* **101,** 219–250 (2012).
71. Dusinska, M. *et al.* Testing strategies for the safety of nanoparticles used in medical applications. *Nanomed.* **4,** 605–607 (2009).
72. Guadagnini, R. *et al.* Toxicity screenings of nanomaterials: challenges due to interference with assay processes and components of classic in vitro tests. *Nanotoxicology* 0–0 (2013). doi:10.3109/17435390.2013.829590
73. Feliu, N. & Fadeel, B. Nanotoxicology: no small matter. *Nanoscale* **2,** 2514–2520 (2010).
74. Bleeker, E. A. J. *et al.* Considerations on the EU definition of a nanomaterial: Science to support policy making. *Regul. Toxicol. Pharmacol.* **65,** 119–125 (2013).
75. Mühlebach, S., Borchard, G. & Yildiz, S. Regulatory challenges and approaches to characterize nanomedicines and their follow-on similars. *Nanomed.* **10,** 659–674 (2015).
76. Savolainen, K. *et al.* Nanosafety in Europe 2015-2025: Towards Safe and Sustainable Nanomaterials and Nanotechnology Innovations. *Hels. Finn. Inst. Occup. Health* (2013).
77. Korzeniowska, B., Nooney, R., Wencel, D. & McDonagh, C. Silica nanoparticles for cell imaging and intracellular sensing. *Nanotechnology* **24,** 442002 (2013).
78. Freitas, L. B. de O. *et al.* Multifunctional mesoporous silica nanoparticles for cancer-targeted, controlled drug delivery and imaging. *Microporous Mesoporous Mater.* **242,** 271–283 (2017).
79. Baek, S. *et al.* Smart multifunctional drug delivery towards anticancer therapy harmonized in mesoporous nanoparticles. *Nanoscale* **7,** 14191–14216 (2015).
80. Li, Z., Barnes, J. C., Bosoy, A., Stoddart, J. F. & Zink, J. I. Mesoporous silica nanoparticles in biomedical applications. *Chem. Soc. Rev.* **41,** 2590–2605 (2012).
81. Kettiger, H., Sen Karaman, D., Schiesser, L., Rosenholm, J. M. & Huwyler, J. Comparative safety evaluation of silica-based particles. *Toxicol. In Vitro* **30,** 355–363 (2015).
82. Kim, I.-Y., Joachim, E., Choi, H. & Kim, K. Toxicity of silica nanoparticles depends on size, dose, and cell type. *Nanomedicine Nanotechnol. Biol. Med.* **11,** 1407–1416 (2015).
83. Cho, M. *et al.* The impact of size on tissue distribution and elimination by single intravenous injection of silica nanoparticles. *Toxicol. Lett.* **189,** 177–183 (2009).
84. Lee, S. *et al.* The comparative immunotoxicity of mesoporous silica nanoparticles and colloidal silica nanoparticles in mice. *Int. J. Nanomedicine* **8,** 147–158 (2013).
85. Fu, C. *et al.* The absorption, distribution, excretion and toxicity of mesoporous silica nanoparticles in mice following different exposure routes. *Biomaterials* **34,** 2565–2575 (2013).
86. He, Q., Zhang, Z., Gao, Y., Shi, J. & Li, Y. Intracellular Localization and Cytotoxicity of Spherical Mesoporous Silica Nano- and Microparticles. *Small* **5,** 2722–2729 (2009).
87. Stöber, W., Fink, A. & Bohn, E. Controlled growth of monodisperse silica spheres in the micron size range. *J. Colloid Interface Sci.* **26,** 62–69 (1968).
88. Ostwald, W. Studien über die Bildung und Umwandlung fester Körper. *Z. Für Phys. Chem.* **22U,** 289–330 (1897).
89. Branda, F., Silvestri, B., Luciani, G. & Costantini, A. The effect of mixing alkoxides on the Stöber particles size. *Colloids Surf. Physicochem. Eng. Asp.* **299,** 252–255 (2007).
90. Porta, F., Lamers, G. E., Zink, J. I. & Kros, A. Peptide modified mesoporous silica nanocontainers(). *Phys. Chem. Chem. Phys. PCCP* **13,** 9982–9985 (2011).
91. Hainfeld, J. F., Slatkin, D. N., Focella, T. M. & Smilowitz, H. M. Gold nanoparticles: a new X-ray contrast agent. *Br. J. Radiol.* **79,** 248–253 (2006).
92. Hainfeld, J. F., Dilmanian, F. A., Slatkin, D. N. & Smilowitz, H. M. Radiotherapy enhancement with gold nanoparticles. *J. Pharm. Pharmacol.* **60,** 977–985 (2008).
93. Curry, T., Kopelman, R., Shilo, M. & Popovtzer, R. Multifunctional theranostic gold nanoparticles for targeted CT imaging and photothermal therapy. *Contrast Media Mol. Imaging* **9,** 53–61 (2014).
94. Zhang, X. Gold Nanoparticles: Recent Advances in the Biomedical Applications. *Cell Biochem. Biophys.* **72,** 771–775 (2015).

95. Alkilany, A. M. & Murphy, C. J. Toxicity and cellular uptake of gold nanoparticles: what we have learned so far? *J. Nanoparticle Res.* **12,** 2313–2333 (2010).
96. Brust, M., Walker, M., Bethell, D., Schiffrin, D. J. & Whyman, R. Synthesis of thiol-derivatised gold nanoparticles in a two-phase Liquid–Liquid system. *J. Chem. Soc. Chem. Commun.* **0,** 801–802 (1994).
97. Turkevich, J., Cooper Stevenson, P. & Hillier, J. A study of the nucleation and growth processes in the synthesis of colloidal gold. *Discuss. Faraday Soc.* **11,** 55–75 (1951).
98. Cobley, C. M., Chen, J., Cho, E. C., Wang, L. V. & Xia, Y. Gold nanostructures: a class of multifunctional materials for biomedical applications. *Chem. Soc. Rev.* **40,** 44–56 (2011).
99. Li, K., Nejadnik, H. & Daldrup-Link, H. E. Next-generation superparamagnetic iron oxide nanoparticles for cancer theranostics. *Drug Discov. Today* (2017). doi:10.1016/j.drudis.2017.04.008
100. Jarockyte, G. *et al.* Accumulation and Toxicity of Superparamagnetic Iron Oxide Nanoparticles in Cells and Experimental Animals. *Int. J. Mol. Sci.* **17,** 1193 (2016).
101. Singh, N., Jenkins, G. J., Asadi, R. & Doak, S. H. Potential toxicity of superparamagnetic iron oxide nanoparticles (SPION). *Nano Rev.* **1,** 10.3402/nano.v1i0.5358 (2010).
102. Hanot, C. C., Choi, Y. S., Anani, T. B., Soundarrajan, D. & David, A. E. Effects of Iron-Oxide Nanoparticle Surface Chemistry on Uptake Kinetics and Cytotoxicity in CHO-K1 Cells. *Int. J. Mol. Sci.* **17,** 54 (2016).
103. Nourafkan, E., Asachi, M., Gao, H., Raza, G. & Wen, D. Synthesis of stable iron oxide nanoparticle dispersions in high ionic media. *J. Ind. Eng. Chem.* **50,** 57–71 (2017).
104. Tombácz, E., Turcu, R., Socoliuc, V. & Vékás, L. Magnetic iron oxide nanoparticles: Recent trends in design and synthesis of magnetoresponsive nanosystems. *Biochem. Biophys. Res. Commun.* **468,** 442–453 (2015).
105. Mahmed, N., Heczko, O., Lancok, A. & Hannula, S.-P. The magnetic and oxidation behavior of bare and silica-coated iron oxide nanoparticles synthesized by reverse co-precipitation of ferrous ion (Fe2+) in ambient atmosphere. *J. Magn. Magn. Mater.* **353,** 15–22 (2014).
106. Häfeli, U. O. *et al.* Cell Uptake and in Vitro Toxicity of Magnetic Nanoparticles Suitable for Drug Delivery. *Mol. Pharm.* **6,** 1417–1428 (2009).
107. Zaloga, J. *et al.* Development of a lauric acid/albumin hybrid iron oxide nanoparticle system with improved biocompatibility. *Int. J. Nanomedicine* **9,** 4847–4866 (2014).
108. Danhier, F. *et al.* PLGA-based nanoparticles: An overview of biomedical applications. *J. Controlled Release* **161,** 505–522 (2012).
109. Makadia, H. K. & Siegel, S. J. Poly Lactic-co-Glycolic Acid (PLGA) as Biodegradable Controlled Drug Delivery Carrier. *Polymers* **3,** 1377–1397 (2011).
110. McCall, R. L. & Sirianni, R. W. PLGA Nanoparticles Formed by Single- or Double-emulsion with Vitamin E-TPGS. *J. Vis. Exp. JoVE* 51015 (2013). doi:10.3791/51015
111. Sieber, S. *et al.* Immobilization of Enzymes on PLGA Sub-Micrometer Particles by Crosslinked Layer-by-Layer Deposition. *Macromol. Biosci.* **17,** n/a-n/a (2017).
112. Dhawan, A., Sharma, V. & Parmar, D. Nanomaterials: A challenge for toxicologists. *Nanotoxicology* **3,** 1–9 (2009).
113. Treuel, L. *et al.* Physicochemical characterization of nanoparticles and their behavior in the biological environment. *Phys. Chem. Chem. Phys.* **16,** 15053–15067 (2014).
114. Kolhatkar, A. G., Jamison, A. C., Litvinov, D., Willson, R. C. & Lee, T. R. Tuning the Magnetic Properties of Nanoparticles. *Int. J. Mol. Sci.* **14,** 15977–16009 (2013).
115. Crist, R. M. *et al.* Common Pitfalls in Nanotechnology: Lessons Learned from NCI's Nanotechnology Characterization Laboratory. *Integr. Biol. Quant. Biosci. Nano Macro* **5,** (2013).
116. Fabricius, A.-L., Duester, L., Meermann, B. & Ternes, T. A. ICP-MS-based characterization of inorganic nanoparticles—sample preparation and off-line fractionation strategies. *Anal. Bioanal. Chem.* **406,** 467–479 (2014).
117. Pyrz, W. D. & Buttrey, D. J. Particle Size Determination Using TEM: A Discussion of Image Acquisition and Analysis for the Novice Microscopist. *Langmuir* **24,** 11350–11360 (2008).

118. Goldstein, A., Soroka, Y., Frušić-Zlotkin, M., Popov, I. & Kohen, R. High resolution SEM imaging of gold nanoparticles in cells and tissues. *J. Microsc.* **256,** 237–247 (2014).
119. Rao, A. *et al.* Characterization of nanoparticles using Atomic Force Microscopy. *J. Phys. Conf. Ser.* **61,** 971 (2007).
120. Li, T., Senesi, A. J. & Lee, B. Small Angle X-ray Scattering for Nanoparticle Research. *Chem. Rev.* **116,** 11128–11180 (2016).
121. Bhattacharjee, S. DLS and zeta potential - What they are and what they are not? *J. Control. Release Off. J. Control. Release Soc.* **235,** 337–351 (2016).
122. Filipe, V., Hawe, A. & Jiskoot, W. Critical Evaluation of Nanoparticle Tracking Analysis (NTA) by NanoSight for the Measurement of Nanoparticles and Protein Aggregates. *Pharm. Res.* **27,** 796–810 (2010).
123. Masarudin, M. J., Cutts, S. M., Evison, B. J., Phillips, D. R. & Pigram, P. J. Factors determining the stability, size distribution, and cellular accumulation of small, monodisperse chitosan nanoparticles as candidate vectors for anticancer drug delivery: application to the passive encapsulation of [14C]-doxorubicin. *Nanotechnol. Sci. Appl.* **8,** 67–80 (2015).
124. Li, Z., Wang, Y., Shen, J., Liu, W. & Sun, X. The measurement system of nanoparticle size distribution from dynamic light scattering data. *Opt. Lasers Eng.* **56,** 94–98 (2014).
125. Cervera Gontard, L., Ozkaya, D. & Dunin-Borkowski, R. E. A simple algorithm for measuring particle size distributions on an uneven background from TEM images. *Ultramicroscopy Amst.* **111,** 101–106 (2011).
126. Brunauer, S., Emmett, P. H. & Teller, E. Adsorption of Gases in Multimolecular Layers. *J. Am. Chem. Soc.* **60,** 309–319 (1938).
127. Nienhaus, G. U., Maffre, P. & Nienhaus, K. Studying the protein corona on nanoparticles by FCS. *Methods Enzym.* **519,** (2013).
128. Grossen, P. *et al.* Functionalized Solid-Sphere PEG-b-PCL Nanoparticles to Target Brain Capillary Endothelial Cells In Vitro, Functionalized Solid-Sphere PEG-b-PCL Nanoparticles to Target Brain Capillary Endothelial Cells In Vitro. *J. Nanomater. J. Nanomater.* **2016, 2016,** e7818501 (2016).
129. Huth, F. *et al.* Nano-FTIR Absorption Spectroscopy of Molecular Fingerprints at 20 nm Spatial Resolution. *Nano Lett.* **12,** 3973–3978 (2012).
130. Carney, R. P. *et al.* Determination of nanoparticle size distribution together with density or molecular weight by 2D analytical ultracentrifugation. *Nat. Commun.* **2,** 335 (2011).
131. Fatisson, J., Quevedo, I. R., Wilkinson, K. J. & Tufenkji, N. Physicochemical characterization of engineered nanoparticles under physiological conditions: effect of culture media components and particle surface coating. *Colloids Surf. B Biointerfaces* **91,** 198–204 (2012).
132. Maiorano, G. *et al.* Effects of cell culture media on the dynamic formation of protein-nanoparticle complexes and influence on the cellular response. *ACS Nano* **4,** 7481–7491 (2010).
133. Nel, A. E. *et al.* Understanding biophysicochemical interactions at the nano-bio interface. *Nat. Mater.* **8,** 543–557 (2009).
134. Docter, D. *et al.* No king without a crown--impact of the nanomaterial-protein corona on nanobiomedicine. *Nanomed.* **10,** 503–519 (2015).
135. Setyawati, M. I., Tay, C. Y., Docter, D., Stauber, R. H. & Leong, D. T. Understanding and exploiting nanoparticles' intimacy with the blood vessel and blood. *Chem. Soc. Rev.* **44,** 8174–8199 (2015).
136. Neagu, M. *et al.* Protein bio-corona: critical issue in immune nanotoxicology. *Arch. Toxicol.* **91,** 1031–1048 (2017).
137. Zhang, L. W. & Monteiro-Riviere, N. A. Use of confocal microscopy for nanoparticle drug delivery through skin. *J. Biomed. Opt.* **18,** 061214 (2013).
138. Zucker, R. M., Ortenzio, J. N. R. & Boyes, W. K. Characterization, detection, and counting of metal nanoparticles using flow cytometry. *Cytom. Part J. Int. Soc. Anal. Cytol.* **89,** 169–183 (2016).
139. Kong, B., Seog, J. H., Graham, L. M. & Lee, S. B. Experimental considerations on the cytotoxicity of nanoparticles. *Nanomed.* **6,** 929–941 (2011).

140. Bahadar, H., Maqbool, F., Niaz, K. & Abdollahi, M. Toxicity of Nanoparticles and an Overview of Current Experimental Models. *Iran. Biomed. J.* **20,** 1–11 (2016).
141. Kroll, A., Pillukat, M. H., Hahn, D. & Schnekenburger, J. Interference of engineered nanoparticles with in vitro toxicity assays. *Arch. Toxicol.* **86,** 1123–1136 (2012).
142. Ong, K. J. *et al.* Widespread Nanoparticle-Assay Interference: Implications for Nanotoxicity Testing. *PLoS ONE* **9,** e90650 (2014).
143. Majno, G. & Joris, I. Apoptosis, oncosis, and necrosis. An overview of cell death. *Am. J. Pathol.* **146,** 3–15 (1995).
144. Manke, A., Wang, L. & Rojanasakul, Y. Mechanisms of Nanoparticle-Induced Oxidative Stress and Toxicity. *BioMed Research International* (2013). doi:10.1155/2013/942916
145. Eruslanov, E. & Kusmartsev, S. Identification of ROS using oxidized DCFDA and flow-cytometry. *Methods Mol. Biol. Clifton NJ* **594,** 57–72 (2010).
146. Tang, S. & Hewlett, I. Nanoparticle-based Immunoassays for Sensitive and Early Detection of Human Immunodeficiency Type 1 Capsid (p24) Antigen. *J. Infect. Dis.* **201,** S59–S64 (2010).
147. Collins, F. S., Gray, G. M. & Bucher, J. R. TOXICOLOGY: Transforming Environmental Health Protection. *Science* **319,** 906–907 (2008).
148. Lawrence, C. The husbandry of zebrafish (Danio rerio): A review. *Aquaculture* **269,** 1–20 (2007).
149. Barros, T. P., Alderton, W. K., Reynolds, H. M., Roach, A. G. & Berghmans, S. Zebrafish: an emerging technology for in vivo pharmacological assessment to identify potential safety liabilities in early drug discovery. *Br. J. Pharmacol.* **154,** 1400–1413 (2008).
150. Fako, V. E. & Furgeson, D. Y. Zebrafish as a correlative and predictive model for assessing biomaterial nanotoxicity. *Adv. Drug Deliv. Rev.* **61,** 478–486 (2009).
151. Jeong, J.-Y. *et al.* Functional and developmental analysis of the blood–brain barrier in zebrafish. *Brain Res. Bull.* **75,** 619–628 (2008).
152. Lyons, M. S., Bell, B., Stainier, D. & Peters, K. G. Isolation of the zebrafish homologues for the tie-1 and tie-2 endothelium-specific receptor tyrosine kinases. *Dev. Dyn.* **212,** 133–140 (1998).
153. Trede, N. S., Langenau, D. M., Traver, D., Look, A. T. & Zon, L. I. The use of zebrafish to understand immunity. *Immunity* **20,** 367–379 (2004).
154. Kimmel, C. B., Ballard, W. W., Kimmel, S. R., Ullmann, B. & Schilling, T. F. Stages of embryonic development of the zebrafish. *Dev. Dyn.* **203,** 253–310 (1995).
155. Karlsson, J., von Hofsten, J. & Olsson, P.-E. Generating Transparent Zebrafish: A Refined Method to Improve Detection of Gene Expression During Embryonic Development. *Mar. Biotechnol.* **3,** 0522–0527 (2001).
156. Lieschke, G. J. & Currie, P. D. Animal models of human disease: zebrafish swim into view. *Nat. Rev. Genet.* **8,** 353–367 (2007).
157. Braunbeck, T. *et al.* The fish embryo test (FET): origin, applications, and future. *Environ. Sci. Pollut. Res. Int.* **22,** 16247–16261 (2015).
158. Basnet, R. M., Guarienti, M. & Memo, M. Zebrafish Embryo as an In Vivo Model for Behavioral and Pharmacological Characterization of Methylxanthine Drugs. *Int. J. Mol. Sci.* **18,** 596 (2017).
159. Walker, M. B. & Kimmel, C. B. A two-color acid-free cartilage and bone stain for zebrafish larvae. *Biotech. Histochem. Off. Publ. Biol. Stain Comm.* **82,** 23–28 (2007).
160. Sieber, S. *et al.* Zebrafish as an early stage screening tool to study the systemic circulation of nanoparticulate drug delivery systems in vivo. *J. Controlled Release* **264,** 180–191 (2017).
161. Detampel, P., Witzigmann, D., Krähenbühl, S. & Huwyler, J. Hepatocyte targeting using pegylated asialofetuin-conjugated liposomes. *J Drug Target* **22,** 232–241 (2014).
162. Lahkar, S. & Das, M. K. Surface modified polymeric nanoparticles for brain targeted drug delivery. **7,** 914–931 (2013).
163. Veronese, F. M. & Pasut, G. PEGylation, successful approach to drug delivery. *Drug Discov. Today* **10,** 1451–1458 (2005).
164. Peng, K. *et al.* Dextran based photodegradable hydrogels formed via a Michael addition. *Soft Matter* **7,** 4881–4887 (2011).

Dr. Stefan Kevin **Siegrist**

10.05.1987 CH / CDN
Amerikanerstrasse 21 4102 Binningen
Stefansiegrist@gmx.ch +41 (0)76 498 93 47
https://www.linkedin.com/in/stefan-siegrist-ph-d-4553babb/

I am a highly motivated and solution-oriented person with working experience under GMP conditions. As a team player, I thrive in multidisciplinary projects and proactively communicate with my co-workers to tackle challenging tasks with a "can-do" mindset.

Professional Experience

06/2018 – present **Senior Scientist (Contractor),** Biopharm. Development, Novartis AG, Basel

- Develop efficient and robust drug manufacturing processes in sterile facilities, e.g. by applying down scale models for critical process steps and implementing new methods/technologies
- Plan, organize, perform, and analyze scientific experiments in collaboration with scientific associates and functional leads
- Author and review scientific documents to hand over to internal partners (e.g. Manufacturing sites, Device Development, RegCMC, Clinics)

09/2017 – 01/2018 **Research Scientist,** Pharm. Technology, University of Basel

- Co-leader in a safety project on in vivo biodistribution of nanomaterials
- Optimizing nanomedicine testing strategies with EMPA and SCAHT
- Validation of a novel safety evaluation guideline for nanomedicines

03/2014 – 09/2017 **Scientist/PhD Candidate,** Pharm. Technology, University of Basel

PhD thesis title *Assessing the safety of engineered nanoparticles for therapeutic use*

- Conduct drug discovery/nanotoxicology studies in vitro and in vivo in collaboration with various (inter)national academic partners and authorities (EU, NanoReg2, EMPA, SCAHT, BAG)
- Design, plan, perform, and evaluate analytical assays and testing strategies in a multidisciplinary environment
- Writing scientific publications and proposals as well as presenting scientific results at (inter)national meetings and conferences

01/2006 – 06/2006 **Trainee,** Analytical Development, Novartis Animal Health, Basel

- Analytical testing of oral dosage forms under GMP conditions
- Translation of equipment specific SOPs from German to English

Advanced Training

02/2016 – 06/2016 *Course on regulatory toxicology and risk assessment*, University of Basel
07/2016 *Nanomaterial Dosimetry Workshop*, 8th Int. NanoTox Conference, Boston
04/2015 *Nanotoxicology Postgraduate Course*, Karolinska Instituet, Stockholm
07/2014 *Summer School on Fluorescence-based Techniques*, FHNW Basel
04/2014 *Practical Introduction to Biophysical Methods*, University of Basel

Education

09/2007 – 03/2014 **BSc & MSc in Pharmaceutical Sciences,** University of Basel

Master thesis *Studying carbohydrate-lectin interactions to develop glycomimetic drugs*

- Master thesis results have extensively contributed to the validation of lead compounds that have moved to clinical development (Phase III).

01/2012 – 08/2012 **Internship,** Molecular Modeling Unit, University of Basel

- Studying toxic potentials (in silico) of antiarrhythmic active agents, method validation, and pinpointing of relevant molecular characteristics

Leadership Experience

03/2014 – 01/2018 **Research Scientist & PhD Candidate,** Pharm. Tech., University of Basel

- Leading graduate courses on semi-solid dosage forms
- Supervision of master theses and one PhD candidate

03/2016 **Rotary Youth Leadership Awards (RYLA),** Rotary Club Switzerland, Basel

- Leadership and management training for selected young professionals
- Communication training and enhancement of problem-solving skills

06/2012 – present **Board Member Head of Junior Handball,** HB Blau Boys Binningen

- Coordination of junior teams and their staff (approx. 100 individuals)
- Coordination of yearly budget and expenses (J+S Coach Diploma)
- Club representative for youth sports in the talent-pool HSG Leimental

03/2003 – 6/2018 **Handball Team Coach,** HB Blau Boys Binningen

- Diploma C adult/youth handball and Diploma children's sports/handball

Languages

Spoken & written	**German:**	native	**French:**	intermediate (level B2)
	English:	native	**Spanish:**	intermediate (level B2)

Computer Skills

Software experience MS Office, Origin, FlowJo, Gimp, ImageJ, JMP, Subway, BioELN, BSM

Recreational interests

- team handball, golf, and soccer
- travelling, cooking, and board games

Publications and granted proposals

09/2018 *Preclinical Hazard Evaluation Strategy for Nanomedicines*
Siegrist S., Cörek E., Detampel P., Wick. P., Sandström J., Huwyler J.; J. of Nanotoxicology

08/2018 *Propagation-basedX-ray Phase Contrast Microtomographyof Zebrafish Embryos to Understand Drug Delivery*
Schulz G., Cörek E., **Siegrist S**., Thalmann P., Dehyle A., Rack A., Huwyler J., Müller B.; Microsc. Microanal. 24 (Suppl 2), 2018

09/2017 *Removing ring artefacts from synchrotron radiation-based hard X-ray tomography data*
Thalmann P., Bikis C., Schulz G., Paleo P., Mirone A., Rack A., **Siegrist S.**, Cörek E., Huwyler J., Müller B.; Proc. SPIE

09/2017 Granted proposal for beam time at the Paul-Scherrer Institue (PSI) in Viligen, Switzerland. Implementing synchrotron radiation phase-contrast micro-computed tomography for monitoring the biodistribution differently coated iron nanoparticles upon injection into zebrafish embryos *in vivo*.

05/2017 *Selective stimulation of the JAK/STAT signaling pathway by silica nanoparticles in human endothelial cells.*
Siegrist S., Kettiger H., Fasler-Kan E., Huwyler J.; Toxicol. In Vitro

04/2017 *Immobilization of Enzymes on PLGA Sub-Micrometer Particles by Crosslinked Layer-by-Layer Deposition*.
Sieber S., **Siegrist S.**, Schwarz S., Porta F., Schenk SH., Huwyler J.; Macromol. Biosci.

02/2016 Granted proposal for beam time at the European Synchrotron Radiation Facility (ESRF) in Grenoble, France. Implementing synchrotron radiation phase-contrast micro-computed tomography for the visualization of silica, gold, and iron nanoparticles upon injection into zebrafish embryos *in situ*.

Manuscripts under review

Biodistribution of metal-based nano-particles in a small vertebrate model traced by synchrotron radiation micro-tomography
Siegrist S., Cörek E., Fluder P., Klados K., Bikis C., Detampel P., Thalmann P., Schulz G., Puchkov M., Alexiou C., Müller B., Huwyler J.

High-Affinity Carbohydrate-Lectin Interactions: How Nature Makes it Possible
Zihlmann P., Jiang X., Sager C.P., Fiege B., Jakob R.P., **Siegrist S.**, Zalewski A., Rabbani S., Eris D., Silbermann M., Pang L., Muhlethaler T., Sharpe T., Maier T., Ernst B.